MINERAL PARAGENESIS AND PEGMATITE FORMATION ASSOCIATED WITH THE EDEN LAKE SYENITE COMPLEX, NORTHERN MANITOBA.

by

KYLA M. ARDEN

A Thesis
submitted to the Faculty of Graduate Studies
in Partial Fulfilment of the Requirements
for the Degree of

MASTER OF SCIENCE

Department of Geological Sciences
University of Manitoba
Winnipeg, Manitoba

October, 1995

ISBN 0-612-12959-4

Canada

MINERAL PARAGENESIS AND PEGMATITE FORMATION ASSOCIATED WITH THE EDEN LAKE SYENITE COMPLEX, NORTHERN MANITOBA

BY

KYLA M. ARDEN

A Thesis submitted to the Faculty of Graduate Studies of the University of Manitoba in partial fulfillment of the requirements of the degree of

MASTER OF SCIENCE

For Glen

Abstract

The Eden Lake syenite complex is a monzonitic intrusion located in the Trans Hudson orogenic terrane. It intrudes granitic rocks between the Lynn Lake and Leaf Rapids greenstone belts in northern Manitoba. Although the complex has not yet been dated, geochemical, textural and mineralogical characteristics support its interpretation as a post-orogenic, metaluminous pluton with alkaline characteristics. The syenite complex comprises mafic and felsic monzonite phases and four types of associated pegmatites. The Type I mafic pegmatites comprise aegirine-augite, magnetite, plagioclase and hornblende; the Type II granitic pegmatites contain quartz, K-feldspar ± plagioclase. Neither of these are rare element pegmatites and neither contain any REE-bearing accessory minerals. The Type III granitic pegmatites are rare element pegmatites; they contain REE-bearing accessory minerals including apatite, titanite and zircon, as well as andradite, aegirine-augite, K-feldspar, plagioclase, quartz and fluorite. The REE-bearing phases are among the earliest minerals to crystallize in the Type III pegmatites; they display a similar stratigraphy of mineral growth, reflected in zoning patterns. The Type IV radioactive pegmatites are significantly REE-enriched; they contain REE-bearing minerals including apatite, titanite, zircon, allanite and britholite, as well as aegirine-augite, K-feldspar, plagioclase, quartz and fluorite. In the Type IV pegmatites, allanite and britholite are interpreted to be the last minerals to crystallize, after the other REE-bearing phases. Britholite has a number of unusual characteristics that suggest that it has been amorphized, annealed and altered by a hydrothermal fluid. Apatite, titanite and zircon display the same sequence of mineral growth as the crystals in the Type III pegmatites.

The Type I and Type II pegmatites represent crystallization of a liquid derived from a melt that had not undergone significant differentiation; this melt was not related to the syenite complex melt, but to a younger intrusion in the Eden Lake area. The Type III pegmatites were produced by crystallization of a residual liquid slightly enriched in incompatible trace elements formed by the fractional crystallization of the mafic and felsic monzonite phases of the syenite complex. The lack of significant REE-enrichment in the Type III pegmatites is the result of separation of a REE-, F-enriched immiscible vapour phase during the crystallization of the main phases of the syenite complex. The Type IV pegmatites are genetically related to the Type III pegmatites; they represent Type III pegmatites that have been altered by reaction with REE-enriched fluids. These fluids were introduced along shear zones and reacted with the pegmatite minerals before crystallizing first allanite, then britholite. The most likely source for these fluids is the REE -and F-enriched immiscible vapour phase that separated from the syenite melt during crystallization. Alteration of minerals within the Type III and IV pegmatites indicates both have been affected by late meteoric or magmatic fluids at elevated temperatures. The Eden Lake syenite complex and the associated REE-bearing pegmatites have undergone a long and complex history of fluid movement and alteration, similar to other REE deposits.

Acknowledgements

The author wishes to acknowledge Dr. N.M. Halden of the University of Manitoba, for his help, boundless enthusiasm and encouragement in finishing this project. This thesis is a tribute to the tireless patience and love of my husband Glen, without whom I would still be writing page one.

Thanks are due to the following technical staff and students at the University of Manitoba for their help: Ron Chapman (EMPA), Neil Ball (XRF), Sergio Mejia (IBAS), Irene Berta (thin sections) and Mark Cooper (for identifying unknowns). Thanks also to Bill Teesdale of the University of Guelph (PIXE). And finally, thanks to the gang for their helpful discussions on all aspects of geology.

Funding for this project was provided by an NSERC Research Grant to N. M. Halden and an NSERC Scholarship to K. M. Arden.

Table of Contents

List of Figures

List of Tables

Chapter 1: Introduction

The Eden Lake syenite complex is located approximately halfway between the towns of Leaf Rapids and Lynn Lake in northern Manitoba, about 1000 km north of Winnipeg (Figure 1.1). The Eden Lake area is accessible from Provincial Highway 391; the main outcrops of the syenite complex are accessible from Eden Lake, approximately 6.5 km by boat south from the highway.

At its present level of erosion, the Eden Lake syenite complex covers an area of 15 square km. It is located in the western part of the Leaf Rapids domain, which is itself part of the Trans Hudson orogenic terrane. The intrusion was informally termed a syenite based on field data, but modal analysis indicates that it is, in fact, a monzonite to quartz monzonite body; however, it will be referred to as a syenite complex for traditional reasons in agreement with existent literature (eg. McRitchie, 1988; 1989; Fedikow et al., 1993; 1994; Halden and Fryer, submitted). The syenite complex is composed of two main intrusive phases, a mafic monzonite and a felsic monzonite. In addition, there are several late pegmatite phases, which are the focus of this thesis. The complex is exposed in three topographically high, north-south, linear ridges on a peninsula on the eastern side of Eden Lake (Figure 1.2); exposure of the Eden Lake syenite complex on the ridge tops is generally good, although moss and lichen growth are prevalent in low lying areas. Shoreline outcrops are very limited, but a few locations on the shores of Kwaskwaypichikun Bay have relatively good exposure.

Previous studies have focussed on the field relations of the Eden Lake syenite

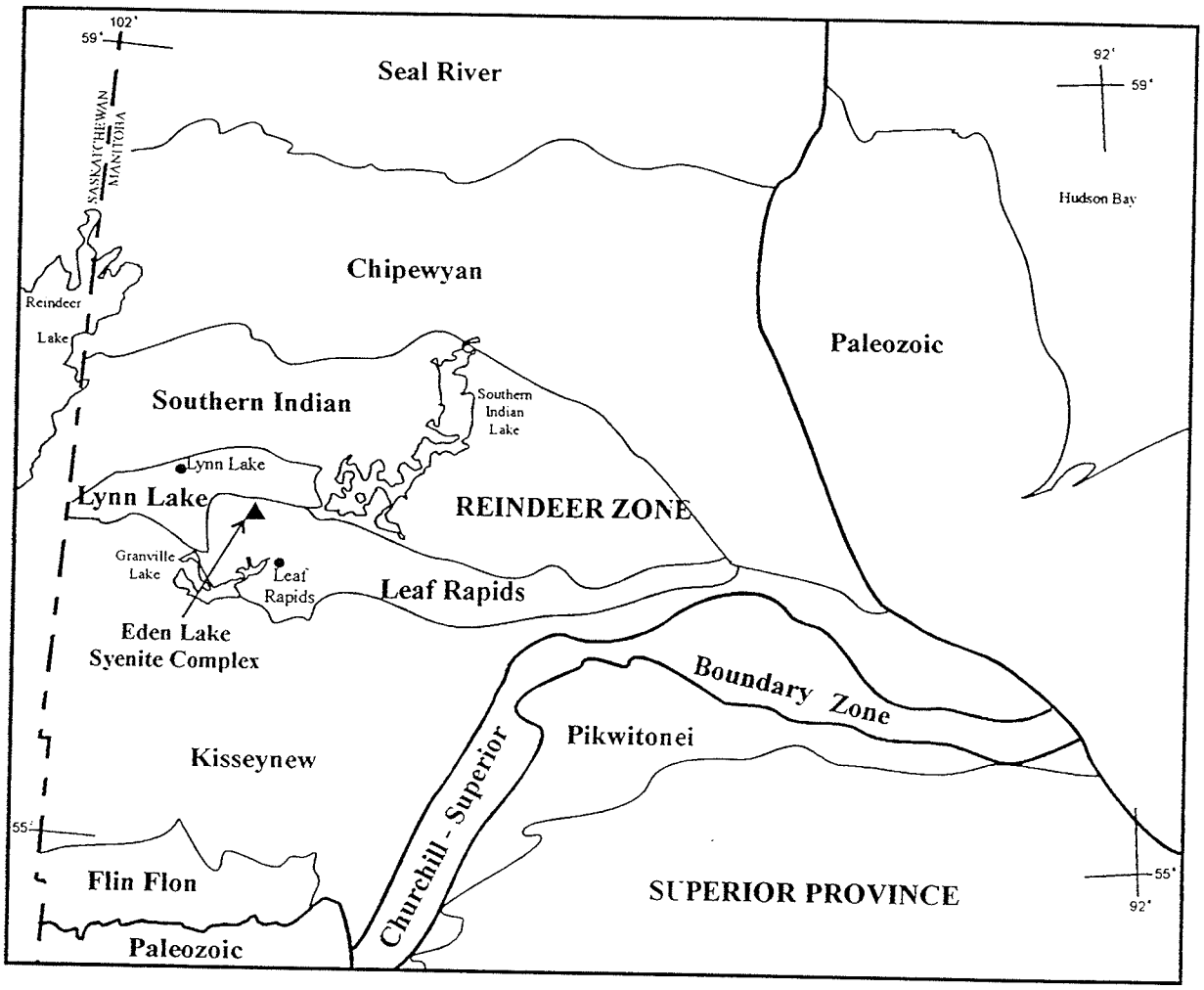

Figure 1.1. Map of part of the Reindeer Zone of the Trans Hudson Orogenic terrane and the adjacent Superior Province in northern Manitoba, showing the principle geological domains and the location of the Eden Lake syenite complex, marked with ▲ (after Zwanzig et al., 1985).

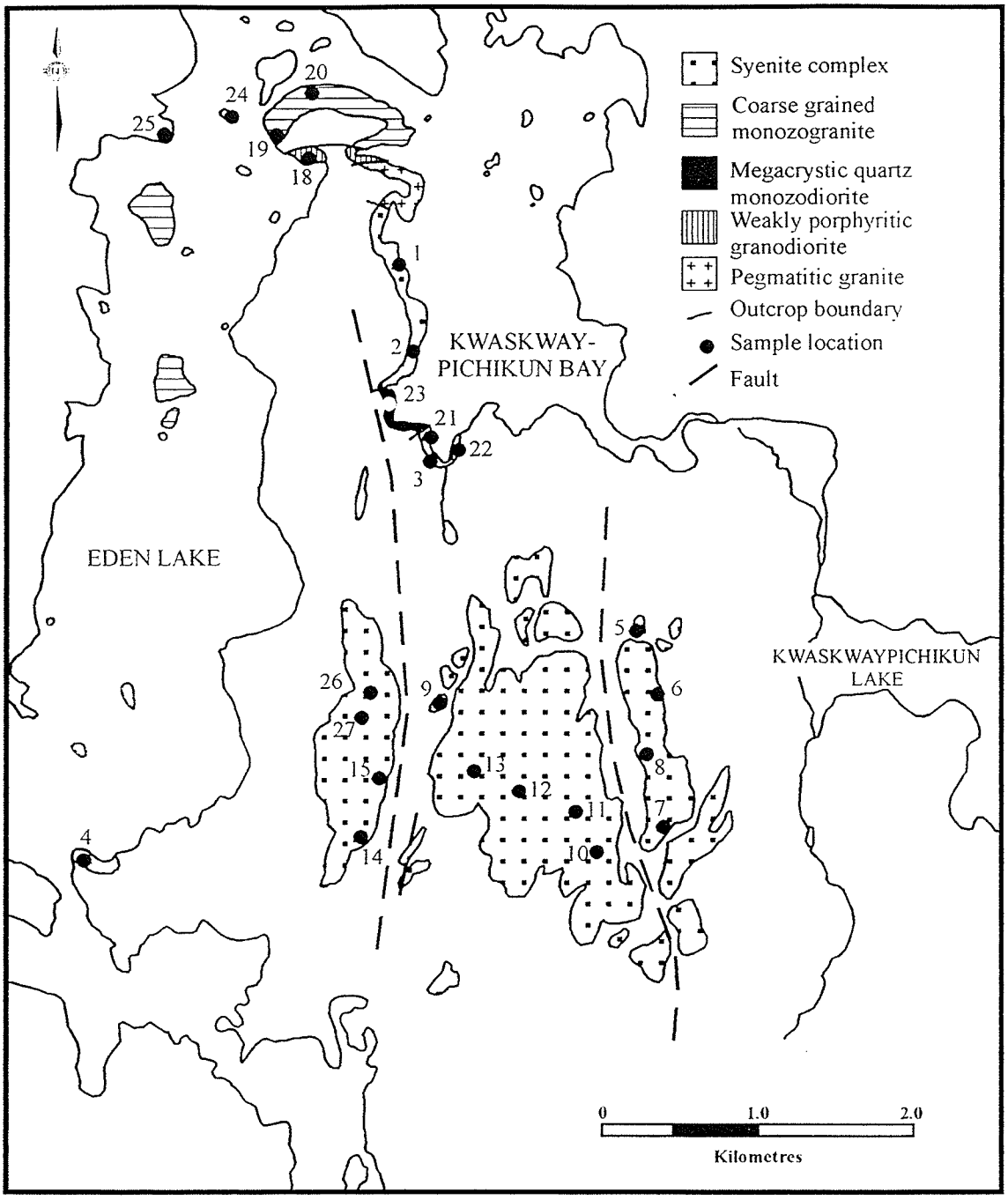

Figure 1.2. Detailed geological map of the Eden Lake syenite complex and the surrounding country rocks (after McRitchie, 1988). Numbered sample locations are shown by ●.

complex to the other rocks of the Eden Lake region (Cameron, 1978; 1988) as well as on some petrologic aspects of the syenite complex itself (McRitchie, 1988; 1989). The geochemical evolution of the main syenite phases has been described by Halden and Fryer (submitted) and other work has shown that the complex is associated with uranium, thorium and potassium anomalies; field work has established that zones with high levels of radioactivity are associated with some of the pegmatite phases (McRitchie, 1988; 1989). Many of the pegmatites are also characterized by high rare earth element (REE) contents and the presence of accessory rare-element minerals, such as fluorite, titanite, apatite, zircon, britholite and allanite.

Intrusive complexes with alkaline or A-type affinities are not uncommon in the Trans Hudson orogen; examples occur at Burntwood Lake, Brezden Lake and McVeigh Lake (McRitchie, 1988). Each of these intrusions contains multiphase intrusive assemblages indicating a complex and extended intrusive history, with an early alkaline phase (McRitchie, 1988). These intrusions represent a late, compositionally distinct magmatic event in the Trans Hudson orogen that postdates major orogenic activity by 10 Ma (Halden and Fryer, submitted). Of all the alkaline intrusions in Manitoba, the Eden Lake syenite complex shows the most exotic mineralogy, hosted within the pegmatite phases, and perhaps the best potential for economic development. A REE-Th deposit with a similar mineralization has been the focus of exploration activity at Rodeo de Los Molles, in Argentina (Lira and Ripley, 1992).

1.1 Previous Work

The Eden Lake area was first investigated by Henderson et al. (1936) during reconnaissance mapping of the Granville Province. They identified a number of granitic intrusive phases, some of which contained rafts of gneissic and volcanic rocks. The first map of the Eden Lake area, at a scale of one inch to four miles, was published in 1936 as part of the east half of the Granville Lake Sheet (Henderson et al., 1936).

Much regional-scale mapping has been done by the Manitoba Department of Energy and Mines. Zwanzig (1974) conducted reconnaissance traverses from Highway 391 and from the shores of Eden Lake. He identified a number of foliated and porphyritic granitoid intrusions, ranging in composition from tonalite to quartz monzonite. McRitchie (1976) began preliminary examinations of granitic rocks in the Outlaw Bay region, to the southeast of Eden Lake. Cameron (1978) mapped the Eden Lake area at a scale of 1:50 000; he found that most of the region was underlain by granitoid intrusions with minor supracrustal rafts. He mapped more than 18 intrusive complexes that ranged in composition from gabbro/diorite to monzogranite (Cameron, 1988). Lenton (1982) examined granitic, two feldspar-biotite-quartz pegmatites associated with granodiorites in the south part of Eden Lake.

The Federal/Provincial Uranium Reconnaissance Program (Geological Survey of Canada, 1977) identified uranium, thorium and potassium anomalies in the Eden Lake area during an airborne gamma-ray spectrometer survey in 1977. These anomalies are concentrated over the syenite complex and monzonites to the east of Eden Lake. Cameron (1988) suggested that the anomalies may be related in part to late local potassium metasomatism that resulted in lenticular microcline megacrysts in a fine- to medium-grained

granitic groundmass within the monzonites. Anomalously high uranium and fluorine contents have also been detected in the water of Eden Lake (Schmitt et al., 1989).

McRitchie (1988) conducted a detailed study of the Eden Lake syenite complex as part of a study of syenitic alkaline intrusions within the Lynn Lake Belt of the Churchill Province. He summarized the major geological characteristics of the complex and documented the occurrence of elevated REE concentrations in pyroxene-enriched pegmatites (McRitchie, 1988). Field work, using a ground scintillometer, showed that some of the anomalously high radioactive measurements associated with the syenite complex were related to pegmatite patches and veins (McRitchie, 1989).

A detailed study of the geochemical characteristics of the Eden Lake syenite complex was undertaken by Halden and Fryer (submitted) in order to constrain the origin of the complex. They concluded that (1) the Eden Lake syenite complex is an alkaline intrusion with elevated REE and fluorine contents that are associated with REE-enriched pegmatites; (2) the complex was derived from a LREE-enriched source; (3) the source was mafic in composition, probably the upper mantle; and (4) crystal fractionation was important for the chemical evolution of the complex, but physical segregation of an F-enriched vapour phase may account for the LREE-enriched pegmatites (Halden and Fryer, submitted).

Fedikow et al. (1993; 1994) began geochemical and radiometric studies of vegetation near the occurrence of a highly radioactive pegmatite vein. Tree twigs and bark were analyzed for rare earth and trace elements in order to assess the potential for using vegetation samples as a medium to locate rare earth element mineralization (Fedikow et al., 1993). The results indicate that the LREE concentrations in alder twigs can be used to delineate the occurrences

of some of the REE-enriched pegmatites associated with the complex (Fedikow et al., 1994).

This study is the first detailed mineralogical description of pegmatites associated with the Eden Lake syenite complex. The objectives are to: (1) characterize the mineralogy of the pegmatite phases associated with the intrusive complex; (2) determine the relationship of the pegmatites with the rest of the syenite complex; (3) characterize the distribution of the REEs and other trace elements such as fluorine, uranium and thorium within the pegmatites; and (4) characterize the alteration events that affected the pegmatites after crystallization. The paragenesis of the pegmatites was examined through field and petrographic studies, as well as detailed chemical analyses of the minerals within the pegmatites.

Chapter 2: Regional Geology

2.1 General Geology

The Eden Lake syenite complex is located in northern Manitoba, within the juvenile Reindeer Zone of the Trans Hudson Orogeny (Figure 1.1). It is a non-foliated to slightly foliated post-orogenic intrusive complex with alkaline characteristics, and it intrudes granitic rocks of the Leaf Rapids domain.

The Trans Hudson orogenic terrane is the largest early Proterozoic orogenic belt on the earth (Meyer et al., 1992); it extends for 5000 km from the north central United States through the Canadian Churchill Province and into Greenland and Labrador (Figure 2.1; Lewry and Collerson, 1990). It is 350 km wide, bounded on the east by the Archean Superior Province and on the west by the Archean Hearne Province (Hoffman, 1988).

The Trans Hudson orogen resulted from collisional and accretionary events between the Superior and Hearne provinces; this collisional event occurred between 1850-1830 Ma (Hoffman, 1988). The sedimentary, structural, metamorphic and magmatic asymmetry of the Trans Hudson terrane suggest that subduction of oceanic lithosphere occurred during collision (Hoffman, 1988). The Trans Hudson orogenic terrane contains foredeep basins, thrust and fold belts and sparse mafic magmatism with low metamorphic grades in the forelands, as well as high metamorphic grades, calc-alkaline magmatic belts and ductile deformation patterns in the hinterlands (Hoffman, 1988). This assemblage is typical of Early Proterozoic mobile belts, including the Thelon and Wopmay orogens in northern Canada (Hoffman, 1988).

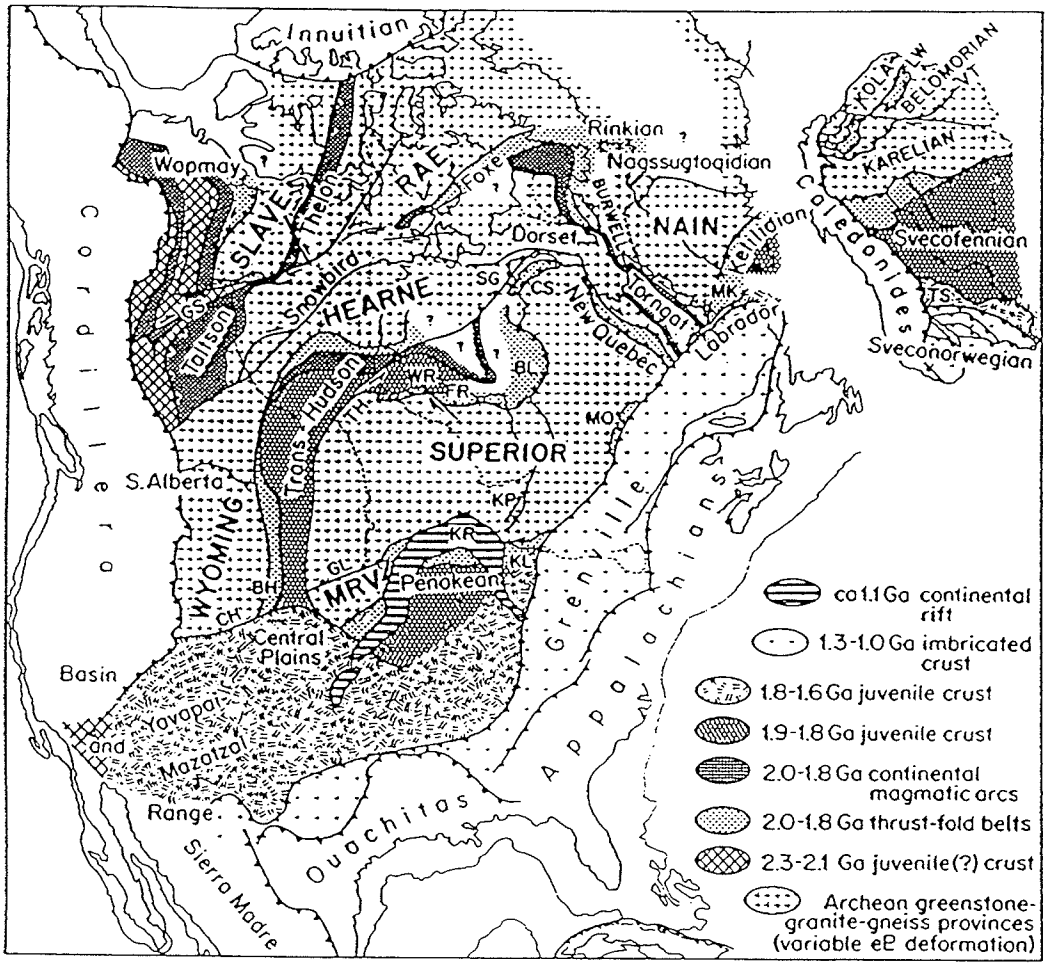

Figure 2.1. Precambrian tectonic elements in North America. Note the large extent of the Trans Hudson orogenic terrane from the south central United States to northern Labrador/P.Q. Abbreviations: BH, Black Hills inlier; BL, Belcher belt; CH, Cheyenne belt; CS, Cape Smith belt; FG, Fox River Belt; GL, Great Lakes tectonic zone; GS, Great Slave Lake shear zone; KL, Killarney magmatic zone; KP, Kapuskasing uplift; KR, Keweenawan rift zone; LW, Lapland-White Sea tectonic zone; MK, Makkovik orogen; MO, Mistassini-Otish basins; MRV, Minnesota River Valley terrane; SG, Sugluk terrane; TH, Thompson belt; TS, Transscandinavian magmatic zone; VT, Vetrenny tectonic zone; WR, Winisk River fault (after Hoffman, 1988).

The Reindeer Lake Zone comprises part of the Thelon Segment of the Trans Hudson orogen (Figure 2.2; Syme, 1990). It consists of a number of intra-oceanic domains that are bounded by ensialic belts (Stauffer, 1984; Syme, 1990). The ensialic belts comprise basal rift valleys overlain by post rift shelf strata (Hoffman, 1988). The ensialic belt rocks are unconformably overlain by foredeep sediments and volcanic rocks that record the transition from continental to oceanic crust (Van Schmus et al., 1987; Hoffman, 1988; Meyer et al., 1992). These structurally dismembered, submarine, mafic through felsic, metavolcanic rocks have island-arc characteristics (Van Schmus et al., 1987; Hoffman, 1988; Meyer et al., 1992). Intrusive rocks comprising synvolcanic gabbro/diorite and tonalite sheets commonly intrude the island-arc volcanic rocks (Hoffman, 1988). Sedimentary rocks are intercalated with, and unconformably overlie, the volcanic piles (Hoffman, 1988; Syme, 1990). Most of the granitic and related magmatism in the Trans Hudson orogen is related to supra-subduction cordilleran and volcanic magmatic arcs, with the peak of activity at 1840-1870 Ma (Halden et al., 1990; Halden and Fryer, submitted). However, there are several plutons with younger ages, including the Burntwood syenite at 1830 Ma (Gordon et al., 1990) and the Thorsteinson batholith at 1710 Ma (Halden et al., 1990), which define an anorogenic magmatic pulse that began a minimum of 10 Ma after the main calc-alkaline magmatic activity (Halden and Fryer, submitted).

The Leaf Rapids domain comprises Precambrian metavolcanic and metasedimentary belts that are separated by younger tonalitic, granitic and minor mafic intrusions (Zwanzig, 1974). The Eden Lake area is bordered to the east by the Rusty Lake

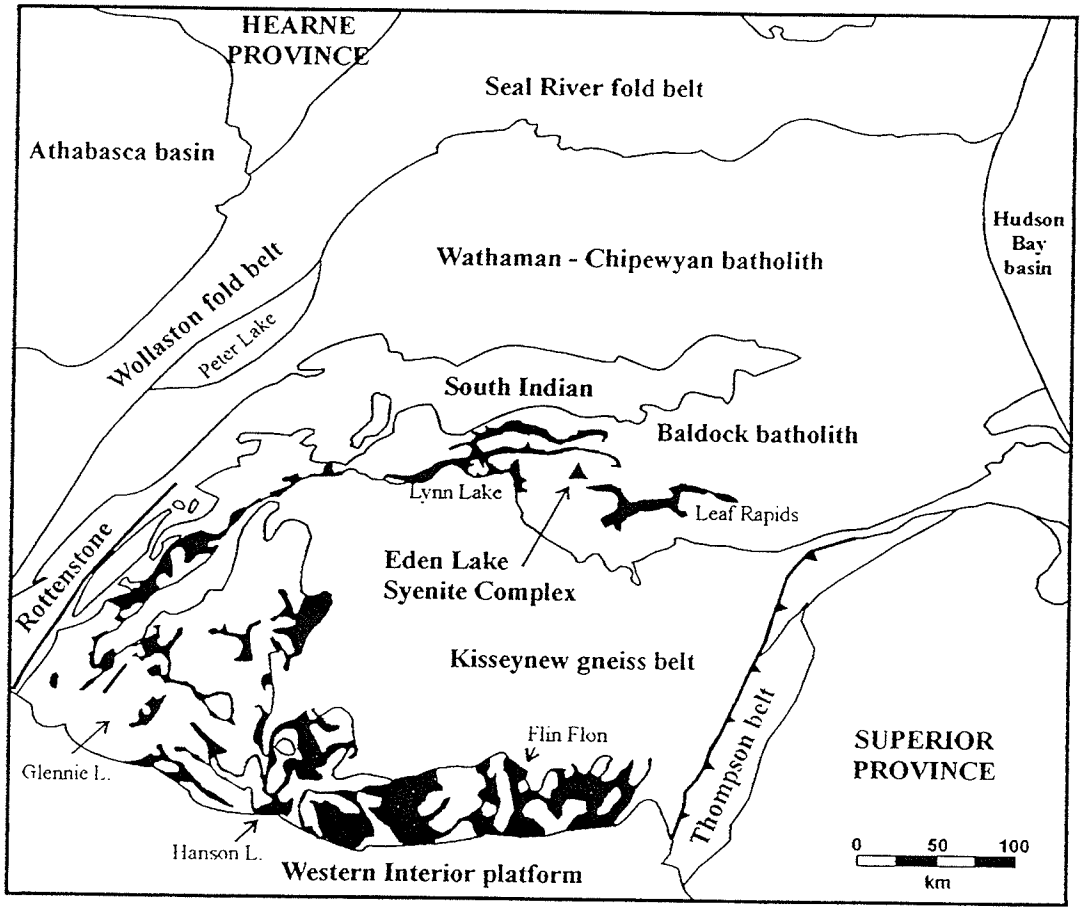

Figure 2.2. Tectonic domains of the Trans Hudson orogen in northern Manitoba and Saskatchewan. Volcanic belts are shown in black; the Eden Lake syenite complex is marked with ▲ (after Hoffman, 1988).

greenstone belt, to the north by the Lynn Lake greenstone belt and to the west and south by the Kisseynew metasedimentary belt (Figure 2.2).

The Rusty Lake greenstone belt comprises metamorphosed volcanic and sedimentary rocks as well as subvolcanic plutons (Baldwin, 1988). Three major faults divide the belt into four blocks; the lithologies across the blocks are not consistent and therefore a regional stratigraphy cannot be determined (Baldwin, 1988).

The Lynn Lake greenstone belt is 35 Ma older than the Rusty Lake belt (Baldwin et al., 1987); they are separated by 10 km of older plutonic orthogneisses (Baldwin, 1988) into which the Eden Lake syenite complex was intruded (Figure 2.2). A regional stratigraphy for the Lynn Lake belt has been established (Syme, 1990). The older Wasekwan Group consists of a mafic platform of tholeiitic and magnesian calc-alkaline basalts, overlain by felsic complexes and an andesitic calc-alkaline suite (Syme, 1990). In places, tholeiitic basalts overlie the felsic complexes. The Sickle Group unconformably overlies the Wasekwan Group; it comprises alluvial sandstones and conglomerates (Syme, 1990).

The Kisseynew gneiss belt consists of both metasedimentary and meta-igneous rocks (Zwanzig, 1990). A general stratigraphy of the belt, from oldest to youngest, is: (1) fine-grained amphibolite and felsic gneisses; (2) Sherridon gneisses, quartz-rich with an uncertain origin; (3) Burntwood Suite, metamorphosed greywacke-mudstone turbidites; (4) Sickle Suite, metamorphosed alluvial sandstones and conglomerates; and (5) Missi Suite, sedimentary gneisses and metavolcanic rocks (Zwanzig, 1990).

2.2 Geology of the Eden Lake area.

The Eden Lake syenite complex is located at the western end of the Leaf Rapids belt (Zwanzig et al., 1985). The geology of the Eden Lake region is dominated by granitoid intrusive rocks, although a few occurrences of supracrustal rocks have been documented (Figure 2.3).

The supracrustal rocks comprise metavolcanic and metasedimentary rocks; these occur only as rafts and discontinuous screens in the vicinity of Eden Lake (Figure 2.3). The metavolcanic rocks consist of sheared mafic to intermediate flows and flow breccias with some dacitic tuff interlayers, as well as rafts of basalt flows and flow breccia mixed with tuffs, iron formation, greywacke and arkose. The metasediments consist of psammitic greywacke, amphibolite, iron formation, arkosic gneiss and grey biotite gneiss of unknown affinity (Figure 2.3; Cameron, 1988). Metamorphism has destroyed many of the primary textures of these supracrustal rocks (Cameron, 1988).

Intrusive complexes in the Eden Lake area range in composition from diorite/gabbro to quartz diorite to tonalite to granodiorite (Figure 2.4). The complexes are of varying ages and many of the intrusions have multistage intrusive histories (Table 2.1; Cameron, 1988).

The oldest intrusive rocks in the Eden Lake region comprise an early quartz diorite suite that ranges in composition from diorite/gabbro to quartz monzodiorite (Figure 2.4; Table 2.1; Cameron, 1988). These intrusions are scattered throughout the region and range in size from small xenoliths in younger rocks to large "inclusions" up to 10 km^2 in area (Cameron, 1988). These rocks are highly foliated and altered.

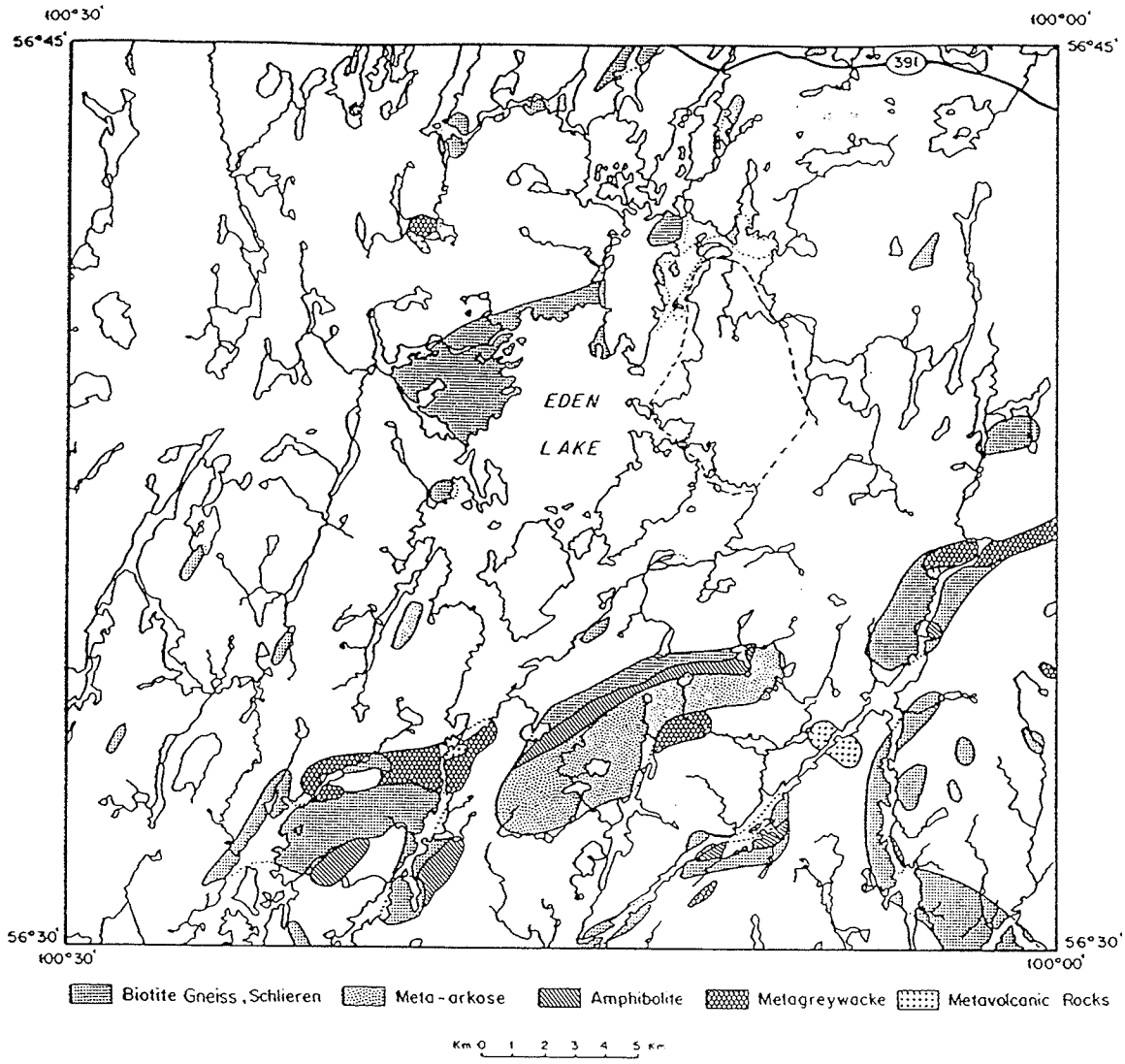

Figure 2.3. Distribution of rafts and inclusions of supracrustal rocks in the Eden Lake area (from Cameron, 1988). The Eden Lake syenite complex is outlined with a dashed line.

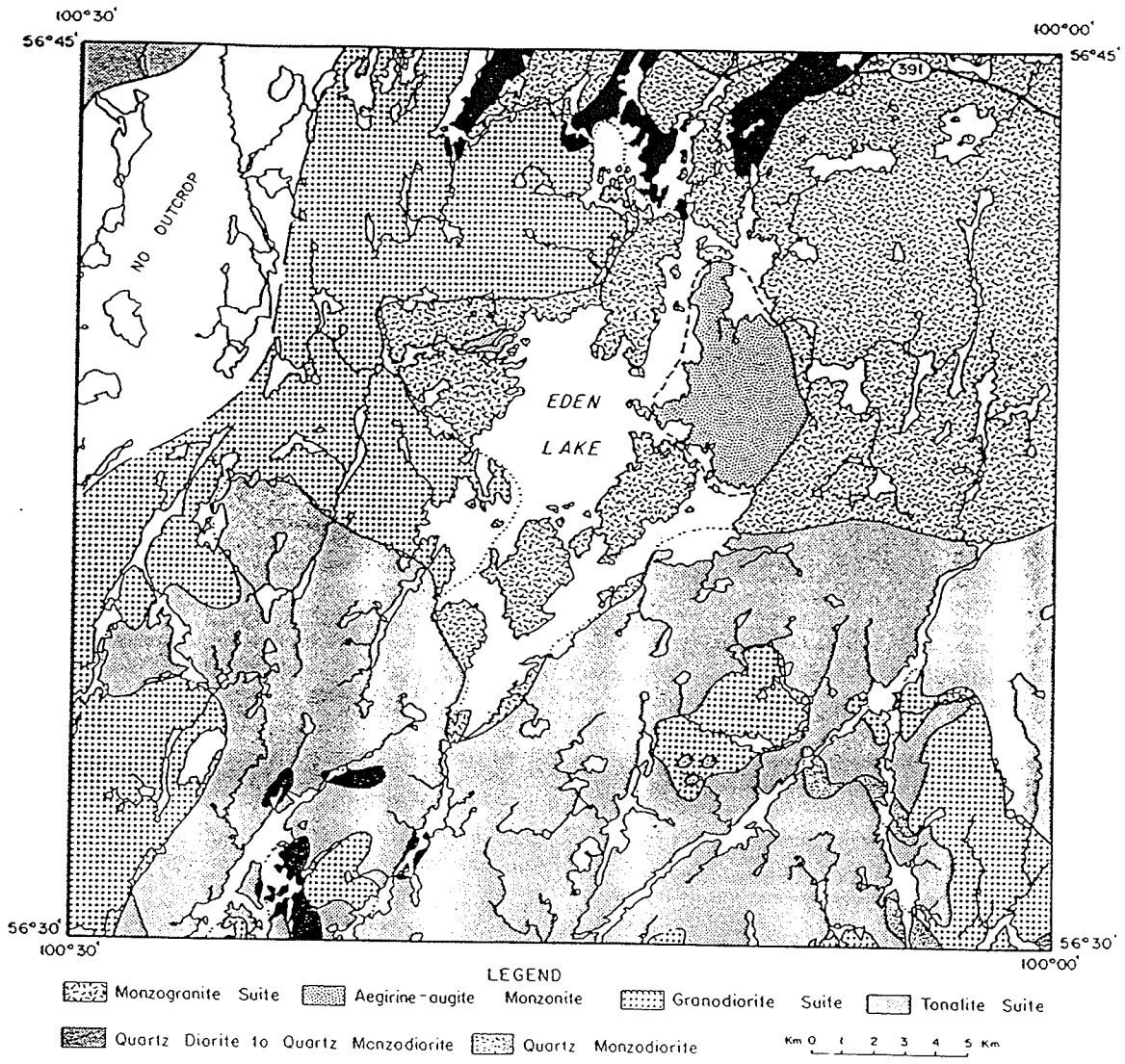

Figure 2.4. Distribution of the major intrusive suites in the Eden Lake area (from Cameron, 1988). The Eden Lake syenite complex is outlined with a dashed line.

Table 2.1. Geological formations exposed in the Eden Lake area (from Cameron, 1988).

Pleistocene and Recent		Sand, gravel, clay and till deposits
		UNCONFORMITY
PRECAMBRIAN (EARLY PROTEROZOIC)	INTRUSIVE AND METAMORPHIC ROCKS	19 Pegmatite, pegmatitic granite, graphic granite, aplite 18 Coarse grained monzogranite 17 Fine grained biotite monzogranite, aplitic granite; (17a) fine grained, weakly porphyritic monzogranite 16 Megacrystic monzogranite 15 Muscovite granodiorite 14 Fine- to medium-grained, weakly porphyritic granodiorite 13 Fine grained, aegirine-augite-bearing monzonite 12 Megacrystic granodiorite (to quartz monzodiorite) 11 Seriate to megacrystic granodiorite; (11a) sheared, epidote-bearing megacrystic granodiorite; (11b) coarse grained, weakly porphyritic granodiorite 10 Granodiorite to tonalite 9 Granodiorite to granite 8 Biotite granodiorite ± hornblende; (8a) porphyroblastic granodiorite 7 Biotite tonalite ± hornblende; (7a) porphyroblastic tonalite 6 Coarse grained to megacrystic quartz diorite; (6a) megacrystic quartz monzodiorite 5 Quartz monzodiorite, highly tectonized 4 Diorite, gabbro; (4a) feldspar cumulophyric metagabbro; (4b) coarse grained gabbro, ultramafic rock; (4c) quartz diorite
		INTRUSIVE CONTACT
	METASEDIMENTARY AND METAVOLCANIC ROCKS OF UNCERTAIN AGE	3 Paragneiss of unknown affinity, grey biotite gneiss, schlieren (subordinate lithology not occurring as map unit.) 2 Metasedimentary rocks; (2a) psammitic metagreywacke ± garnet; (2b) amphibolite, fine grained, layered; (2c) iron formation; (2d) arkosic gneiss ± hornblende ± magnetite 1 Metavolcanic rocks; (1a) mafic volcanic rocks, basalt flows and flow breccia; (1b) felsic volcanic rocks, dacite, dacitic tuff

The tonalite suite is the second oldest suite of intrusive rocks in the Eden Lake area (Figure 2.4); it comprises both biotite tonalite and biotite granodiorite (Table 2.1). These massive to weakly foliated plutons dominate to the south and east of the Eden Lake syenite complex (Figure 2.4). In general, contacts between the tonalite and granodiorite are gradational and are defined only in terms of chemistry (Cameron, 1988).

The granodiorite suite is the third oldest suite (Figure 2.4; Table 2.1). It consists of massive to well foliated, coarse grained to megacrystic granodiorites that outcrop to the south and west-southwest of Eden Lake. These rocks intrude the older tonalite suite and contain rafts of both the tonalite suite and supracrustal rocks; (Cameron, 1988).

The Eden Lake syenite complex is the second youngest intrusion in the Eden Lake area (Table 2.1) and will be discussed in detail in Chapter 4. The youngest group of intrusive rocks is a monzogranite suite that surrounds both the syenite complex and Eden Lake (Table 2.1; Figure 2.4). The monzogranite forms a zoned complex with textures ranging from aplitic to megacrystic; it is massive to non-foliated and is associated with pegmatites and pegmatitic granites (Cameron, 1988). Rafts of the quartz diorite, tonalite and granodiorite suites as well as supracrustal rocks are present within some of the monzogranite plutons.

Chapter 3: Research Methods

3.1 Field work

Field work at Eden Lake was done during the summer of 1993; the principle focus of the work was to establish the relationships between the intrusive complex and the surrounding country rocks; between the intrusive phases within the syenite; between the complex and associated pegmatites and between the different pegmatites. A sample suite, comprising 24 stations and 63 samples, was collected. The sample locations were based partially on previous work (Cameron, 1988; McRitchie, 1988; 1989) and partially on field observations; the locations of the stations are shown on Figure 1.2. Sampling of the radioactive pegmatites was based on the earlier work done by McRitchie (1988; 1989); radioactive anomalies were used as a general guide. In addition, pegmatites with no reported radioactivity were sampled from various sites throughout the syenite complex.

The bulk of the sample suite (49 samples) was obtained from the aegirine-augite quartz monzonite to monzonite and associated pegmatites (Table 3.1). Of the remaining samples, two were taken from the quartz monzodiorite to the north of the Eden Lake syenite complex (Figure 1.2; Table 3.1), eight from the porphyritic granodiorite to the north (Figure 1.2; Table 3.1) and four from the monzogranite to the north (Figure 1.2; Table 3.1); these include both representative "whole rock" and pegmatite samples.

3.2. Laboratory analysis

Fifty-four polished thin sections and twenty-five polished mineral mounts were

Table 3.1. List of station locations, sample numbers and lithologies. Station locations are shown on Figure 2.1.

Station number	Sample number	Lithology
KA-93-1	1A	Felsic monzonite unit
	1B	Felsic monzonite unit
	1C	Felsic monzonite unit
KA-93-2	2	Pegmatite Type I
KA-93-3	3A	Felsic monzonite unit
	3B	Pegmatite Type II
	3C	Pegmatite Type III
	3D	Mafic monzonite unit
	3E	Mafic monzonite unit
	3F	Mafic monzonite unit
	3G	Mafic monzonite unit
	3H	Mafic monzonite unit
KA-93-4	4	Pegmatite Type III
KA-93-5	5A	Pegmatite Type III
	5B	Pegmatite Type III
KA-93-6	6A	Pegmatite Type IV
KA-93-7	7A	Mafic & felsic monzonite unit
	7B	Mafic monzonite unit
	7C	Pegmatite Type III
	7D	Pegmatite Type III
	7E	Pegmatite Type III
	7F	Felsic syenite unit
	7G	Pegmatite Type I
	7H	Pegmatite Type I
KA-93-8	8A	Pegmatite Type III
	8B	Pegmatite Type III
KA-93-10	10A	Felsic monzonite unit
	10B	Pegmatite Type III
	10C	Pegmatite Type III
	10D	Pegmatite Type III
KA-93-11	11A	Pegmatite Type III
	11B	Pegmatite Type III
KA-93-12	12A	Pegmatite Type II
KA-93-13	13A	Pegmatite Type II
KA-93-14	14A	Pegmatite Type III
KA-93-15	15A	Mafic monzonite unit
	15B	Pegmatite Type III

Table 3.1 continued.

KA-93-18	18A 18B	Porphyritic granodiorite Pegmatite from granodiorite
KA-93-19	19A 19B 19C 19D 19E 19F	Porphyritic granodiorite Monzogranite Pegmatite from monzogranite Porphyritic granodiorite Porphyritic granodiorite Porphyritic granodiorite
KA-93-20	20A	Coarse grained monzogranite
KA-93-21	21A 21B	Mafic monzonite unit Pegmatite Type III
KA-93-22	22A 22B	Pegmatite Type III Mafic monzonite unit
KA-93-23	23A 23B	Quartz monzodiorite Pegmatite from monzodiorite
KA-93-24	24A 24B	Monzogranite Monzogranite
KA-93-25	25A	Monzogranite
KA-93-26	26A 26B 26C 26D	Carbonate from ELSC Felsic monzonite unit Carbonate from ELSC Carbonate from ELSC
KA-93-27	27A 27B 27C 27D	Pegmatite Type III Pegmatite Type III Pegmatite Types II and III Pegmatite Type III

prepared for further study. The polished thin sections were examined using a transmitted light microscope; the grains mounts were examined under a reflecting microscope. The textures and minerals present were determined and recorded and sites for chemical analysis of each mineral were selected.

Chemical analysis of the minerals were obtained by several methods. The bulk of the chemical data was obtained using the electron microprobe; several minerals were selected for detailed trace-element analysis using proton induced x-ray emission (PIXE). X-ray diffraction patterns were collected for one mineral (zircon); structural information for one mineral was collected using a precession camera (britholite). Scans of back-scattered electron images of all minerals analyzed were collected by the IBAS image analyzer during EMPA. Water contents in one mineral (britholite) were determined using a moisture meter.

EMPA was done on the Cameca SX50 electron microprobe at the University of Manitoba for apatite, titanite, zircon, britholite, allanite, fluorite, andradite, aegirine-augite, K-feldspar and plagioclase. Major and minor elements (Si, Fe, Al, Na, Ca, Ti, Mn, Mg, Sr, Ba, V, Zr, Hf, K, P, Cl, F) were analyzed with a specimen current of 20 nA, an excitation voltage of 15 KV and a peak count time of 20 seconds. Rare earth and some trace elements (La, Ce, Pr, Nd, Sm, Eu, Gd, Dy, Yb, Lu, Y, Th, U) were analyzed with a specimen current of 40 nA, an excitation voltage of 20 kv and a peak count time of 40 seconds. For apatite, F was analyzed with a specimen current of 40 nA, an excitation voltage of 10 KV and a peak count time of 40 seconds. Standards and spectrometer crystals used are listed in Table 3.2. Overlap corrections were used to resolve the peaks

Table 3.2. Standards and crystals used during microprobe analyses.

Analyte	Line	Crystal	Standard
Si	Kα	TAP	Diopside, Pyrope
Fe	Kα	LIF	Almandine, Fayalite
Al	Kα	TAP	Kyanite, Anorthite, Pyrope
Na	Kα	LIF	Albite
Ca	Kα	PET	Diopside, Anorthite
Ti	Kα	PET	Sphene
K	Kα	PET	Orthoclase
Mn	Kα	LIF	Spessartine
Mg	Kα	TAP	Olivine, Pyrope
Sr	Kα	PET	$SrTiO_3$
Ba	Lα	LIF	Sanidine
V	Kα	LIF	VP_2O_7
Zr	Lα	PET	Zircon
Hf	Mα	TAP	ZrO_2
P	Kα	PET	Monazite
Cl	Kα	PET	Tugtup
F	Kα	TAP	Riebeckite
La	Lα	PET	$LaVO_4$
Ce	Lα	PET	CeO_2
Pr	Lβ	LIF	REE glass
Nd	Lα	LIF	REE glass
Sm	Lβ	LIF	REE glass
Eu	Lα	LIF	REE glass
Gd	Lα	LIF	REE glass
Dy	Lβ	LIF	REE glass
Yb	Lα	LIF	REE glass
Lu	Lβ	LIF	REE glass
Y	Lα	TAP	REE glass
U	Mβ	PET	UO_2
Th	Mα	PET	ThO_2

of the rare earth elements.

Samples of zircon, titanite, apatite, britholite and allanite were selected for detailed trace element analysis using the PIXE at the University of Guelph. Point and line analyses as well as area scans were collected. For all minerals, the proton beam was set to 3 MeV; the beam current was typically about 2.86 nA. For zircon, a 125 μm mylar beam filter was used; for the other minerals, a 106 μm Al filter was used in addition to the 125 μm mylar filter to reduce x-ray counts from major elements in the mineral. For titanite and apatite, data was collected to an accumulated charge of 1.5 μC, for zircon, 0.2-0.5 μC and for britholite and allanite, 2.5 μC. Data was processed using GUPIX (Guelph thin/thick target PIXE program; Maxwell et al., 1989); for titanite, apatite, britholite and allanite, matrix elements were entered from previous EMPA analyses and trace-element abundances were calculated. For zircon, a matrix calculation was performed using the GUPIX software.

Continuous scan X-ray diffraction data from a zircon sample were collected on a Philips automated diffractometer system PW1710, using a PW1050 Bragg-Brentano goniometer equipped with incident- and diffracted-beam Soller slits, 1.0 divergence and anti-scatter slits, a 0.2 mm receiving slit and a curved graphite diffracted-beam monochromator at the University of Manitoba. The normal-focus Cu X-ray tube was operated at 40 KV and 40 nA, using a take-off angle of 6°. The pattern was collected using a step width of 0.010° 2θ, with a counting time of 0.40 sec/step, over a range of $10\text{-}50^{\circ}$ 2θ.

BSE images of all the minerals examined were taken with the electron microprobe; these images were edited and enhanced using the IBAS system at the University of Manitoba. Prints and slides were obtained of these images using a Datagraph computer image recorder

CIR-300 series.

The degree of crystallinity of britholite was determined qualitatively using the Buerger Precession Camera at the University of Manitoba. Experimental conditions were set to 40 KV and 20 nA. Britholite samples were exposed to unfiltered radiation and slowly rotated for ten minutes while photographs were exposed.

Water analysis of five britholite samples was performed on a Mitsubishi Moisture Meter, Model CA-06, at the University of Manitoba. This instrument uses the coulometric Karl Fischer titration method which is based on a quantitative reaction of water with iodine. Samples of the radioactive pegmatites were crushed and the britholite was separated. Five samples were placed in an oven at 110° C for at least 72 hours to remove any external water and then run through the moisture meter.

Chapter 4: Local Geology

4.1 Geology of the Eden Lake syenite complex.

The Eden Lake syenite complex comprises a number of intrusive units with complex inter-relationships and irregular distributions; the relative ages of the various units can be determined from cross-cutting field relationships. The complex was named informally in the field as a syenite (McRitchie, 1988); subsequent modal analysis indicated that it is monzonitic (McRitchie, 1988; Cameron, 1988). However, as mentioned in Chapter 1, the intrusion will be referred to as a syenite complex in keeping with existent literature. An earlier weakly-foliated mafic monzonite and a late non-foliated felsic monzonite are the two dominant intrusive units of the syenite complex. Contacts between the mafic and felsic monzonitic units of the complex are irregular and vary from sharp to gradational over several metres. Several late, coarse-grained pegmatitic units intrude both of the syenite phases; these pegmatites have the same mineralogy, with a few exceptions, as the syenite complex. The syenite complex displays a strong marginal foliation, caused by regional metamorphism (McRitchie, 1988). The contacts between the Eden Lake syenite complex and the country rocks are not observed.

The oldest intrusive unit is a medium grained, homogeneous, equigranular monzonite with a slightly mafic composition. This mafic monzonite contains 15-40% ferromagnesian minerals, dominantly aegirine-augite pyroxene with minor amphibole (hornblende) and magnetite (Table 4.1). The aegirine-augite crystals form clots 1-4 mm in size. In places, 1 to 100 cm thick layers of mafic minerals, comprising aegirine-augite

Table 4.1. Mineralogy of the mafic and felsic monzonite units of the syenite complex; mineral abundance was determined at the outcrop scale.

Minerals	Abundances	
	Mafic monzonite	Felsic monzonite
Aegirine-augite	15-40%	5-15%
Hornblende		
Magnetite		
K-feldspar	15-30%	40-50%
Plagioclase (albite to andesine)	10-25%	20-35%
Quartz	<1-5%	5%
Titanite	<1%	<1%
Apatite	<1%	<1%
Zircon	0%	<1%

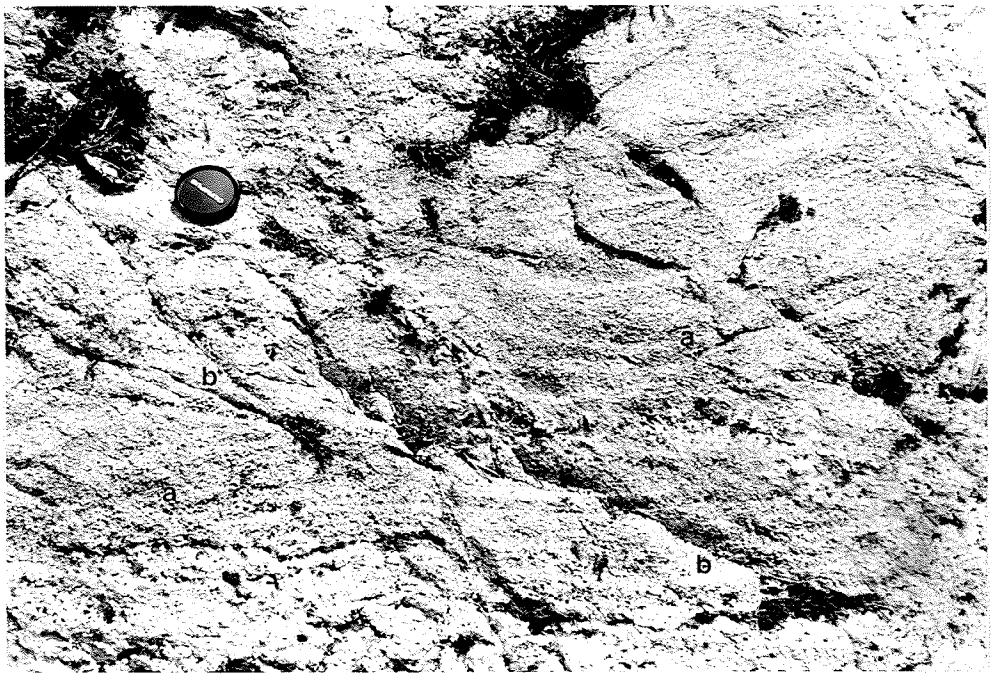

Figure 4.1. Photograph of layers of mafic minerals (aegirine-augite and magnetite) within the mafic monzonite unit of the syenite complex (a). The layers are offset by a Type II pegmatite vein (b). Note darker coloured diorite inclusion (c).

and hornblende, are present (Figure 4.1). Mafic segregations form dyke networks 1-4 cm in length (McRitchie, 1988); in a few locations scattered ferromagnesian schlieren 1-3 cm thick and 30-40 cm long are present (McRitchie, 1988). Pink-weathering K-feldspar and white plagioclase grains constitute the remainder of the mafic monzonite mineralogy; quartz grains are rare (Table 4.1). Accessory minerals comprise titanite and apatite. In massive phases, oikocrystic microcline grains containing inclusions of ferromagnesian minerals have been observed (McRitchie, 1988). Fine-grained amphibolitic or dioritic rafts and schlieren are rare but are locally abundant, especially at the southern end of the western ridge; these form hybridized contamination zones (McRitchie, 1988).

The felsic monzonite contains 5-15% ferromagnesian minerals, comprising aegirine-augite, amphibole and magnetite, as well as pink K-feldspar, white plagioclase and minor quartz (Table 4.1). Accessory minerals comprise zircon, titanite and apatite. Pyroxene megacrysts, ranging in size from 2 to 3 cm, are present in some coarser-grained areas. This unit is also homogeneous and equigranular, but is finer-grained than the mafic monzonite. In places, blocky and angular mafic monzonite inclusions with sharp contacts with the felsic monzonite are present; rare rafts and schlieren of amphibolite or diorite are also observed.

Several faults are associated with the Eden Lake syenite complex (Figure 1.2). North-south faults are inferred to exist between the three north-south outcrop ridges due to the presence of vertical cliff faces at the ridge edges (McRitchie, 1988) and field observations of horizontal slickensides on the cliff faces. In addition, several north- and west-trending fractures are exposed on the outcrop ridges (Figure 1.2). These are 30 cm to 1.5 m long with splayed terminations and are recessively weathered, rusty coloured and contain pyrite and

magnetite as well as fluorite (McRitchie, 1989; Fedikow et al., 1993). Narrow, 1 mm to 20 cm, vertical, north trending cataclastic zones, exposed in the centre of the complex, contain finely ground quartz and cryptocrystalline crushed granite (McRitchie, 1988). An extensive subhorizontal, 20 cm thick, recessively-weathered fault zone with intensely microbrecciated granite suggests that the intrusion may in large part be structurally bound and allochthonous (McRitchie, 1988). This zone is exposed for 50 m in a 15 m high vertical face in the south-east part of the syenite complex (Figure 1.2; McRitchie, 1988).

4.2. Pegmatites associated with the syenite complex.

There are four pegmatite units associated with the Eden Lake syenite complex, characterized on the basis of mineralogy. These include mafic pegmatites, two types of granitic pegmatites and radioactive pegmatites.

4.2.1: Type I: Mafic Pegmatites.

These pegmatite stringers cross-cut both the mafic and felsic monzonite units, and in places, are cut by the Type II pegmatites; all observed contacts are sharp. The stringers are up to 2 m long and 20 cm wide but are discontinuous and commonly pinch out. The stringers contain coarse-grained aegirine-augite up to 2.5 cm long, with hornblende and magnetite as well as K-feldspar and quartz (Figure 4.2).

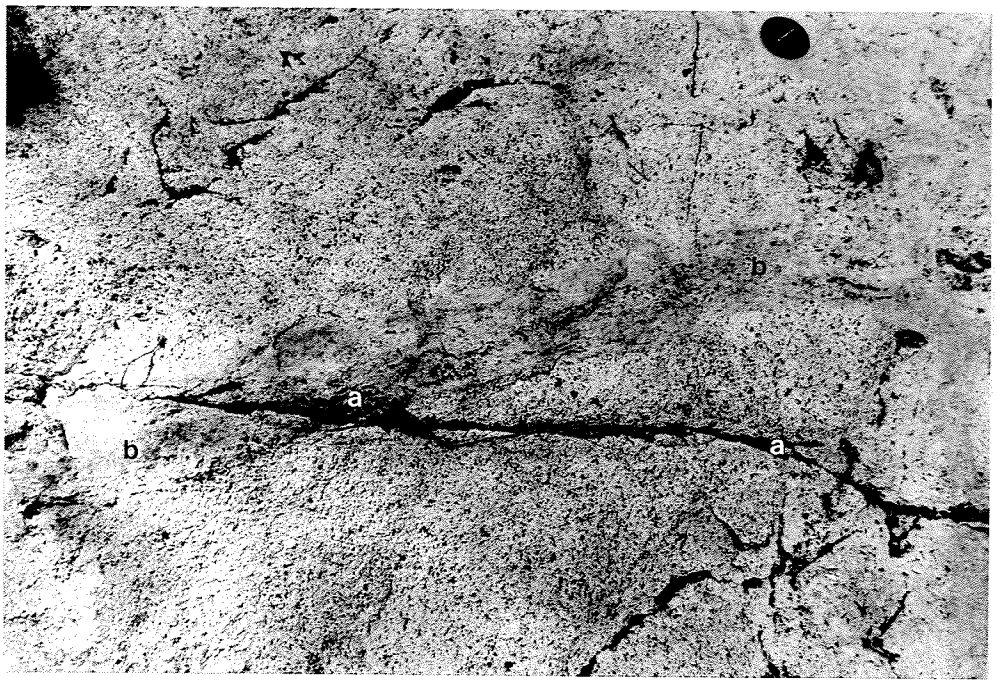

Figure 4.2. Photograph of a Type I mafic pegmatite (a) crosscut by Type II granitic pegmatites (b).

4.2.2: Type II: Granitic pegmatites.

These pegmatites are the second most abundant pegmatitic unit of the syenite complex; they crosscut both the mafic and felsic monzonite units with sharp contacts. Field relations indicate that the Type II pegmatites are younger than the Type I pegmatites, but their ages relative to the Type III and IV pegmatites are unknown. Type II pegmatites occur as patches and veins that range in size from a few cm wide to 50 cm wide; they can commonly be traced across outcrop exposures and have exposed lengths from 10 to 30 m. Type II pegmatites contain blocky quartz and K-feldspar (Figure 4.2), commonly with a graphic intergrowth. Occasionally, albitic plagioclase is present. Some of the veins are zoned, with pink K-feldspar at the margins, buff coloured K-feldspar closer to the centre and blocky quartz in the centre of the vein. The minerals have a variable size range, up to a maximum of 2 cm. Some of these pegmatite veins are associated with a few cm of displacement of linear features such as layering within mafic and felsic monzonite units (Figure 4.1).

4.2.3: Type III: Granitic pegmatites.

These pegmatites are the most abundant type associated with the Eden Lake syenite complex. They comprise irregularly shaped pegmatitic patches that are found in both the mafic and felsic monzonite units, but they predominate in the felsic monzonite. Contacts with the main monzonite units are gradational over a few cm, and the patches range in size from a few cm^2 to 10 m^2. These pegmatites differ from the Type II pegmatites in that in addition to K-feldspar, quartz and plagioclase, they contain aegirine-augite, magnetite, fluorite, zircon, andradite, apatite, titanite, strontianite and burbankite; the abundance of each mineral species

varies between pegmatites (Table 4.2). The grain size within the pegmatites is variable, with a maximum of 3 cm.

4.2.4: Type IV: Radioactive pegmatites.

The Type IV pegmatites are the least abundant of the pegmatite units and are found only on the easternmost outcrop ridge, associated with shear zones. The veins crosscut both the mafic and felsic monzonite units of the complex; contacts are sharp but irregular. These pegmatites are particularly prominent on radiometric maps of the Eden Lake area, due to their radioactive character. In general, the veins are discontinuous with maximum widths from 30 to 40 cm (Figure 4.3). One pegmatite vein was traced 80 m along a shear before it disappeared into the overburden; most veins pinch out after a length of about 10 m. The minerals found in Type IV pegmatites include aegirine-augite, quartz, K-feldspar, plagioclase, magnetite, titanite, britholite, allanite, apatite, fluorite, zircon and weloganite (Table 4.3). The grain size is variable, with a maximum size of 3 cm.

4.3. Geochemical Characteristics of the Eden Lake syenite complex.

The geochemical character of the Eden Lake syenite complex has been described by Halden and Fryer (submitted); this work has highlighted some unusual geochemical characteristics. It is one of several plutons in the Reindeer Zone of the Trans-Hudson Orogen that display alkaline geochemical characteristics; others include the intrusions at

Table 4.2. Abundance of minerals within the Type III granitic pegmatites; abundance determined at the outcrop and thin section scales.

Mineral phase	Abundance
Aegirine-augite	5-25%
K-feldspar Microcline Orthoclase	5-55%
Plagioclase (albite to andesine)	0-30%
Quartz	0-20%
Fluorite	0-5%
Andradite	0-10%
Apatite	0-5%
Zircon	0-2%
Titanite	0-10%
Allanite	0-trace
Thorite	0-trace
Burbankite	0-trace
Strontianite	0-trace

Figure 4.3. Photograph of a Type IV pegmatite vein. The darker areas are concentrations of mainly britholite, allanite and aegirine-augite.

Table 4.3. Mineral abundance in the Type IV radioactive pegmatites; abundance determined at both the outcrop and thin section scale.

Mineral phase	Abundance
Aegirine-augite	5-30%
K-feldspar Microcline Orthoclase	0-30%
Quartz	1-10%
Plagioclase (albite to oligoclase)	0-25%
Fluorite	0-5%
Apatite	0-35%
Zircon	0-trace
Titanite	0-5%
Britholite	0-70%
Allanite	0-20%
Weloganite	0-trace

Brezden, McVeigh and Burntwood Lakes (McRitchie, 1988; Halden and Fryer, submitted).

The Eden Lake syenite complex has many characteristics that support the view that it is an A-type granitoid. These include high Na_2O+K_2O values (11-13 weight %), significant F abundances (200-4000 ppm), relatively constant Y/Nb and Yb/Ta ratios and a characteristic mineral assemblage consisting of magnetite, fluorite, titanite, aegirine-augite, apatite and zircon. The Shand Index for samples from the syenite complex is shown in Figure 4.4; samples plot close to the peralkaline field but would be classified as metaluminous (Halden and Fryer, submitted).

The SiO_2 content of the syenite complex ranges from 57-76 weight percent with a continuous fractionation trend from low to high silica phases (Halden and Fryer, submitted). Major-element trends for CaO, MgO, TiO_2 and $Fe_2O_3^T$ (total iron) show continuous decrease with increasing silica (Figure 4.5); Al_2O_3 and total alkalies increase with increasing SiO_2 until 64 weight% SiO_2, whereupon the abundances decrease (Figure 4.5). These element trends indicate an early fractionating assemblage dominated by a mafic mineral such aegirine-augite; the inflection point suggests that at a later stage, the fractionating assemblage consisted of aegirine-augite and K-feldspar.

The rocks of the Eden Lake syenite complex can be divided into three groups based on trace element characteristics and silica content (Halden and Fryer, submitted): (1) a low silica group (LSG) with SiO_2 contents ranging from 57-62 weight % that has elevated U, P and total REE contents; (2) the main phase syenite (MPS) with 64-71 weight % SiO_2; and (3) a high silica group (HSG) with 71-77 weight % SiO_2, that has

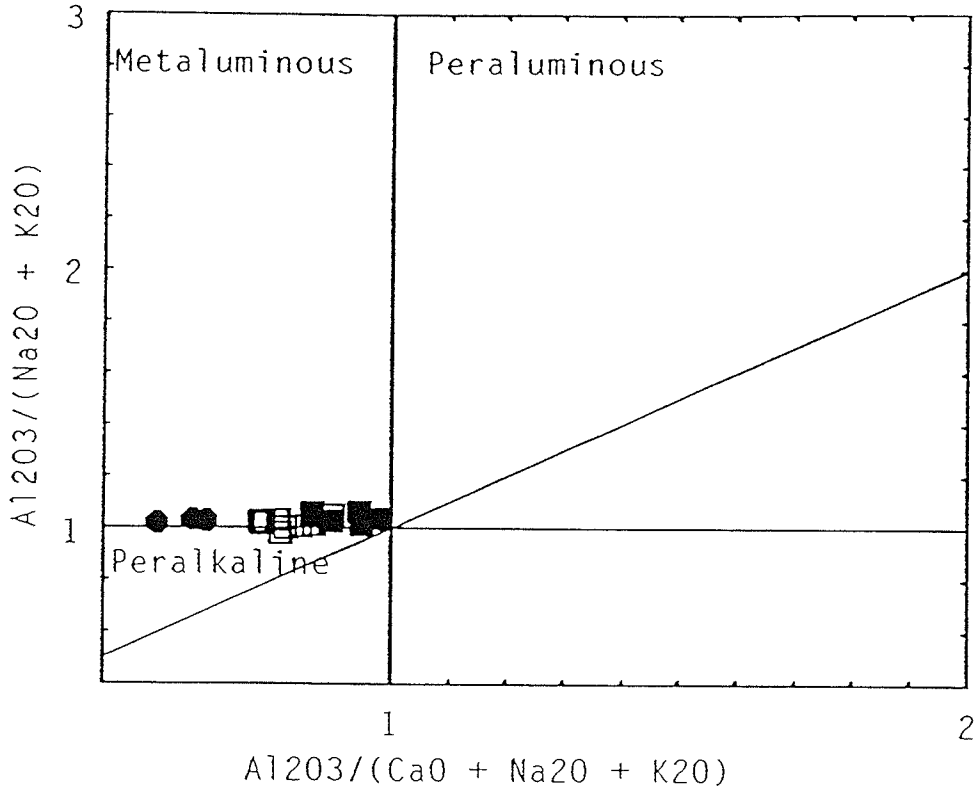

Figure 4.4. Shand Index for samples from the Eden Lake syenite complex (from Halden and Fryer, submitted). Field boundaries and designations after Maniar and Piccoli (1989). Samples from the LSG are shown by ●, samples from the MPS are shown by □ and samples from the HSG are shown by ■.

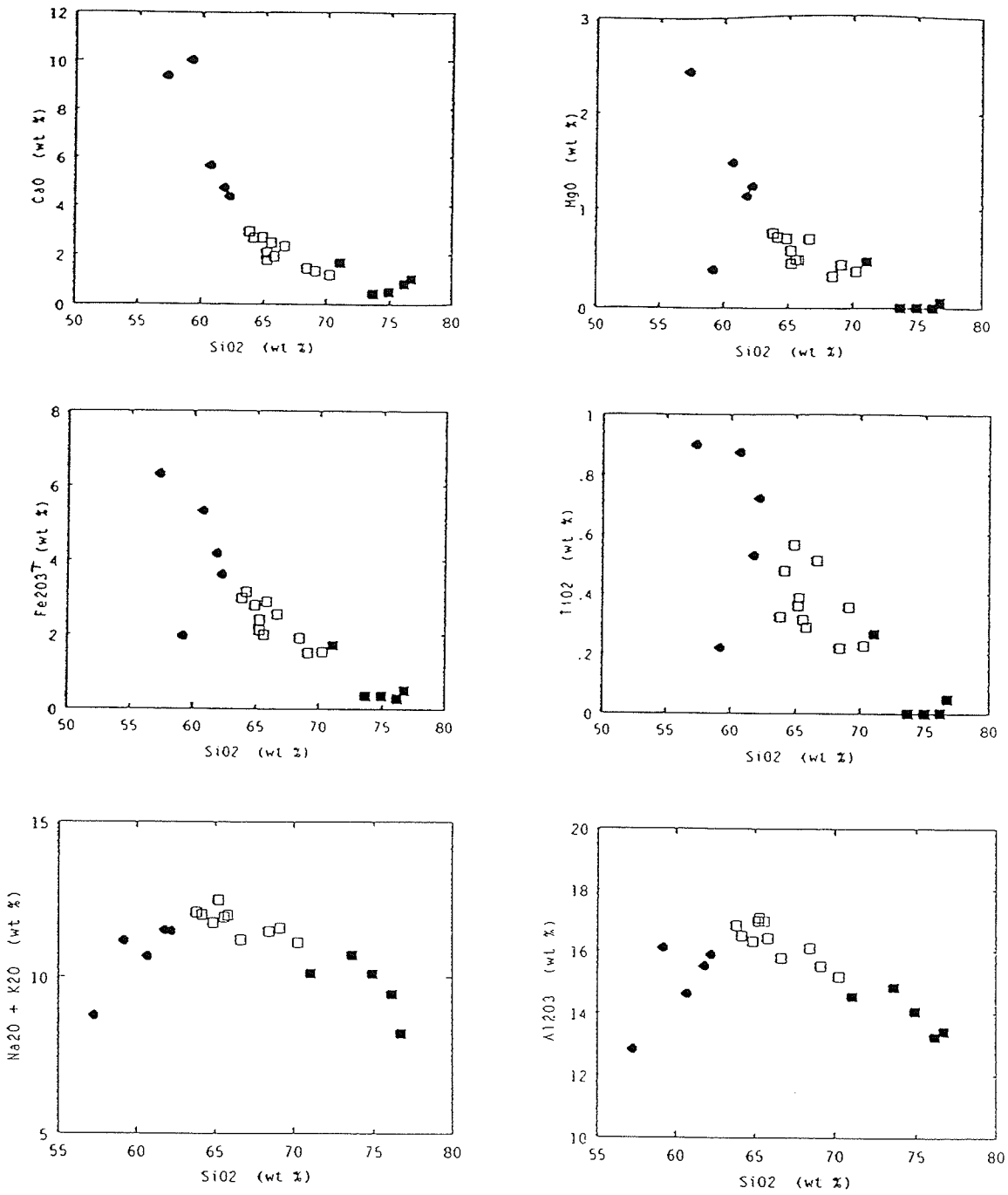

Figure 4.5. Major element plots showing continuous decrease of $Fe_2O_3^T$, CaO, MgO and TiO_2 vs SiO_2, and inflections in the trends of Al_2O_3 and K_2O+Na_2O versus SiO_2 (from Halden and Fryer, submitted). Symbols as in Figure 4.4.

similar trace element patterns as the LSG but with lower trace element and REE abundances.

Chondrite-normalized REE plots for the syenite complex are shown in Figure 4.6; the plots are light REE-enriched and lack europium anomalies. Of importance is the fact that the total REE content decreases with increasing SiO_2 content. This is somewhat unexpected as the main mineral phases dominating major element fractionation (K-feldspar and aegirine-augite) have a bulk distribution coefficient less than one, which would result in incompatibility of the REEs. The early stages of crystal fractionation have also been influenced by the separation of a significant amount of REE-compatible accessory minerals, including titanite and apatite; the result is that the more evolved, silica-rich rocks of the syenite complex tend to be depleted in REEs (Halden and Fryer, submitted). There is a distinct compositional gap between the main phase syenites and the silica-rich rocks where the latter are significantly depleted in REEs; this is inconsistent with a smooth uninterrupted liquid line of descent dominated by crystal fractionation. The spatial association of the pegmatites with the syenite complex, and their compositional similarities to the syenite complex, suggest there is a genetic association (Halden and Fryer, submitted). The compositional gap in terms of REE content, between the main phase and the more evolved silica-rich rocks, might be explained by the physical separation of a REE-enriched vapour phase. Such a REE-enriched phase will also have been rich in F and P, therefore the REEs would have been scavenged as ionic complexes (Halden and Fryer, submitted).

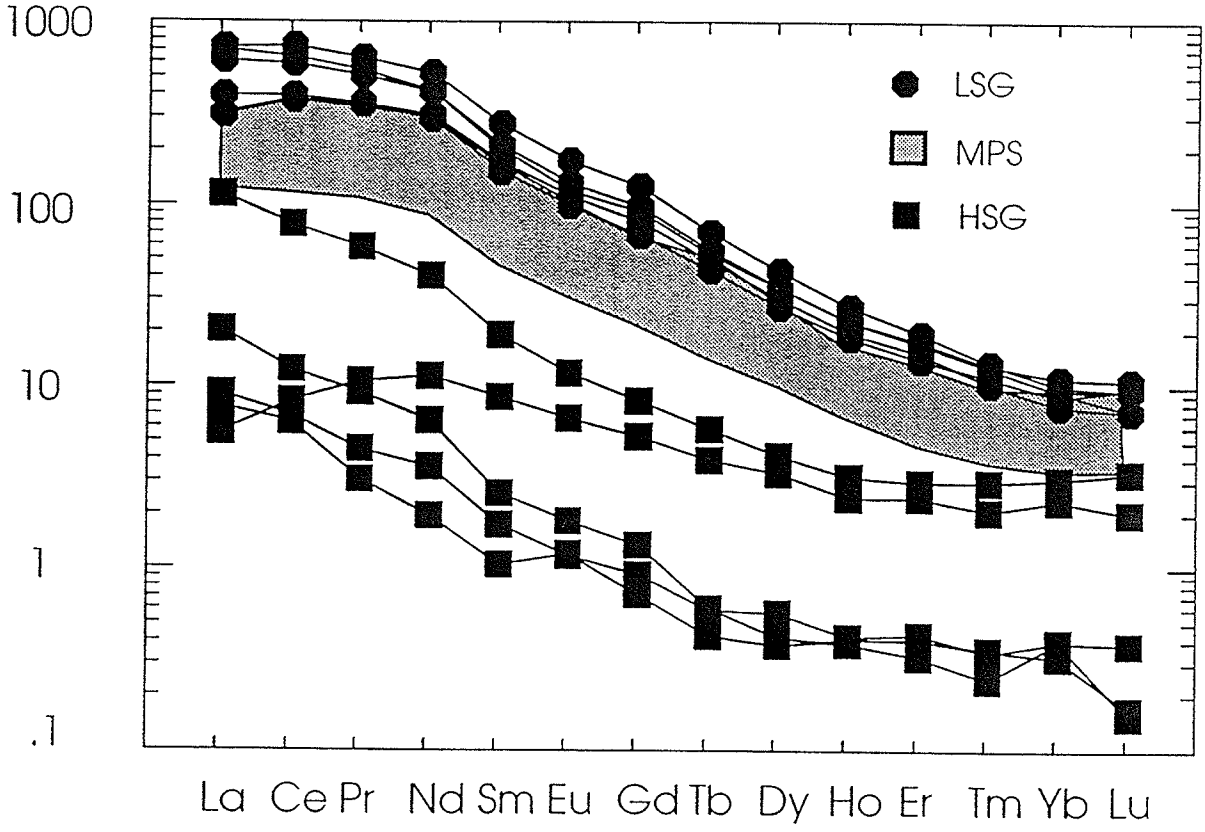

Figure 4.6. Chondrite-normalized REE plot of the rocks from the Eden Lake syenite complex (from Halden and Fryer, submitted). Symbols as in Figure 4.4. Normalization values are from Sun (1982).

Chapter 5: Pegmatite Mineral Phases

To constrain (i) the origin of the pegmatites associated with the Eden Lake syenite complex and (ii) the distribution of the trace elements within these pegmatites, petrologic and chemical data were collected from the accessory, REE-bearing mineral phases. The study focuses on the minerals in the Type III and IV pegmatites as they contain the more complex mineralogy; minerals examined include apatite, titanite, zircon, britholite, allanite, andradite, fluorite, aegirine-augite, K-feldspar, and plagioclase. A suite of REE-bearing carbonates was also observed; preliminary microprobe and diffraction analyses suggest this suite includes burbankite, weloganite and strontianite.

5.1. Apatite.

Apatite, $Ca_5(PO_4)_3$ (OH, F, Cl), is a common accessory mineral in syenitic rocks and associated pegmatites, as well as hydrothermal veins and cavities (Deer et al., 1986; Ronsbo, 1989). It is the most abundant P-bearing mineral in syenites; fluorapatite is usually host for the majority of the REEs (up to 16 weight % in alkaline rocks; Clark, 1984; Ronsbo, 1989). Apatite is present in both the Type III and Type IV pegmatites.

Apatite occurs in the Type III pegmatites as both separate grains and as inclusions within aegirine-augite and titanite. In thin section, the apatite crystals are clear, euhedral to anhedral (Figure 5.1). Anhedral grains have rounded shapes with curved grain boundaries; euhedral grains tend to have straight boundaries (Figure 5.1). Grain size ranges from 0.18 to 0.45 mm; where present, apatite abundance varies from trace amounts

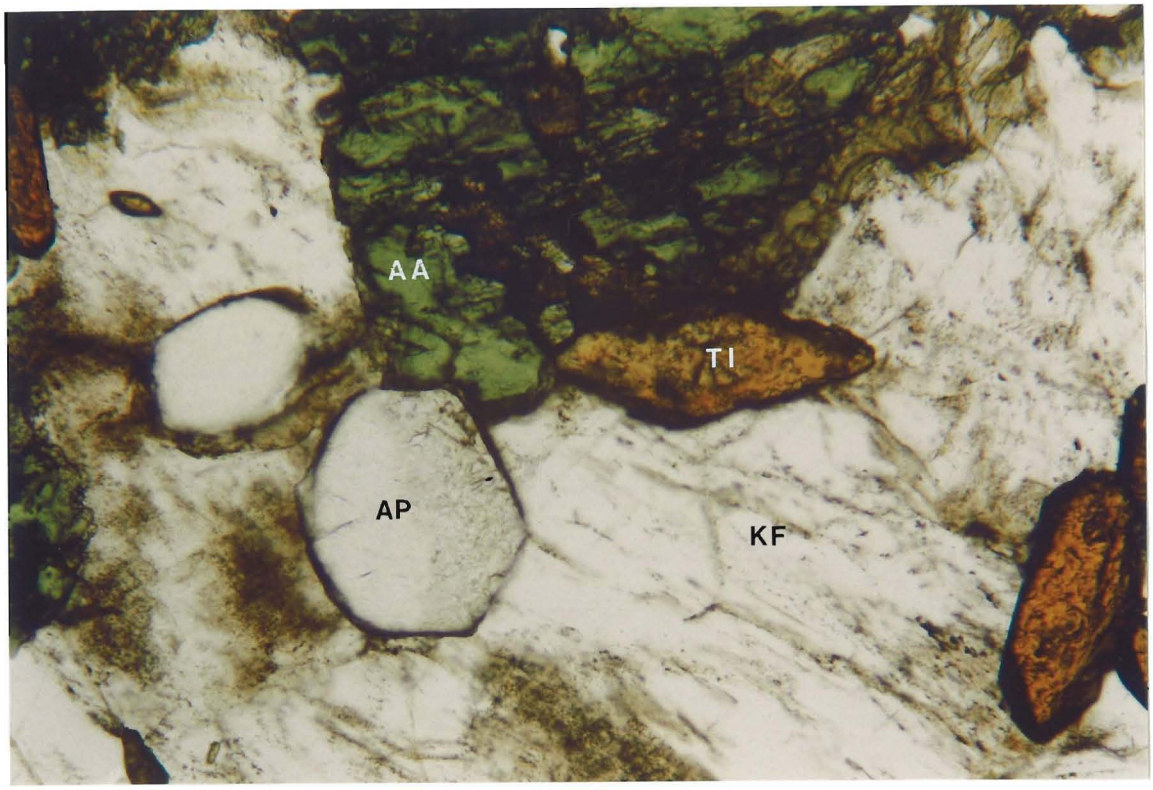

Figure 5.1. Photomicrograph of euhedral to subhedral apatite in the Type III pegmatites. Field of view is 0.7 mm. Mineral abbreviations are as follows: AP - apatite, KF - K-feldspar, TI - titanite, AA - aegirine-augite.

to 5%. Apatite inclusions within titanite are anhedral, with slightly curved irregular margins (Figure 5.2B).

Examination of back-scattered electron (BSE) images of apatite grains indicates that they are compositionally homogeneous; however, a few grains appear to have a faint oscillatory zoning while others have a patchy discontinuous zoning (Figure 5.2A). Contacts between the oscillatory zones are straight and regular; contact between the patchy zones are curved (Figure 5.2A). BSE images of apatite inclusions within titanite crystals reveals that the inclusions have a patchy discontinuous zoning (Figure 5.2B). The presence of unzoned apatite grains as well as two different zoning patterns within apatite suggests that there was several different stages of apatite crystallization.

The chemistry of apatite grains in the Type III pegmatites is shown in Table 5.1. The oscillatory zoning reflects changing trace-element contents; the bright zones have higher abundances of Si, Na, REEs but lower Cl than the dark zones (Table 5.1). The unzoned apatite crystals have the same range of element abundances as both the bright and dark oscillatory zones (Table 5.1). The light patches within apatite inclusions within titanite have a higher REE content that the dark patches (Table 5.1). Apatite inclusions have higher Ca and lower Si contents than the oscillatory zoned and unzoned apatite grains (Table 5.1). REE plots for apatite grains from the Type III pegmatites are shown in Figure 5.3. The plots are LREE-enriched and they are similar for both the separate apatite grains and the inclusions.

In the Type IV pegmatites, apatite crystals are euhedral to anhedral, with curved to straight edges (Figure 5.4). Anhedral grains commonly have curved or scalloped

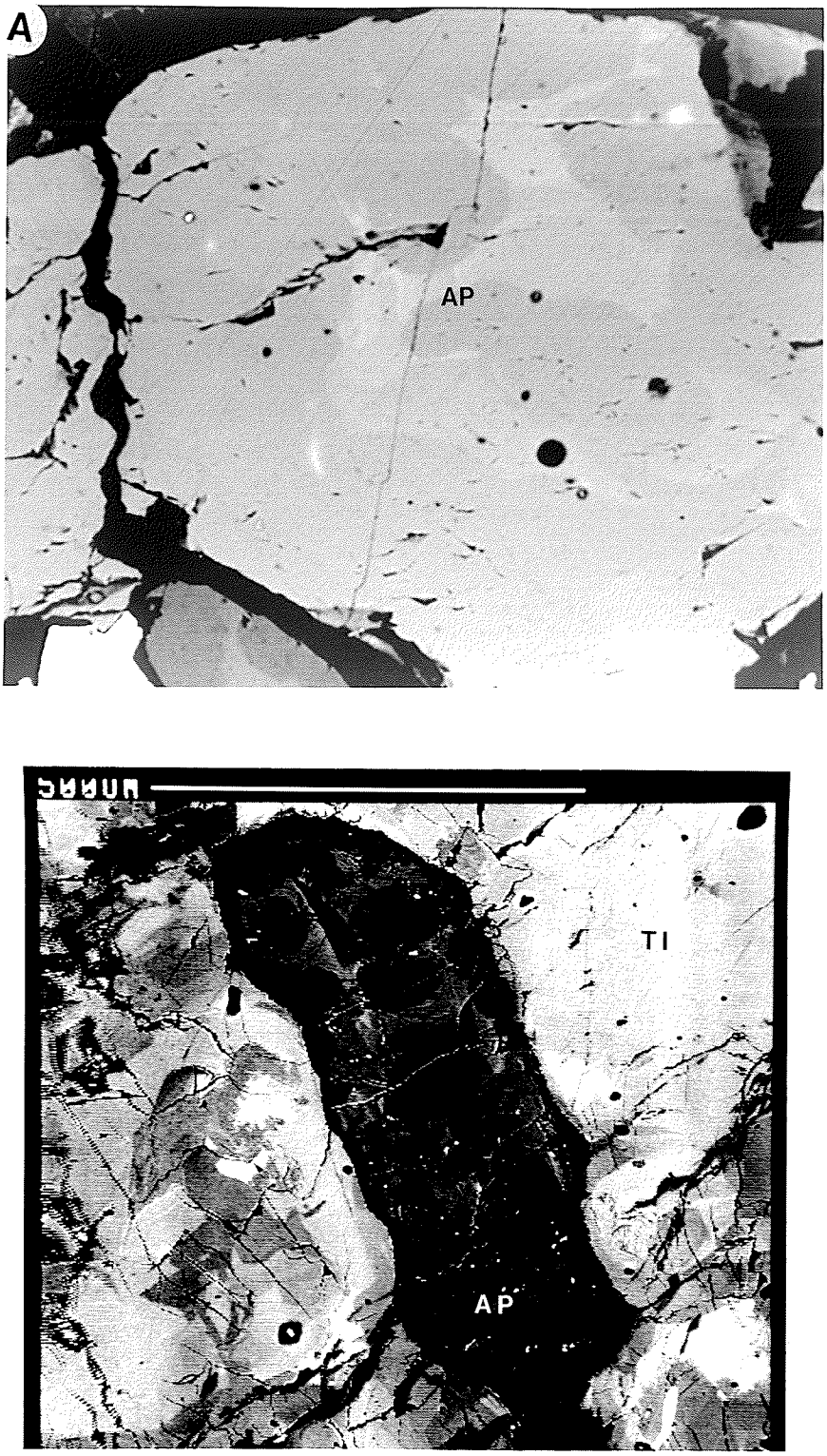

Figure 5.2. A. Photograph of a BSE image of separate apatite grain in the Type III pegmatites. Note the slight colour variation suggesting patchy zoning. Field of view is 200 microns in the long dimension. *B.* Photograph of a BSE image of an anhedral apatite inclusion within titanite. The apatite has patchy, irregular zoning and irregular, slightly curved grain boundaries. Bar scale is 500 microns long.

Table 5.1. Representative apatite chemical compositions for samples from the Type III and Type IV pegmatites. Further compositions are presented in Appendix I.

Oxide (weight percent)	Pegmatite III					Pegmatite IV	
	Unzoned	Dark Oscillatory Zone	Bright Oscillatory Zone	Dark Patch	Bright Patch	Unaltered	Altered
CaO [1]	52.920	52.531	52.471	54.032	53.814	51.508	52.536
P_2O_5	39.568	39.369	38.944	38.958	38.243	35.837	37.789
SiO_2	0.451	0.438	0.787	0	0	2.263	1.535
FeO^T [2]	0.024	0.008	0.006	0.005	0	0	0.022
MnO	0.017	0.036	0.025	0.048	0.043	0.003	0.039
Na_2O	0	0.090	0.148	-	-	-	-
BaO	-	0.011	0.034	0.253	0.185	1.391	4.154
F	3.988	3.982	3.947	4.068	4.000	3.975	4.007
Cl	0.032	0.017	0.005	0.009	0	0.007	0.010
REE_2O_3 [3]	-	0.754	1.339	2.503	1.535	8.914	15.154
TOTAL	97.000	97.227	97.764	99.625	97.636	102.514	111.09
Ni [4,5]	-	-	-	0	0	40	35
Cu	-	-	-	18	12	44	35
Zn	-	-	-	0	18	22	53
As	-	-	-	65	59	234	289
Sr	-	6720	7220	6390	6740	6387	6934
Y	-	435	1465	1074	1423	3528	4266
La	-	445	900	2583	2102	19512	31261
Ce	-	2345	3785	3425	3673	30585	64342
Nd	-	2605	3945	3032	4006	15819	20981
Sm	-	460	915	754	879	3325	4648
Gd	-	130	330	409	494	1687	2097
Dy	-	-	-	162	221	810	891
Er	-	-	-	98	135	402	440
Yb	-	-	-	71	98	241	264
Pb	-	-	-	96	137	348	622
Bi	-	-	-	0	0	0	23
Th	-	-	-	689	1016	410	406
U	-	-	-	86	118	422	866
Formulas calculated on basis of 12 oxygen + 1 (F, Cl)							
Ca^{2+}	4.99	4.966	4.959	5.074	5.139	4.871	4.7
P^{5+}	2.948	2.941	2.908	2.891	2.885	2.678	2.672
Si^{4+}	0.04	0.039	0.07	0	0	0.199	0.128
Fe^{2+}	0.001	0.001	0.001	0.000	0	0	0.001
Mn^{2+}	0.001	0.003	0.001	0.004	0.003	0	0.003
Na^+	0	0.015	0.026	0	0	0	0
Ba^{2+}	0	0	0.001	0.009	0.006	0.048	0.136
Ce^{3+} [6]	0	0.024	0.043	0.08	0.05	0.288	0.463
Cation sum	7.981	7.989	8.009	8.058	8.083	8.085	8.103
F-	1.111	1.111	1.099	1.128	1.128	1.108	1.059
Cl-	0.004	0.003	0.002	0.001	0	0.001	0.001

1.Ca, P, Si, Fe, Mn, Na, F, Cl abundances from EMPA.

2. Total iron expressed as FeO^T.

3. Sum of REE abundance.

4. Ba, Ni, Cu, Zn, As, Sr, Y, La, Ce, Nd, Sm, Gd, Dy, Er, Yb, Pb, Bi, Th, U abundances from PIXE.

5. Element abundance in ppm.

6. Total REEs expressed as Ce^{3+}.

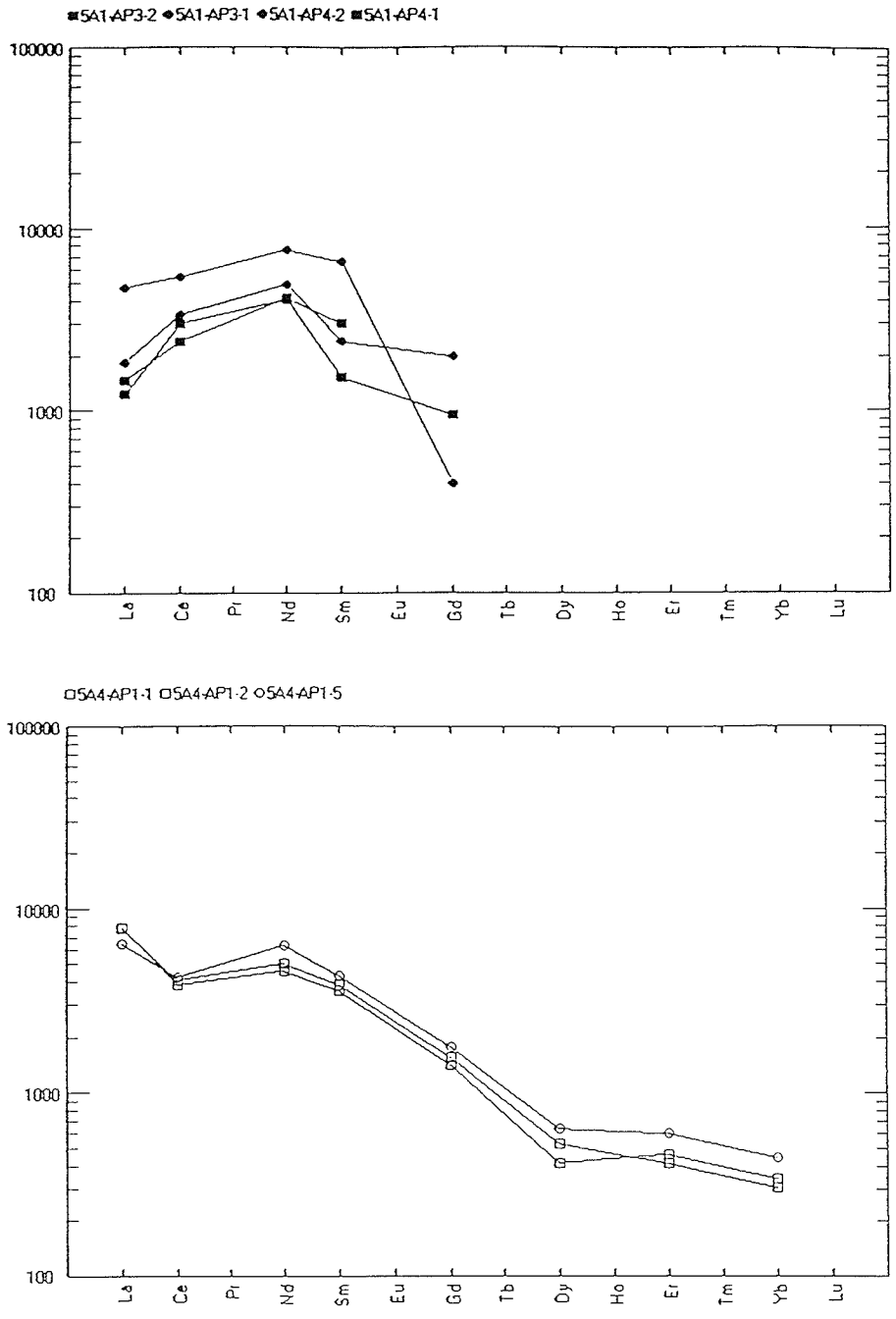

Figure 5.3. A. Chondrite-normalized REE plots for separate apatite grains in the Type III pegmatites. REE values are from EMPA. Dark oscillations are shown by ■; bright oscillations are shown by ●. *B.* Chondrite-normalized REE plots for apatite inclusions within the Type III pegmatites. REE values are from PIXE analysis. Dark patches are shown by □; bright patches are shown by ○.

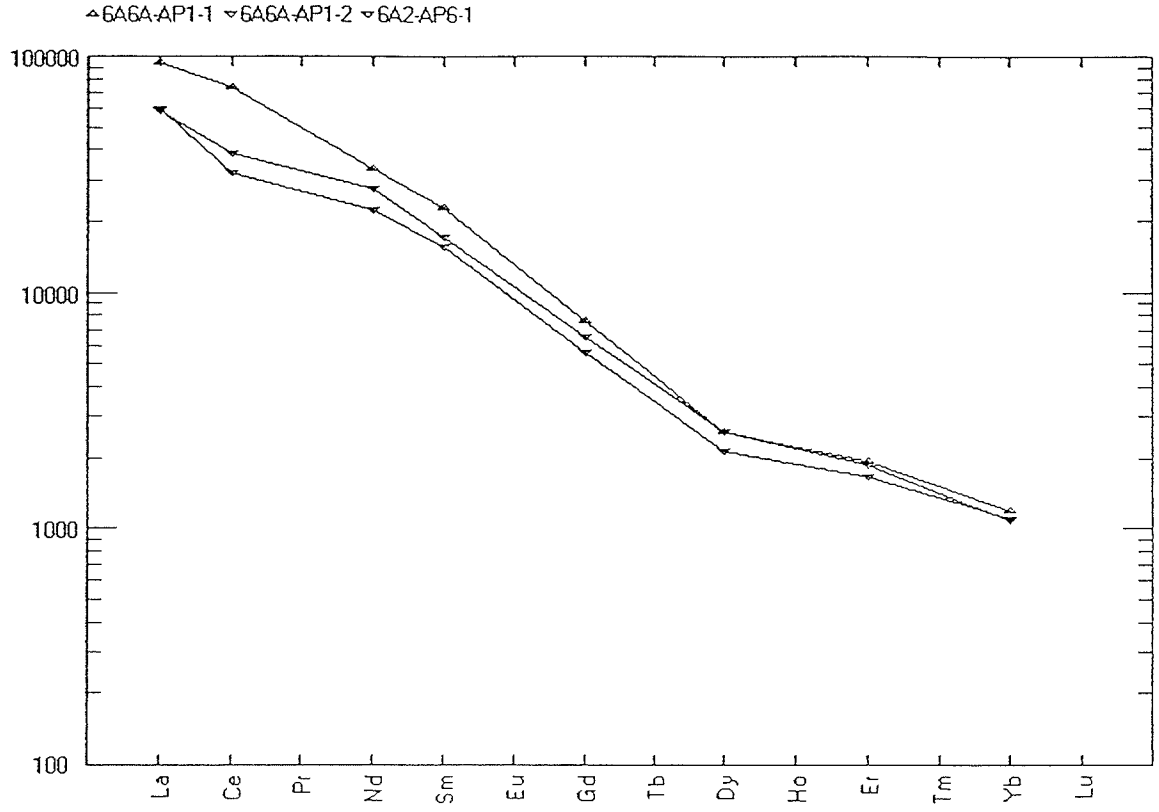

Figure 5.3. continued. C. Chondrite-normalized REE plots for apatite grains from the Type IV pegmatites. REE values are obtained from PIXE analysis. Unaltered apatite are shown by ▽; altered apatite are shown by △. Normalization values are from Sun (1982).

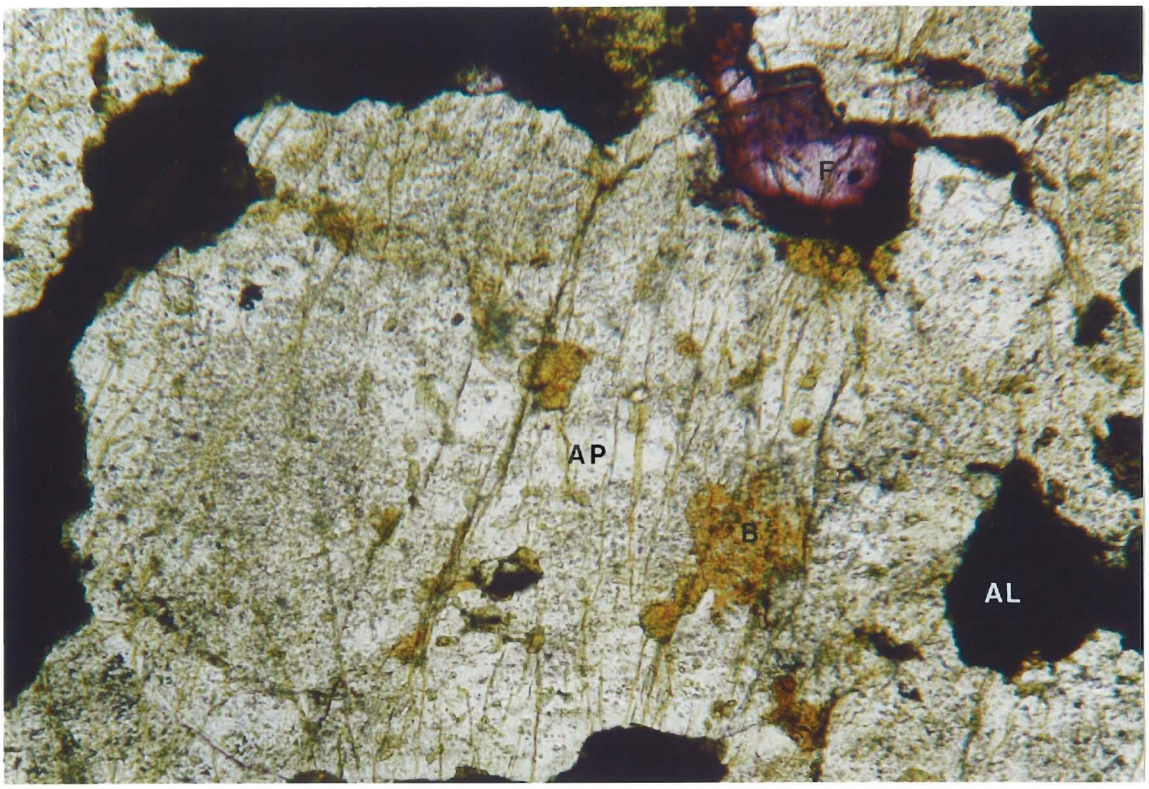

Figure 5.4. Photomicrograph of anhedral apatite with irregular grain boundaries from the Type IV pegmatites. Apatite near britholite is commonly fractured. Field of view in the long dimension is 2.8 mm. Mineral abbreviations are as follows: AP - apatite, AL - allanite, B - britholite, F - fluorite.

margins whereas euhedral grains have straight edges and occur only as inclusions within britholite and aegirine-augite. Apatite crystals are generally cloudy due to the presence of very fine grained, irregularly shaped fluid inclusions (Figure 5.4); small corrosion pits of britholite are observed in some grains. Apatite crystals range in size from 0.45 mm to 5.4 mm and range in abundance from 5 to 35%. Apatite grains commonly contain subparallel cracks, some of which are filled by fluorite and others with REE-enriched apatite (Figure 5.4, 5.5); these cracks are more numerous close to britholite (Figure 5.4) and in places, radiate away from britholite grains.

Chemical compositions of apatite grains from the Type IV pegmatites are presented in Table 5.1. There are differences in grey level within apatite grains near britholite and allanite and associated with the subparallel cracks that are observed in BSE images (Figure 5.5); these areas are irregular and patchy with slightly curved margins. These most likely result from chemical alteration of the apatite, which may be related to metamictization of the adjacent britholite. There may be some primary igneous zoning in some of the apatite grains, defined by light and dark regions with sharp straight contacts, but this is partially to completely overprinted by the irregular alteration. The ranges of element abundances are similar in both the darker, altered and lighter, unaltered apatite; however, altered apatite has a higher amount of Fe and total REEs and a lower Si content than the unaltered apatite grains (Table 5.1). REE plots for the Type IV apatite crystals are shown in Figure 5.3; they are very light REE-enriched and are not the same as the plots for Type III apatite crystals.

The major element abundances in the Type IV apatite grains are, in general,

Figure 5.5. Photograph of a BSE image of an apatite grain from the Type IV pegmatites. The patchy colouring within the apatite is due to alteration; the bright fractures are filled with REE-enriched apatite. Field of view is 300 microns in the long dimension. Mineral abbreviations are as follows: AP - apatite, B - britholite.

similar to those in the Type III apatite grains, except that Si contents are higher in the Type IV apatite grains. Trace element abundances (Ni, Mn, Zn, As, Ba, Pb, Y and REEs) are also significantly higher in the Type IV apatite crystals; only Sr and Bi have similar abundances (Table 5.1). The significance of the different trace element abundances in the apatite crystals will be discussed in Chapter 6.

5.2. Titanite.

Titanite, $CaTiOSiO_4$, is a common accessory mineral in syenitic rocks, where it is an important host for the REEs (Henderson, 1980; Clark, 1984; Deer et al., 1989; Hawthorne et al., 1990; Pan et al., 1993). Pegmatitic titanite grains tend to have higher LREE content than titanite crystals from any other location (Clark, 1984; Russell et al., 1994). Titanite grains are found in both the Type III and IV pegmatites associated with the syenite complex; they are also present as an accessory mineral in the main units of the syenite complex where titanite is an important host for the REEs.

Titanite in the Type III pegmatites.

Titanite crystals within the Type III pegmatites appear euhedral to subhedral and typically have a brown to black colour. In thin section, the titanite grains are tan to red brown to brown in colour with a tan to red-brown pleochroism. Titanite occurs both as separate grains (Figure 5.6A) and as inclusions within andesine (Figure 5.6B), indicating co-crystallization of titanite and andesine. Where present, titanite ranges in abundance from trace amounts to 10%. Titanite grains are subhedral to anhedral, have straight crystal faces (Figure 5.6A) and have a size range from 0.1 to 6.5 mm. Titanite grains within

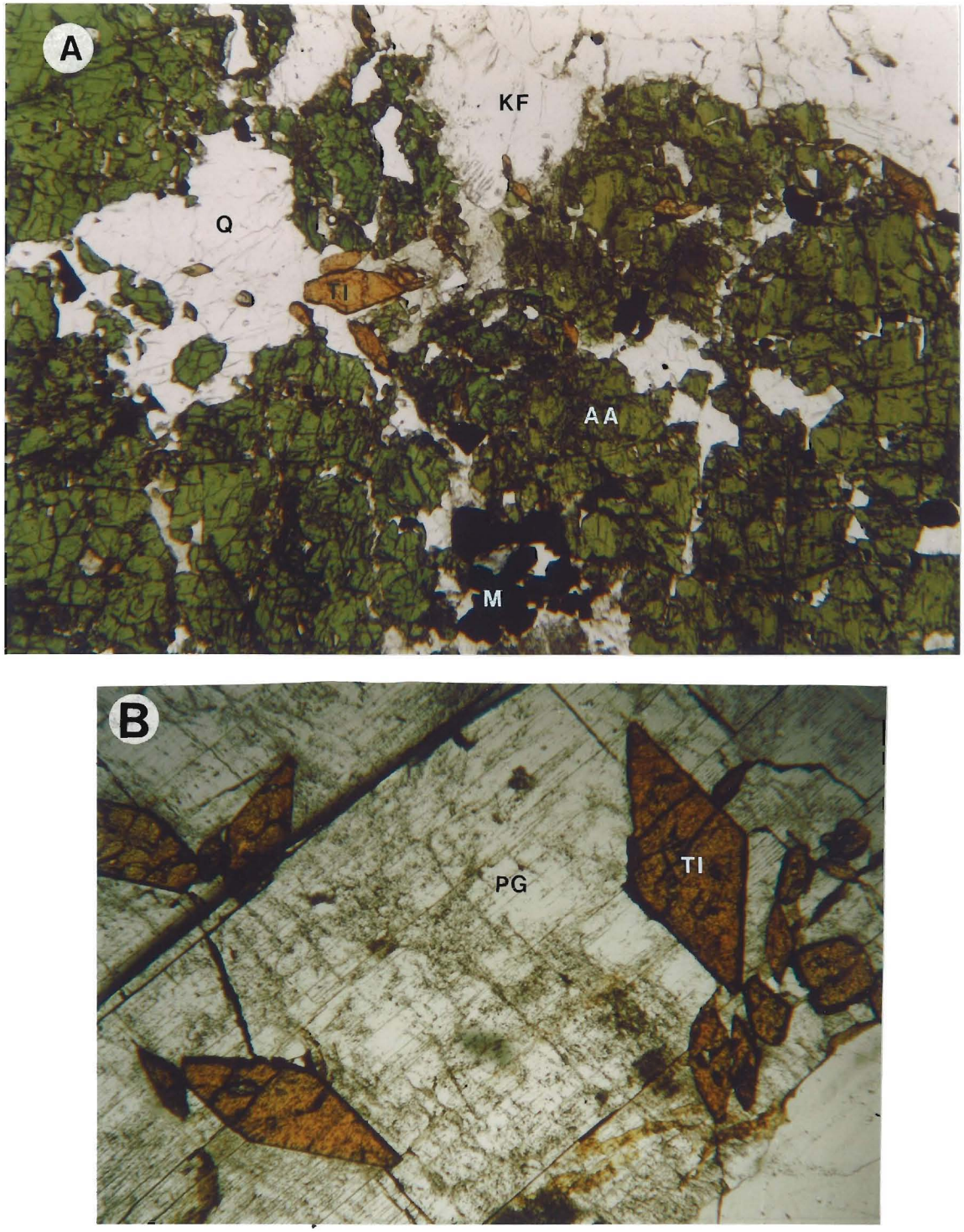

Figure 5.6.A. Photomicrograph of titanite and aegirine-augite crystals in the Type III pegmatites. The titanite grains have euhedral to subhedral lozenge-shapes; the aegirine-augite has subhedral shapes. Field of view is 2.8 mm in the long dimension. *B.* Photomicrograph of titanite inclusions within andesine plagioclase. Field of view is 2.8 mm in the long dimension. Mineral abbreviations are as follows: AA - aegirine-augite, KF - K-feldspar, M - magnetite, PG - plagioclase, TI - titanite, Q - quartz.

plagioclase are euhedral to subhedral with straight grain boundaries and range in size from 0.12 to 0.8 mm. Inclusions present within titanite crystals comprise apatite, thorite, oscillatory zoned allanite and strontianite.

Examination of BSE images of titanite grains from the Type III pegmatites reveals that the grains are chemically zoned. There are four types of zoning observed: (1) a patchy zoning defined by discontinuous, randomly distributed bright and dark patches, roughly circular to oval in shape (Figure 5.7A); (2) oscillatory zoning defined by alternating light and dark linear bands with sharp margins; the width of the bands ranges from 1 to 70 microns (Figure 5.7A,B); (3) sector zoning of crystal growth planes (Figure 5.7C); the {111} form of titanite crystal faces appear darker in BSE images while the {100} and {001} forms are lighter; contacts between the sectors are sharp and straight; and (4) discontinuous rims or overgrowths characterized by a bright rim around crystal margins (Figure 5.7).

Within the Type III pegmatites, we can define two types of titanite grains on the basis of zoning patterns; this suggests that there have been several stages of titanite growth and resorption. Type A titanite grains contain three major growth regions, separated by irregular undulatory surfaces (Figure 5.7A,B). The first region is characterized by patchy zoning, the second region by oscillatory zoning and the third by an overgrowth (Figure 5.7A,B). Some Type A titanite crystals contain only the oscillatory zoning and the overgrowth, but this may be a result of the section orientation and cut. Type B titanite grains contain two major growth regions (Figure 5.7C), again separated by irregular undulatory contacts. The first region is characterized by sector zoning and the

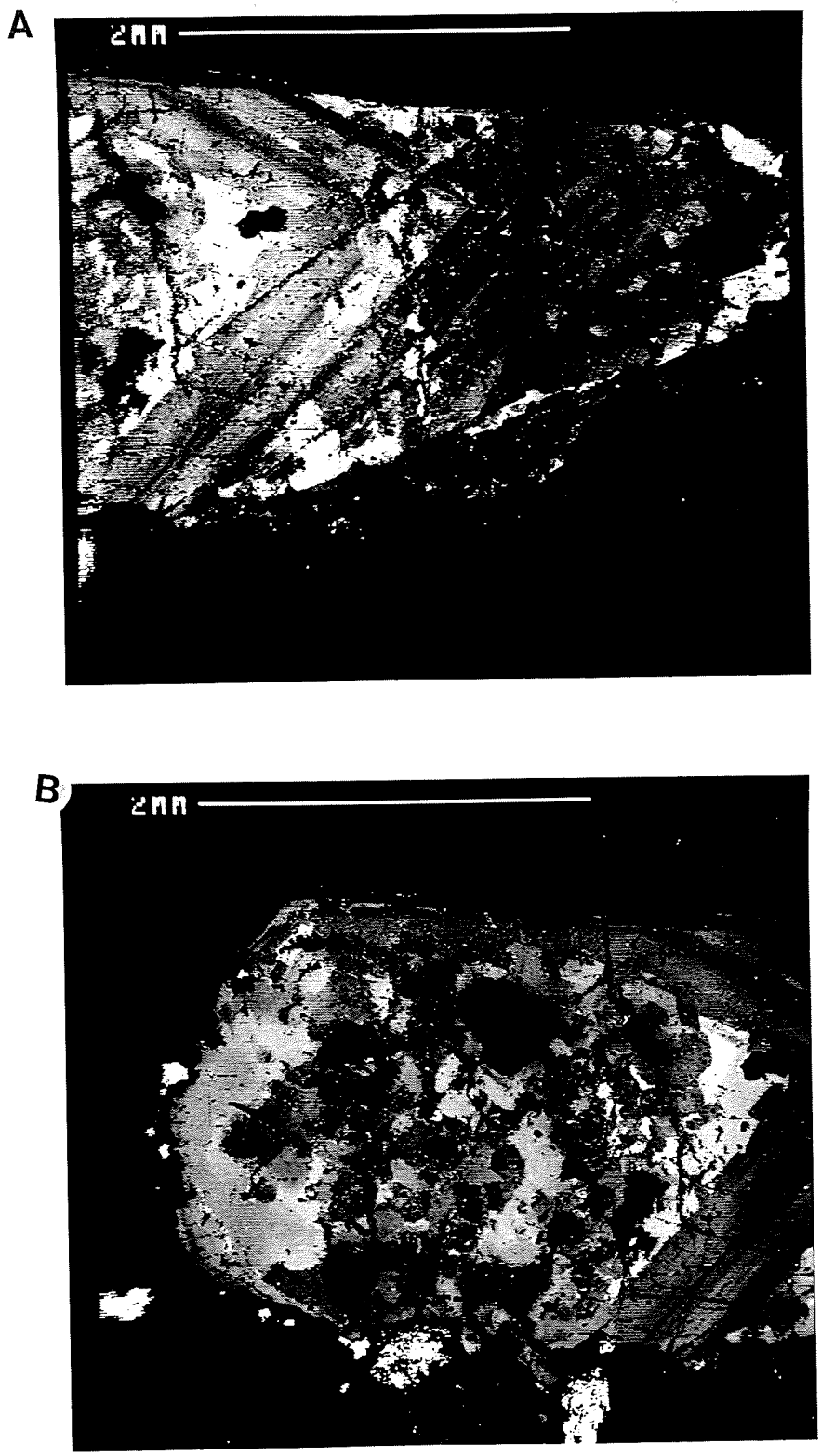

Figure 5.7. A & B. Two photographs of BSE images of a Type A titanite grain in the Type III pegmatites. Patchy discontinuous zoning, oscillatory zoning and a bright overgrowth are all visible; these are separated by irregular, sutured contacts. Scale bar is 2 mm long.

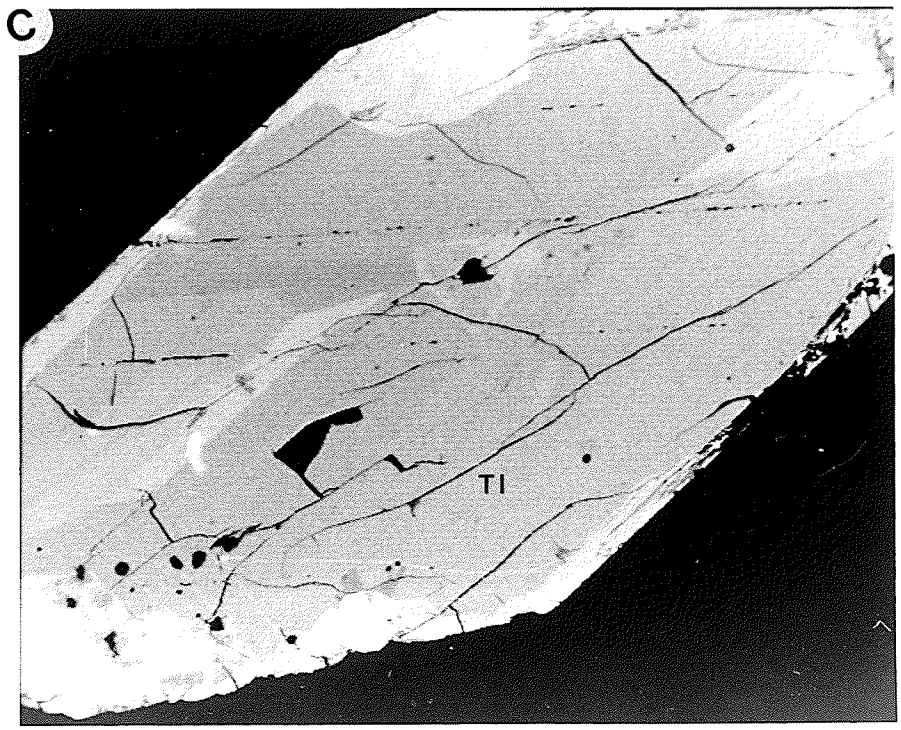

Figure 5.7. continued. C. Photograph of a BSE image of a Type B titanite grain in the Type III pegmatites. Sector zoning and a bright overgrowth are visible, separated by an undulatory contact. Field of view is 200 microns in the long dimension.

second by an overgrowth (Figure 5.7C). Table 5.2A lists representative chemical compositions for the different growth regions in the Type A titanite grains. Chemical differences exist between the different growth regions as well as different brightness zones within each growth region. Chemical variations in the patchy growth zones are related to Fe, Sr, Zr, Pb, Th, U, REE and F abundances. The darker patches have significantly higher Sr, Zr, Nb, Pb and F contents whereas the lighter patches have higher Fe, Y, La, Ce, Sm, Th and U contents (Table 5.2A). Oscillatory zoning reflects variation in Ti, Sr, Fe, Cu, Zn, Zr, Nb, Nb, Pb, Th, U, REE and F contents. The dark oscillatory zones have higher concentrations of Ti and Sr, while Fe, Cu, Zn, Zr, Nb, Nb, Pb, Th, U, Y, REEs and F are concentrated in the light oscillatory zones (Table 5.2A). Regions with patchy zoning contain higher abundances of Zr and Nb than either of the other two regions and the overgrowths have the highest concentration of La and F.

Table 5.2B lists representative chemical compositions for each of the growth regions in the Type B titanite grains. Differences in brightness levels within the sector zoned regions are related to variations in Mn, Na, REE and F. The darker sectors, {111}, have a high concentration of Sm and F and the brightest sectors, {100}, have the highest amounts of Mn, Na and Y. In comparison with the regions with sector zoning, the overgrowths have higher REE, Mn, Sn, Na and Sr contents but lower Al contents (Table 5.2B).

While the major element chemistry of the overgrowths in the Type A and B titanite crystals is similar, there are some differences in terms of trace element chemistry (Table 5.2). The overgrowths of the Type A titanite crystals have higher Sr, REE, Fe, Zr,

Table 5.2.A. Chemical compositions for Type A titanite crystals from the Type III pegmatites. Additional compositions are presented in Appendix II.

Oxide (weight percent)	Dark Patch	Bright Patch	Dark Oscillatory Zone	Bright Oscillatory Zone	Overgrowth
SiO_2 [1]	29.869	29.674	30.397	30.051	29.679
TiO_2	36.557	34.073	35.680	33.016	32.849
CaO	27.435	26.922	27.977	27.628	27.402
FeO^T [2]	1.946	3.031	2.528	3.133	2.997
Al_2O_3	0.886	1.366	1.031	1.887	1.988
Na_2O	0.122	0.062	0.020	0.071	0.032
REE_2O_3 [3]	2.184	2.144	1.722	2.352	3.533
F	0.601	0.717	0.858	1.368	1.463
TOTAL	99.6	97.989	100.213	98.506	99.943
Mn [4, 5]	396	375	122	471	366
Sr	1140	395	956	685	379
Co	115	193	120	172	165
Cu	17	16	5	56	13
Zn	15	7	2	25	8
Zr	2854	1035	3045	3338	1053
Nb	3084	2306	1528	2190	2451
Ta	153	103	121	115	120
Pb	198	89	12	691	94
Y	945	1129	452	1042	1190
La	6495	6403	6637	6915	7877
Ce	5701	5379	5136	6871	6068
Nd	3629	3413	1646	3732	3388
Sm	1204	1305	600	1039	1291
Gd	556	528	175	366	469
Yb	72	82	30	52	98
Th	106	303	25	205	293
U	128	240	51	186	265
Formulas calculated on basis of 4 oxygen + 1 F					
Si^{4+}	0.999	1.011	1.009	1.01	1
Ti^{4+}	0.919	0.873	0.89	0.834	0.832
Ca^{2+}	0.983	0.983	0.994	0.995	0.989
Fe^{2+}	0.054	0.086	0.07	0.088	0.085
Al^{3+}	0.035	0.055	0.04	0.075	0.079
Na^{+}	0.008	0.004	0.001	0.005	0.002
Ce^{3+} [6]	0.027	0.027	0.021	0.029	0.044
Cation sum	3.024	3.038	3.026	3.034	3.03
F-	0.063	0.078	0.09	0.146	0.156

1. Si, Ti, Ca, Fe, Al, Na, F were determined by EMPA.
2. Total iron expressed as FeO.
3. Sum of REE abundance.
4. Mn, Sr, Co, Cu, Zn, Zr, Nb, Ta, Pb, Y, La, Ce, Nd, Sm, Gd, Yb, Th, U were determined by PIXE.
5. Element abundance in ppm.
6. Total REEs expressed as Ce^{3+}.

Table 5.2B. Chemical compositions for Type B titanite crystals from the Type III pegmatites. Additional compositions are presented in Appendix II.

Oxide (weight percent)	Dark Sector {111}	Bright Sector {100}or{001}	Overgrowth
SiO_2 [1]	30.244	30.355	30.081
TiO_2	32.357	32.300	32.500
CaO	28.028	27.879	27.837
FeO^T [2]	2.476	3.942	1.360
Al_2O_3	2.001	2.110	1.422
Na_2O	0	0.002	0.028
REE_2O_3 [3]	0.744	0.62	1.416
F	1.697	1.666	1.805
TOTAL	88.803	98.254	95.033
Mn [4,5]	239	379	488
Sr	74	-	154
Co	0	-	58
Cu	10	-	54
Zn	17	-	42
Zr	257	-	150
Nb	1710	-	1313
Ta	160	-	122
Pb	59	-	171
Sn	110	-	358
Mo	33	-	0
Y	505	1390	5172
La	2790	490	3338
Ce	1985	540	0
Nd	634	2410	682
Sm	297	360	1003
Gd	50	-	687
Yb	52	-	821
Th	40	-	17
U	68	-	47
Formulas calculated on basis of 4 oxygen + 1F.			
Si^{4+}	1.022	1.017	1.029
Ti^{4+}	0.823	0.814	0.836
Ca^{2+}	1.015	1.001	1.02
Fe^{2+}	0.07	0.11	0.039
Al^{3+}	0.08	0.083	0.057
Na^{+}	0	0	0.02
Ce^{3+} [6]	0.09	0.08	0.018
Cation sum	3.019	3.035	3.001
F-	0.182	0.176	0.195

1. Si, Ti, Ca, Fe, Al, Na, F were determined by EMPA.
2. Total iron expressed as FeO.
3. Sum of REE abundance.
4. Mn, Sr, Co, Cu, Zn, Zr, Nb, Ta, Pb, Y, La, Ce, Nd, Sm, Gd, Yb, Th, U were determined by PIXE.
5. Element abundance in ppm.
6. Total REEs expressed as Ce^{3+}.

Table 5.2C. Chemical compositions for titanite crystals from the Type IV pegmatites. Additional compositions of titanite crystals from the Type IV pegmatites are given in Appendix II.

Oxide (weight percent)	Dark Oscillatory Zone	Bright Oscillatory Zone	PIXE Analysis
SiO_2 [1]	29.807	29.426	-
TiO_2	34.558	33.554	-
CaO	27.597	26.509	-
FeO [1,2]	3.258	3.230	3.319
Al_2O_3	1.003	3.340	-
Na_2O	0.021	0.043	-
F	0.875	1.010	-
REE_2O_3 [3]	1.057	2.5	5.496
TOTAL	98.176	99.612	-
(ppm)			
Mn [4,5]	8	93	2345
Sr	1035	457	2463
Co	-	-	171
Cu	-	-	25
Zn	-	-	38
Zr	-	-	2028
Nb	-	-	1485
Sn	-	-	62
Ta	-	-	70
Pb	-	-	1173
Y	655	940	2045
La	600	2700	12275
Ce	2130	8260	18014
Nd	4775	7977	10996
Sm	840	1437	2363
Gd	-	-	998
Yb	-	-	139
Th	-	-	56
U	-	-	935
Formulas calculated on basis of 4 oxygen + 1F			
Si^{4+}	1.019	0.985	-
Ti^{4+}	0.888	0.845	-
Ca^{2+}	1.024	0.951	-
Fe^{2+}	0.093	0.09	-
Al^{3+}	0	0.132	-
Na^{+}	0.001	0.003	-
Ce^{3+} [6]	0.013	0.031	
Cation sum	3.04	3.037	
F-	0.094	0.107	-

1. Si, Ti, Ca, Fe, Al, Na, F were determined by EMPA.
2. Total iron expressed as FeO.
3. Sum of REE abundance.
4. Mn, Sr, Co, Cu, Zn, Zr, Nb, Ta, Pb, Y, La, Ce, Nd, Sm, Gd, Yb, Th, U were determined by PIXE.
5. Element abundance in ppm.
6. Total REEs expressed as Ce^{3+}.

Nb, Th and U contents whereas the overgrowths of the Type B titanite grains have slightly higher Mn, Y and F contents. The similarity of the compositions suggests that the overgrowths are cogenetic; this will be discussed further in Chapter 6.

Rare earth element plots for titanite from the Type III pegmatites are shown in Figure 5.8. The plots for Type A titanite grains are light REE-enriched (Figure 5.8A); Type B plots are relatively flat and have lower LREE and higher HREE contents (Figure 5.8B).

Titanite in the Type IV pegmatites.

In the Type IV pegmatites, titanite grains are red-brown to light brown to light tan in colour with a tan to red-brown pleochroism (Figure 5.9). Grains are euhedral, lozenge-shaped to subhedral, oval shapes (Figure 5.9). Where present, titanite crystals range in abundance from trace amounts to 3%, and they have a size range from 0.13 to 2.25 mm. Some clusters of titanite grains up to 0.3 mm are visible. Titanite crystals are associated with aegirine-augite, britholite, apatite and allanite and they are commonly included within britholite grains. Rarely, titanite grains contain "inclusions" of weloganite, a REE-bearing Sr, Zr carbonate. Some grains are completely fractured and contain subparallel cracks that are filled with britholite (Figure 5.9; 5.10).

Examination of these titanite grains using BSE imaging reveals that they are zoned. The zoning appears to be oscillatory in nature, with thick compositional bands up to 75 microns thick; sector zoning similar to that observed in the Type B titanite grains in the Type III pegmatites is also visible (Figure 5.10). Bright overgrowths are observed in some grains, but no patchy-zoned titanite crystals are observed.

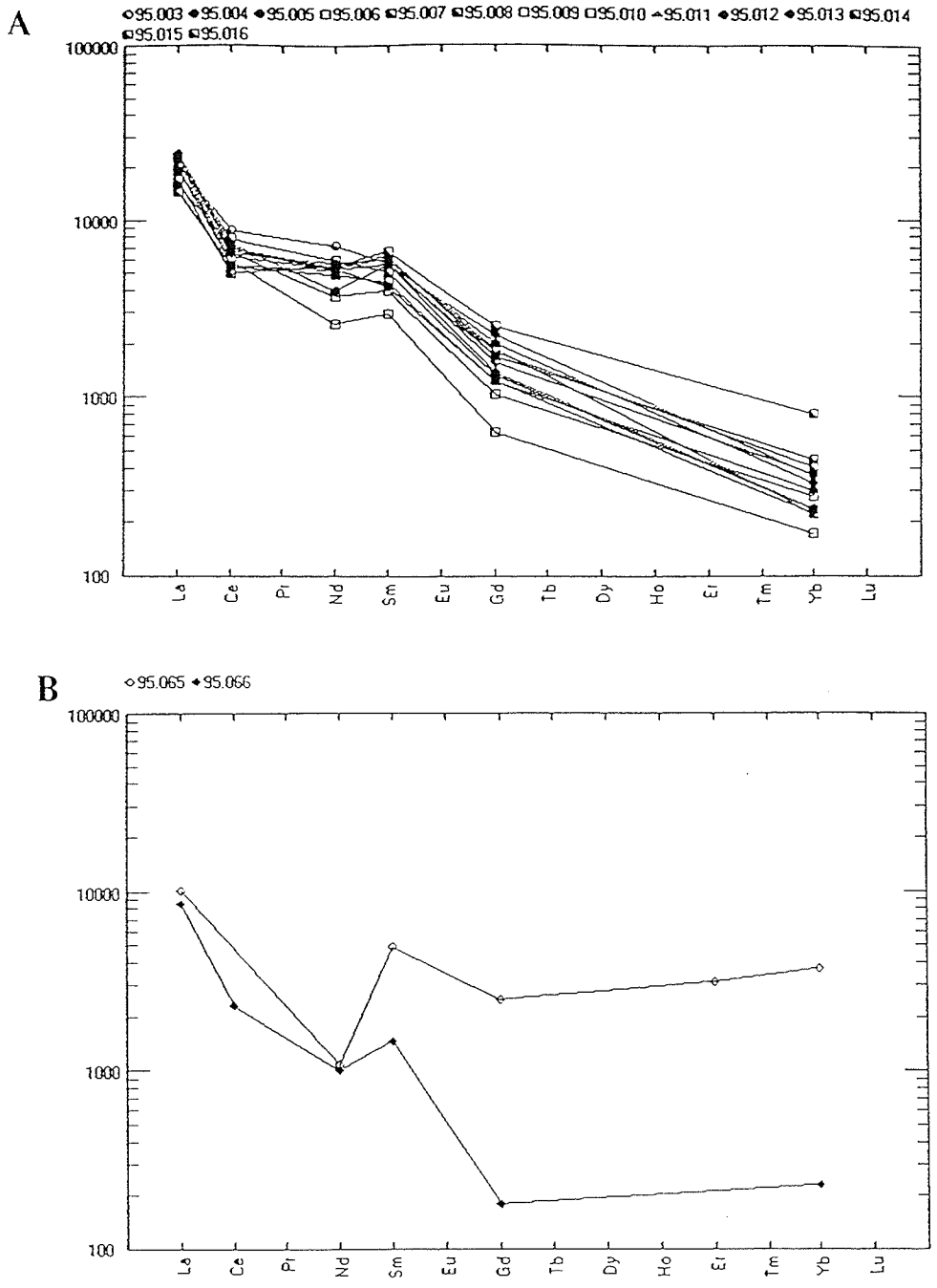

Figure 5.8. A. Chondrite-normalized REE plots for Type A titanite crystals in the Type III pegmatites. REE values from PIXE analysis. Dark patches are shown by ●, bright patches are shown by ○, Dark oscillatory zones are shown by □, bright oscillations are shown by ■ and bright overgrowth are shown by ▵. *B.* Chondrite-normalized REE plots for Type B titanite crystals. REE data from PIXE analysis. Dark sectors are shown by ♦, bright overgrowths are shown by ◇.

C

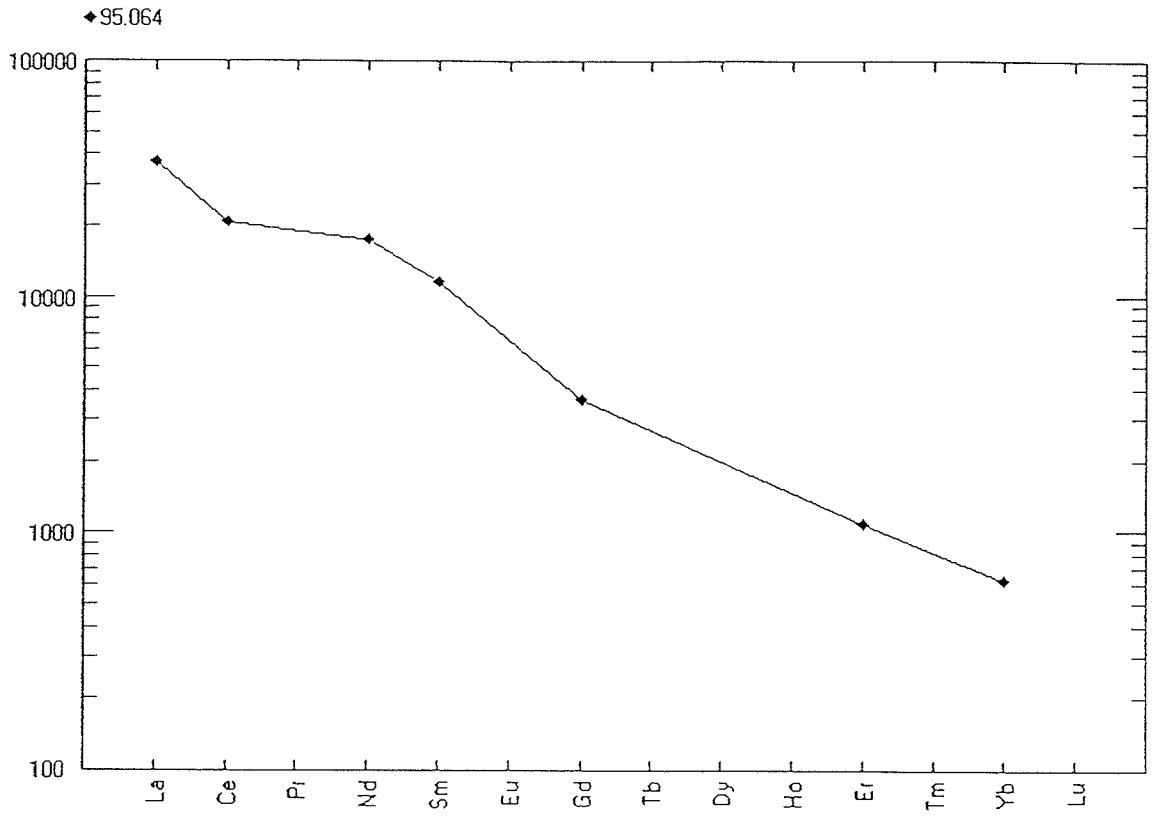

Figure 5.8. continued. C. Chondrite-normalized REE plots for titanite grains in the Type IV pegmatites. REE data from PIXE analysis. Normalization values are from Sun (1982).

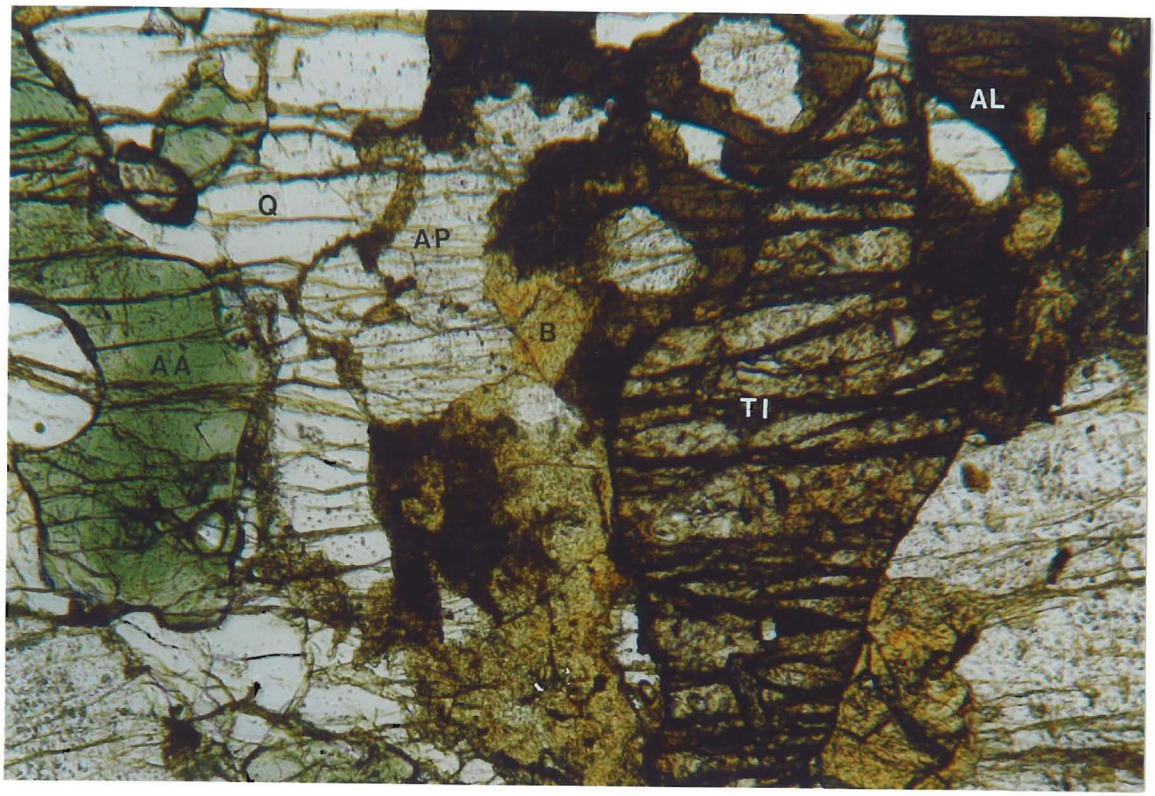

Figure 5.9. Photomicrograph of a titanite crystal in the Type IV pegmatites. The grain is euhedral, with a lozenge-shape and is pervasively cracked. Field of view is 2.8 mm in the long dimension. Mineral abbreviations are as follows: AA - aegirine-augite, AP - apatite, AL - allanite, B - britholite, TI - titanite, Q - quartz.

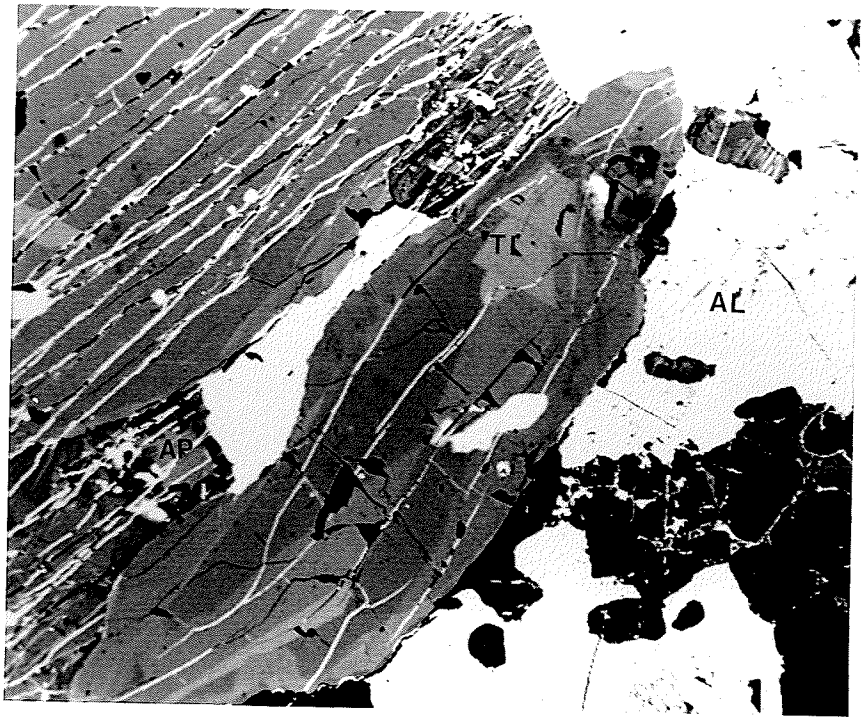

Figure 5.10. Photograph of a BSE image of a titanite grain from the Type IV pegmatites. The brightness differences represent oscillatory zoning. The bright veinlets are filled with britholite. Field of view is 400 microns in the long dimension. Mineral abbreviations are as follows: AL - allanite, TI - titanite.

Chemical data for the titanite crystals in Type IV pegmatites are presented in Table 5.2C. The oscillatory zoning observed within the titanite crystals from the Type IV pegmatites is related to variable Fe, Al, Na, Y, REE and F abundances. Dark zones contain higher Al, Fe, Y and F contents and bright zones have higher Na and REEs. REE plots for Type IV titanite grains are shown in Figure 5.8C; they show light REE-enrichment and the slopes and abundances are similar to plots of the Type A titanite crystals in the Type III pegmatites.

Chemical compositions for the Type IV titanite grains are remarkably similar to those of the Type A titanite grains (Table 5.2A and 5.2C). The most significant difference is that Y, REE and some trace elements are more abundant in the titanite grains of the Type IV pegmatites (Table 5.2); this may be due to a higher degree of fractionation in the Type IV pegmatites or may be an artifact of alteration of the Type IV titanite crystals. In general, the bright zone of each growth pattern has the highest REE contents (Table 5.2). The similarity of the chemical composition of titanite grains from the two pegmatites suggests that the titanite grains within the two pegmatites have a similar genesis; this will be discussed further in Chapter 6.

5.3. Zircon.

Zircon is a common accessory mineral in alkaline and peralkaline rocks and associated pegmatites (Deer et al., 1989). The chemistry of zircon is relatively simple; usually ZrO_2, HfO_2 and SiO_2 comprise more than 99 weight% (Hinton and Upton, 1991). However, substitution of Zr by LREEs, Y, Th, U and PO_4 are common, according to the reaction Y^{3+}

(or REE^{3+}) + P^{5+} ↔ Zr^{4+} + Si^{4+} (Romans et al., 1975; Speer, 1980; Clark, 1984). Zircon crystals are found in both the Type III and IV pegmatites as well as in the main units of the complex where they may have played a role in concentrating the REEs in the early crystallized phases.

Zircon grains are present only in amounts up to 2% in the Type III pegmatites. They are red to red brown in colour with a maximum size of 0.5 cm; shapes are euhedral to subhedral, with straight crystal faces (Figure 5.11). Examination of these zircon grains using BSE imaging reveals that they are zoned. There are two patterns observed: (1) oscillatory zoning (Figure 5.12A); and (2) discontinuous overgrowths similar to those observed in the Type III titanite crystals (Figure 5.12B). Some zircon grains also have core regions that are characterized by a slightly different brightness in BSE images (Figure 5.12C). These cores are less fractured than either the interior or the overgrowth. Both the oscillatory zoned regions and the overgrowths have embayed margins, indicating several stages of zircon growth and resorption. The similarity of titanite and zircon zoning patterns within the Type III pegmatites indicates a stratigraphy of mineral growth that may be applied to more than one mineral phase; this will be discussed further in Chapter 6. Mottled patterns within zircon crystals are also apparent from BSE imaging (Figure 5.12); these patterns suggest alteration of the zircon grains that might be related to metamictization.

Chemical compositions of zircon crystals from the Type III pegmatites are presented in Table 5.3A. The oscillatory zoning reflects changing abundances of both major and trace elements (Table 5.3A). The darker zones have higher Mo, Ba, Ca and Na

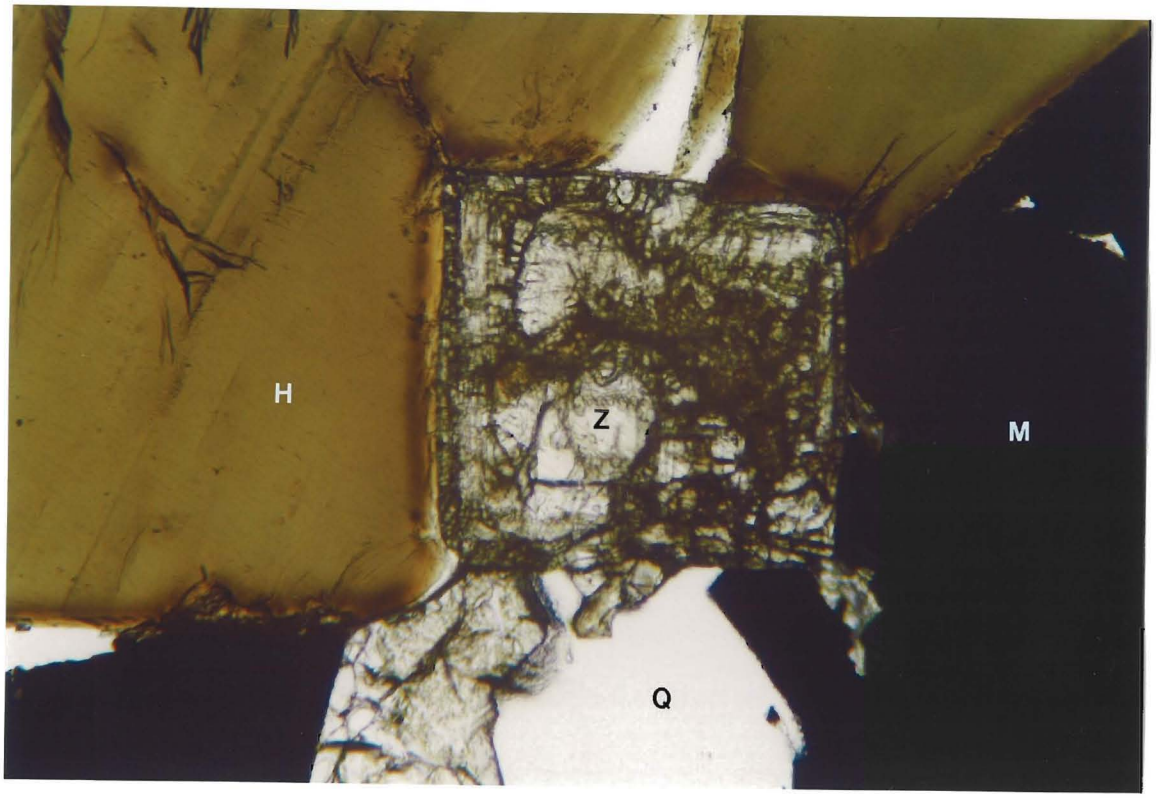

Figure 5.11. Photomicrograph of a square section across a euhedral zircon crystal in the Type III pegmatites. Field of view is 0.7 mm in the long dimension. Mineral abbreviations are as follows: M - magnetite, H - hornblende, Q -quartz, Z - zircon.

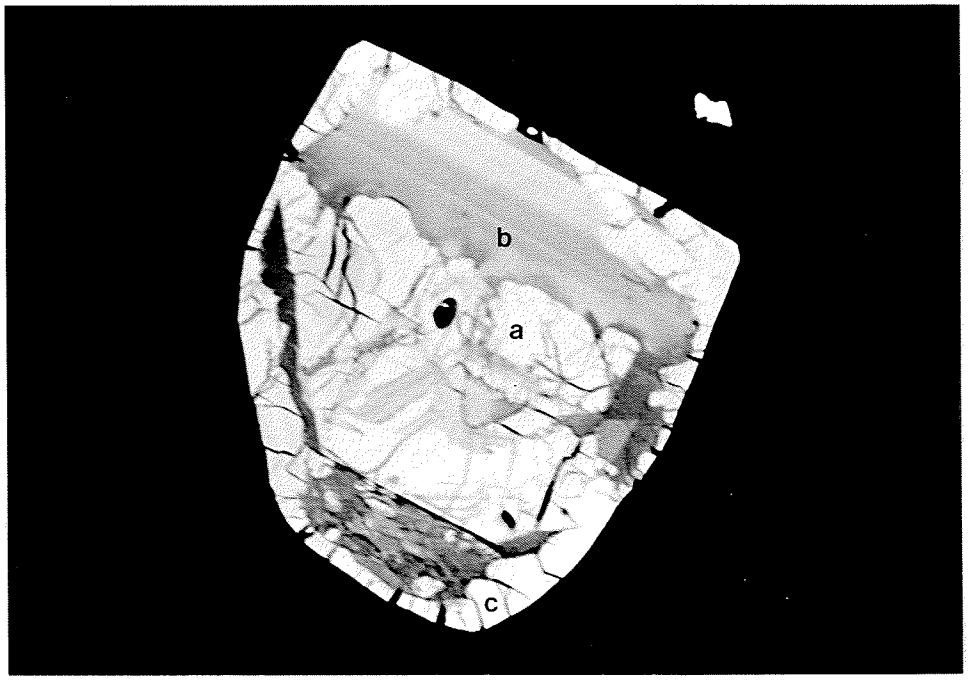

Figure 5.12. Photograph of a BSE image of a zircon crystal in the Type III pegmatites. A less fractured core (a), oscillatory zoning (b) and a bright overgrowth (c) are visible. The zircon crystal is 100 microns wide.

Table 5.3.A. Chemical compositions of zircon grains from the Type III pegmatites. Major element data were obtained using EPMA; trace element data are from PIXE analysis. Additonal compositions are presented in Appendix III.

Oxide (weight percent)	Bright Core	Dark Oscillatory Zone	Medium Oscillatory Zone	Bright Oscillatory Zone	Dark Overgrowth	Bright Overgrowth
ZrO_2	60.897	62.796	56.947	66.077	56.532	62.300
SiO_2	28.951	30.020	29.730	31.035	29.444	28.900
CaO	1.545	0.822	2.216	0.239	2.662	1.577
FeO^{T} [1]	2.226	0.232	0.657	0.002	0.531	1.471
HfO_2	0.256	0.202	0.165	0.207	0.159	0.356
Al_2O_3	0.501	0.042	0.427	0.026	0.340	0.088
MgO	0	0	0.017	0	0.003	0
Na_2O	0	0.593	0	0	0.558	0
TiO_2	0	0	0.005	0	0.026	0
P_2O_5	0	0.012	0	0.017	0	0.021
UO_2	1.838	1.040	2.895	0.158	1.789	0.715
REE_2O_3 [2]	2.182	0.605	1.328	0.088	0.76	1.106
TOTAL	96.214	95.759	93.059	97.761	92.044	95.428
Cr [3]	41	0	23	0	0	0
Mn	1314	865	1679	7	3483	1748
Co	578	602	642	514	492	396
Ni	94	44	52	46	27	52
Cu	73	70	81	76	62	98
Zn	59	86	116	7	56	23
Br	67	13	42	7	53	25
Sr	5286	273	657	22	891	1141
Mo	0	1956	1827	0	2157	0
Ba	1133	187	0	134	65	142
Y	3926	2954	6661	635	3589	2529
La	3583	0	0	0	0	704
Ce	8393	93	921	0	261	3057
Nd	0	16	244	21	126	1728
Sm	0	59	84	16	184	184
Gd	406	179	326	17	284	163
Dy	0	242	513	7	368	0
Er	766	370	777	3	430	531
Yb	1281	1055	1325	0	1000	372
Tl	118	56	79	43	83	0
Pb	471	2412	5045	449	1853	440
Th	1230	1007	4654	0	1788	295
Formula calculated on basis of 4 oxygen						
Zr^{4+}	0.959	0.988	0.919	1.014	0.92	0.99
Si^{4+}	0.935	0.969	0.984	0.977	0.983	0.941
Ca^{2+}	0.053	0.028	0.078	0.008	0.095	0.055
Fe^{2+}	0.06	0.006	0.018	0	0.015	0.04
Hf^{4+}	0.002	0.002	0.002	0.002	0.002	0.003
Al^{3+}	0.019	0.002	0.017	0.001	0.013	0.003
Mg^{2+}	0	0	0.001	0	0	0
Na^{+}	0	0.037	0	0	0.036	0
Ti^{4+}	0	0	0	0	0.001	0
P^{5+}	0	0	0	0.001	0	0.001

U^{4+}	0.013	0.007	0.021	0.001	0.013	0.005
Ce^{3+} [4]	0.026	0.007	0.016	0.001	0.009	0.013
Cation sum	2.068	2.047	2.057	2.004	2.088	2.051

1. Total iron expressed as FeO.
2. Total REE abundance expressed as REE_2O_3.
3. Trace element abundance in ppm.
4. Total REEs expressed as Ce^{3+}.

Table 5.3.A. continued.

Oxide (weight percent)	Dark part of Mottled Area	Bright part of Mottled Area
ZrO_2	60.117	54.288
SiO_2	28.659	28.291
CaO	1.263	3.959
FeO^T	1.414	3.712
HfO_2	0.178	0.166
Al_2O_3	0.058	0.535
MgO	0	0
Na_2O	0	0
TiO_2	0	0
P_2O_5	0	0
UO_2	1.578	1.494
REE_2O_3 [2]	1.097	1.597
TOTAL	93.267	92.445
Cr [3]	70	0
Mn	1557	1626
Co	945	655
Ni	0	129
Cu	0	119
Zn	82	70
Br	33	86
Sr	1538	5798
Mo	0	1606
Ba	379	666
Y	5358	2650
La	0	3227
Ce	213	4975
Nd	236	0
Sm	323	0
Gd	457	830
Dy	0	0
Er	1049	785
Yb	1352	1005
Tl	37	0
Pb	2168	287
Th	2140	4908
Formula calculated on basis of 4 oxygen		
Zr^{4-}	0.987	0.91
Si^{4-}	0.965	0.973
Ca^{2+}	0.045	0.146
Fe^{2-}	0	0
Hf^{4-}	0.002	0.002
Al^{3-}	0.002	0.021
Mg^{2-}	0	0
Na^{-}	0	0
Ti^{4-}	0	0
P^{5-}	0	0
U^{4-}	0.012	0.011
Ce^{3-} [4]	0.013	0.02

Cation sum	2.027	2.083

1. Total iron expressed as FeO.
2. Total REE abundance expressed as REE_2O_3.
3. Trace element abundance in ppm.
4. Total REEs expressed as Ce^{3+}.

Table 5.3. B. Chemical compositions of zircon grains from the Type IV pegmatites. Major element data were obtained using EPMA; trace element data are from PIXE analysis. Additonal compositions are presented in Appendix III.

Oxide (weight percent)	Bright Core	Unzoned Interior	Bright Overgrowth	Bright Mottled Area
ZrO_2	67.699	64.886	68.191	65.927
SiO_2	32.145	31.044	32.367	31.294
CaO	0.049	0.303	0.179	0.358
FeO^{T} [1]	0	0.044	0.017	0.069
HfO_2	0.180	0.200	0.173	0.198
Al_2O_3	0.008	0.038	0.026	0.012
MgO	0.004	0	0	0
Na_2O	0	0	0	0
TiO_2	0.032	0.008	0.025	0.009
P_2O_5	0.042	0.027	0.044	0.040
UO_2	0.100	0.071	1.141	0.165
REE_2O_3 [2]	0.312	0.886	2.527	1.403
TOTAL	100.571	97.507	104. 69	99.475
V [3]	-	-	85	-
Cr	-	-	231	-
Mn	-	-	0	-
Co	-	-	1319	-
Ni	-	-	89	-
Cu	-	-	102	-
Zn	-	-	0	-
Br	-	-	21	-
Sr	-	-	2841	-
Mo	-	-	0	-
Ba	-	-	0	-
Ta	-	-	473	-
Y	715	2445	13707	805
La	75	486	73	4890
Ce	865	2433	480	3915
Nd	650	1193	2174	1830
Sm	40	115	1173	120
Gd	-	-	966	-
Dy	-	-	656	-
Er	-	-	368	-
Yb	70	515	369	215
Lu	200	200	540	150
Pb	-	-	3475	-
Bi	-	-	383	-
Th	0	0	7935	20
Formula calculated on basis of 4 oxygen				
Zr^{4+}	1.009	1.0	0.996	1.002
Si^{4+}	0.983	0.982	0.969	0.975
Ca^{2+}	0.002	0.01	0.006	0.012
Fe^{2+}	0	0.001	0.001	0.002
Hf^{4+}	0.002	0.002	0.001	0.002
Al^{3+}	0	0.001	0.001	0
Mg^{2+}	0	0	0	0

Na^{-}	0	0	0	0
Ti^{4-}	0.001	0	0	0
P^{5+}	0.001	0.001	0.001	0.001
U^{4+}	0.001	0	0.008	0.001
Ce^{3-} [4]	0.003	0.01	0.028	0.016
Cation sum	2.002	2.008	2.01	2.011

1. Total iron expressed as FeO.
2. Total REE abundance expressed as REE_2O_3.
3. Trace element abundance in ppm.
4. Total REEs expressed as Ce^{3-}.

and the analysis totals are lower than those of the bright or medium bright zones in BSE images. Bright oscillatory zones have the highest Zr contents, while medium bright oscillatory zones have the highest Mn, Fe, Sr, Y, REEs, Pb, Th and U contents. The overgrowths have variable trace-element chemistry (Table 5.3A); dark overgrowths have higher Ca, Na, Mn, Mo, Y, Pb, Th and U contents, while bright overgrowths have higher P, Hf, Zr, Fe, Sr and REE contents. The bright overgrowths have the highest compositional totals (96%), whereas the dark overgrowths have the lowest totals (91%), probably resulting from considerable alteration or metamictization due to the high U and Th contents (Rubin et al., 1989). Chemical differences are also apparent in the mottled regions of zircon grains (Table 5.3A). The dark parts of mottled areas have higher Si, Na, Hf, Pb, U and heavy REE contents while the bright parts of mottled areas have higher Fe, Ca, Th and light REE values. The compositional totals for both of the mottled areas are generally low (~90%).

If we compare the chemistry of the different growth regions, it is apparent that (i) the highest REE contents are in the bright centres of the zircon crystals; (ii) the overgrowths have high Al, P, La, Ce, Nd, Sm and low Yb concentrations; (iii) the mottled areas have the lowest overall Zr and Hf contents; and (iv) the highest abundances of Zr are in the oscillatory zones (Table 5.3A). Metamictization of zircon is usually associated with high U and Th contents (Rubin et al., 1989); these range from 1400 ppm to 30 000 ppm in zircon grains from the Type III pegmatites (Table 5.3A). X-ray diffraction data obtained from a zircon crystal from the Type III pegmatites lacks any recognizable peaks in the spectrum (Appendix III), suggesting that the zircon grains are metamict, and that the structure has been completely destroyed. The REE abundances range from 5000 ppm to 18 000 ppm (Table 5.3A). REE

plots are shown in Figure 5.13; plots from both the different growth regions and from different zones of brightness within each region have different slopes, suggesting that the zoning cannot be directly related to REE distribution.

Zircon crystals are less common in the Type IV pegmatites than in the Type III pegmatites and are present only in trace amounts. The zircon crystals appear square to slightly rhombic in shape, highly fractured (Figure 5.14), and range in size from 0.18 to 0.4 mm. Zircon crystal boundaries are generally straight but contacts with allanite and britholite are irregular and embayed (Figure 5.14). The Type IV zircon grains contain irregular patches of britholite and apatite (Figure 5.14). The zircon grains are not isotropic in cross-polars as suggested by Chakoumakos et al. (1987) for metamict zircon crystals.

Examination of Type IV zircon grains using BSE imaging reveals that the zircon grains display a sequence of internal growth stratigraphy similar to that observed in the Type III zircon crystals (Figure 5.15): (i) a core region that is slightly brighter in BSE images and is generally less fractured than the rest of the grain; (ii) an unzoned interior; and (iii) overgrowths. Mottled areas are also present within the unzoned interior of zircon grains (Figure 5.15), suggesting alteration due to metamictization.

Chemical compositions of the Type IV zircon grains are presented in Table 5.3B. The core regions are characterized by low REE, U, Fe and Ca concentrations, the unzoned interiors have high concentrations of Fe, Ca, Hf, Y and Yb concentrations, whereas the overgrowths have the highest La, Ce, Nd, Sm, Lu, U and Zr concentrations. The mottled parts of zircon crystals have the lowest Zr and the highest Ca contents.

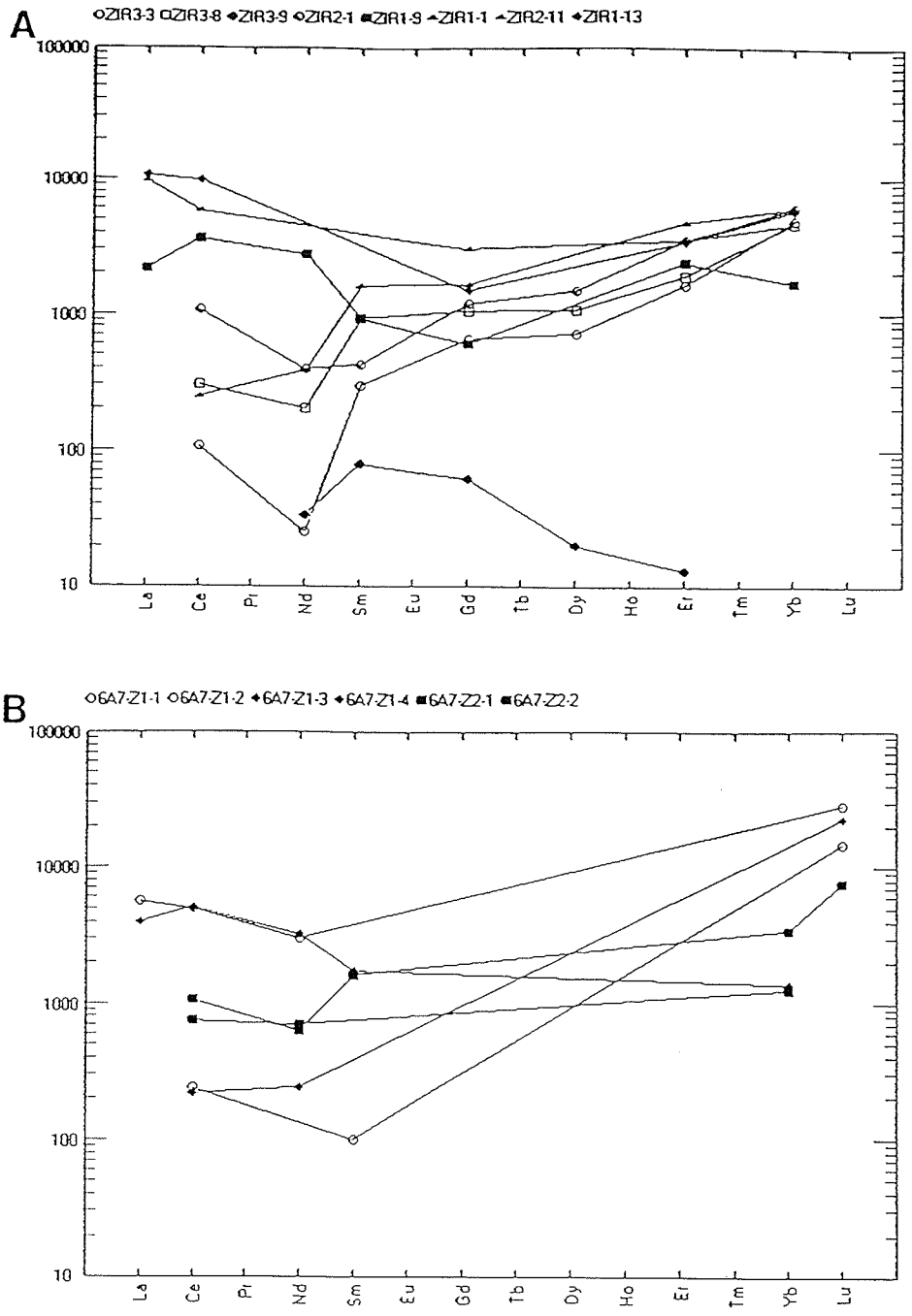

Figure 5.13. A. Chondrite-normalized REE plots for zircon crystals from the Type III pegmatites. REE values from PIXE analysis. Bright centres are shown by ♦, dark oscillatory zones are shown by ○, bright oscillatory zones are shown by ●, medium bright oscillatory zones are shown by ○, dark rims are shown by □, bright rims are shown by ■, dark parts of mottled areas are shown by △, and bright parts of mottled areas are shown by ▲. *B.* Chondrite-normalized REE plots for zircon crystals from the Type IV pegmatites. REE values from EMPA. Centres are shown by ♦, dark interiors are shown by ■, and bright rims are shown by ○. Normalization values are from Sun (1982).

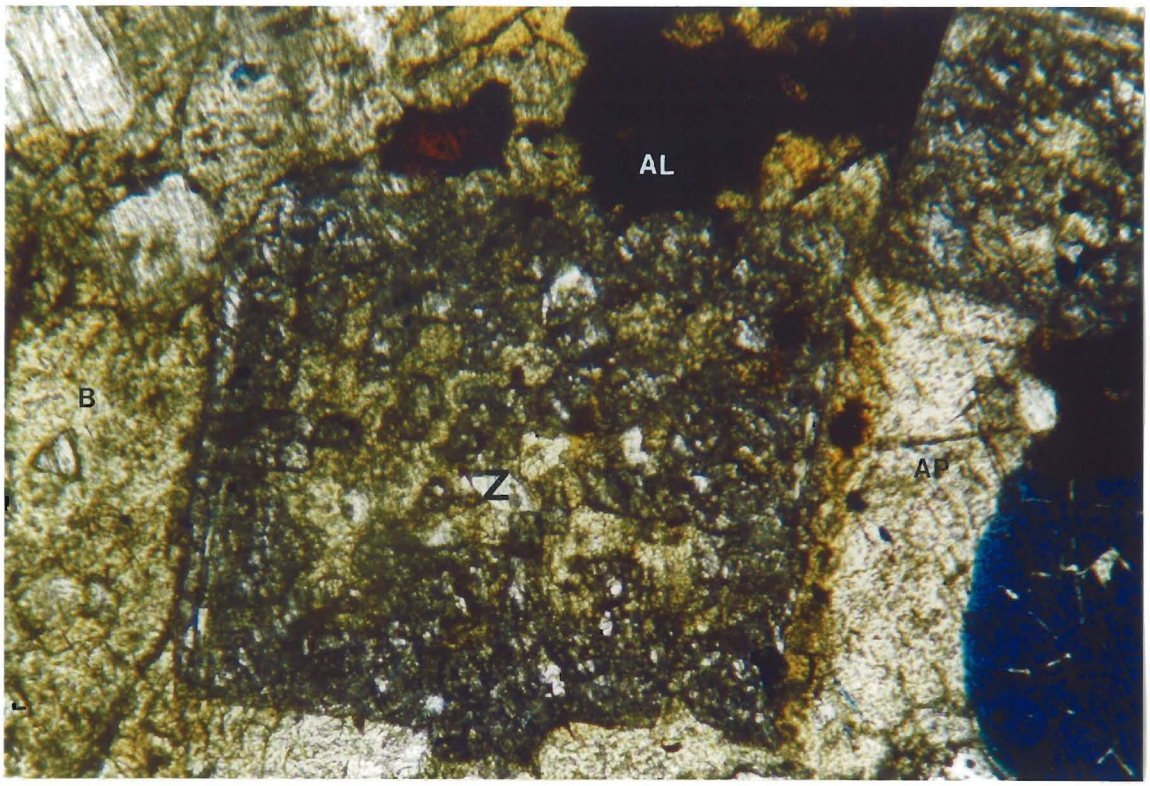

Figure 5.14. Photomicrograph of two zircon grains from the Type IV pegmatites. The crystals are very similar to the zircon crystals in the Type III pegmatites (see Figure 5.11). The crystal margins are straight to irregular. Field of view is 2.8 mm in the long dimension. Mineral abbreviations are as follows: AL - allanite, AP - apatite, B - britholite, Z - zircon.

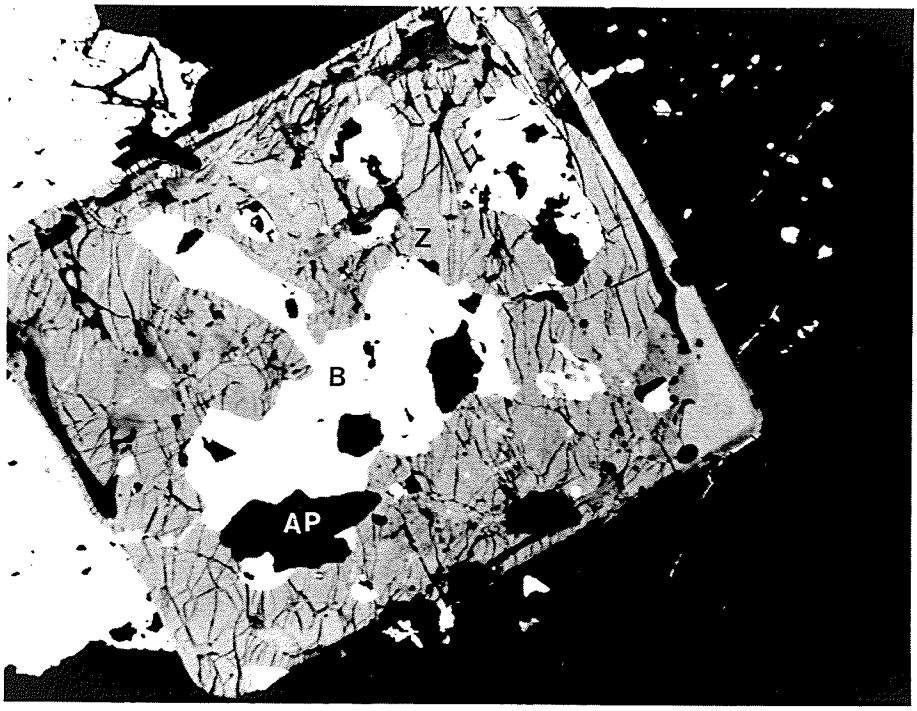

Figure 5.15. Photograph of a BSE image of a zircon crystal in the Type IV pegmatites. The grain contains a less fractured core and a brighter overgrowth. The mottled pattern suggests alteration of the zircon. The grain is 225 microns in width. Mineral abbreviations are as follows: AP - apatite, B - britholite, Z - zircon.

Comparing the chemistry of zircon grains in the Type III and IV pegmatites, the range of abundances of Si, Ti, Mg, Ca, P, Hf, Zr and REEs are similar. However, Y, Th, U and Na abundances are lower in the Type IV zircon crystals than in the Type III. In general, the bright zones of each zoning pattern have the high REE contents. The similar chemistry between the Type III and IV zircon crystals suggests that zircon crystals from the two pegmatites are genetically related.

5.4. Britholite.

Britholite, $(Ca,Ce,Y)_5(SiO_4,PO_4)_3(F,OH)$, is a member of an isomorphous series with apatite (Khudolozhkin et al., 1973). Britholite is a rare mineral; most of the documented occurrences are in alkaline intrusions (nepheline syenite complexes) in Russia, in the Oka carbonatite, and in a quartz monzonite in Argentina, the Rodeo de Los Molles deposit (Hughson and Sen Gupta, 1964; Khudolozhkin et al., 1973; Lira and Ripley, 1990; Mariano, 1989). REE abundance can be up to 60% (Hughson and Sen Gupta, 1964).

Britholite is only found within the Type IV pegmatites, where it occurs as anhedral irregularly-shaped masses with no observed cleavage. Britholite is brown, with a resinous to vitreous lustre, and a conchoidal fracture. It varies in abundance from 2 to 70% within the Type IV veins. In thin section, the britholite is yellow to light orange in colour, non-pleochroic and isotropic; some grains have a darker orange-coloured edge (Figure 5.16A). The britholite forms anhedral and irregular grains; within some grains, a polygonal pattern

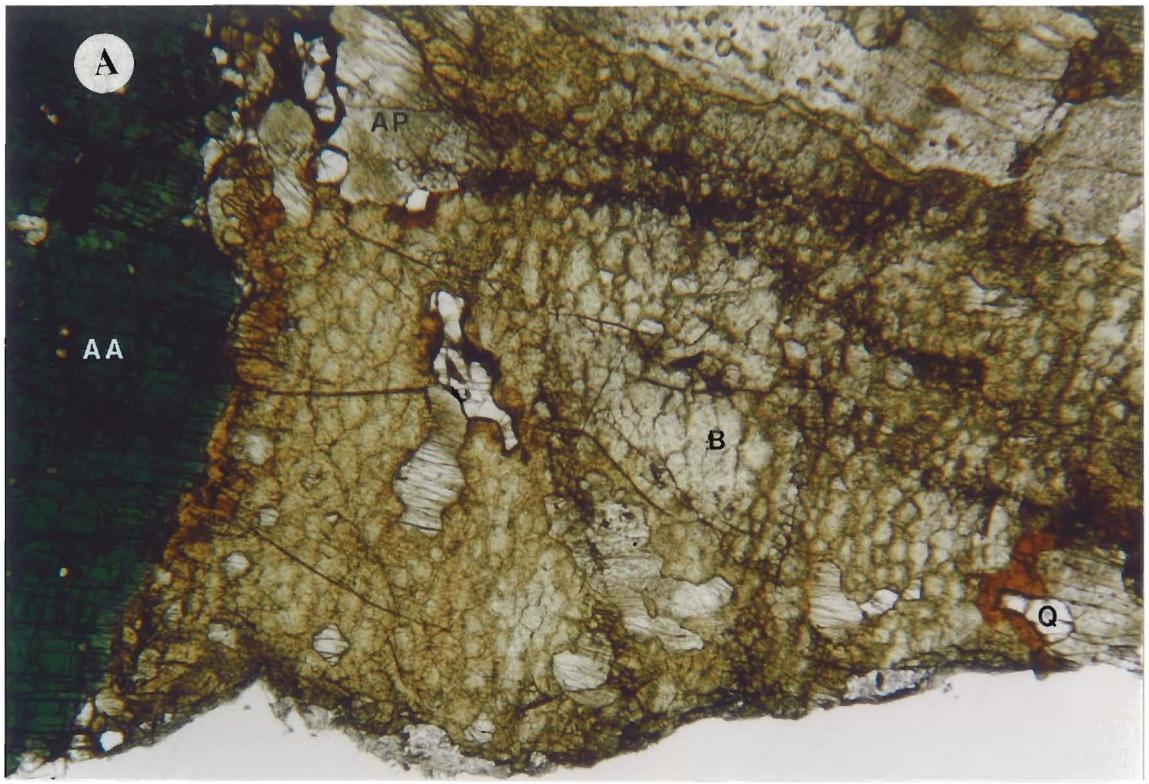

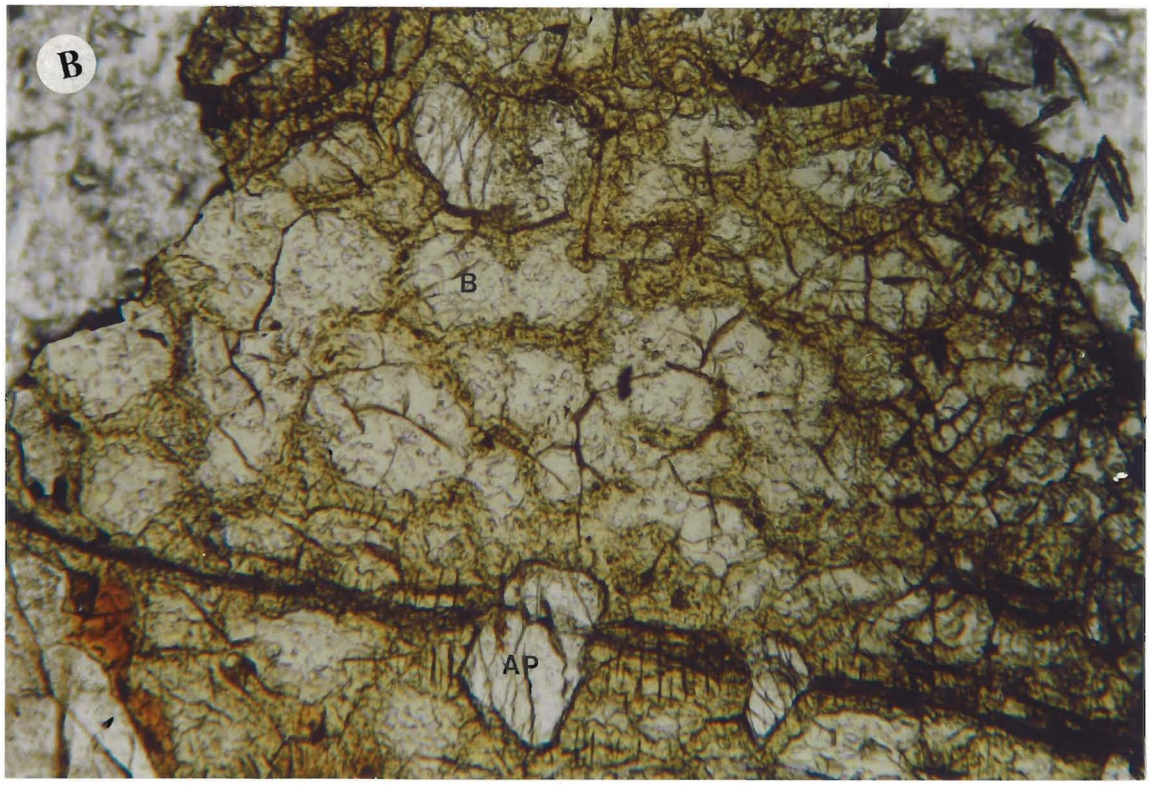

Figure 5.16. A. Photomicrograph of an anhedral, cracked, irregularly-shaped yellow britholite grain. The contacts with all other minerals are irregular and embayed. Field of view is 2.8 m in the long dimension. *B.* Photomicrograph of part of a britholite grain. Darker coloured, fractured areas highlight a polygonal pattern. Field of view is 0.7 mm in the long dimension.

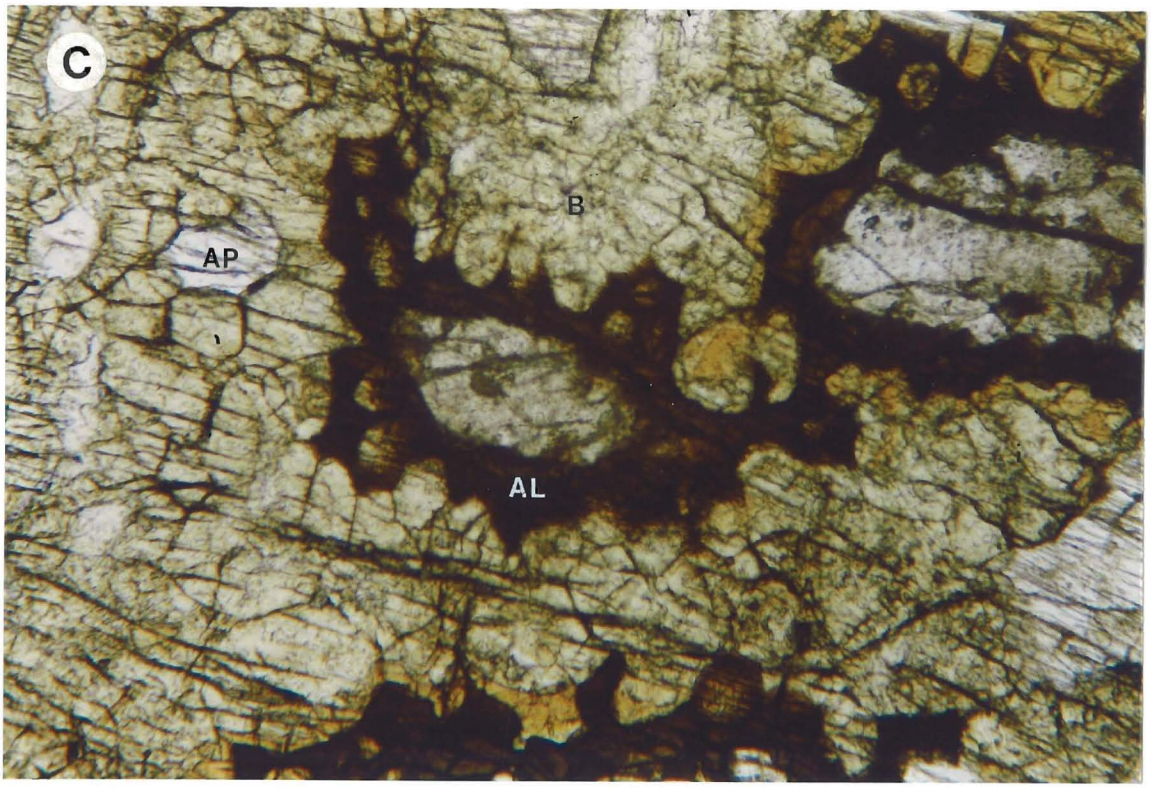

Figure 5.16. continued. C. Photomicrograph of part of a britholite grain. The contacts with allanite are very irregular and sutured, although on a smaller scale they appear straight. Field of view is 0.7 mm in the long dimension. Mineral abbreviations are as follows: AP - apatite, AL - allanite, AA - aegirine-augite, B - britholite, Q - quartz.

can be observed (Figure 5.16B). Margins of the anhedral grains vary from straight to sutured, whereas the margins of the polygons are straight (Figures 5.16A,B). The britholite grains range in size from 0.6 mm to 5 cm. Britholite is intimately associated with apatite, allanite and fluorite and surrounds grains of apatite, titanite, aegirine-augite, allanite, fluorite and a U-Pb phase. Britholite grains are commonly rimmed by allanite (Figure 5.16C); the contacts between britholite and allanite crystals tend to be straight along the edges of polygons, but are sutured where polygons cannot be distinguished. Britholite is commonly pervasively cracked and associated minerals, including aegirine-augite, titanite, quartz, K-feldspar, apatite and allanite, are also commonly cracked (Figure 5.16A)

Examination of the anhedral britholite grains using BSE imaging reveals that grains are made up of a number of smaller polygons (Figure 5.17); this is the same pattern that is apparent in thin sections. The polygons range in size from 20 to 200 microns, averaging from 50 to 100 microns. Polygon boundaries intersect at triple junctions with interfacial angles ranging from 60-180°, although an average triple junction has angles of 120° (based on measurements from 87 triple junctions; Appendix IV). This suggests that the polygons are in a stable arrangement where growth occurred during conditions of equal free energy of the grain surfaces (Vernon, 1976); this will be discussed further in Chapter 6. In some britholite polygons, a faint oscillatory zoning pattern concentric about a central core is apparent, while in others, a patchy discontinuous pattern is observed (Figure 5.17). Anhedral to subhedral crystals of apatite occur ubiquitously in the margins between the britholite polygons (Figure 5.17). These range

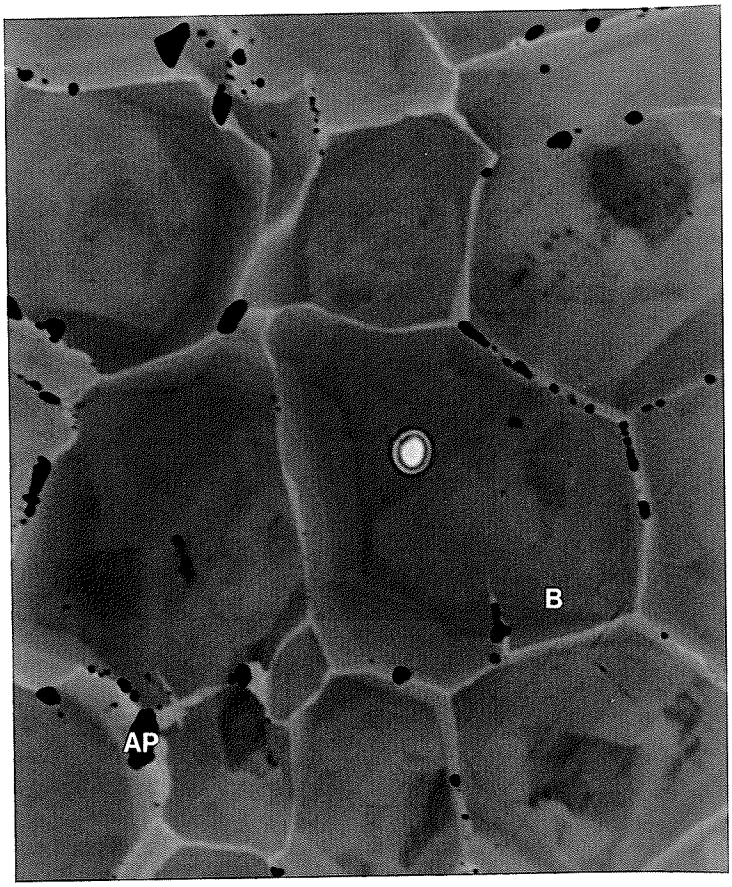

Figure 5.17. Photograph of a BSE image of part of a britholite grain (B). Britholite polygons are separated by boundaries that appear brighter due to topographic effects. All boundaries intersect at triple junctions. Some polygons contain oscillatory zoning, others patchy zoning. Apatite (AP) grains occur in the polygonal boundaries. Field of view is 200 microns in the short dimension.

in size from 10 to 100 microns, and lack well defined crystal margins (Figure 5.17).

Further examination of the BSE images reveals that many of the britholite polygons are altered (Figure 5.18). The alteration has a vermicular to colloform appearance and is concentrated along the margins of the britholite polygons (Figure 5.18A). The alteration advances from the polygon boundary to the centre; polygons range from partially to completely altered (Figure 5.18). In the most altered samples, the polygonal boundaries are completely obliterated, but in partially altered grains, the boundaries can still be seen (Figure 5.18). The less altered polygons tend to be in the centre of the anhedral grains, whereas the more altered britholite tends to be in contact with other pegmatite minerals, near the margins of the anhedral grains. In some polygons, more than one alteration front is apparent (Figure 5.18C); fractures in the altered britholite closest to the polygon interior are cut off by younger alteration fronts (Figure 5.18C). The shapes of the interstitial apatite grains do not appear to be affected by the alteration. In thin section, the altered britholite has a darker tan colour and is more fractured (Figure 5.16B).

The altered britholite has a different brightness in BSE images suggesting a different composition than the unaltered britholite. In order to characterize these compositional differences, chemical compositions were obtained for both the altered and unaltered britholite polygons. These compositions are summarized in Table 5.4. The major element oxide abundances in both the unaltered and altered britholite are similar to those reported in the literature (Table 5.4). The britholite contains both U and Th; the amount of Th is 5 times lower than that reported by Hughson and Sen Gupta (1964; Table 5.4).

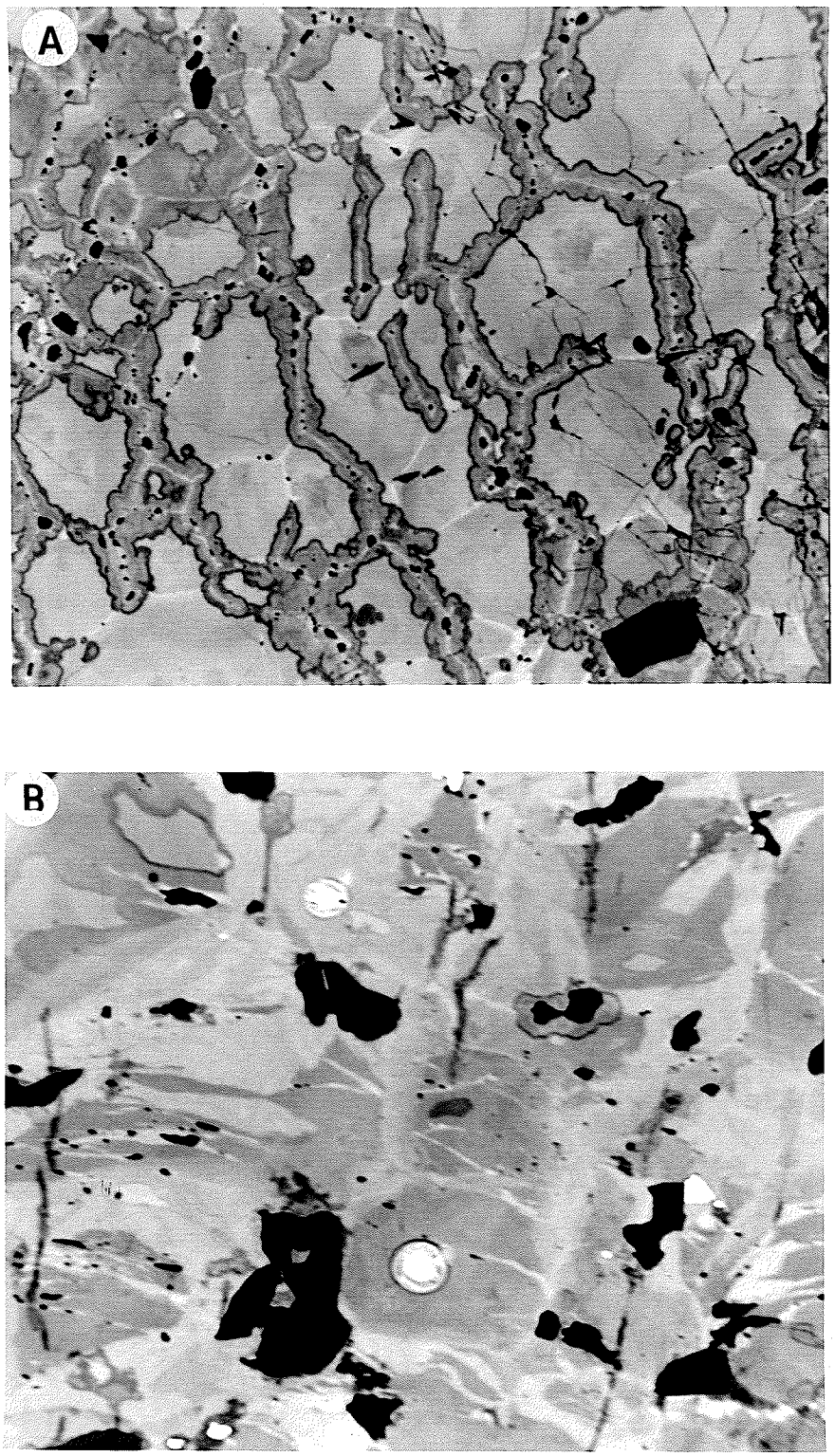

Figure 5.18. Photographs of BSE images showing altered britholite. *A.* Very slightly altered britholite; note the control of the polygonal boundaries on the alteration. Field of view 400 microns in the long dimension. *B.* Complete alteration of the britholite polygons; boundaries have been completely destroyed. Field of view 200 microns in the long dimension.

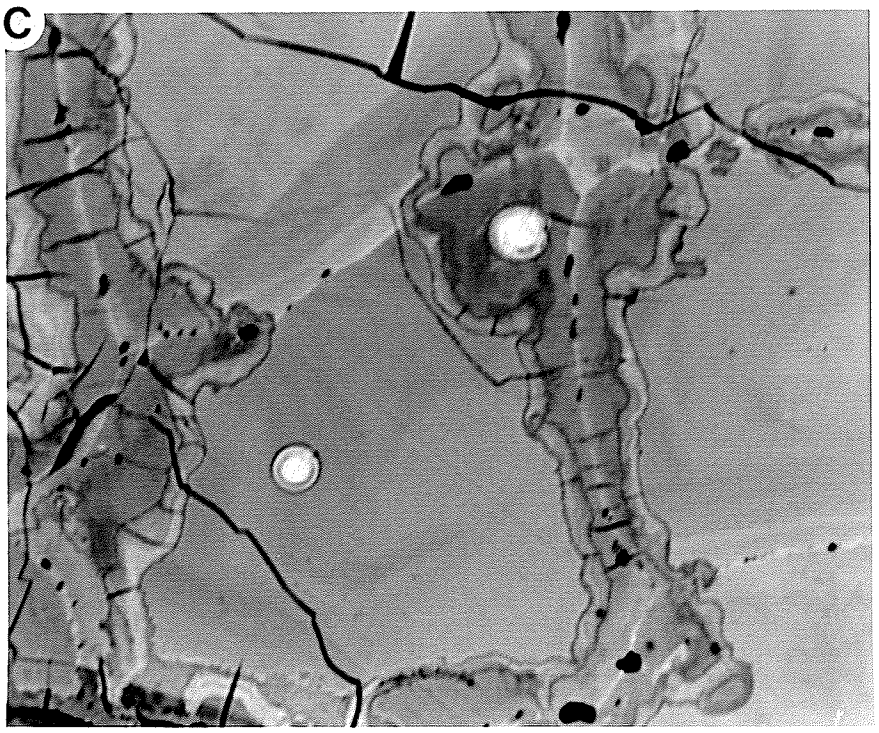

Figure 5.18. continued. C. Detail of altered polygonal boundaries; two fronts of alteration are visible along the boundary. Fractures within the older front are cut off by the younger front. Field of view is 150 microns in the long dimension.

Table 5.4. Representative chemical compositions of britholite grains from the Type IV pegmatites; all data were obtained using EPMA. Additional compositions are presented in Appendix IV.

Oxide (weight percent)	Pegmatite IV - Altered	Pegmatite IV - Unaltered	Boggild (1905)	Hughson and Sen Gupta (1964)	Nash (1972)
SiO_2	19.05	19.45	16.77	12.28	16.20
FeO	0.005 [1]	0	-	-	-
Fe_2O_3	-	-	0.43	0.14	0.08
CaO	15.23	15.79	11.28	28.84	16.60
Al_2O_3	0.04	0.13	-	0.47	0.09
TiO_2	0.01	0.01	-	-	-
BaO	-	-	-	-	0.07
SrO	-	-	-	-	0.46
PbO	-	-	-	-	0.24
MgO	-	-	0.13	-	0.02
K_2O	-	-	-	-	0.07
UO_2	0.81	0.79	-	-	-
ThO_2	0.94	0.84	-	5.62	-
Y_2O_3	1.91	1.92	Σ60.54 [2]	Σ33.43 [2]	0.40
La_2O_3	8.23	8.71			16.3
Ce_2O_3	23.94	24.92			22.50
Nd_2O_3	12.94	13.10			6.92
Sm_2O_3	1.90	1.92			1.66
Eu_2O_3	0.31	0.30			0.61
Gd_2O_3	-	-			2.85
Dy_2O_3	0.49	0.52			0.29
Ho_2O_3	-	-			0.98
Er_2O_3	-	-			0.26
Yb_2O_3	-	-			0.18
Nb_2O_5	-	-	-	-	0.13
P_2O_5	3.62	3.73	6.48	16.96	7.03
F	2.56	3.13	1.33	2.10	3.80
Cl	0.11	0.04	-	-	0.28
OH	1.468		1.27	0.54	-
S	-	-	-	-	0.07
TOTAL	96.46	99.57	98.23	100.38	98.09
Formulas calculated on basis of 12 oxygen and 1 (F,Cl)					
Si^{4+}	2.623	2.583	2.291	1.369	2.061
Fe^{2+}	0.001	0	0.044	0.012	0.008
Ca^{2+}	2.247	2.247	1.651	3.446	2.263
Al^{3+}	0.006	0.02	0	0.062	0.013
Ti^{4+}	0.001	0.001	0	0	0
U^{4+}	0.025	0.023	0	0	0
Th^{4+}	0.029	0.025	0	0.143	0
Ce^{3+} [3]	2.507	2.498	3.027	1.365	2.597
P^{5+}	0.422	0.419	0.749	1.601	0.757
Cation sum	7.862	7.817	7.762	7.997	7.699
F-	1.115	1.315	0.575	0.741	1.529
Cl-	0.026	0.009	0	0	0.06

1. Total iron expressed as FeO.
2. Sum of all REE abundances.
3. Total REEs expressed as Ce^{3+}.

Total REE contents in the britholite range from 52.8% to 54.56%; these values are similar to the total REE content reported by Nash (1972). However, the Type IV britholite has higher Nd and lower La values than the britholite documented by Nash (1972).

Differences in the chemistry between the altered and unaltered britholite are as follows: (i) The weight present totals of the altered britholite are consistently lower than the totals for the unaltered britholite (Table 5.4), suggesting a higher volatile content in the altered britholite. Independent water determinations on bulk britholite samples (ones that contain both altered an unaltered britholite) indicate the presence of about 1.5% water (Table 5.4; Appendix IV). This suggests that the volatile phase present within the altered britholite is water. (ii) The ratio of fluorine to chlorine is lower in altered britholite than in unaltered britholite. (iii) The REE abundance also varies. Although the ratio of Ce to La remains constant, the amount of La+Ce is lower in the altered britholite (Table 5.4). The REE patterns for both the unaltered and altered britholite polygons are shown in Figure 5.19 A and B; the patterns are essentially identical, with LREE enrichment and a small negative europium anomaly.

Analysis of britholite grains using precession camera methods reveals that the britholite has little to no crystal structure (Figure 5.20). This suggests that either the britholite structure has been destroyed by post-crystallization processes such as metamictization or amorphization, or that the britholite formed without a coherent structure; this will be discussed in Chapter 6.

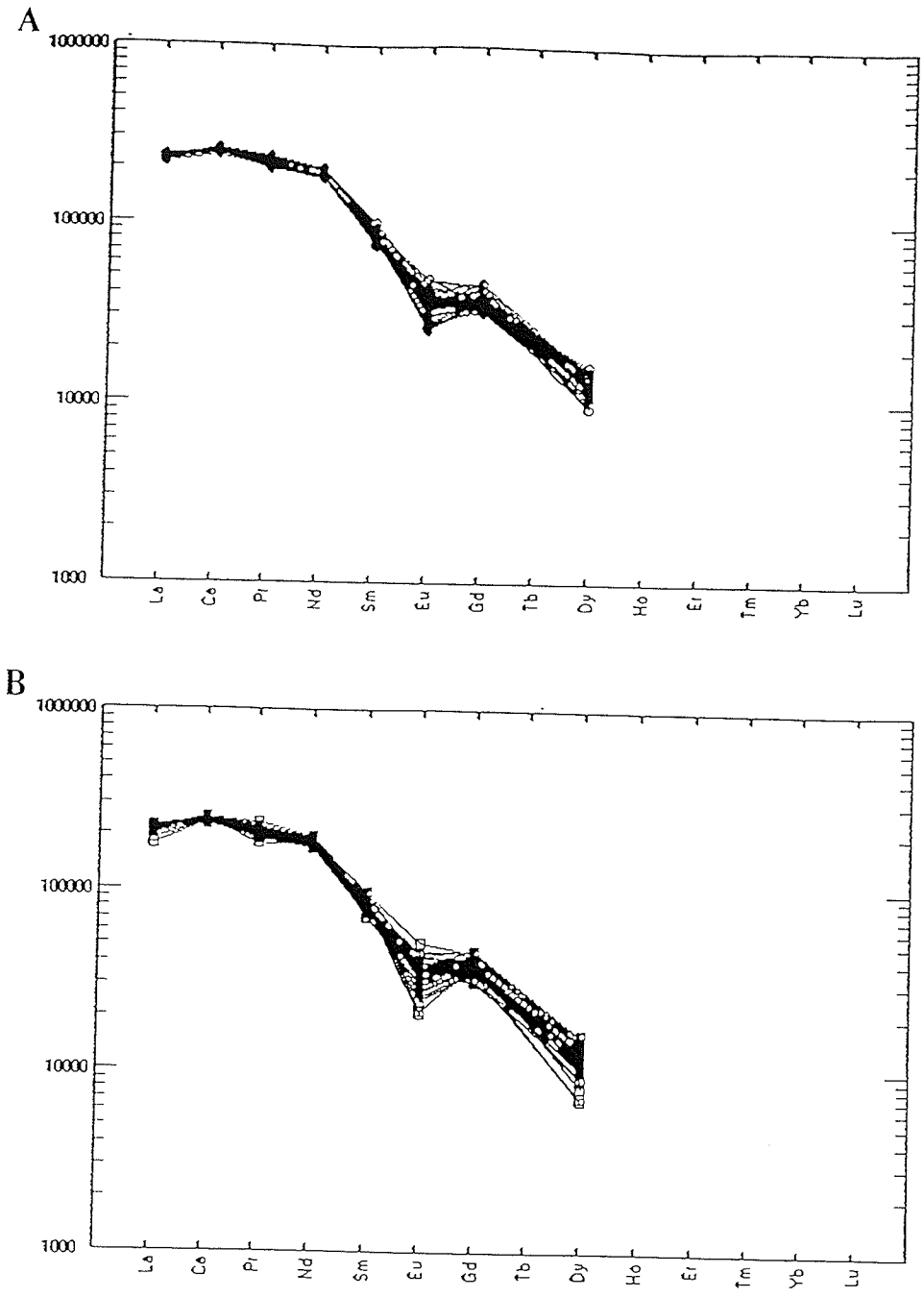

Figure 5.19. Chondrite-normalized REE plots for *A* unaltered and *B* altered britholite. Unaltered britholite are shown by ○; altered britholite are shown by □. Normalization values are from Sun (1982).

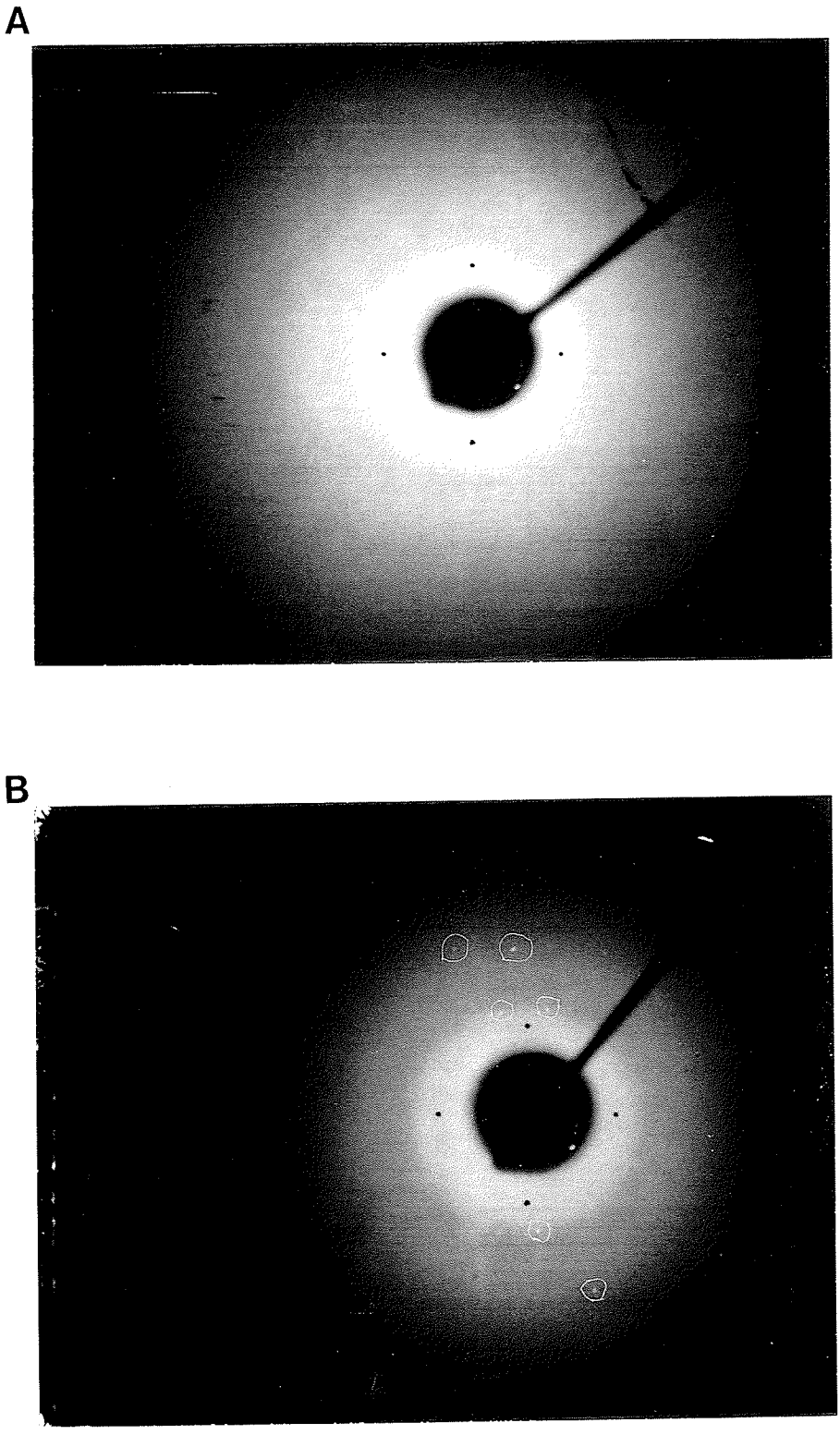

Figure 5.20. Precession camera photos of britholite samples. *A.* The lack of significant diffraction spots suggest the britholite is amorphized. *B.* The presence of a few diffraction spots (highlighted by the white circles) indicates that the britholite has some remnant structure.

5.5. Allanite.

Allanite, $(Ca,REE)_2(Fe,Ti,Al)Si_3O_{12}(OH,F,Cl)$, is a REE and ferrous iron-bearing member of the epidote group (Deer et al., 1986). It is a common accessory mineral in many granites, granodiorites, monzonites and syenites and occurs in high abundances in some pegmatites (Morin, 1977; Clark, 1984; Deer et al., 1986). Allanite has also been documented from the Rodeo de Los Molles deposit in Argentina where it occurs in association with britholite (Ripley and Lira, 1990). Allanite is a significant host for the REEs; it is usually Ce-rich (Clark, 1984).

Allanite is only found in the Type IV pegmatites associated with the Eden Lake syenite complex. In hand samples, the allanite cannot be distinguished from the anhedral britholite masses; in thin section, the allanite is red brown to black in colour (Figure 5.16A,C) and has brown to black pleochroism. Allanite grains are irregular and anhedral and occur as rims around britholite and apatite or as inclusions within aegirine-augite (Figure 5.16A,C). Crystal margins are generally scalloped and irregular, although straight contacts have been observed where allanite rims britholite (Figure 5.16C). Allanite abundance within the Type IV pegmatites ranges from 1 to 20%.

In BSE images, most allanite grains appear to be compositionally homogeneous (Figure 5.21A,B). However, a few grains have a discontinuous and irregular zoning (Figure 5.21A); this is probably a result of metamictization of associated britholite (Morin, 1977; Pan and Fleet, 1990). Allanite grains associated with britholite contain abundant subparallel cracks, some of which are filled with britholite (Figure 5.21A). Allanite inclusions within aegirine-augite are also fractured, but to a lesser degree (Figure 5.21B).

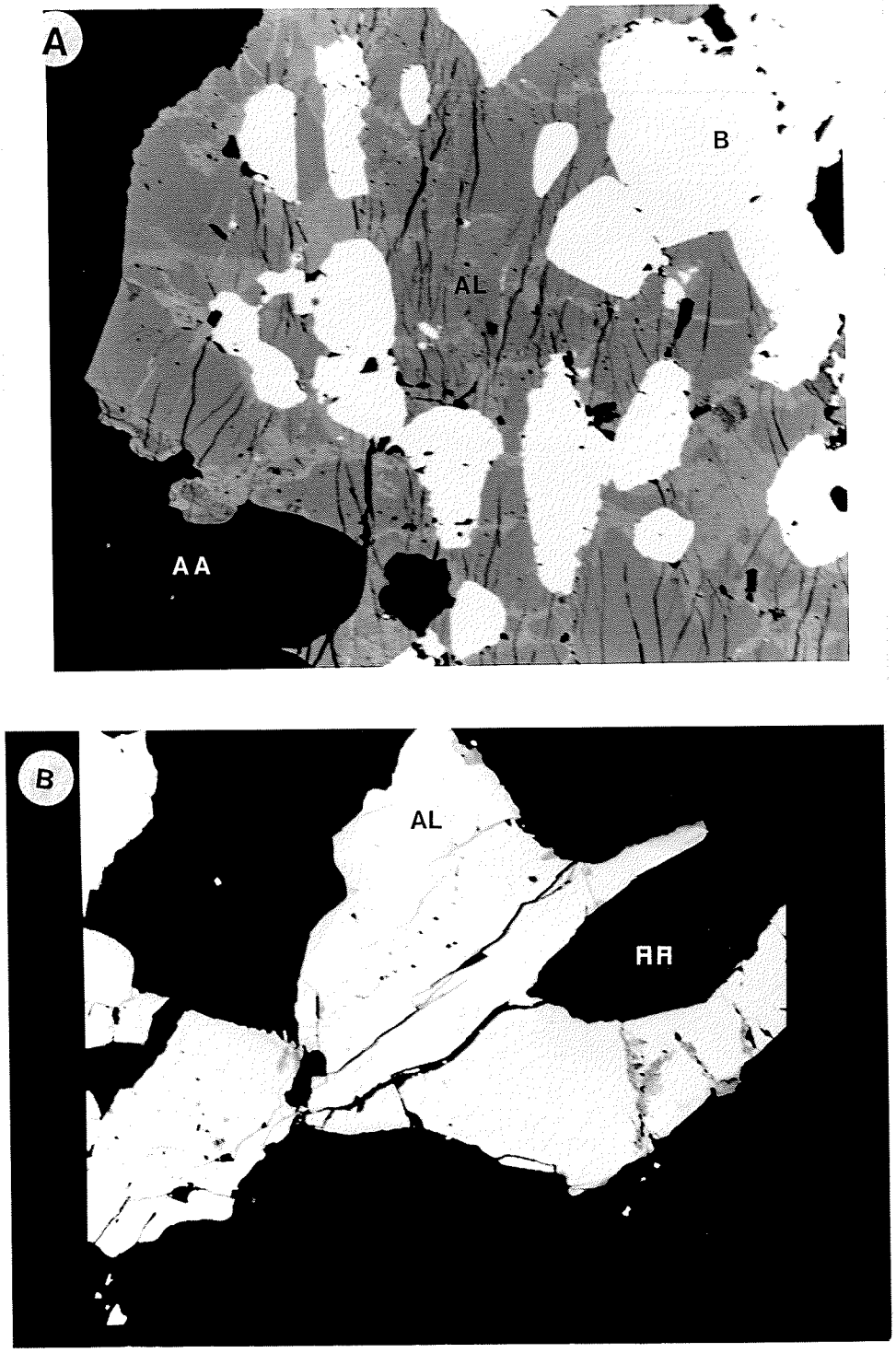

Figure 5.21. Photographs of BSE images of allanite grains. *A.* Allanite associated with britholite; note the random irregular zoning and prevalent fractures. Field of view is 400 microns in the long dimension. *B.* Allanite associated with aegirine-augite. This grains appears compositionally homogeneous and contains less fractures. Field of view is 200 microns in the long dimension. Mineral abbreviations are as follows: AA - aegirine-augite, AL - allanite, B - britholite.

Chemical compositions of allanite grains are presented in Table 5.5. The allanite compositions, in terms of the major and minor oxides, are similar to those published in the literature (Smith et al., 1957; Ghent, 1972; Pan and Fleet, 1990). Compositional totals are about 95 to 96 weight % oxide; these are similar to totals of altered and metamict allanite recorded by Ghent (1972). The discontinuous zoning reflects Al, Mg, Ca variations; the darker zones have higher Ca while the brighter zones have higher Al and Mg values. REE abundances range from 23-27 weight% and are the same in the dark and bright zones (Table 5.5). Rare earth element plots for allanite are shown in Figure 5.22; these are LREE-enriched.

5.6. Andradite.

Garnets are characteristic of metamorphic rocks, but may also be found in igneous rocks. Andradite garnet, $Ca_3(Fe^{3+},Ti)_2Si_2O_{12}$, can occur in alkaline rocks such as nepheline syenite (Deer et al., 1989). Rarely is the pure andradite end-member found, although garnet with up to 95% andradite has been documented (Deer et al., 1989). Andradite generally has low REE abundances, but it does tend to concentrate the heavy REEs (Henderson, 1984). Andradite grains are present only in some of the Type III pegmatites associated with the syenite complex.

In hand sample, the andradite crystals are black in colour, appear euhedral and have a size range of 0.75 mm to 2 cm. They range in abundance from 5 to 10% where present. In thin section, andradite crystals are brown to tan in colour and isotropic with subhedral to anhedral, pseudo-dodecahedral shapes (Figure 5.23A). Crystal boundaries are

Table 5.5. Representative chemical compositions of allanite crystals from the Type IV pegmatites. Major element data were obtained using EPMA; trace element data is from PIXE analysis. Additional compositions are presented in Appendix V.

Oxide (weight percent)	Unzoned	Dark Zone	Bright Zone	Ghent (1972)[1]	Pan and Fleet (1990)[2]
SiO_2	28.771	28.587	28.853	32.20	33.37
FeO^{T} [3]	20.563	20.069	20.249	16.80	7.93
Al_2O_3	8.010	8.236	7.787	14.10	20.60
CaO	9.948	9.586	9.373	6.20	13.12
MnO	0.570	0.564	0.715	0.10	1.29
MgO	0.590	0.671	0.790	0.60	1.20
TiO_2	0.859	0.832	1.055	2.40	0.15
Y_2O_3	0.015	0.034	0.111	0.100	0.223
La_2O_3	6.911	5.993	5.315	4.0	4.48
Ce_2O_3	13.709	8.847	9.292	5.7	9.0
Nd_2O_3	3.35	1.767	2.518	0.5	4.15
Sm_2O_3	0.141	0.217	0.145	0.2	0.56
Gd_2O_3	0.001	0.053	0.029	-	-
Yb_2O_3	0.011	0.005	0.012	-	0.06
ThO_2	0.15	0.085	0.201	0.8	0.1
P_2O_5	0.027	0.025	0.005	-	-
F	0.269	0.196	0.254	0.20	0.50
Cl	0.006	0.011	0.003	-	0.86
TOTAL	93.901	85.474	86.528	83.90	89.99
Co [4]	-	1111	1136	-	-
Ni	-	23	39	-	-
Cu	-	9	23	-	-
Zn	-	697	606	-	-
Ga	-	29	32	-	-
Sr	-	2356	2650	-	-
Mo	-	4	6	-	-
Pb	-	88	428	-	-
U	-	125	1065	-	-
Formula calculated on basis of 12 oxygen + 1 F, Cl					
Si^{4+}	3.223	3.343	3.352	3.458	3.123
Fe^{2+}	1.926	1.963	1.968	1.509	0.621
Al^{3+}	1.058	1.134	1.067	1.785	2.272
Ca^{2+}	1.194	1.200	1.167	0.713	1.316
Mn^{2+}	0.054	0.055	0.07	0.009	0.102
Mg^{2+}	0.099	0.117	0.137	0.096	0.167
Ti^{2+}	0.072	0.073	0.092	0.194	0.011
Ce^{3+} [5]	0.99	0.724	0.741	0.413	0.65
Th^{4+}	0.004	0.002	0.005	0.02	0
P^{5+}	0.003	0.002	0.001	0	0
Cation sum	8.624	8.614	8.599	8.196	8.263
F-	0.096	0.07	0.092	0.068	0.148
Cl-	0.002	0.002	0	0	0.136

1. Analysis of portion of altered allanite crystal.
2. Total iron is expressed as FeO^{T}.
3. Average of 10 analyses of REE-rich margin of allanite crystal.
4. Trace element abundance in ppm.
5. Total REEs expressed as Ce^{3+}.

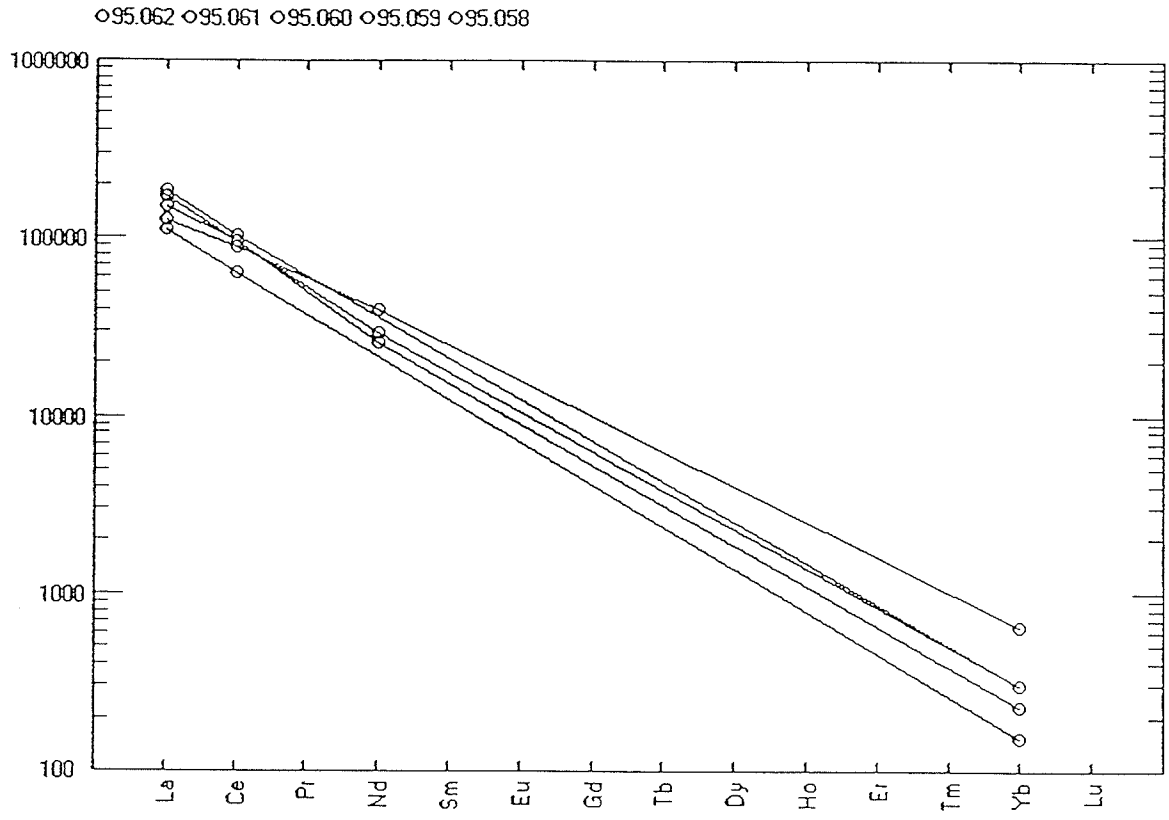

Figure 5.22. Chondrite-normalized REE plots for allanite from the Type IV pegmatites. REE values from PIXE analysis. Normalization values are from Sun (1982).

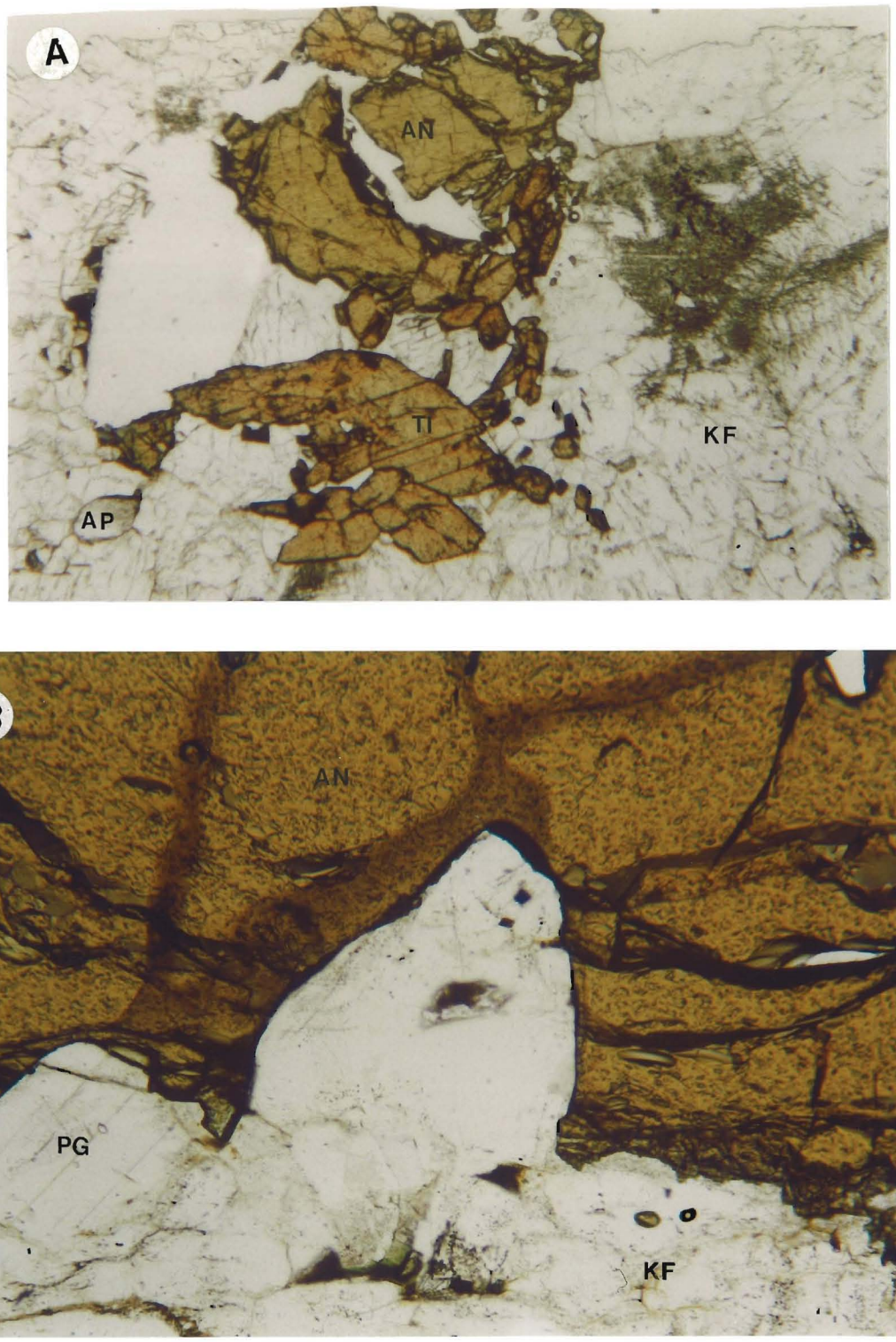

Figure 5.23. A. Photomicrograph of subhedral andradite crystals, associated with lozenge-shaped titanite grains, in the Type III pegmatites. Field of view is 2.8 mm in the long dimension. *B.* Photomicrograph showing part of andradite crystal margin with large embayment. The darker brown colour within the andradite results from alteration of the andradite. Field of view is 0.7 mm in the long dimension. Mineral abbreviations are as follows: AP - apatite, AN - andradite, KF - K-feldspar, PG - plagioclase, Q -quartz, TI - titanite.

straight to slightly curved. Rare embayments along the edges of the andradite crystals are observed; the largest is 0.4 mm wide and extends 0.4 mm into the andradite grain (Figure 5.23B). Parts of the garnet grains near the embayments have a darker brown colour (Figure 5.23B); these darker areas extend into the crystal and are probably the result of alteration of the garnet.

Examination of BSE images of andradite crystals shows that the grains are not zoned and are compositionally homogeneous (Figure 5.24). The darker brown areas associated with the embayments have a brighter colour in BSE images, indicating they have a different chemistry than the rest of the garnets. Chemical compositions for andradite grains are presented in Table 5.6; the altered andradite has higher Fe and lower Al abundances than the unaltered andradite (Table 5.6). REE plots for andradite are shown in Figure 5.25; as expected, they are HREE-enriched. However, the REEs are not very abundant within the garnet; they total only ~1000 ppm (Table 5.6).

5.7. Fluorite.

Fluorite, CaF_2, can be found as an accessory mineral in granites, syenites and related pegmatites where it occurs as a late stage crystallization, mainly hydrothermal mineral (Deer et al., 1989). Most fluorite compositions are at least 99% CaF_2, but the REEs can substitute for Ca in the mineral structure (Deer et al., 1989). Fluorite grains are present in Type III and IV pegmatites.

Fluorite grains in the Type III pegmatites have an irregular shape and a purple colour. In thin section, the fluorite is purple to clear in colour, with the darker purple

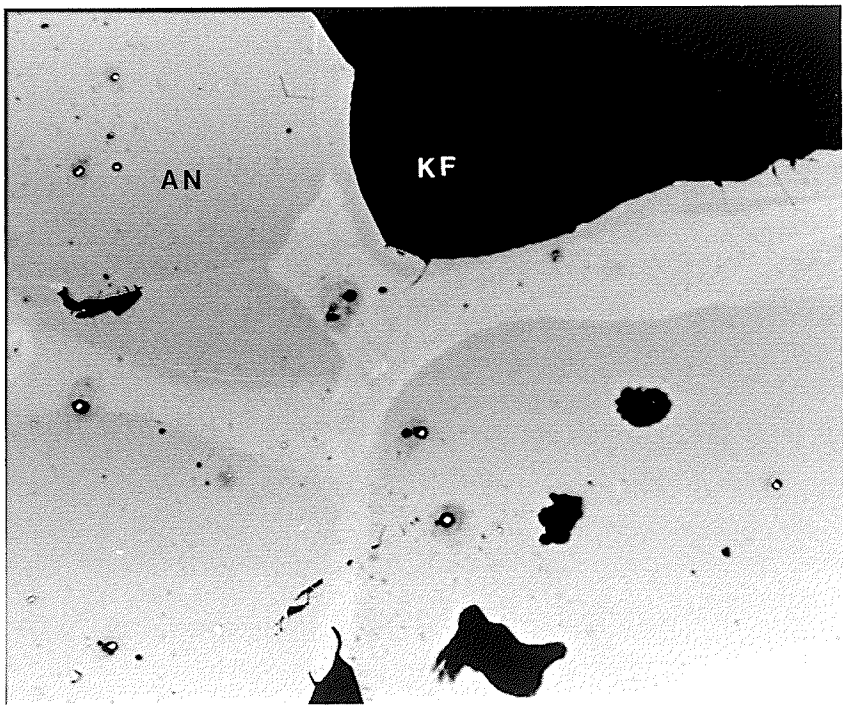

Figure 5.24. Photograph of BSE image of andradite grain; it is compositionally homogeneous, except for the brighter altered areas. Field of view is 600 microns in the long dimension. Mineral abbreviations are as follows: An - andradite, KF - K-feldspar.

Table 5.6. Representative chemical compositions of andradite crystals from the Type III pegmatites. All chemical data were obtained from EPMA. Additional compositions are presented in Appendix VI.

Oxide (weight percent)	Unaltered	Unaltered	Altered
SiO_2	35.072	35.118	34.669
CaO	31.538	31.346	30.396
Fe_2O_3[1]	28.296	29.032	30.081
Al_2O_3	1.957	1.555	1.037
TiO_2	0.944	0.733	0.619
MnO	1.002	1.09	1.365
MgO	0	0	0.003
TOTAL	98.809	98.874	98.170
V[2]	1117	840	1095
Zr	221	206	345
Y	2391	2166	2610
La	24	12	50
Ce	91	14	290
Nd	312	198	295
Yb	385	572	215
Lu	129	114	650
U	77	78	180
Formulas calculated on basis of 12 oxygen			
Si^{4+}	2.972	2.982	2.976
Ca^{2+}	2.864	2.851	2.795
Fe^{3+}	1.805	1.855	1.943
Al^{3+}	0.196	0.155	0.105
Ti^{4+}	0.06	0.047	0.04
Mn^{2+}	0.072	0.078	0.099
Mg^{2+}	0	0	0
Cation sum	7.968	7.967	7.959
Mol. %			
Andradite	97.5	97.3	96.6
Spessartine	2.5	2.7	3.4
Pyrope	0	0	0

1. Total iron expressed as $Fe_2O_3^T$.
2. Trace element abundance in ppm.

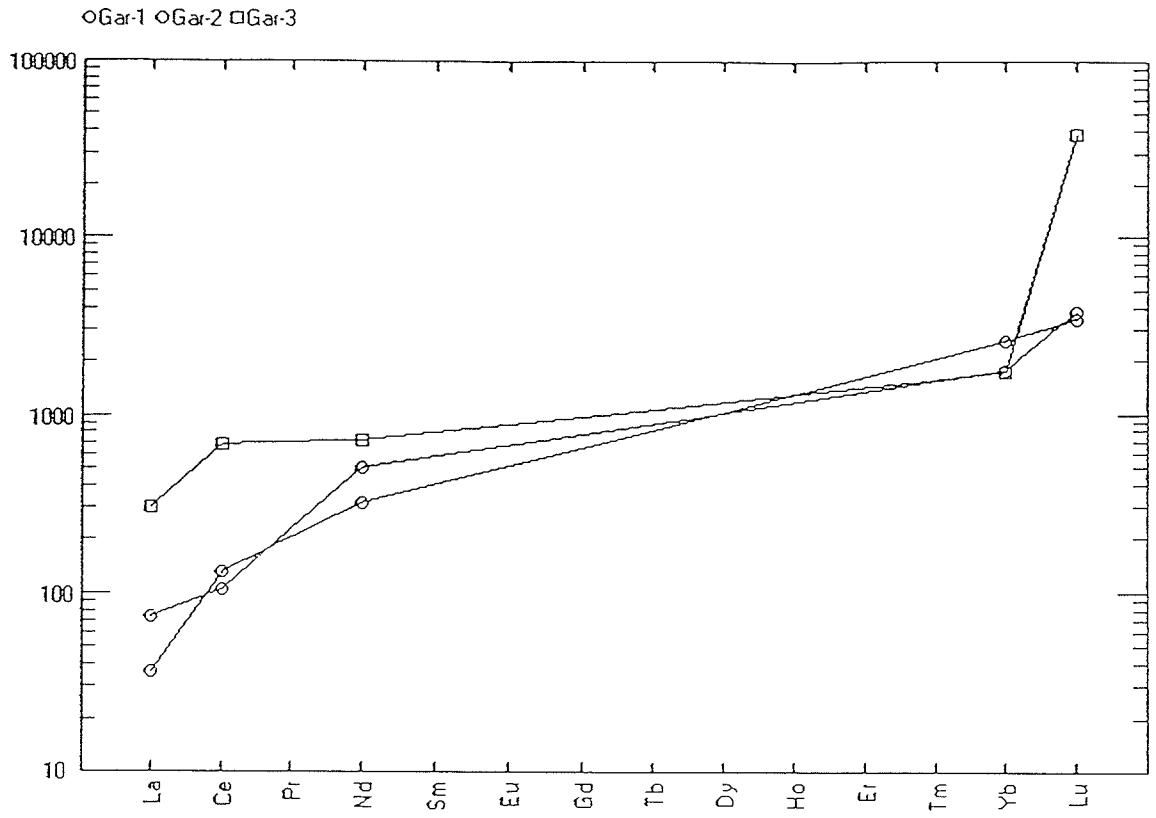

Figure 5.25. Chondrite-normalized REE plots for andradite grains from the Type III pegmatites. REE values are from EMPA. Unaltered andradite are shown by ○; altered andradite is shown by □. Normalization values are from Sun (1982).

colour at the margins (Figure 5.26). Fluorite grains are subhedral to anhedral, with straight to slightly curved margins, and range in size from 0.01 mm to 1.0 cm. BSE images from the Type III pegmatites reveal that the fluorite is homogeneous (Figure 5.27). Chemical analyses indicates the fluorite is pure CaF_2.

Fluorite grains in the Type IV pegmatites range in size from 0.1 to 0.9 mm, and in abundance from 0 to 5%. In thin section, fluorite grains are anhedral and irregularly shaped interstitial aggregates with curved to slightly curved margins, although contacts with allanite and britholite are very irregular to sutured. The aggregates are purple to clear in colour, with the darkest purple in the centre of the grain fading to clear at the margins (Figure 5.28). BSE images from the Type IV pegmatites are shown in Figure 5.29; these indicate that the fluorite is homogeneous. Again, chemical analyses indicate the fluorite is pure CaF_2.

5.8. Aegirine-augite.

Aegirine-augite, $(Na,Ca)(Fe,Mg,Mn)Si_2O_6$, is a clinopyroxene that is commonly found in alkaline rocks such as quartz syenite, syenite and nepheline syenite (Deer et al., 1989). Aegirine-augite usually forms as a product of late -age crystallization of alkaline magmas (Deer et al., 1989). The REEs are not common constituents of aegirine-augite (Henderson, 1984). Aegirine-augite grains are found in the Type I, III and IV pegmatites.

In samples of the Type III pegmatites, aegirine-augite appears black and anhedral. In thin section, the pyroxene is green with a dark green to olive green pleochroism (Figure 5.6A). The grains are dominantly subhedral, range in size from 0.15 mm to 2.0

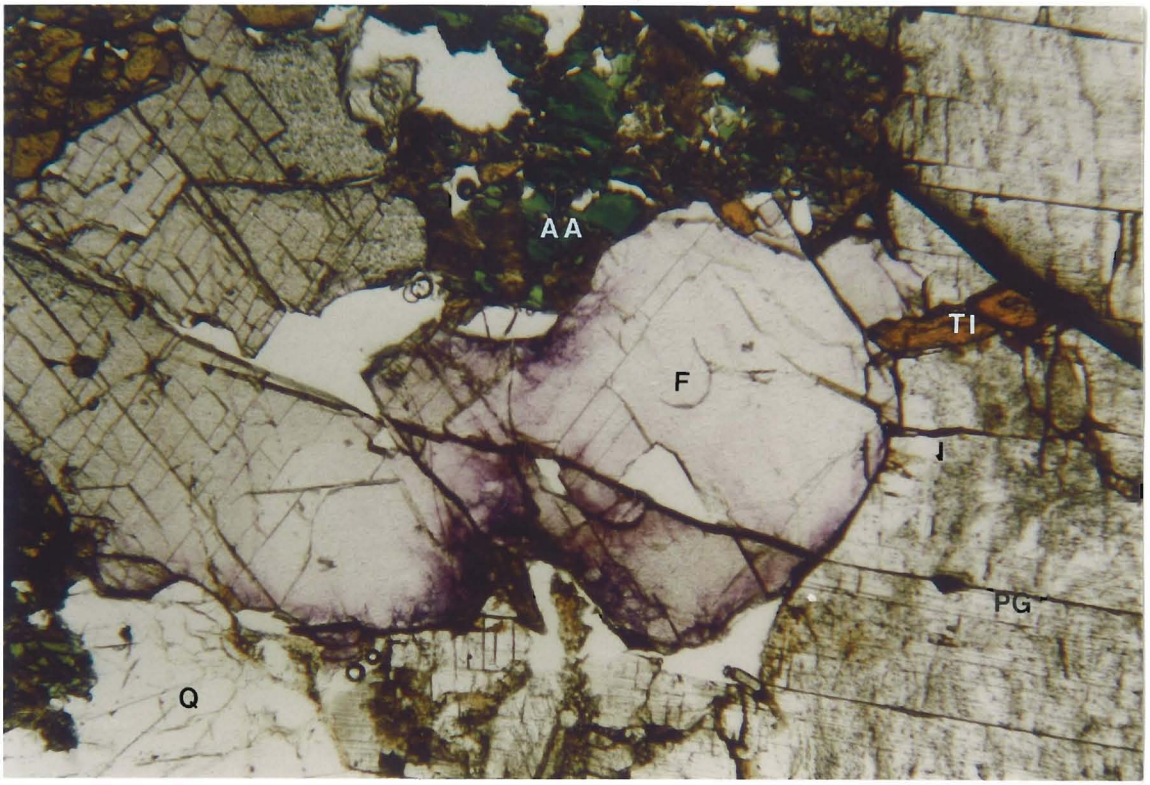

Figure 5.26. Photomicrograph of anhedral fluorite grains from the Type III pegmatites. The purple colour is darkest near the grain boundaries. Field of view is 2.8 mm in the long dimension. Mineral abbreviations are as follows: AA - aegirine-augite, F - fluorite, PG - plagioclase, Q - quartz, TI - titanite.

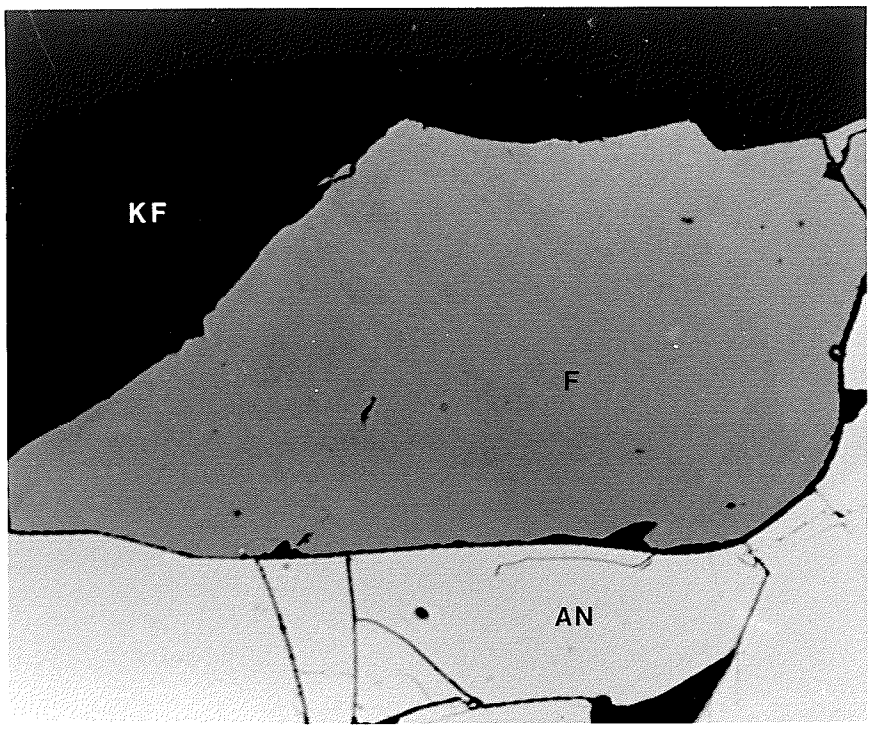

Figure 5.27. Photograph of a BSE image of a homogeneous fluorite grain from the Type III pegmatites. Field of view is 250 microns in the long dimension. Mineral abbreviations are as follows: AN - andradite, F - fluorite, KF - K-feldspar.

Figure 5.28. Photomicrograph of anhedral fluorite grains from the Type IV pegmatites. The purple colour is darkest near the grain centres. Field of view is 0.7 mm in the long dimension. Mineral abbreviations are as follows: AA - aegirine-augite, AL - allanite, AP - apatite, B - britholite, F - fluorite.

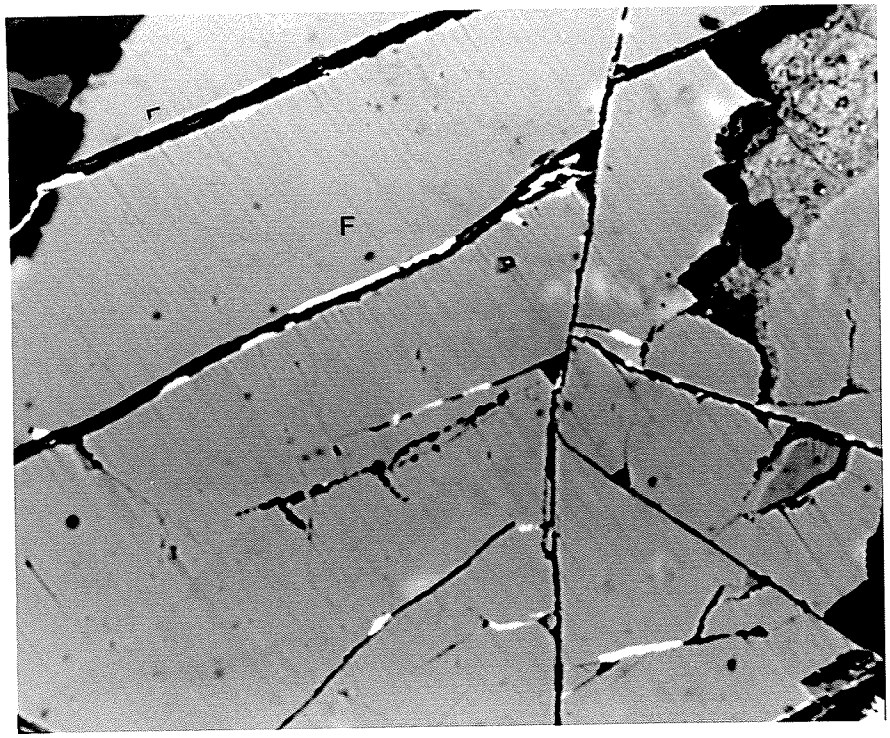

Figure 5.29. Photograph of a BSE image of a homogeneous fluorite grain from the Type IV pegmatites. Field of view is 175 microns in the long dimension. Mineral abbreviations are as follows: F - fluorite.

cm and range in abundance from 5-30%. Commonly, clusters of pyroxene grains, with magnetite and titanite, up to 2 cm in length are visible (Figure 5.6A). BSE images of Type III aegirine-augite indicate an irregular and discontinuous zoning (Figure 5.30). Contacts between the lighter and darker zones are sharp, and the zoning appears to be associated with fractures and grain boundaries, indicating the zoning is probably the result of alteration (Figure 5.30). The chemistry of the Type III aegirine-augite grains is presented in Table 5.7. The zoning pattern reflects varying amounts of Fe and Mg; the darker zones have lower Fe and higher Mg than the lighter zones.

The aegirine-augite in the Type IV pegmatites has similar physical and optical characteristics as that in the Type III pegmatites. In hand samples, the grains are black and anhedral; in thin section, the pyroxene is euhedral to subhedral, green in colour with a dark to olive green pleochroism. The aegirine-augite is pervasively fractured where it is associated with britholite (Figure 5.16A). Aegirine-augite grains range in size from 1 cm to 2 mm and in abundance from 5-30%. Pyroxene grains from the Type IV pegmatites also display the compositional variations observed in the Type III pyroxene (Figure 5.31). The darker areas in BSE images are associated with the grain boundaries, where aegirine-augite is in contact with apatite, quartz and britholite/allanite, again suggesting alteration (Figure 5.31). Chemical compositions of Type IV pyroxene are listed in Table 5.7. The darker zones have a lower Fe and Na abundance, but a higher Mg abundance than the lighter zones.

The data in Table 5.7 show that aegirine-augite crystals from the two pegmatites have similar composition, in terms of both major and trace elements. The chemical

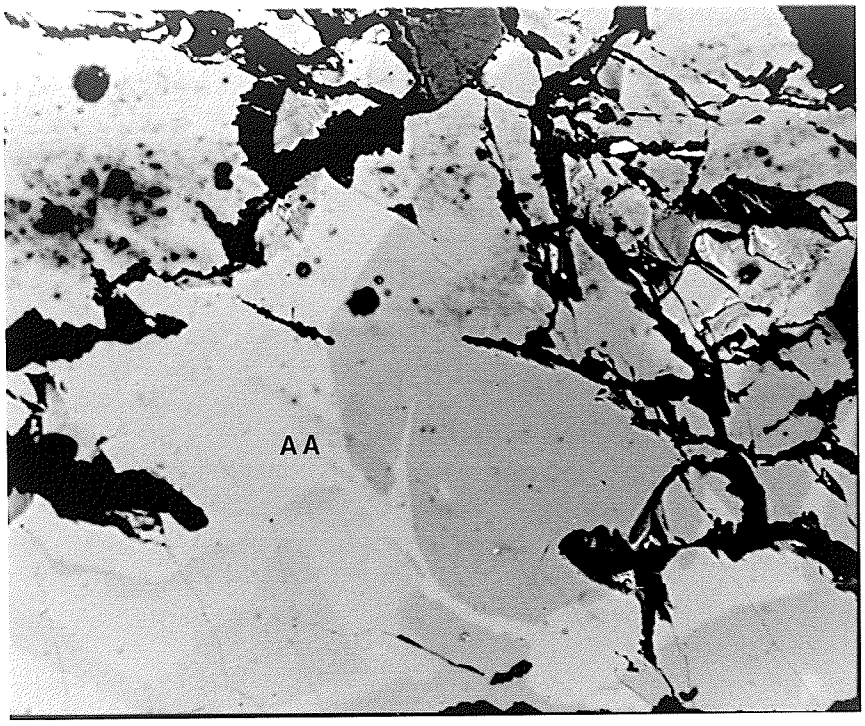

Figure 5.30. Photograph of a BSE image of aegirine-augite in the Type III pegmatites. Brightness differences indicate either primary zoning or alteration. Field of view is 300 microns of the long dimension. Mineral abbreviations are as follows: AA -aegirine-augite.

Table 5.7. Chemical compositions of aegirine-augite crystals from the Type III and Type IV pegmatites. All chemical data were obtained from EPMA. Additional compositions are presented in Appendix VII.

Oxide (weight percent)	Pegmatite III		Pegmatite IV	
	Unaltered	Altered	Unaltered	Altered
SiO_2	51.212	51.773	50.688	52.215
TiO_2	0.027	0.024	0.020	0.019
Al_2O_3	0.658	0.694	0.848	0.297
$Fe_2O_3^{T}$ [1]	19.535	16.272	20.737	14.155
MnO	0.819	1.035	1.138	1.038
MgO	6.537	8.877	5.874	9.588
CaO	19.631	18.870	19.309	21.905
Na_2O	2.092	1.704	2.131	1.070
V_2O_5	0.036	0.019	0.055	0.015
La_2O_3	0.002	0	0.001	0.001
Ce_2O_3	0.028	0.042	0.015	0.015
Yb_2O_3	0.002	0.002	0.008	0.004
Lu_2O_3	0	0.425	0	0
TOTAL	100.579	99.737	100.824	100.322
Formulas calculated on basis of 6 oxygen				
Si^{4+}	1.929	1.952	1.914	1.95
Ti^{4+}	0.001	0.001	0.001	0.001
Al^{3+}	0.029	0.031	0.038	0.013
Fe^{3+}	0.554	0.462	0.589	0.398
Mn^{2+}	0.026	0.003	0.036	0.033
Mg^{2+}	0.367	0.499	0.330	0.534
Ca^{2+}	0.792	0.762	0.781	0.876
Na^{2+}	0.153	0.124	0.156	0.077
V^{5+}	0.001	0	0.001	0
Cation sum	3.853	3.863	3.848	3.882

1. Total iron expressed as $Fe_2O_3^{T}$.

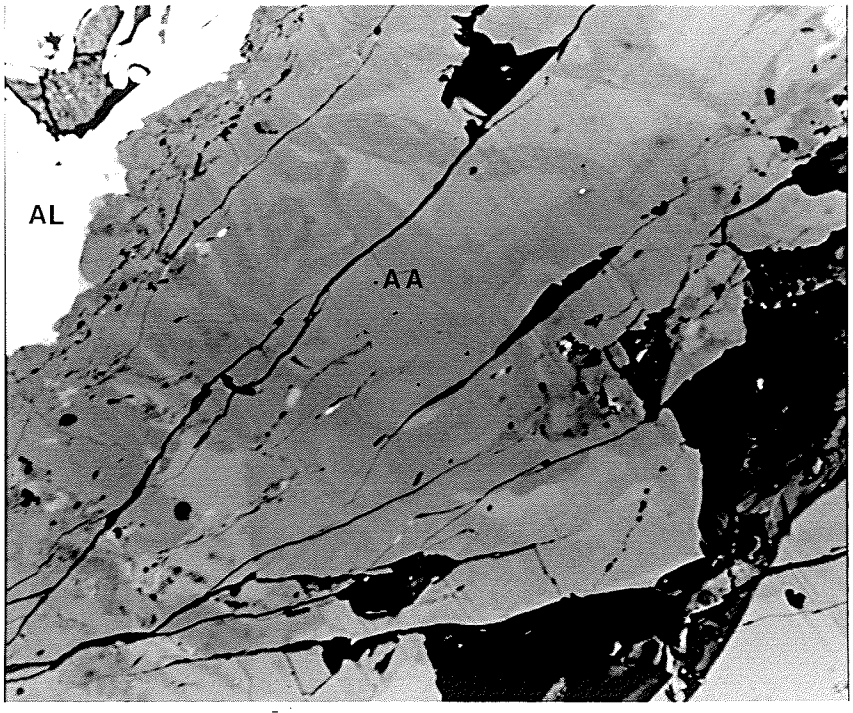

Figure 5.31. Photograph of a BSE image of aegirine-augite from the Type IV pegmatites. Note the brightness differences similar to those in Figure 5.30. Field of view is 300 microns in the long dimension. Mineral abbreviations are as follows: AA - aegirine-augite, AL - allanite.

differences caused by alteration are similar in aegirine-augite grains from each pegmatite: variable Fe, Na and high Mg; this will be discussed further in Chapter 6.

5.9. Feldspar.

Albite plagioclase and K-feldspar are very common constituents of felsic rocks, especially syenites and associated pegmatites. Typically, they are not important hosts for the REEs as the distribution coefficients for all the REEs (except Eu) are less than one (Henderson, 1984). Plagioclase and K-feldspar are present in the Type I, II, III and IV pegmatites associated with the Eden Lake syenite complex.

In the Type III pegmatites, K-feldspar is red to pink in colour and has a maximum size of 3 cm. Both microcline and orthoclase are observed, with abundances ranging from 5-75% (Table 4.2). Grain shapes range from anhedral to subhedral, with straight to curved crystal margins (Figure 5.1). Some grains appear cloudy due to presence of very fine-grained inclusions. Perthite with worm-like albite inclusions with a maximum size of 5 mm is visible.

The appearance of K-feldspar in the Type IV pegmatites is similar to that of K-feldspar in the Type III pegmatites. It weathers red to pink with a maximum size of 3 cm. Grain shapes are dominantly anhedral with scalloped to straight margins, but some subhedral shapes are present (Figure 5.16A). Orthoclase and microcline are both present, with abundances ranging from 5-40%. K-feldspar grains associated with britholite are commonly fractured (Figure 5.16A).

The composition of K-feldspar from the Type III and IV pegmatites is given in Table 5.8. In terms of the major and minor elements, the compositions are identical, although for

certain trace elements, the Type III K-feldspar grains have a wider range of abundance (Table 5.8). The amount of REEs present within the K-feldspar is the same in samples from both the Type III and IV pegmatites, ranging from 1700 to 1900 ppm with Ce the most abundant REE (Table 5.8); this REE content is higher than listed in the literature (Deer et al., 1989). In addition, K-feldspar grains from both the Type III and IV pegmatites contain very low Na_2O abundances, from 0.2 weight % to 0.8 weight % (Table 5.8; Appendix VIII).

Plagioclase in the Type III pegmatites weathers white and has a maximum size of 3 cm. Compositions range from albite to andesine (An7 to An35, Michel-Levy method), with the abundance ranging from 15-50%. Both albite and pericline twinning are visible. Grain shapes range from anhedral to subhedral and crystal margins are straight to curved (Figure 5.6B).

The plagioclase in the Type IV pegmatites weathers white, with a maximum grain size of 2 cm. Grains are mostly anhedral, but there are a few subhedral grains; crystal boundaries are straight to scalloped (Figure 5.16A). Compositions range from albite to oligoclase (An8 to An12; Michel-Levy method). Both untwined and albite-twinned plagioclase are present; the abundance ranges from 0-60%.

Chemical compositions of plagioclase grains in the Type III and IV pegmatites are listed in Table 5.8; in terms of major and minor elements, the data is very similar for samples from the two pegmatites. The abundance of some of the trace elements varies slightly between the pegmatites: Ba contents are higher in the Type III plagioclase, while

Table 5.8. Representative chemical compositions of K-feldspar and plagioclase grains in the Type III and Type IV pegmatites. All chemical data were obtained using EPMA. Additional compositions are presented in Appendix VIII.

Oxide (weight percent)	Pegmatite III		Pegmatite IV	
	K-Feldspar	Plagioclase	K-Feldspar	Plagioclase
SiO_2	64.062	68.007	63.678	68.527
Al_2O_3	18.622	20.095	18.788	20.379
$Fe_2O_3^{T}$ [1]	0.150	0.189	0.146	0.251
CaO	0	0.132	0	0.455
Na_2O	0.437	11.354	0.568	11.250
K_2O	16.289	0.114	15.935	0.162
BaO	0.399	0.017	0.430	0.031
SrO	0.097	0.123	0.185	0.217
TOTAL	100.333	100.059	100.027	101.313
La [2]	17	0	0	0
Ce	1348	34	1545	94
Nd	77	34	77	69
Sm	69	78	43	129
Eu	44	79	44	44
Yb	79	44	70	18
Hf	729	0	738	0
Formula units calculated on basis of 8 oxygen				
Si^{4+}	2.976	2.972	2.967	2.963
Al^{3+}	1.019	1.035	1.032	1.04
Fe^{3+}	0.005	0.006	0.005	0.008
Ca^{2+}	0	0.006	0	0.021
Na^{+}	0.039	0.962	0.051	0.943
K^{+}	0.965	0.006	0.947	0.009
Ba^{2+}	0.007	0	0.008	0.009
Sr^{2+}	0.003	0.003	0.005	0.001
Cation sum	5.014	4.991	5.014	0.006
Mol. %				
Or	96.2	0.61	94.9	0.92
Ab	3.8	98.7	5.1	96.9
An	0	0.61	0	2.2

1. Total iron expressed as $Fe_2O_3^{T}$.
2. Trace element abundance in ppm.

Fe and Ca contents are higher in the Type IV plagioclase. The REEs total 350-500 ppm and similar amounts are present in plagioclase crystals from both pegmatites.

Chapter 6: Discussion

Examination of the pegmatite phases associated with the Eden Lake syenite complex enables us to characterize the nature and origin of these pegmatites. In addition, models for the genesis of the REE-enriched minerals within these pegmatites can be established.

Granitic rare element pegmatites have the most diversified and most enriched rare element assemblages (Cerny, 1991a). This class of pegmatites was originally defined by Ginsburg et al. (1976), and can be divided into a number of subtypes based on bulk chemistry, geochemical signature of accessory minerals, internal structure and P, T conditions during crystallization (Cerny, 1991a). Rare-element pegmatites represent late residual differentiates that crystallize from volatile-enriched and rare-element-bearing melts that form as a result of granitic differentiation on a plutonic scale (Cerny and Meintzer, 1988). Many rare-element pegmatites are extensively mineralized and contain high amounts of the rare elements; however, the main controls on the exploitation of such pegmatites are the shapes and sizes (Cerny, 1991a).

Anorogenic plutons are commonly associated with rare-element pegmatites (Cerny, 1991a). Granite + rare element pegmatite systems of post-orogenic to anorogenic tectonic affiliation are generally related to subvertical dilation structures; the pegmatites are located either within the granite or along its margins (Cerny, 1991a). Most models for the generation of rare-element pegmatites involve differentiation within the parent granite. Volatiles and rare elements concentrate in pools or pods of residual melt during crystallization of the pluton; the pegmatites form as these pools intrude into the already solidified parts of the pluton (Cerny,

1991b). Emplacement of the pegmatites occurs by three different mechanisms (Cerny, 1991b): (i) filter pressing and/or gravitation convection, resulting in pegmatite concentration near the top of the pluton or in a carapace of country rocks; (ii) crystal melt fractionation, resulting in pegmatite concentration in a somewhat lower part of the pluton; and rarely (iii) buoyant rise of local pegmatite-melt segregations, resulting in pegmatite concentration at one level within the pluton.

7.1. Type I and Type II pegmatites.

The Type I and The Type II pegmatites are coarse-grained units with a similar chemistry as the main monzonites and contain no unusual rare element-bearing accessory minerals. The lack of a trace-element-enriched mineral population suggests that the melts from which these pegmatites crystallized did not contain elevated amounts of rare elements, suggesting (i) they were derived from melts depleted in incompatible elements, or (ii) the melts had not undergone extreme differentiation that would have concentrated incompatible elements. In this latter case, later melts were emplaced into a solidified syenite complex carapace before they had undergone significant differentiation, and rare-element enrichment (Figure 6.1). The different mineral assemblages observed in these two pegmatite units suggests that there were several stages of melt emplacement into the syenite complex, probably from an external source. The more mafic composition of the Type I pegmatites is consistent with them representing an earlier and more primitive

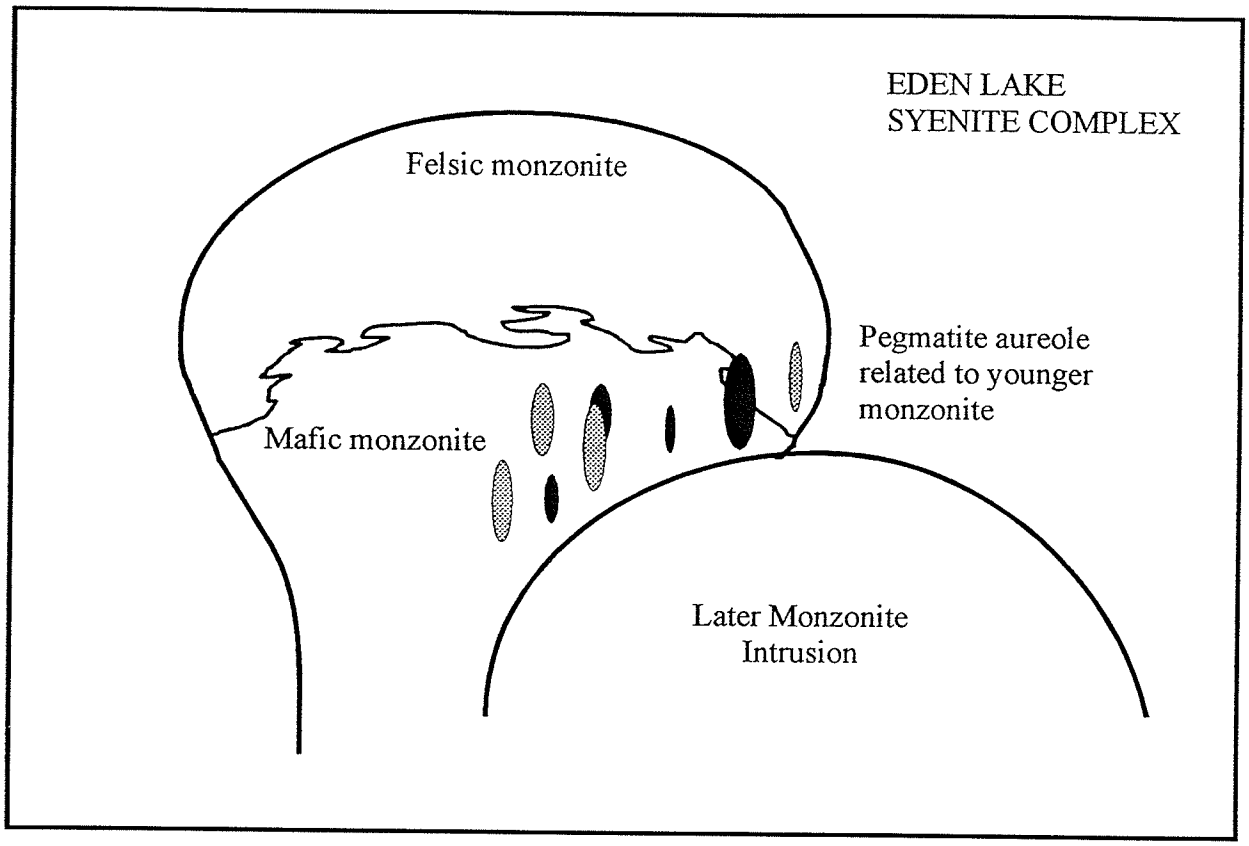

Figure 6.1. Schematic diagram illustrating the model for the origin of the Type I and II pegmatites associated with the Eden Lake syenite complex (modified from Simmons et al., 1987). The Type I pegmatites are shown in black and the Type II in the stippled pattern.

magma injection. Two stages of melt injection would account for the crosscutting field relations that indicate that the Type I pegmatites are older than the Type II pegmatites. As these veins crosscut the mafic and felsic monzonite units, it is suggested that they are derived from a younger monzonitic melt. A possible magmatic source for these melts is the younger monzonite suite that surrounds the syenite complex (Figure 2.4; Table 2.1).

7.2 Type III pegmatites

MINERAL CRYSTALLIZATION

The sequence of mineral crystallization in the Type III pegmatites can be determined from the relationships between minerals and has important connotations for the evolving chemistry of the melt from which the minerals formed. A general paragenetic diagram is shown in Figure 6.2; the crystallization sequence has been subdivided into early, middle and late stages of crystallization (Figure 6.2).

Early crystallization

The early stages of crystallization are represented by inclusions within minerals. these include oscillatory-zoned allanite, thorite and apatite (Figure 6.2). Strontianite and burbankite occur as inclusions within titanite. This is somewhat problematic. If these minerals are early-formed inclusions, it would require an early stage of pegmatite melt saturation with respect to CO_2. Alternatively, if they represent alteration products of the titanite grains (cf. Schuiling and Vink, 1967; Pan et al, 1993), it would be consistent with a later period of hydrothermal alteration by a CO_2-rich fluid. Based on the current incomplete evidence of the chemistry and structure of these carbonate minerals, it is not

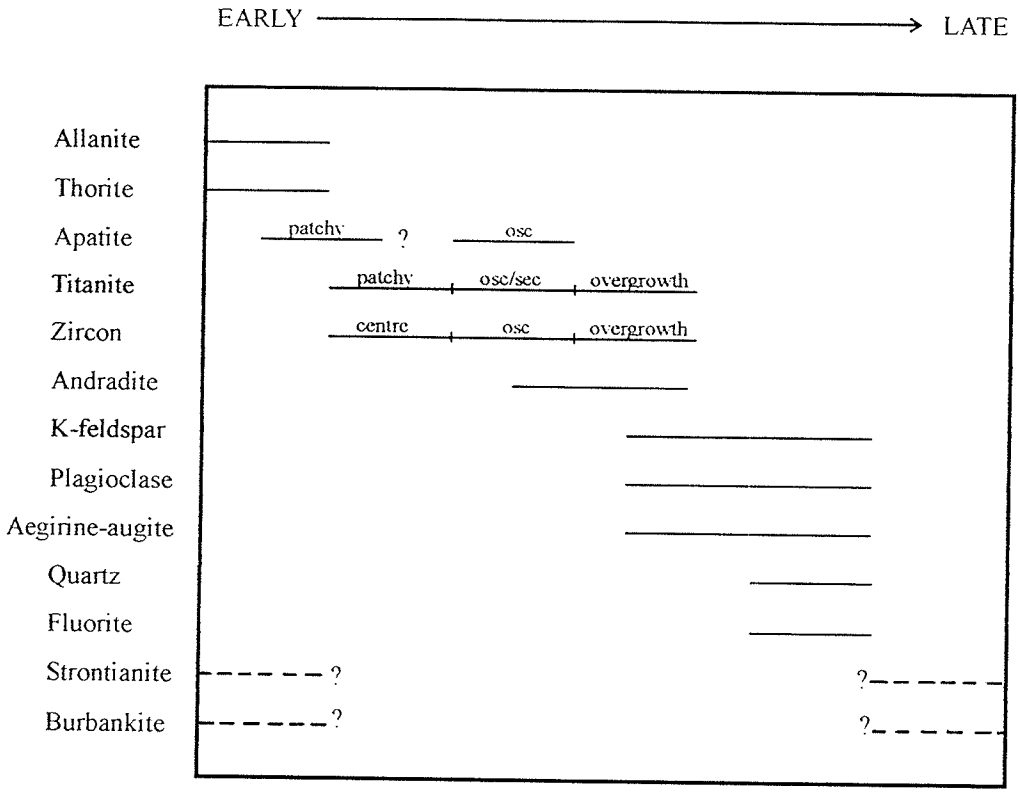

Figure 6.2. General paragenetic diagram illustrating the sequence of mineral crystallization within the Type III pegmatites.

possible to categorically deduce their origin.

Middle crystallization

Titanite and zircon crystals from the Type III pegmatites display a similar internal stratigraphy of mineral growth. The growth history can be summarized as an early period of random growth in the core, followed by a period of oscillatory growth followed by crystallization of an overgrowth; these are separated by irregular contacts. To some degree, this stratigraphy is observed in apatite crystals; apatite inclusions have a patchy zoning, while non-included grains contain oscillatory zoning. Titanite grains also have a sector zoning pattern not observed in either zircon or apatite. Irregular contacts between areas within crystals that contain different zoning patterns have been interpreted by Van Breemen et al. (1987) as representing a period of crystal resorption. The period of resorption occurs as a result of melt-mineral disequilibrium; the melt chemistry changes as a result of the influx of new chemical components due to movement within the melt. The characteristics of the zoning patterns observed within apatite, titanite and zircon suggest that the zoning patterns crystallized concurrently. The similarity of the internal growth stratigraphy suggests the crystal growth mechanism was changing at the same time for all three minerals.

Apatite occurs both as separate grains and as inclusions within titanite crystals. There were two stages of apatite growth: the early stage produced small, patchy zoned apatite crystals that were incorporated into titanite during growth; the late stage produced oscillatory and unzoned crystals. The slightly curved grain boundaries of the apatite inclusions indicate that these have undergone dissolution; there must have been a period of apatite-melt chemical disequilibrium between the two stages of apatite crystallization. The chemistry of the apatite

inclusions within titanite and the separate apatite grains are very similar, suggesting that the melts from which they formed had a similar chemistry. However, during the early stage of apatite crystallization, the melt was relatively enriched in Ce and La; at a later stage, the melt was enriched in Si and Cl (see Table 5.1). During the late stage of apatite crystallization, incorporation of varying amounts of Si into the growing crystal contributed to the oscillatory zoning pattern.

Titanite grains have a very complicated crystallization history. The Type A and Type B titanite grains have different internal characteristics with three consecutive zoning patterns; thus, there have been at least three stages of titanite growth. The embayed and irregular contacts between these growth stages suggests there were at least three stages of titanite-melt disequilibrium that resulted in partial dissolution of the titanite crystals. The first stage of titanite growth produced patchy, discontinuously zoned crystals; darker patches incorporated Sr, Zr, Nb, Pb and F while the brighter patches incorporated REEs, Fe, Th and U. The latest stage of titanite crystallization produced an overgrowth or rim, with high REE and F contents, around the margins of pre-existing titanite crystals. The middle stage(s) of titanite growth produced both oscillatory zoning and sector zoning. The brighter oscillatory zones incorporated trace elements, REEs and F. The {111} sectors incorporated F and Sm while the {100} and {001} sectors incorporated Mn, Na and Y. These two zoning patterns may represent either more than one stage of crystallization or coeval crystallization in different parts of the pegmatite melt. The absence of some of these zoning patterns within some titanite crystals is probably a result of thin section orientation and cut.

Zircon contains three types of consecutive zoning patterns, suggesting at least three

stages of zircon growth from the melt. The embayed outer margins of each of these zoning types suggests at least three periods of resorption of the zircon grains. The earliest stage of zircon growth produced the less fractured cores observed in BSE images; the melt from which this zircon crystallized was enriched with respect to the REES. The second stage of zircon growth was characterized by the development of oscillatory zoning. Some crystals appear to lack cores, probably as a result of thin section cut and orientation. The latest stage of zircon growth is represented by the rims and overgrowths that surround zircon grains; these rims incorporated Al, P, and REEs. The mottled areas within zircon crystals are not related to crystal growth, but rather result from chemical alteration of the zircon grains due to metamictization. The low Zr and Hf contents, and the low analysis totals, within these zones are consistent with chemical analyses of metamict and altered zircons (Rubin et al., 1989).

Middle to late crystallization

The minerals in the Type III pegmatite that characterize middle to late crystallization do not display a sequence of internal zoning patterns; these include andradite, K-feldspar, plagioclase, aegirine-augite, quartz and fluorite. This suggests that there was only one stage of crystallization from the pegmatite melt for each of these minerals. Andradite grains have irregular embayments on the crystal faces, suggesting that these crystals were resorbed into the melt as a result of chemical disequilibrium. The irregular grain boundaries observed for K-feldspar, plagioclase, fluorite and quartz are likely a result of grain boundary interference during crystal growth, rather than a period of dissolution.

Several minerals within the Type III pegmatites have been altered after crystallization,

including andradite and aegirine-augite. The andradite underwent a period of alteration that occurred after or at the same time as the development of the embayed outer margins. This alteration produced darker coloured areas concentrated at the crystal margins near embayments and along cracks within the andradite. These areas lost Al and gained Fe during the alteration event. Darker coloured areas in BSE images of aegirine-augite grains suggest that the pyroxene underwent a period of alteration. These signify that hydrothermal fluids have invaded the Type III pegmatites after crystallization.

K-feldspar crystals from the Type III (and IV) pegmatites have Or contents of Or95 to Or96 (Table 5.8). In syenites and associated pegmatites, K-feldspar commonly occurs as perthite, cryptoperthite or microcline perthite (Deer et al., 1989). However, perthite occurs in relatively low abundances within the Type III pegmatites and in most grains, no solid solution between K-feldspar and albite is visible. These features indicate that the K-feldspar is not now of plutonic origin (Deer et al., 1989); it is more likely that the K-feldspar crystals have undergone recrystallization. Recrystallization of the K-feldspar due to interaction of a hydrothermal fluid can cause changes in the coarseness and regularity of exsolution (or perthitic) textures (Parsons and Brown, 1984). This recrystallization would have occurred at temperatures less than 400°C and resulted in the removal of Na from the K-feldspar (Parsons and Brown, 1984). The elevated REE contents within K-feldspar crystals in the Type III (and IV) pegmatites might also be related to recrystallization by the hydrothermal fluid, but more likely, they are related to the original crystallization of the K-feldspar.

DEVELOPMENT OF MINERAL ZONING IN TYPE III PEGMATITES

Compositional zoning patterns in crystals can provide a detailed record of growth processes (Reeder et al., 1990). The two principle zoning patterns observed in minerals include concentric or oscillatory zoning and sector zoning (Reeder et al., 1990). Random, discontinuous zoning patterns are also found (Vance, 1965; Anderson, 1984). Compositional zoning may reflect: (i) depletion or change in the supply of chemical constituents during crystal growth; (ii) reaction or homogenization after initial growth; or (iii) chemical inequalities produced during growth along different crystallographic directions (Kwak, 1981). The presence of several zoning patterns within one crystal reflects changing melt conditions; these may be the result of movement of the crystal to a new location within the melt, or an influx of certain chemical components into the areas where the crystal is forming. Equilibrium conditions between the crystal and the melt favour the development of zones of slightly variable composition.

Patchy, discontinuous zoning is not commonly described in the literature. Anderson (1984) suggests that patchy zoned regions in oscillatory zoned plagioclase developed during episodes of greater plagioclase supersaturation and faster crystal growth. Vance (1965) suggests that patches of unzoned plagioclase within oscillatory zoned plagioclase formed by resorption and deposition. Intense corrosional channelling of the interior of zoned plagioclase cores and relatively weak attack on their outer portions caused the patchy appearance. Resorption of the plagioclase resulted from a decrease in the hydrostatic pressure related to boiling off of late stage volatiles (Vance, 1965). Renewed magmatic crystallization filled patches within the zoned plagioclase cores (Vance, 1965). Neither of these models explain

the features observed in the patchy-zoned regions; these may represent amalgamation of a number of discrete nuclei that were formed during a period of melt supersaturation with respect to apatite and titanite.

Oscillatory zoning is a common and normal form of crystal growth and has been documented in many accessory minerals (eg. Jamtveit, 1991; Halden et al., 1993). It is most commonly interpreted as reflecting temporal changes in bulk composition, redox state, temperature or pressure within the fluid from which crystallization of the mineral occurred (Reeder et al., 1990). Oscillatory zoning has also been interpreted to represent non-linear dynamical interplay between growth rate and solute diffusion through crystal boundary layers or surface adsorption of growth inhibitors as well as self-organization during crystal growth (Reeder et al., 1990; Wang and Merino, 1992). Oscillatory zoning always varies between two compositional extremes. During the development of the oscillatory zoning, the magma surrounding the growing crystal is quiescent; the rate of crystallization is therefore less than would be the case if the crystal had moved around. Diffusion-limited crystal growth in a multiply-saturated chemical system invites kinematically controlled feedback, whereby the crystal disturbs the chemistry of the melt surrounding it. The oscillatory zoning in apatite, titanite and zircon resulted from a period of diffusion-controlled growth mechanics.

Sector zoning is related to crystal growth by addition of new material on rational crystal faces, suggesting chemical disequilibrium between the crystals and the melt (Paterson and Stephens, 1992). Sector zoning refers to a compositional difference between coeval growth sectors or portions of growth sectors within a crystal (Reeder and Paquette, 1989). It is a consequence of the non-equivalence of surface cation sites on growing crystal faces and

it is preserved where crystal growth occurred at a faster rate than the rate of diffusion (Nakamura, 1973; Searl, 1990). The presence of sector zoned Type B titanite grains indicates disequilibrium partitioning that was the result of directionally non-uniform growth kinetics of individual titanite crystals (Paterson and Stephens, 1992).

The overgrowths represent a last period of mineral saturation within the melt; this resulted in crystal growth around old nuclei. These overgrowth reflect a change in the chemistry of the surrounding melt, or a different fluid source (Rubin et al., 1989).

The unfractured, unzoned cores in zircon crystals may represent either early crystallization of homogeneous zircon or solid state recrystallization of early oscillatory zoned zircon (Pidgeon, 1992). The high contaminant content (REEs, Th and U) distort the zircon structure, making it unstable and susceptible to recrystallization at low temperatures, without changing the crystal shape (Pidgeon, 1992). Recrystallization may have occurred immediately after crystallization at high temperatures or later, as a result of low temperature sustained for a long period of time (Pidgeon, 1992).

ORIGIN OF THE TYPE III PEGMATITES

The Type III pegmatites contain trace element-enriched minerals, including titanite, apatite, zircon, andradite, oscillatory zoned allanite, thorite and burbankite. The melt from which Type III pegmatites formed was enriched in volatiles and trace elements. This means that the Type III pegmatites are rare-element pegmatites according to the definition of Cerny and Meintzer (1988). The melt from which the pegmatite formed was a late residual differentiate; the similarity of mineral assemblages found in the Type III pegmatites and the

mafic and felsic monzonites suggests that these pegmatites represent the last stages of crystallization from the syenite complex melt.

It is difficult to constrain the source of the REEs present within titanite, apatite, zircon and the early inclusions within the Type III pegmatites There are two possible sources: (i) concentration during crystallization of the main phase syenite; the pegmatites are therefore the result of pluton-scale differentiation due to crystal fractionation; or (ii) re-introduction and mixing of the REE- and volatile-enriched immiscible vapour phase that separated from the main phases of the complex during crystallization (see Chapter 4). The former model seems the most likely; the REEs were concentrated in the Type III pegmatites as the result of fractional crystallization of the felsic monzonite melt. The separation of the REE- and volatile-enriched vapour phase during the evolution of the main syenite complex removed the bulk of these elements from the residual melt (Halden and Fryer, submitted). Some of the residual incompatible elements were incorporated into minerals such as apatite, titanite and zircon in the high silica group (see Chapter 4). Fractional crystallization of the syenite melt would have concentrated the rest of the incompatible elements in the residual melt (Arth, 1976).

The model for the formation of the Type III pegmatites is shown schematically in Figure 6.3. As the intrusion cooled, fractional crystallization controlled the composition evolution of the complex from the mafic to felsic monzonite. Type III pegmatites formed, as irregular patches, where there were concentrations of volatiles (Figure 6.3). The Type III pegmatite mineralogy can vary, and this may be due to various volatile-rich pockets having slightly different bulk compositions.

7.3. Type IV pegmatites

MINERAL CRYSTALLIZATION

The Type IV pegmatites contain, in general, the same minerals as the Type III pegmatites, except for the REE-bearing phases allanite and britholite; the occurrence of allanite is different than in the Type III pegmatites as within the Type IV pegmatites, allanite occurs as irregularly shaped grains, not as inclusions within titanite (see Chapter 5). Mineral relationships within the Type IV pegmatites indicate that the sequence of mineral crystallization is almost the same as that of the Type III pegmatites (Figure 6.4). However, the sequence of crystallization is complicated by allanite and britholite; both of these are interpreted to represent late stage crystallization within the Type IV pegmatites (Figure 6.4).

Apatite

There are some small difference in the characteristics of apatite in the Type IV pegmatites compared to the apatite grains in the Type III pegmatites. The apatite grains within the Type IV pegmatites do not occur as inclusions within titanite, but this is probably the result of thin section cut and orientation. The extensive alteration observed in the Type IV apatite crystals is not observed in samples from the Type III pegmatites. The chemistry of apatite grains from the Type IV pegmatites is also significantly different, in terms of trace element abundance, especially REE content, than the chemistry of apatite crystals in the Type III pegmatites (Table 5.1).

Titanite

Titanite crystals in the Type IV pegmatites are equivalent to Type A titanite crystals from the Type III pegmatites, without patchy-zoned cores, but this is probably the result of

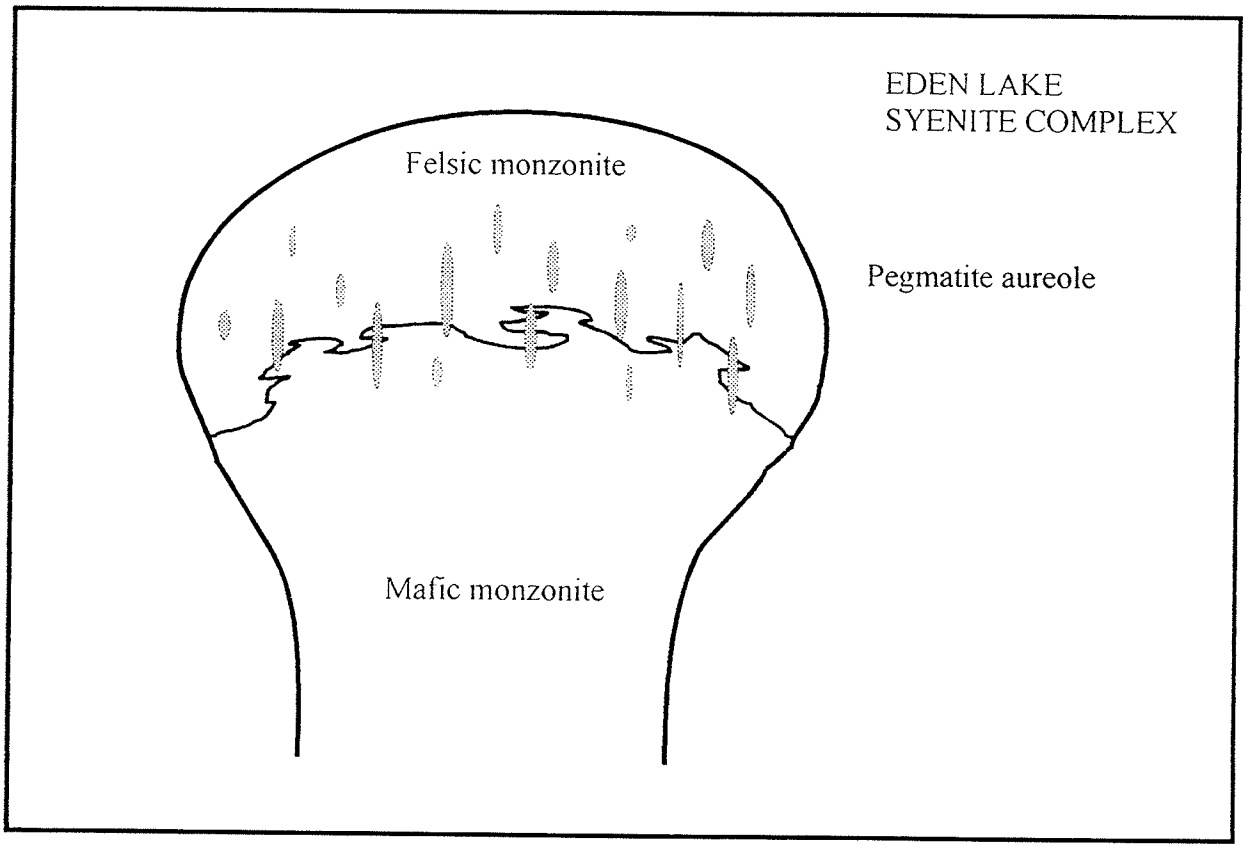

Figure 6.3. Schematic diagram illustrating the model for the origin of the Type III pegmatites, shown in the light stippled pattern (modified after Simmons et al., 1987). They formed by crystallization of pools of volatile-enrichment.

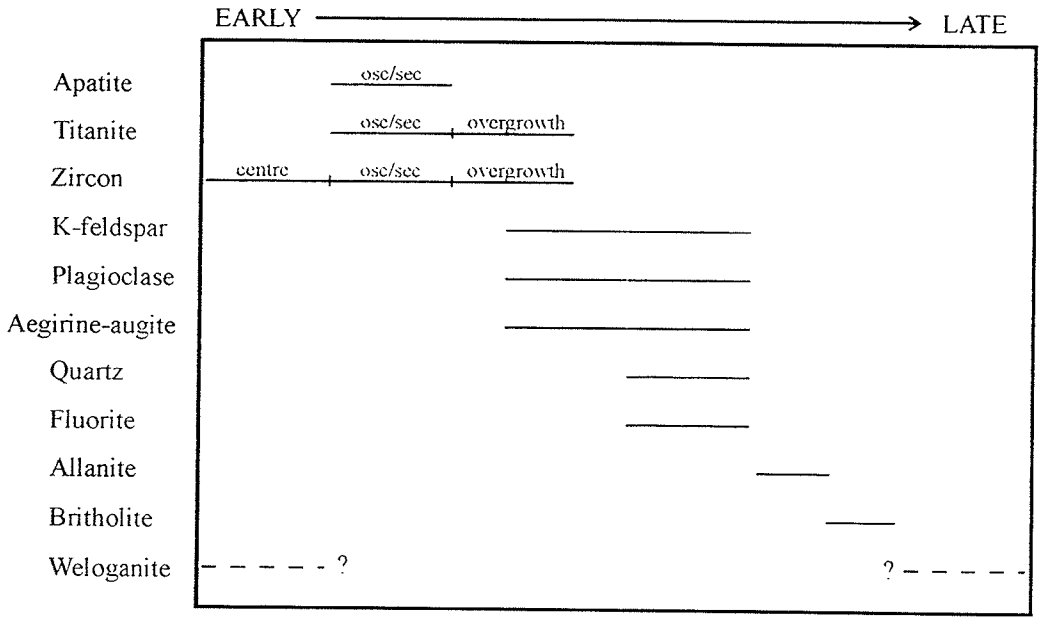

Figure 6.4. General paragenetic diagram showing the sequence of mineral crystallization within the Type IV pegmatites.

thin section cut and orientation.

K-feldspar

K-feldspar grains within the Type IV pegmatites lack perthitic textures and have high Or contents that suggest recrystallization of these grains has occurred, as in the Type III pegmatites.

REE-carbonate

Weloganite is the REE carbonate found within titanite grains in the Type IV pegmatites. It is interpreted to have the same origin as the carbonate minerals within the Type III pegmatites discussed earlier.

Allanite

Allanite is one of the last minerals to form in the Type IV pegmatites. Several unusual features constrain its origin, including: (i) its unusual chemistry with respect to the other pegmatite minerals (except britholite); (ii) its embayed and irregular contacts with other pegmatite minerals including britholite; and (iii) its occurrence as rims around other pegmatite minerals.

The chemistry of allanite is quite dissimilar from the silicate minerals (aegirine-augite, K-feldspar, plagioclase, quartz) and apatite with which it occurs. Compared to these, allanite is significantly enriched in REEs, thus it must have crystallized from a REE-enriched fluid. The irregular and embayed contacts observed between allanite and the other pegmatite minerals such as apatite, feldspar, aegirine-augite, quartz and zircon, suggests that its growth was not in chemical equilibrium with the host minerals. The rims of allanite were formed as a REE-enriched fluid moved into the pegmatites. Since the easiest passages were the grain

boundaries between crystallized minerals, the fluid likely moved along these boundaries. As a result of the chemical disequilibrium between the pegmatite minerals and the fluid, dissolution occurred, and allanite was precipitated in the resulting void space. The irregularity of the contacts is consistent with the reaction of a fluid with different chemistry with aegirine-augite, K-feldspar, plagioclase, quartz, apatite and zircon. Possible sources of the allanite-producing, REE-enriched fluid will be discussed in a later section.

The irregular contacts observed between allanite and britholite suggest that the two minerals were not in chemical equilibrium with one another during growth. The problem becomes a matter of determining whether allanite or britholite crystallized first in the Type IV pegmatites. It is therefore important to examine allanite-britholite contacts in detail. In some areas, allanite outlines britholite polygons and allanite rims follow polygonal boundaries into the britholite (Figure 5.16C). This suggests that the fluid which produced allanite moved along polygonal boundaries within the britholite; therefore the britholite polygons formed first, before crystallization of allanite. Allanite and britholite should have formed from different REE-enriched fluids injected into the pegmatites at different times.

The argument against this model is one of scale. Individual britholite polygons have a maximum size, determined from BSE images, of 200 microns; those polygons outlined by allanite are on the order of several mm (Figure 5.16C; Figure 5.17). Therefore, allanite does not outline individual polygons of britholite and the fluid that produced allanite could not have moved along individual britholite polygonal boundaries. The irregularity of the contacts between allanite and britholite represent a reaction texture similar to what is observed between allanite and the other pegmatite minerals. Therefore, allanite must have been present

in the Type IV pegmatites before the formation of britholite. The reaction texture suggests that although both allanite and britholite formed from REE-enriched fluids, they did not form at the same time, and probably not from the same fluid. However, if they formed from the same fluid, its chemistry must have been modified after the crystallization of allanite by further reaction with the other pegmatite minerals, in order to achieve saturation with respect to britholite, again suggesting that the crystallization of allanite and britholite is not coeval.

Random, discontinuous zoning is observed in only a minority of allanite grains, signifying it is most likely a result of alteration. The almost completely isotropic nature of allanite in the Type IV pegmatites indicates that it is metamict (Smith et al., 1957; Morin, 1977). Allanite contains 900-7000 ppm U and Th (Table 5.5; Appendix V) and associated britholite contains 14000-15000 ppm U and Th (Table 5.4; Appendix IV); allanite alteration can therefore be attributable to metamictization by either allanite or britholite (Pan and Fleet, 1990). Fractures within allanite, and within associated silicate minerals and apatite, are the result of expansion due to alteration and hydration of either the allanite or britholite (Deer et al., 1986).

Britholite

Britholite is the last mineral to crystallize in the Type IV pegmatites, after other REE-bearing accessory phases such as apatite, titanite, zircon and allanite (Figure 6.4). The most unusual features of the britholite are: (i) its unique chemistry with respect to the host minerals, except allanite; (ii) its irregular and embayed contacts with the host minerals; (iii) its lack of a well defined crystal structure; and (iv) its distinct polygonal texture.

Like allanite, britholite chemistry is quite distinct from that of the other pegmatite

minerals; compared to these, it is REE-, F- and P- enriched. The embayed and irregular contacts observed between britholite and other pegmatite minerals suggest that the fluid that produced britholite reacted with these minerals.

The absence of well-defined crystal structures in the britholite polygons might be explained by metamictization of the britholite. If this were the case, however, preservation of the distinct, sharp polygon boundaries, assuming they represent an original crystallization texture, would be unlikely. The absence of a crystal structure might also be explained by amorphization of the britholite. Amorphization is the transition from a crystalline to an aperiodic or amorphous state; it is the result of radiation-induced phase instability (Weber, 1992). Amorphization results from a high local defect concentration that leads to the spontaneous collapse of both the local crystal structure and long range order when the free energy of the high defect region becomes equal to that of the amorphous state (Swanson et al., 1971; Weber, 1992). Self-amorphization is the result of the emission of alpha-decay events in the U and Th radionuclide series within the mineral of interest (Eby et al., 1991), thus the amorphization of the britholite might have been caused by the decay of U and Th within the britholite.

Polygonal textures with straight to slightly curved grain boundaries formed during conditions of minimum surface free energy of any incipient structures (Vernon, 1976). Such textures are common in annealed and sintered materials (Vernon, 1976). If the polygonal texture represents an annealed or sintered amorphized britholite, then this would require a period of elevated temperatures that post-dates the crystallization and amorphization of the britholite. This is problematic as the rest of the minerals within the pegmatites have a clearly

distinguishable igneous texture with no evidence of any dynamothermal metamorphism. The temperature required for the annealing process must have been high enough to anneal the britholite and low enough not to have affected any of the other pegmatite minerals.

It is possible that the production of the polygonal texture may be related to heat generated during the amorphization process. However, this is unlikely as heat produced by amorphization would be insufficient to cause annealing of the britholite (B. Finch, personal communication). Studies on amorphized $Ca_2La_8(SiO_4)_6O_2$ crystals with the apatite structure indicate that self-annealing does not occur at temperatures up to 500°C (Weber and Wang, 1993). Alternatively, and more likely, the heat might have been imposed on the system from an external source, but it did not cause significant recrystallization in anything but the britholite, and possible the K-feldspar (see pages 124 and 131).

Britholite alteration.

The vermicular texture seen at the polygon grain boundaries points to the britholite having undergone a period of hydrothermal alteration after development of the polygonal texture. The fluid that altered the britholite grains was forced through the britholite along the polygonal boundaries; alteration proceeded from the polygon margins into the interiors. The contacts of britholite and other pegmatite minerals must have also controlled the fluid mobility, as the most altered portions of the britholite grains tend to occur closest to contacts with other minerals. The presence of more than one alteration front can be explained if: (i) there were several stages of fluid ingress into the britholite, where during each event, the polygonal boundaries acted as the loci for fluid movement; or (ii) chemical buffering of the fluid chemistry occurred as a result of initial alteration of the britholite by the fluid. The timing

of fluid(s) ingress into the britholite is constrained to after the formation of the polygonal boundaries.If this fluid was at elevated temperatures, then it is possible that heat preceding the hydrothermal alteration of britholite caused annealing of britholite. The possible sources of this hydrothermal fluid will be discussed in a later section.

The britholite grains in the Type IV pegmatites have undergone hydration and exchange reactions. The fluid was rich in OH and Cl; as it moved along polygon boundaries, it removed F, Ce and La from the britholite while OH and Cl were incorporated into the britholite. The REEs and F were probably transported out of the system as complexes (Humphris, 1984). Further comparison of the chemistry of the altered and unaltered britholite highlights some unusual features. The mole proportion of U and Th in the altered and unaltered britholite is constant, suggesting that they were not affected by the fluid alteration. This contradicts previous work which suggests that U and Th are mobile under hydrothermal conditions (Pan et al., 1993).

ORIGIN OF TYPE IV PEGMATITES

There are a number of features common to both the Type III and IV pegmatites, evident from comparative studies of samples from the two pegmatites. Similar features include: (i) pegmatite mineralogy, except for allanite and britholite in the Type IV pegmatites; (ii) mineral chemistry, in terms of major, trace and REE abundance, in titanite, zircon, aegirine-augite, K-feldspar, plagioclase, fluorite and quartz; and (iii) mineral growth histories in titanite, apatite and zircon where early crystallization is characterized by a period of irregular growth and late crystallization is characterized by oscillatory patterns. These

similarities indicate that the Type III and IV pegmatites are genetically related.

There are two possible models that can explain the genetic association of the Type III and IV pegmatites: (i) the Type IV pegmatites represent further differentiation of the melt that produced the Type III pegmatites; or (ii) the Type IV represent Type III pegmatites that have reacted with REE-enriched fluids. Key observations in deciding which is the most reasonable model are: (i) the very REE-enriched signature of the Type IV pegmatites; (ii) the presence of the extremely REE-enriched minerals allanite and britholite compared to the other REE-bearing minerals; and most importantly, (iii) the irregular and embayed contacts indicative of chemical disequilibrium observed between allanite and britholite and the other pegmatite minerals. All of these features suggest that a chemically reactive fluid was introduced late to some of the Type III pegmatites and then reacted with the mineral assemblage.

The Type IV pegmatites are associated with shear zones within the syenite complex. Shear zones and faults are zones of weakness within rocks and frequently act as paths for fluid migration. It is possible, therefore, that the REE-enriched fluids were introduced to the Type III pegmatites along shear zones. This places a time constraint on the origin of the Type IV pegmatites; they must have been formed after the crystallization of the Type III pegmatites and after the solidification of the mafic and felsic monzonite and after the development of the shear zones.

ORIGIN OF ALLANITE AND BRITHOLITE FLUIDS

Possible sources for the REE-enriched fluids that crystallized allanite and britholite in the Type IV pegmatites include: (i) a fluid of magmatic origin genetically related to the

syenite complex that is enriched in trace and incompatible elements; or (ii) a genetically unrelated fluid of either meteoric or magmatic provenance that was enriched in REEs. The association of the pegmatites with the syenite complex and their compositional similarities suggest some sort of genetic association. The most evolved silica-rich rocks associated with the Eden Lake syenite complex have very low REE contents; it was postulated earlier that separation of a F-, P- REE-enriched vapour phase, late in the evolution of the complex, might account for depletion of the REEs in the high silica group and enrichment of the REEs in the pegmatites (Chapter 4; Halden and Fryer, submitted). The nature of this enrichment is difficult to constrain in the absence of experimental data. The corroded contacts between the allanite/britholite assemblage and the other pegmatite minerals within the Type IV pegmatites is consistent with alteration by a late fluid; however, the source of such a fluid is unclear. If the syenite intrusion continued to solidify inwards after crystallization of the mafic and felsic monzonite units, the F-, P-, REE-enriched fluid may represent the last residua of crystallization that was ultimately trapped in the interior of the intrusion. The suggestion that there was separation of a vapour phase during the evolution of the complex implies something different, however. In this case, REE-enrichment might have been achieved by a sudden change in pressure or temperature, resulting in the nucleation of a F-, P-enriched vapour phase that scavenged REEs. In either case, the chemically reactive fluid appears to (i) have migrated along fractures and (ii) pervasively and irregularly altered Type III pegmatites to Type IV pegmatites.

7.4. Nature and origin of fluids.

The model described in Section 7.3 for the formation of the Type IV pegmatites requires the reaction of one F-, P-, REE-enriched fluid with the Eden Lake syenite complex to produce the allanite and britholite. However, it was noted that the britholite polygonal boundaries have also been altered, suggesting later ingress of fluids to the intrusion. These later fluids may have been of hydrothermal origin. They may even represent alteration of the intrusion by fluids whose circulation and convection were caused by the intrusion itself. What is not clear is how much time had elapsed between the formation of the allanite and britholite and alteration of the britholite polygons.

F-, P-, REE-enriched phase: physical and chemical constraints

The dominant volatile phase in the melt imposes significant controls on the behaviour of the syenite melt (Dingwell, 1988). Bulk chemical analyses of the samples from the Eden Lake syenite complex indicate elevated fluorine contents but low water contents (Halden and Fryer, submitted), suggesting that fluorine is the dominant volatile phase. Fluorine acts as a complexing agent responsible for the aqueous phase transport of various elements (Dingwell, 1988). With respect to a hydrous vapour phase, fluorine preferentially partitions into the granitic pegmatite melt phase, but in the absence of a significant amount of water, a cooling fluorine-bearing vapour phase would deplete fluorine in the syenitic melt (Flynn and Burnham, 1978; Dingwell, 1988).

Experimental studies have reported the presence of silicate-fluoride liquid immiscibility textures in granitic melts (eg. Levin et al., 1964; Anfilogov et al., 1973; Kovalenko, 1978). An investigation by Manning (1981) suggests that if immiscible fluoride and silicate liquids

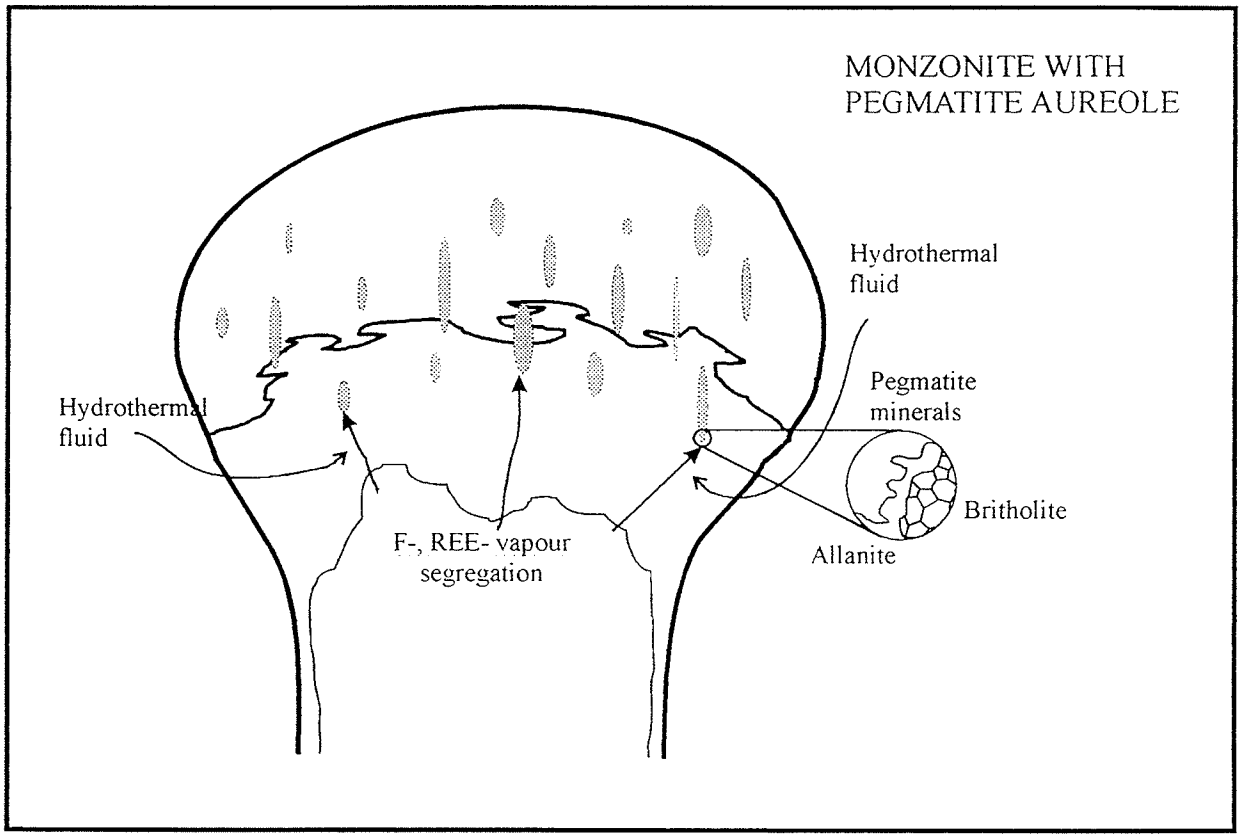

Figure 6.5. Schematic diagram illustrating the origin of the Type IV pegmatites associated with the Eden Lake syenite complex; the Type III pegmatites are shown in a stippled pattern (modified after Simmons et al., 1987). The Type IV pegmatites were formed by reaction of Type III pegmatites with a REE- and volatile-enriched magmatic fluid. Subsequent hydrothermal alteration has also affected the pegmatites; in this case, the hydrothermal fluid is unrelated to the complex.

do exist, then they must exist only in extremely F-rich melts with F concentrations of several weight percent (Kovalenko, 1978). These experiments were done in the presence of excess water, not in a system where F is the dominant volatile phase (Manning, 1981), as is the case with the Eden Lake syenite melt. The transport of the rare-earth elements in hydrothermal fluids for any distance requires the formation of carbonate, fluoride or sulphate complexes (Humphris, 1984). Cerium is easily transported because of its conversion to a 4^+ oxidized state which enables it to be re-mobilized more readily than the other rare earth elements; lanthanum often shows similar behavioral trends although it does not oxidize (Humphris, 1984).

Distribution of the F-, P-, REE-enriched phase

During the late stages of fractional crystallization of the syenite melt, it is possible that the REEs (and other incompatible trace elements such as Y, U, Th) were removed from the syenite melt by complexing with fluorine; such a vapour phase could then be re-introduced to the syenite complex to reacted with some of the pegmatites associated with the complex. It is not reasonable to assume that the vapour phase was introduced to only a few shear zones and reacted only with pegmatite minerals that it encountered in the shear zones. Rather, we would expect a wider distribution, interaction and reaction between the vapour phase and the main units of the syenite complex. Other parts of the syenite complex not associated with shear zones should therefore show the effects of some reaction with the vapour phase. This type of effect can be seen on the hand sample scale (cf McRitchie, 1989). As mentioned earlier, a considerable proportion of the intrusion is obscured by overburden, so it is hard to estimate the volume of the F-, P-, REE-enriched fluid that has altered the complex. It is

interesting to note that the overburden contains significant amounts of Sr, Ba and REEs (Fedikow et al., 1993; 1994) which might suggest the alteration was widespread.

Fluids responsible for britholite alteration

The fluid alteration of britholite occurred late in the history of the Type IV pegmatites; it probably occurred at elevated temperatures in order to cause annealing of the britholite. The source of the fluids responsible for the alteration of the britholite polygons is unknown. This is a question that might be addressed by fluid inclusions and stable isotope studies. It is worth noting that other minerals such as andradite, aegirine-augite and K-feldspar do show some effects of recrystallization. It is also possible, if the REE-bearing carbonates found as inclusions within titanite, that these could also be connected with a late, possibly hydrothermal alteration event.

Fluid activity associated with other REE deposits

Fluid activity, both magmatic and meteoric, is important for the development of many REE deposits hosted in granitic rocks. These include both the Strange Lake deposit, Labrador/P.Q., and the Rodeo de Los Molles deposit, Argentina.

The Strange Lake pluton is a peralkaline granite, located within the Nain Province of the Canadian Shield (Currie, 1985). The Strange Lake pluton has been dated at 1189 ± 32 Ma (Pillet et al., 1989) and therefore it has been suggested that the pluton is related to the Gardar anorogenic event in Greenland (Upton, 1974; Currie, 1985; Pillet et al., 1989; Salvi and Williams-Jones, 1990). The pluton contains an unusual niobium-zirconium-rare earth deposit (Zajac et al., 1984). Evolution of the Strange Lake pluton is unusual because the concentration in Be, Zr, and REEs was marked by a decrease in alkali content, decrease in

agpaitic index and increase in Ca content (Currie, 1985). This can be accounted for by alteration of the pluton by an anhydrous F- (and Ca-) enriched fluid that contained REEs and Zr complexed with F (Currie, 1985). Fluid inclusion studies indicate that a number of successive alteration events occurred (Salvi and Williams-Jones, 1990). An early Ca metasomatic event involved the interaction of two immiscible fluids, one of high salinity $CaCl_2$ and the other of CH_4, with a third low salinity fluid containing NaCl. The Y and REE mineralization occurred after significant mixing of the high and low salinity fluids; fluorite deposition caused a reduction of ligand concentration which allowed precipitation of the REE-bearing minerals to occur at temperatures less than 200°C (Salvi and Williams-Jones, 1990). The high salinity fluids were associated with basement gneisses near the Strange Lake pluton; they represent ground or formational waters that were heated by the intrusion of the Strange Lake pluton. The low salinity fluids represent oxidizing ground waters that circulated within the pluton. The REEs, Zr and Y were already present within the pluton and were locally remobilized and concentrated (Salvi and Williams-Jones, 1990).

The Rodeo de Los Molles REE and Th deposit is located in granitic rocks of the Las Chacras batholith in central Argentina (Lira and Ripley, 1990). The Las Chacras batholith has been dated at 320-335 Ma (K/Ar; Brogioni, 1987); it formed during the last stages of a continental arc cycle in the Lower Carboniferous (Rapela et al., 1990). The deposit is hosted within a hydrothermally altered zone of alkali feldspar granite and syenite within a biotite monzogranite (Lira and Ripley, 1992). The mineralogy of the REE deposit is markedly similar to that of the Type IV pegmatites within the Eden Lake syenite complex. The primary mineral assemblage includes apatite, titanite, and alteration products include fluorite, britholite and

allanite (Lira and Ripley, 1992). Fluid inclusion studies indicate that there has been a complex history of open-system fluid migration and interaction with the host rocks (Lira and Ripley, 1990). The fluids that produced allanite and britholite were of magmatic origin and were channelled from the base of the intrusion to the top (Lira and Ripley, 1992). Later meteoric fluids were involved in alteration of the REE minerals at temperatures less than 200°C (Lira and Ripley, 1992). The REEs were present in other minerals within the pluton and were redistributed and concentrated by the magmatic fluids.

The Type IV pegmatites associated with the Eden Lake syenite complex underwent fluid alteration similar to the model proposed for the Rodeo de Los Molles deposit. The fluid that produced the REE deposits was magmatic in origin and was channelled into the pegmatites along shear zones to the top of the complex (Figure 6.4). The fluid reacted with pegmatite minerals to produce a REE-enriched pegmatite. Like the Rodeo de Los Molles and the Strange Lake deposits, a number of hydrothermal events have altered the Eden Lake pegmatites after REE mineralization. Unlike the Rodeo de Los Molles and the Strange Lake deposits, the REEs were already concentrated in a fluid phase by complexing with F during separation of an immiscible vapour phase; the REEs were not remobilized from other minerals within the syenite complex.

Chapter 7: Conclusions

The Eden Lake syenite complex is a multiphase anorogenic intrusion with alkaline characteristics that is associated with four different pegmatite units. Mineralogical and geochemical studies of these pegmatites indicate they have complex and varied origins. In addition, the Eden Lake syenite complex and associated pegmatites have been affected by a number of fluid alteration events, similar to other granitic intrusions that host REE deposits.

The Type I and Type II pegmatites contain no REE-enriched accessory minerals and are not genetically related to the syenite complex. Rather, these pegmatites represent multiple injections of undifferentiated granitic melt from a younger monzonite suite in the Eden Lake areas. The Type I mafic pegmatites represent the oldest injection from this magma.

Pools of residual melt with high volatile content and a slight enrichment in incompatible rare elements crystallized to form the Type III pegmatites after crystallization of the mafic and felsic monzonites. Within the Type III pegmatites, REEs, and other trace elements such as U and Th, were incorporated into apatite, titanite and zircon, as well as strontianite and burbankite. Apatite, titanite and zircon display a similar crystallization history; the early stage of growth is characterized by the development of discontinuous, patchy zoning, the result of supersaturation within the pegmatite melt. The second stage of growth is characterized by the development of both oscillatory and sector zoning that result from diffusion-controlled growth. The last stage of growth resulted in the formation of an overgrowth around pre-existing crystals. These REE-bearing phases are among the earliest to crystallize in the pegmatites; later minerals include andradite, aegirine-augite, K-feldspar, plagioclase, quartz and fluorite. Decay of U and Th within zircon crystals has resulted in

metamictization of the Type III zircons.

A number of characteristics suggest the Type IV pegmatites represent Type III pegmatites that have been altered by REE-enriched fluids, including mineralogy, mineral chemistry, both major and trace element abundances, and mineral growth histories. The REE-enriched fluids were introduced to some Type III pegmatites along shear zones and fractures within the syenite complex. Reactions between the fluids and the pre-existing pegmatite minerals, including apatite, titanite, zircon, aegirine-augite, quartz, K-feldspar, plagioclase and fluorite, occurred, followed by the crystallization of first allanite, then britholite. The source of the REE-enriched fluids is most likely a F-. P-, REE-enriched vapour phase that separated from the syenite complex during crystallization of the mafic monzonite. The decay of U and Th within britholite caused amorphization of the britholite, alteration of allanite and resulted in the fracturing of associated minerals. The polygonal texture observed in the britholite is the result of annealing of amorphized britholite. The heat responsible for the annealing was related to late hydrothermal alteration of the britholite; the alteration post-dates the annealing. The hydrothermal fluid moved along britholite polygonal boundaries and may have been chemically buffered by the britholite.

As this study is the first to examine the minerals within the pegmatites associated with the Eden Lake syenite complex in detail, it raises several questions that need to be considered in future work. (i) What are the sources and relations of the various hydrothermal fluids that have altered both the Type III and Type IV pegmatites? (ii) What is the origin of the inclusions, thorite and oscillatory-zoned allanite, in the Type III pegmatites (iii) What are the origin and relationships of the strontium carbonate minerals, strontianite, burbankite, and

weloganite associated with titanite? Much work remains to be done in order to fully comprehend the REE-enriched pegmatites associated with the Eden Lake syenite complex.

References

Anderson, A.T., 1984. Probable relations between plagioclase zoning and magma dynamics, Fuego Volcano, Guatemala. Amer Min, Vol 69, p 660-676.

Anfilogov, V. N., Bushlyakov, I. N., Vilisov, V. A., and Bragina, B. I., 1977. Distribution of fluorine between coexisting biotite and amphibole and granitic melts at 780°C and 1000 atm pressure. Geochem Int., Vol 19, p 95-98.

Arth, J. G., 1976. Behaviour of trace elements during magmatic processes - a summary of theoretical models and their applications. U.S. Geological Survey Journal of Research, Vol 4, p 41-47.

Baldwin, D. A., 1988. Mineral deposits and occurrences in the Lynn Lake area, NTS 64C/14. Manitoba Energy and Mines, Geological Services, 130 pp.

Brogioni, N., 1987. El batolito de Las Chacras-Piedras Coloradas, provincia de San Luis, Geologia y edad. Intl Symp Circum Pacific Phanerozoic Granites: X Cong Geol Arg, Vol IV, p 115-118.

Cameron, H.D.M., 1978. Eden Lake, *in* Manitoba Mineral resources Division, Report of Field Activities 1978, p 16-19.

Cameron, H.D.M., 1988. Geology of the Eden Lake area. Manitoba Energy and Miners Geological Report GR84-2, 18pp.

Cerny, P., 1991a. Rare-element granitic pegmatites. Part I: Anatomy and internal evolution of pegmatite deposits, *in* Ore Deposit Models. Geoscience Canada Reprint Series 6, p 29-47.

Cerny, P., 1991b. Rare element granitic pegmatites. Part II: Regional to global environments and petrogenesis, *in* Ore Deposit Models. Geoscience Canada Reprint Series 6, p 49-62.

Cerny, P. and Meintzer, R. E., 1988. Fertile granites in the Archean and Proterozoic fields of rare-element pegmatites: crustal environment, geochemistry and petrogenetic relationships, *in* Taylor, R. P. and Strong, D. F., Eds., Recent advances in the geology of granite-related mineral deposits. Can Inst Min Met Spec Vol 39, p 170-207.

Chakoumakos, B. C., Murakami, T., Lumpkin, G. R, and Ewing, R. C., 1987. Alpha-decay-induced fracturing in zircon: the transition from the crystalline to the metamict state. Science, Vol 236, p 1556-1559.

Clark, A. M., 1984. Mineralogy of the rare earth elements, *in* Henderson, P., Ed, Rare earth element geochemistry. Elsevier, New York, p 33-62.

Currie, K. L., 1985. An unusual peralkaline granite near Lac Brisson, Quebec-Labrador, *in* Current Research, Part A, GSC, Paper 85-1A, p 73-80.

Deer, W. A., Howie, R. A. and Zussman, J., 1986. Allanite, *in* Deer, W. A., Howie, R. A. and Zussman, J., Eds, Rock-forming minerals, Second Edition, Vol Disilicates and Ring silicates. Wiley, New York, p 151-179.

Deer, W. A., Howie, R. A. and Zussman, J., 1989. An introduction to the rock forming minerals. John Wiley and Sons, New York, 525 pp.

Dingwell, D. B., 1988. The structures and properties of fluorine-rich magmas: a review of experimental studies, *in* Taylor, R. P., and Strong, D. F., Eds., Recent advances in the geology of granite-related mineral deposits, Can Inst Min Met Spec Vol 39, p 1-12.

Eby, R. K., Wang, L. M., Arnold, G. W., and Ewing, R. C., 1991. Ion-irradiation study of the exotic mineral neptunite: $LiNa_2K(Fe, Mg,Mn)_2Ti_2Si_8O_{24}$. Mat Res Soc Symp Proc, Vol 201, p 283-288.

Fedikow, M.A., Dunn, C. E. and Kowalyk, E., 1993. A vegetation geochemical and radiometric study of part of the Eden Lake aegirine-augite syenite, northwestern Manitoba, *in* Manitoba Energy and Mines, Minerals Division, Report of Activities, 1993, p 5-10.

Fedikow, M. A., Dunn, D. E. and Kowalyk, E., 1994. Preliminary observations from a vegetation geochemical survey over part of the Eden Lake aegirine-augite syenite, Lynn Lake areas (NTS 64C/9), *in* Manitoba Energy and Mines, Minerals Division, Report of Activities, 1994, p 11-15.

Flynn, R. T. and Burnham, C. W., 1978. An experimental determination of rare earth partition coefficients between a chloride containing vapour phase and silicate melts. Geochim Cosmochim Acta, Vol 42, p 685-701.

Geological Survey of Canada, 1977. Uranium Reconnaissance Program Map 35364G.

Ghent, E. D., 1972. Electron microprobe study of allanite from the Mt Falconer quartz monzonite pluton, lower Taylor Valley, South Victoria Land, Antarctica. Can Min, Vol 11, p 526-530.

Ginsburg, A. I., Timofeyev, I. N. and Feldman, L. G., 1979. Principles of geology of the granitic pegmatites. Nedra, Moscow, 296 p. [In Russian]

Gordon, T. M., Hunt, P. A., Bailes, A. H. and Syme, E. C., 1990. U-Pb ages from the Flin Flon and Kisseynew belts, Manitoba: chronology of crust formation at an Early Proterozoic accretionary margin, *in* Lewry, J. F. and Stauffer, M. R., Eds, The Early Proterozoic Trans-

Hudson Orogen of North America. Geol Ass Canada, Spec Pap 37, p 177-200.

Halden, N. M., Clark, G. S., Corkery, M. T., Lenton, P. G. and Schledewitz, D.C.P., 1990. Trace-element and Rb-Sr whole-rock isotopic constraints on the origin of the Chipewyan, Thorsteinson and Baldock batholiths, Churchill Province, Manitoba, *in* Lewry, J. F. and Stauffer, M. R., Eds, The Early Proterozoic Trans-Hudson Orogen of North America. Geol Ass Canada, Spec Pap 37, p 201-214.

Halden, N. M., Hawthorne, F. C., Campbell, J. L., Teesdale, W. J., Maxwell, J. A., and Higughi, D., 1993. Chemical characterization of oscillatory zoning and overgrowths in zircon using a 3MeV μ-PIXE. Can Min, Vol 31, p 637-647.

Halden, N. M. and Fryer, B. J., submitted. Geochemical characteristics of the Eden Lake syenite: late anorogenic magmatism in the Trans-Hudson Orogen.

Hawthorne, F.C., Groat, L.A., Raudsepp, M., Ball, N.A., Kimata, M., Spike, F.D., Gaba, R., Halden, N.M., Lumpkin, G.R., Ewing, Greegor R.B., Lytle, F.W., Ercit, T.S., Rossman, G.R., Wicks, F.J., Ramik, R.A., Sherriff, B.L. Fleet, M.E., and McCammon, C., 1991. Alpha decay damage in titanite. Amer Min, Vol 76, p 370-396.

Henderson, J. E., Norman, G.W.H. and Downie, D. L., 1936. Granville Lake (east half) area, Manitoba. Geological Survey of Canada, Map 344A.

Henderson, P., 1980. Rare element partition between sphene, apatite and other co-existing minerals of the Kangerdlugssuag intrusion, East Greenland. Contrib Min Pet, Vol 72, p 81-85.

Hinton, R. W. and Upton, B.C.J., 1991. The chemistry of zircon: variations within and between large crystals from syenite and alkali basalt xenoliths. Geochim Cosmochim, vol 55, p 3287-3302.

Hoffman, P., 1988. United Plates of America, the birth of a craton: Early Proterozoic assembly and growth of Laurentia. Ann Rev Earth Planet Sci, Vol 16, p 543-603.

Hughson, M. R. and Sen Gupta, J. G., 1964. A thorian intermediate member of the britholite-apatite series. Canadian Mineralogist, vol 49, p 937-951.

Humphris, S. E., 1984. The mobility of the rare earth elements in the crust, *in* Henderson, P., Ed, Rare earth element geochemistry. Elsevier, New York, p 317-342.

Jamtveit, B., 1991. Oscillatory zonation patterns in hydrothermal grossular-andradite garnet: nonlinear dynamics in regions of immiscibility. Amer Min, Vol 76, p 1319-1327.

Khudolozhkin, V. O., Urusov, V. S. and Tobelko, K. I., 1973. Dependence of structural

ordering of rare earth atoms in the isomorphous series apatite-britholite (abukumalite) on composition and temperature. Geochem Int, vol 10, p 1171-1177.

Kovalenko, V. I., 1978. The reactions between granite and aqueous hydrofluoric acid in relation to the origin of fluorine-bearing granites. Geochem Int, Vol 14, p 108-118.

Kwak, T.A.P., 1981. Sector-zoned $annite_{85}phlogopite_{15}$ micas from the Mt. Lindsay Sn-W-F(-Be) deposit, Tasmania, Australia. Can Min, Vol 19, p 643-650.

Lenton, P. G., 1982. Granite-pegmatite studies, Lynn Lake region, *in* Manitoba Department of Energy and Mines, Mineral Resources Division, Report of Field Activities 1982, p 19-23.

Levin, E. M., Robbins, C. R. and McCurdie, H. F., 1964. Phase diagrams for ceramists. The American Ceramists Society.

Lewry, J. F., Sibbald, T.I.I. and Schledewitz, D.C.P., 1985. Variation in character of Archean rocks in the western Churchill province and its significance, *in* Ayres, L. D., Thurston, P., Card, K. and Weber, W., Eds. Evolution of Archean Supracrustal sequences. Geol Assn Can Spec Pap 28, p 239-261.

Lewry, J. F. and Collerson, K. D., 1990. The Trans-Hudson orogen: extent, subdivisions and problems, in Lewry and Stauffer, Eds. The early Proterozoic trans-Hudson Orogen of North America. Geol Assn Can Sp Paper 37, p 1-14.

Lira, P. and Ripley, E. M., 1990. Fluid inclusion studies of the Rodeo de Los Molles REE and Th deposit, Las Chacras Batholith, Central Argentina. Geochim Cosmochim, vol 54, p 663-671.

Lira, P. and Ripley, E. M., 1992. Hydrothermal alteration and REE-Th mineralization at the Rodeo de los Molles deposit, Las Chacras batholith, central Argentina. Contrib Min Pet, vol 110, p 370-386.

Maniar, P. D. and Piccoli, P. M., 1989. Tectonic discrimination of granitoids. Geol Soc Amer Bull, Vol 101, p 635-643.

Manning, D.A.C., 1981. The effect of fluorine on liquidus phase relationships in the system Qz-Ab-Or with excess water at 1 kbar. Contrib Min Pet, Vol 76, p 206-215.

Mariano, 1989. Economic geology of rare earth elements, *in* Lipin and McKay, Eds, Geochemistry and Mineralogy of Rare Earth elements, Reviews in Mineralogy, Vol 21, p 309-337.

Maxwell,J. A., Campbell, J. L. and Teesdale, W. J., 1989. The Guelph PIXE software

package. Nucl Instrumentation Methods Phys Res, Vol B43, p 218-230.

McRitchie, W. D., 1976. Paskwachi-Waskaiowaka regional compilation. Manitoba Mineral Resources Division, Geological Survey, Report of Field Activities 1976, p 13-23.

McRitchie, W. D., 1988. Alkaline intrusions of the Churchill Province Eden Lake and Brezden Lake, *in* Manitoba Energy and Mines, Minerals Division, Report of Field Activities, 1988, p 5-11.

McRitchie, W. D., 1989. Ground scintillometer reconnaissance of the Eden Lake aegirine-augite monzonite, *in* Manitoba Energy and Mines, Minerals Division, Report of Field Activities, 1989, p 7-12.

Meyer, M. T., Bickford, M. E., and Lewry, J. F., 1992. The Wathaman batholith: an early Proterozoic continental arc in the Trans-Hudson orogenic belt. Geol Soc Am Bull, Vol 104, p 1073-1085.

Morin, J. A., 1977. Allanite in granitic rocks of the Kenora-Vermilion Bay area, Northwestern Ontario. Can Min, Vol 15, p 297-302.

Nakamura, Y., 1973. Origin of sector-zoning or igneous clinopyroxenes. Amer Min, Vol 58, p 986-990.

Nash, W. P., 1972. Apatite chemistry and phosphorus fugacity in a differentiated igneous intrusion. Amer Min, Vol 57, p 877-886.

Pan, Y. and Fleet, M., 1990. Halogen-bearing allanite from the White River gold occurrence, Hemlo area, Ontario. Can Min, Vol 28, p 67-75.

Pan, Y., Fleet, M., and MacRae, N. D., 1993. Late alteration in titanite ($CaTiSiO_5$): redistribution and remobilization of rare earth elements and implications for U/Pb and Th/Pb geochronology and nuclear waste disposal. Geochim Cosmochim, Vol 57, p 355-367.

Parsons, I., and Brown, W. L., 1984. Feldspars and the thermal history of igneous rocks, *in* Brown, W. L., Ed., Feldspars and Feldspathoids: structures, properties and occurrences. D. Reidel Publishing Co., Boston, p 317-372.

Paterson, B. A. and Stephens, W. E., 1992. Kinetically induced compositional zoning in titanite: implications for accessory-phase/melt partitioning of trace elements. Contrib Min Pet, Vol 109, p 373-385.

Pidgeon, R. T., 1992. Recrystallisation of oscillatory zoned zircon: some geochronological and petrological implications. Contrib Min Pet, vol 110, p 463-472.

Pillet, D., Bonhomme, M. G., Duthou, J. L. and Shenevoy, M., 1989. Chronologie Rb/Sr et K/Ar du granite peralkalin du lac Brisson, Labrador central, Noveau-Quebec. Can Jour Earth Sci, Vol 26, p 328-332.

Rapela, C. W., Toselli, A. J., Heaman, L., and Saavedra, J., 1990. Granite plutonism of the Sierras Pampeanas: an inner cordilleran Paleozoic arc in the Southern Andes, *in* Kay, S. M. and Rapela, C. W., Eds, Plutonism from Antarctica to Alaska. Geol Soc Amer Spec Paper Vol 241.

Reeder, R. J., and Paquette, J., 1989. Sector zoning in natural and synthetic calcites. Sed Geol, Vol 65, p 239-247.

Reeder, R. J., Fagioli, R. O., and Meyers, W. J., 1990. Oscillatory zoning of Mn in solution-grown calcite crystals. Earth Science Reviews, Vol 29, p 30-46.

Romans, P. A., Brown, L. L., and White, J. C., 1975 . An electron microprobe study of yttrium, rare element and phosphorus distribution in zoned and ordinary zircon. Amer Min, Vol 60, p 475-480.

Ronsbo, J. G., 1989. Coupled substitutions involving REEs and Na and Si in apatites in alkaline rocks from the Ilimaussaq intrusion, South Greenland and the petrological implications. Amer Min, Vol 74, p 896-901.

Rubin, J. N., Henry, C. D. and Price, J. G., 1989. Hydrothermal zircons and zircon overgrowths, Sierra Blanca Peaks, Texas. Amer Min, Vol 74, p 865-869.

Russell, J. K., Groat, L. A. and Halleran, A.A.D., 1994. LREE-rich nioban titanite from Mount Bisson, British Columbia: chemistry and exchange mechanisms. Can Min, Vol 32, p 575-587.

Salvi, S. and Williams-Jones, A. E., 1990. The role of hydrothermal processes in the granite hosted Zr, Y, REE deposit at Strange Lake, Quebec/Labrador: evidence from fluid inclusions. Geochim Cosmochim, Vol 54, p 2403-2418.

Searl, A., 1990. Complex sector zonation in ankerite: geochemical controls on crystal morphology and intersector element partitioning. Min Mag, Vol 54, p 501-507.

Schmitt, H. R, Hornbrooke, E. H., and Friske, P.W.B., 1989. Geochemical results and interpretations of a lake sediment and water survey in the Lynn Lake-Leaf Rapids region, northern Manitoba. Geological Survey of Canada Open File 1959.

Schuiling, R. D. and Vink, B. W., 1967. Stability relations of some titanitium-minerals (sphene, perovskite, rutile, anatase). Geochin et Cosmoshim, Vol 31, p 2399-2412.

Simmons, W. B., Lee, M. T. and Brewster, R. H., 1987. Geochemistry and evolution of the South Platte granite-pegmatite system, Jefferson County, Colorado. Geochem et Cosmochim Acta, Vol 51, p 455-471.

Smith, W. L., Franck, M. L. and Sherwood, A. M., 1957. Uranium and thorium in the accessory allanite of igneous rocks. Amer Min, Vol 42, p 367-378.

Speer, J. A., 1980. Zircon, *in* Ribbe, P. H., Ed, Orthosilicates. Rev Min 5, p 67-112.

Stauffer, M. R., 1984. Manikewan: an Early Proterozoic ocean in central Canada, its igneous history and orogenic closure. Precambrian Research, Vol 25, p 257-81.

Sun, S. S., 1982. Chemical composition and origin of the Earth's primitive mantle. Geochimica et Cosmochimica Acta, Vol 46, p 179-192.

Swanson, M. L., Parsons, J. R. and Hoelke, C. W., 1971, *in* Corbett, J. W. and Watkins, G. D., Radiation effects in Semiconductors. Gordon and Breach, New York, 359 pp.

Syme, E. C., 1990. Stratigraphy and geochemistry of the Lynn Lake and Flin Flon metavolcanic belts, Manitoba, *in* Lewry, J. F. and Stauffer, M. R., Eds, The early Proterozoic trans-Hudson orogen of North America. Geol Assn Can Sp Paper 37, p 143-161.

Upton, B.C.J., 1974. The alkaline province of southwest Greenland, *in* Sorenson, H., Ed, The Alkaline rocks. Interscience, p 221-238.

Van Breemen, O., Henderson, J. B., Loveridge, W. D. and Thompson, P. H., 1987. U-Pb zircon and monazite geochronology and zircon morphology of granulites and granite from the Thelon Tectonic Zone, Healey Lake and Artillery Lake map areas, N.W.T., *in* Current Research, Part A. Geol Surv Canada Paper 87-1A, p 783-801.

Van Schmus, W. R., Persons, S. S., Macdonald, R. and Sibbald, T.I.I., 1986. Preliminary results from U-Pb zircon geochronology of the Uranium City region, northwest Saskatchewan, *in* Summary of Investigations 1986. Saskatchewan Geol Surv Misc Rep 86-4, p 108-111.

Vance, J. A., 1965. Zoning in igneous plagioclase: patchy zoning. Journal Geology, Vol 73, p 636-651.

Vernon, R. H., 1976. Metamorphic processes: reactions and microstructure development. George Allan & Unwin, Ltd, London, 243 pp.

Wang, Y. and Merino, E., 1992. Dynamic model of oscillatory zoning of trace elements in calcite: double layer, inhibition and self-organization. Geochimica et Cosmochimica Acta, Vol

56, p 587-596.

Weber, W. J., 1992. Radiation-induced amorphization in complex silicates. Nuclear Instruments and Methods in Physics Research, Vol B65, p 88-92.

Weber, W. J. and Wang, Y., 1993. Ion beam amorphization of $Ca_2La_8(SiO_4)_6O_2$ single crystals.

Zajac, I. S., Miller, R., Birkett, T., and Nantel, S., 1984. The Strange Lake deposit, Quebec-Labrador. Can Inst Min Metall Bull, Vol 77, p 60.

Zwanzig, H. V., 1974. Lynn Lake volcanic studies, *in* Manitoba Mineral Resources Division, Report of Field Activities 1974, p 13-16.

Zwanzig, H. V., 1990. Kisseynew gneiss belt in Manitoba: stratigraphy, structure and tectonic evolution, *in* Lewry, J. F. and Stauffer, M. R., Eds, The early Proterozoic Trans-Hudson orogen of North America. Geol Assn Can Sp Paper 37, p 95-120.

Zwanzig, H. V., Parker, J.S.D., Schledewitz, D.C.P. and Van Schmus, 1985. Lynn Lake regional compilation and geochronology, *in* Manitoba Mineral Resources Division, Report of Field Activities 1985, p 6-8.

Appendices

For each composition listed, sample locations are listed by thin section number, crystal number and point of analysis, and by PIXE reference number, if necessary. Zoning refers to the type of zoning pattern, if any, at point of analysis.

APPENDIX I: APATITE

Chemical compositions of separate apatite grains in the Type III pegmatites.

Location	5A1-AP3-2	5A1-AP4-1	5A1-AP2-2	5A1-AP3-1	5A1-AP4-2	5A1-AP1-1
Zoning	Dark	Dark	Light	Light	Light	Unzoned
CaO (1)	53.051	52.011	52.538	52.749	52.194	52.759
P2O5	39.637	39.101	38.569	39.45	38.438	39.4
SiO2	0.312	0.565	0.785	0.65	0.925	0.522
FeO	0.019	0	0.093	0	0.012	0.009
MnO	0.061	0.011	0.011	0.016	0.035	0.054
MgO	0	0	0	0	0	0
Na2O	0.107	0.073	0	0.163	0.133	0
SrO	0.8	0.79	-	0.983	0.756	-
F	3.805	4.16	3.801	3.765	4.13	3.895
Cl	0.003	0.031	0.03	0.001	0.01	0.047
REE2O3 (2)	0.714	0.794	-	1.705	1.017	-
TOTAL	98.524	97.543	95.827	99.482	97.719	96.686
Ba (ppm)	134	63	-	0	618	-
Y	290	580	-	1950	980	-
La	480	410	-	1570	610	-
Ce	2090	2600	-	4660	2910	-
Nd	2620	2590	-	4800	3090	-
Sm	610	310	-	1340	490	-
Gd	0	260	-	110	550	-

Location	5A1-AP1-2	5A1-AP1-3	5A1-AP2-1
Zoning	Unzoned	Unzoned	Unzoned
CaO (1)	53.121	53.121	52.679
P2O5	39.839	40.334	38.7
SiO2	0.377	0.137	0.769
FeO	0.001	0.085	0
MnO	0	0.013	0
MgO	0	0	0
Na2O	0	0	0
SrO	-	-	-
F	3.799	4.415	3.842
Cl	0.047	0.007	0.027
REE2O3 (2)	-	-	-
TOTAL	97.184	98.112	96.017
Ba (ppm)	-	-	-
Y	-	-	-
La	-	-	-
Ce	-	-	-
Nd	-	-	-
Sm	-	-	-
Gd	-	-	-

(1) Major and trace element abundance (in weight percent oxide and ppm, respectively) from EPMA.

(2) REE2O3 is sum of REE abundances

APPENDIX I: APATITE

Chemical compositions of apatite inclusions within titanite grains in the Type III pegmatites.

Location	**5A7-AP1-4**	**5A7-AP2-1**	**5A4-AP1-4**	**5A4-AP1-5**	**5A4-AP2-2**
PIXE				**Apr10_95.**	
Zoning	**Dark Patch**	**Dark Patch**	**Light Patch**	**Light Patch**	**Light Patch**
CaO (1)	54.6	54.939	53.845	53.814	54.669
P2O5	39.755	40.273	38.725	38.243	39.949
SiO2	0	0	0	0	0
FeO	0.06	0	0	0.166	0
MnO	0	0.067	0.061	0.038	0.011
MgO	0	0	0	0	0
SrO	-	-	-	0.168	-
F	4.304	4.276	3.885	4.001	4.098
Cl	0.005	0.024	0.002	0	0
REE2O3 (2)	-	-	-	1.535	-
TOTAL	98.724	99.579	96.518	97.965	98.727
Ni (ppm) (3)	-	-	-	0	-
Cu	-	-	-	12	-
Zn	-	-	-	18	-
As	-	-	-	59	-
Y	-	-	-	1423	-
Ba	-	-	-	1662	-
La	-	-	-	2102	-
Ce	-	-	-	3673	-
Nd	-	-	-	4006	-
Sm	-	-	-	879	-
Gd	-	-	-	494	-
Dy	-	-	-	221	-
Er	-	-	-	135	-
Yb	-	-	-	98	-
Pb	-	-	-	137	-
Bi	-	-	-	0	-
Th	-	-	-	1016	-
U	-	-	-	118	-

(1) Major element abundance (in weight percent oxide) from EMPA.
(2) REE2O3 is sum of REE abundances.
(3) Trace element abundance in ppm, from PIXE.

APPENDIX I: APATITE

Chemical compositions of apatite inclusions within titanite grains in the Type III pegmatites.

Location	**5A4-AP2-3**	**5A7-AP1-2**	**5A7-AP1-3**	**5A7-AP2-2**
PIXE				
Zoning	**Light Patch**	**Light Patch**	**Light Patch**	**Light Patch**
CaO (1)	53.271	54.11	53.934	53.846
P2O5	37.38	38.775	37.748	38.848
SiO2	0	0	0	0
FeO	0.057	0.036	0.031	0.002
MnO	0.002	0	0.03	0.035
MgO	0	0	0	0
SrO	-	-	-	-
F	4.027	4.172	4.194	4.31
Cl	0.025	0.002	0.013	0.014
REE2O3 (2)	-	-	-	-
TOTAL	94.762	97.095	95.95	97.055
Ni (ppm) (3)	-	-	-	-
Cu	-	-	-	-
Zn	-	-	-	-
As	-	-	-	-
Y	-	-	-	-
Ba	-	-	-	-
La	-	-	-	-
Ce	-	-	-	-
Nd	-	-	-	-
Sm	-	-	-	-
Gd	-	-	-	-
Dy	-	-	-	-
Er	-	-	-	-
Yb	-	-	-	-
Pb	-	-	-	-
Bi	-	-	-	-
Th	-	-	-	-
U	-	-	-	-

(1) Major element abundance (in weight percent oxide) from EMPA.
(2) REE2O3 is sum of REE abundances.
(3) Trace element abundance in ppm, from PIXE.

APPENDIX I: APATITE

Chemical compositions of unaltered and altered apatite grains in the Type IV pegmatites.

Location	6A2-AP1-2	6A2-AP2-1	6A2-AP2-3	6A2-AP3-1	6A2-AP4-2	6A2-AP6-1
	Unaltered	Unaltered	Unaltered	Unaltered	Unaltered	Unaltered
SiO2 (1)	3.573	2.519	1.27	2.017	1.789	1.838
FeO	0.168	0.001	0	0.006	0.021	0
MnO	0.127	0.032	0	0.039	0	0.006
MgO	0.178	0	0	0	0	0
CaO	48.192	51.318	52.691	52.428	52.429	52.286
P2O5	34.086	34.868	37.919	37.176	37.413	37.149
F	3.865	4.031	4.1	3.954	3.955	3.928
Cl	0.003	0.019	0	0.005	0	0
TOTAL	90.192	92.788	95.98	95.625	95.607	95.207

Location	6A8A-AP1-1	6A8A-AP2-3	6A8A-AP2-5	6A5-AP2-4	6A5-AP3-1	6A5-AP3-4
	Unaltered	Unaltered	Unaltered	Unaltered	Unaltered	Unaltered
SiO2 (1)	1.353	2.434	2.717	2.351	1.439	1.988
FeO	0	0.048	0	0	0.025	0.018
MnO	0.002	0.018	0	0	0	0
MgO	0	0	0	0	0	0
CaO	52.719	51.279	50.577	51.398	53.146	52.103
P2O5	38.007	35.345	34.428	36.124	38.363	36.839
F	3.84	4.092	3.999	3.8	3.925	3.977
Cl	0	0.016	0.021	0	0.027	0
TOTAL	95.921	93.232	91.742	93.673	96.925	94.925

Location	6A5-AP4-3	6A5-AP4-4	6A1C-AP1-1	6A1C-AP3-1	6A1C-AP3-3	6A1C-AP4-1
	Unaltered	Unaltered	Unaltered	Unaltered	Unaltered	Unaltered
SiO2 (1)	3.104	3.177	3.043	2.732	3.064	3.498
FeO	0	0.06	0	0	0.037	0.017
MnO	0	0	0	0	0.004	0
MgO	0	0	0	0	0	0
CaO	50.223	50.602	51.511	51.993	51.467	50.96
P2O5	34.29	33.589	34.844	35.142	34.756	33.754
F	3.95	4.223	3.92	3.755	3.923	3.907
Cl	0	0	0.001	0.005	0.001	0.003
TOTAL	91.567	91.651	93.319	93.627	93.252	92.139

(1) Element abundance in weight percent oxide from EMPA

APPENDIX I: APATITE

Chemical compositions of unaltered and altered apatite grains in the Type IV pegmatites.

Location	6A5-AP1-1	6A5-AP1-3	6A6A-AP1-3	6A6A-AP2-3	6A2-AP6-3	6A4-AP1-3
	Unaltered	Unaltered	Unaltered	Unaltered	Unaltered	Unaltered
SiO2 (1)	2.208	0.748	2.866	2.51	1.622	2.477
FeO	0.494	0.016	0	0.027	0.019	0.065
MnO	0	0	0	0	0.001	0.019
MgO	0.234	0	0	0	0.021	0
CaO	52.196	54.477	50.037	51.423	52.662	51.041
P2O5	37.907	39.857	34.064	34.989	37.829	35.609
F	3.751	3.785	4.159	3.886	3.777	3.967
Cl	0	0	0.015	0.012	0	0.016
TOTAL	96.79	98.883	91.141	92.847	95.931	93.194

Location	6A4-AP1-1	6A4-AP2-1	6A4-AP2-3	6A4-AP3-1	6A4-AP4-1	6A4-AP4-4
	Unaltered	Unaltered	Unaltered	Unaltered	Unaltered	Unaltered
SiO2 (1)	2.646	2.168	2.173	1.972	2.778	2.226
FeO	0.019	0	0.001	0.183	0	0.105
MnO	0	0.024	0	0.018	0	0.035
MgO	0	0.02	0	0	0	0
CaO	50.754	51.968	51.817	51.825	50.002	51.585
P2O5	32.213	36.606	36.322	36.591	34.123	36.314
F	4.123	4.046	3.834	3.997	3.911	4.064
Cl	0.002	0.012	0.001	0.004	0.006	0.002
TOTAL	89.757	94.844	94.148	94.59	90.82	94.331

Location	6A2-AP5-1	6A8A-AP1-2	6A6A-AP1-1	6A6A-AP2-1	6A5-AP1-4	6A5-AP2-1
	Unaltered	Unaltered	Unaltered	Unaltered	Unaltered	Unaltered
SiO2 (1)	2.611	2.522	2.447	2.724	2.225	2.586
FeO	0	0	0	0	0.285	0.218
MnO	0	0.014	0	0.013	0	0
MgO	0	0	0	0	0.106	0
CaO	51.083	50.903	51.33	50.723	52.039	51.464
P2O5	34.473	34.895	35.198	34.604	37.083	36.098
F	3.81	3.9	4.066	3.958	4.108	4.021
Cl	0.02	0.02	0.011	0.006	0.004	0.008
TOTAL	91.997	92.254	93.052	92.028	95.85	94.395

(1) Element abundance in weight percent oxide from EMPA

APPENDIX I: APATITE

Chemical compositions of unaltered and altered apatite grains in the Type IV pegmatites.

Location	6A1C-AP3-2	6A1C-AP4-2	6A2-AP6-4	6A6A-AP1-4	6A6A-AP2-2	6A4-AP1-2
	Unaltered	Unaltered	Altered	Altered	Altered	Altered
SiO2 (1)	2.484	2.548	1.682	1.789	1.281	2.18
FeO	0	0	0.04	0	0.044	0.044
MnO	0	0.006	0.016	0.038	0.04	0
MgO	0	0	0	0	0	0
CaO	52.324	51.681	52.859	51.776	53.296	51.369
P2O5	35.78	35.563	37.038	37.099	38.479	36.408
F	4.081	3.823	3.95	4.011	3.997	4.056
Cl	0.011	0.024	0.006	0	0.022	0.028
TOTAL	94.68	93.645	95.591	94.713	97.159	94.085

Location	6A4-AP2-2	6A4-AP2-4	6A4-AP3-2	6A4-AP4-2	6A4-AP4-3	6A2-AP1-3
	Altered	Altered	Altered	Altered	Altered	Altered
SiO2 (1)	1.122	1.219	2.588	1.483	0.802	1.186
FeO	0.065	0.019	0.346	0	0.019	0
MnO	0	0	0.042	0.044	0	0.036
MgO	0	0	0.754	0	0	0
CaO	52.861	53.179	50.555	52.481	53.44	53.519
P2O5	38.861	38.993	37.031	37.739	39.423	38.662
F	4.19	4.054	4.174	4.137	4.126	3.672
Cl	0	0.013	0.007	0	0	0.003
TOTAL	97.099	97.477	95.497	95.884	97.81	97.078

Location	6A2-AP1-4	6A2-AP2-4	6A2-AP3-2	6A2-AP4-1	6A2-AP5-2	6A2-AP6-2
	Altered	Altered	Altered	Altered	Altered	Altered
SiO2 (1)	0.905	0.796	1.063	0.777	1.498	1.268
FeO	0	0	0	0.01	0	0
MnO	0.004	0	0	0.039	0	0.064
MgO	0	0	0	0	0	0.149
CaO	53.476	54.094	53.574	54.288	53.238	53.406
P2O5	39.136	39.837	38.765	39.913	37.667	39.052
F	3.957	4.251	3.986	4.155	3.924	3.998
Cl	0	0	0	0.005	0.009	0.007
TOTAL	97.478	98.978	97.388	99.187	96.336	97.944

(1) Element abundance in weight percent oxide from EMPA

APPENDIX I: APATITE

Chemical compositions of unaltered and altered apatite grains in the Type IV pegmatites.

Location	6A8A-AP1-3	6A8A-AP1-4	6A8A-AP2-1	6A8A-AP2-4	6A6A-AP1-2	6A6A-AP2-4
	Altered	Altered	Altered	Altered	Altered	Altered
SiO2 (1)	1.479	1.188	2.215	1.404	1.337	2.266
FeO	0	0.01	0.033	0.012	0	0.079
MnO	0	0.002	0.147	0	0	0.027
MgO	0	0	0.169	0	0	0
CaO	52.673	52.94	49.727	52.723	53.296	51.559
P2O5	37.279	38.01	35.989	37.731	38.112	36.022
F	4.188	4.153	3.852	4.087	3.955	3.976
Cl	0.025	0.011	0.011	0.018	0.006	0.019
TOTAL	95.644	96.314	92.143	95.975	96.706	93.948

Location	6A5-AP1-2	6A5-AP2-2	6A5-AP2-3	6A5-AP4-1	6A5-AP4-2	6A1C-AP3-4
	Altered	Altered	Altered	Altered	Altered	Altered
SiO2 (1)	1.039	2.3	0.808	0.937	0.78	3.473
FeO	0.055	0.038	0	0.113	0.101	0.025
MnO	0.028	0	0.02	0.023	0.044	0
MgO	0	0	0	0.015	0	0
CaO	54.006	51.213	54.032	54.124	54.055	50.79
P2O5	38.4	36.497	39.952	39.684	39.545	33.844
F	4.182	4.087	4.045	4.063	4.133	4.011
Cl	0	0.027	0.017	0.006	0	0
TOTAL	97.71	94.162	98.874	98.965	98.658	92.143

Location	6A8A-AP2-2	6A1C-AP2-2	6A2-AP2-2	6A5-AP3-2	6A5-AP3-3	6A1C-AP1-2
	Altered	Altered	Altered	Altered	Altered	Altered
SiO2 (1)	2.084	1.663	2.363	0.884	0.995	2.965
FeO	0	0.006	0.882	0	0.028	0.346
MnO	0	0.025	0.05	0.03	0	0
MgO	0	0	0	0	0	0.015
CaO	51.659	53.497	49.981	53.748	53.883	52
P2O5	35.972	37.517	35.533	39.218	39.627	35.624
F	4.061	4.014	3.733	3.876	4.109	3.82
Cl	0	0.013	0.01	0	0.018	0
TOTAL	93.776	96.735	92.552	97.756	98.66	94.77

(1) Element abundance in weight percent oxide from EMPA

APPENDIX I: APATITE

Chemical compositions of unaltered and altered apatite grains in the Type IV pegmatites.

Location	6A1C-AP2-1	6A1C-AP4-3
	Altered	Altered
SiO2 (1)	2.632	2.055
FeO	0	0.008
MnO	0	0.021
MgO	0	0
CaO	51.593	52.797
P2O5	35.116	37.36
F	3.95	3.692
Cl	0.017	0
TOTAL	93.308	95.933

(1) Element abundance in weight percent oxide from EMPA

APPENDIX 1: APATITE

Trace element compositions of unaltered and altered apatite grains from the Type IV pegmatites.

Location	6A2	6A6A	6A6A	6A7	6A6A
PIXE	Apr10_95.050	Apr10_95.056	Apr10_95.055	Apr10_95.063	Apr10_95.057
	Unaltered	Unaltered	Unaltered	Altered	U-rich crack
FeO (1)	0	0	0.018	0.38	0
MnO	0.055	0.023	0.093	0.025	0.129
SrO	0.811	0.7	0.82	1.209	0.65
REE2O3	8.336	9.49	15.16	6.261	6.078
Ni (2)	34	47	36	38	26
Cu	42	46	36	40	31
Zn	20	25	53	32	88
As	198	296	289	57	272
Y	3402	3656	4267	3488	2427
Ba	13402	11511	37204	8006	30260
La	19694	19331	31262	9899	15281
Ce	27717	33455	64342	20300	18568
Nd	14089	17551	20981	13829	11386
Sm	3165	3486	4648	2713	2104
Gd	1558	1817	2097	1606	1141
Dy	740	881	891	866	494
Er	379	426	441	370	225
Yb	243	240	264	204	136
Pb	360	337	622	160	752
Bi	0	0	23	0	83
Th	417	403	406	1258	113
U	455	390	867	525	10207

(1) Element abundances in weight percent oxide.

(2) Element abundances in ppm.

APPENDIX II: TITANITE

Chemical compositions of Type A titanite crystals from the Type III pegmatites.

Location	5A4-T1-1	5A4-T1-2	5A4-T1-3	7B-TIT2-DS	7B-TIT3-DK	5A2-TI1-DK
PIXE	Apr10_95.012		Apr10_95.013			
Zoning	Dark Patchy Zone	Dark Patchy Zone	Dark Patchy Zone	Dark Patchy Zone	Dark Patchy Zone	Dark Patchy Zone
SiO2 (1)	29.95	29.689	29.999	30.157	29.623	29.142
TiO2	34.28	33.484	34.102	39.722	37.088	32.88501
CaO	27.435	27.06	27.183	27.637	27.577	27.296
FeO T (2)	2.531	2.943	2.589	0.76	2.034	3.376
Al2O3	1.345	1.645	1.598	0.151	0.361	1.955
Na2O	0.066	0.06	0.044	0.534	0.28	0.146
F	1.036	0.991	1.08	0.513	0.786	1.765
TOTAL	96.643	95.872	96.595	99.474	97.749	96.565
Mn (3)	201	116	316	85	310	929
Sr	491	450	645	470	890	500
Co	98	-	158	-	-	-
Cu	23	-	14	-	-	-
Zn	10	-	7	-	-	-
Zr	3468	-	2367	-	-	-
Nb	2295	-	2197	-	-	-
Ta	102	-	108	-	-	-
Pb	43	-	23	-	-	-
Sn	-	-	-	-	-	-
Mo	-	-	-	-	-	-
Y	959	680	870	40	0	410
La	5290	640	8030	0	0	50
Ce	6090	900	6506	0	420	2040
Nd	3369	4150	2508	1410	2330	3910
Sm	859	1000	1149	730	770	130
Gd	342	-	382	-	-	-
Yb	66	-	53	-	-	-
Lu	0	520	780	0	0	240
Th	115	-	77	-	-	-
U	83	-	71	-	-	-

(1) Element abundance in weight percent oxide.
(2) Total iron expressed as FeO.
(3) Trace element abundance in ppm.

APPENDIX II: TITANITE

Chemical compositions of Type A titanite crystals from the Type III pegmatites.

Location	5A2-TI2-DK	5A2-TI3-DK	5A7-T1-3	5A7-T1-4	7B-TIT2-LT
PIXE			Apr10_95.004	Apr10_95.005	
Zoning	Dark Patchy Zone	Dark Patchy Zone	Dark Patchy Zone	Dark Patchy Zone	Medium Patchy Zone
SiO2 (1)	30.044	29.678	29.694	29.869	29.71
TiO2	36.685	32.709	33.064	36.577	36.809
CaO	27.778	24.857	27.602	27.435	26.976
FeO T (2)	2.646	3.738	3.21	1.946	2.29
Al2O3	0.458	1.728	1.617	0.886	0.469
Na2O	0.208	0.344	0.031	0.122	0.259
F	0.863	1.42	1.051	0.601	0.691
TOTAL	98.682	94.474	96.269	97.436	97.204
Mn (3)	472	1216	263	396	635
Sr	1190	370	559	1140	1130
Co	-	-	187	115	-
Cu	-	-	8	17	-
Zn	-	-	4	15	-
Zr	-	-	3002	2854	-
Nb	-	-	3426	3084	-
Ta	-	-	143	153	-
Pb	-	-	47	198	-
Sn	-	-	-	-	-
Mo	-	-	-	-	-
Y	30	930	1315	945	360
La	0	0	6331	6495	0
Ce	430	1590	4910	5701	2360
Nd	3040	3730	3301	3629	3980
Sm	250	720	1137	1204	950
Gd	-	-	625	556	-
Yb	-	-	79	72	-
Lu	10	0	0	0	810
Th	-	-	90	106	-
U	-	-	107	128	-

(1) Element abundance in weight percent oxide.
(2) Total iron expressed as FeO.
(3) Trace element abundance in ppm.

APPENDIX II: TITANITE

Chemical compositions of Type A titanite crystals from the Type III pegmatites.

Location	**5A2-TI3-ME**	**7B-TIT3-BR**	**7B-TIT3-BS**	**5A2-TI2-BR**	**5A2-TI3-BR**	**5A7-T1-2**
PIXE						
Zoning	**Medium Patchy Zone**	**Bright Patchy Zone**	**Bright Patchy Zone**	**Bright Patchy Zone**	**Bright Patchy Zone**	**Bright Patchy Zone**
SiO2 (1)	29.728	29.364	29.661	29.485	29.622	29.674
TiO2	33.129	36.584	33.103	32.887	33.387	34.073
CaO	27.193	27.069	27.451	26.529	27.293	26.922
FeO T (2)	3.158	2.112	3.213	2.969	3.276	2.818
Al2O3	1.957	0.49	1.892	1.901	1.719	1.366
Na2O	0.091	0.312	0.047	0.181	0.089	0.062
F	1.267	0.806	1.517	1.126	1.223	0.717
TOTAL	96.523	96.737	96.884	95.078	96.609	95.632
Mn (3)	325	62	813	217	937	
Sr	0	930	0	140	160	210
Co	-	-	-	-	-	-
Cu	-	-	-	-	-	-
Zn	-	-	-	-	-	-
Zr	-	-	-	-	-	-
Nb	-	-	-	-	-	-
Ta	-	-	-	-	-	-
Pb	-	-	-	-	-	-
Sn	-	-	-	-	-	-
Mo	-	-	-	-	-	-
Y	820	360	1100	940	1010	770
La	230	0	0	180	1280	1430
Ce	3660	1210	120	3220	6820	4570
Nd	5170	4090	4340	5740	6740	6240
Sm	530	600	1300	940	1150	790
Gd	-	-	-	-	-	-
Yb	-	-	-	-	-	-
Lu	0	1190	0	330	270	0
Th	-	-	-	-	-	-
U	-	-	-	-	-	-

(1) Element abundance in weight percent oxide.
(2) Total iron expressed as FeO.
(3) Trace element abundance in ppm.

APPENDIX II: TITANITE

Chemical compositions of Type A titanite crystals from the Type III pegmatites.

Location	5A7-T1-1	5A7-T1-5	5A7-T1-6	5A7-T1-7	5A7-T1-10	5A7-T1-13
PIXE	Apr10_95.003	.pr10_95.006			Apr10_95.009	
Zoning	Bright Patchy Zone	Dark Oscillatory Zone	Dark Oscillatory Zone	Dark Oscillatory Zone	Dark Oscillatory Zone	Dark Oscillatory Zone
SiO2 (1)	29.64	29.762	29.811	30.032	30.053	29.97
TiO2	33.956	34.72	35.251	34.717	36.065	35.106
CaO	27.102	27.658	27.551	27.456	27.911	27.258
FeO T (2)	2.5	2.527	2.566	2.696	2.958	2.704
Al2O3	1.434	1.3	1.239	1.302	0.827	0.808
Na2O	0.023	0.046	0.068	0.087	0.062	0.041
F	0.728	0.751	0.897	1.043	0.777	0.845
TOTAL	95.383	96.764	97.383	97.333	98.653	96.732
Mn (3)	227	316		39	408	310
Sr	895	847	780	570	794	700
Co	99	183	-	-	174	-
Cu	18	16	-	-	31	-
Zn	8	7	-	-	32	-
Zr	4966	2811	-	-	2622	-
Nb	3896	2635	-	-	1480	-
Ta	183	122	-	-	98	-
Pb	65	29	-	-	166	-
Sn	-	-	-	-	-	-
Mo	-	-	-	-	-	-
Y	1031	782	620	590	676	310
La	6881	7093	930	570	6361	300
Ce	7652	5419	1860	1750	5810	0
Nd	4538	3332	5080	4760	2341	2750
Sm	1162	1230	820	670	806	380
Gd	438	516	-	-	290	-
Yb	81	49	-	-	61	-
Lu	0	0	450	710	490	0
Th	139	84	-	-	93	-
U	157	58	-	-	114	-

(1) Element abundance in weight percent oxide.
(2) Total iron expressed as FeO.
(3) Trace element abundance in ppm.

APPENDIX II: TITANITE

Chemical compositions of Type A titanite crystals from the Type III pegmatites.

Location	5A7-T1-11	5A7-T1-14	5A4-T1-4	5A4-T1-5	5A4-T1-6
PIXE	Apr10_95.010			Apr10_95.015	Apr10_95.014
Zoning	Dark Oscillatory Zone	Dark Oscillatory Zone	Bright Oscillatory Zone	Bright Oscillatory Zone	Bright Oscillatory Zone
SiO2 (1)	30.397	29.888	29.77	29.751	29.916
TiO2	35.68	35.748	33.321	34.462	32.447
CaO	27.977	27.98	27.05	27.414	27.179
FeO T (2)	2.528	2.658	3.26	3.555	3.113
Al2O3	1.031	0.739	1.621	1.906	1.995
Na2O	0.02	0.054	0.044	0.015	0.068
F	0.858	0.863	1.425	1.463	1.323
TOTAL	98.491	97.93	96.491	98.566	96.041
Mn (3)	122	201	132	494	312
Sr	956	750	310	548	395
Co	120	-	-	145	198
Cu	5	-	-	26	10
Zn	2	-	-	19	7
Zr	3045	-	-	330	1013
Nb	1528	-	-	2457	2210
Ta	121	-	-	118	104
Pb	12	-	-	93	103
Sn	-	-	-	-	-
Mo	-	-	-	-	-
Y	452	170	1050	2095	1182
La	6637	180	830	5564	7680
Ce	5136	0	3140	4376	6100
Nd	1646	3360	5310	3461	3282
Sm	600	290	1470	1343	1133
Gd	175	-	-	696	474
Yb	38	-	-	178	98
Lu	0	0	110	910	260
Th	25	-	-	131	285
U	51	-	-	164	248

(1) Element abundance in weight percent oxide.
(2) Total iron expressed as FeO.
(3) Trace element abundance in ppm.

APPENDIX II: TITANITE

Chemical compositions of Type A titanite crystals from the Typ

Location PIXE Zoning	5A7-T1-8 Apr10_95.007 Bright Oscillatory Zone	5A7-T1-9 Apr10_95.008 Bright Oscillatory Zone	5A7-T1-12 Apr10_95.011 Overgrowth
SiO2 (1)	29.931	30.051	29.679
TiO2	33.903	33.016	32.849
CaO	27.509	27.628	27.402
FeO T (2)	2.242	3.133	2.997
Al2O3	1.029	1.887	1.988
Na2O	0.008	0.071	0.032
F	0.974	1.368	1.463
TOTAL	95.596	97.154	96.41
Mn (3)	267	471	366
Sr	934	685	379
Co	136	172	165
Cu	12	56	13
Zn	5	25	8
Zr	2573	3338	1053
Nb	2388	2190	2451
Ta	120	115	120
Pb	27	691	94
Sn	-	-	-
Mo	-	-	-
Y	679	1042	1190
La	4809	6915	7877
Ce	4757	6871	6068
Nd	3125	3732	3388
Sm	918	1039	1291
Gd	342	366	469
Yb	49	52	98
Lu	0	0	140
Th	80	205	293
U	46	186	265

(1) Element abundance in weight percent oxide.
(2) Total iron expressed as FeO.
(3) Trace element abundance in ppm.

APPENDIX II: TITANITE

Chemical compositions of Type B titanite crystals from the Type III pegmatites.

Location PIXE	27A-TI-1	27A-TI-2	27A-TI-3	27A-TI-4	27ATI-4-1	27ATI-4-2	27ATI-1-1
Zoning	Unzoned	Unzoned	Unzoned	Unzoned	Unzoned	Unzoned	Dark Sector Zone
SiO2 (1)	30.476	30.485	30.649	30.124	29.856	30.118	30.467
TiO2	31.491	31.471	32.28	31.798	32.188	31.98	33.318
CaO	28.167	28.041	28.338	28.243	27.981	27.891	28.226
FeO T (2)	4.306	4.283	3.874	3.432	3.968	3.557	3.148
Al2O3	2.23	2.187	2.087	2.199	2.087	2.084	1.902
Na2O	0.023	0.01	0	0.039	0.014	0.039	0.048
F	1.577	1.753	1.669	1.516	1.813	1.362	1.501
TOTAL	98.27	98.23	98.897	97.351	97.907	97.031	98.61
Mn (3)	472		325	31	565	465	627
Sr	0	20	60	0	0	0	0
Co	-	-	-	-	-	-	-
Cu	-	-	-	-	-	-	-
Zn	-	-	-	-	-	-	-
Zr	-	-	-	-	-	-	-
Nb	-	-	-	-	-	-	-
Ta	-	-	-	-	-	-	-
Pb	-	-	-	-	-	-	-
Sn	-	-	-	-	-	-	-
Mo	-	-	-	-	-	-	-
Y	900	650	360	530	680	1080	610
La	0	0	0	0	0	0	0
Ce	0	0	0	0	0	0	0
Nd	1590	2340	1270	1880	2160	2490	2010
Sm	340	810	0	770	830	20	610
Gd	-	-	-	-	-	-	-
Yb	-	-	-	-	-	-	-
Lu	960	520	0	0	270	0	530
Th	-	-	-	-	-	-	-
U	-	-	-	-	-	-	-

(1) Element abundance in weight percent oxide.
(2) Total iron expressed as FeO.
(3) Trace element abundance in ppm.

APPENDIX II: TITANITE

Chemical compositions of Type B titanite crystals from the Type III pegmatites.

Location	27ATI-1-3	27ATI-2-1	27ATI-3-1	27A-T1-1	27A-T1-2	27A-T2-3	27A-T2-4
PIXE Zoning	Dark Sector Zone	Dark Sector Zone	Dark Sector Zone	Dark Sector Zone	Dark Sector Zone	Dark Sector Zone	Dark Sector Zone
SiO2 (1)	30.571	30.255	29.734	30.211	30.139	30.16	30.442
TiO2	32.505	32.167	32.672	32.512	32.659	32.554	32.292
CaO	28.299	28.117	28.05	28.399	28.36	28.332	28.093
FeO T (2)	3.944	4.197	3.758	3.914	3.92	3.993	4.042
Al2O3	1.972	2.177	1.94	2.033	1.972	2.006	2.052
Na2O	0.038	0.03	0.021	0.09	0.023	0.013	0.024
F	1.705	2.099	1.677	1.514	1.534	1.363	1.278
TOTAL	99.034	99.042	97.852	98.673	98.607	98.421	98.223
Mn (3)	759	527		395	325	364	565
Sr	0	0	170	0	0	0	0
Co	-	-	-	-	-	-	-
Cu	-	-	-	-	-	-	-
Zn	-	-	-	-	-	-	-
Zr	-	-	-	-	-	-	-
Nb	-	-	-	-	-	-	-
Ta	-	-	-	-	-	-	-
Pb	-	-	-	-	-	-	-
Sn	-	-	-	-	-	-	-
Mo	-	-	-	-	-	-	-
Y	570	880	560	520	380	230	780
La	0	0	0	0	0	0	0
Ce	0	0	0	0	0	0	0
Nd	1360	2260	1810	1600	1200	1700	1760
Sm	210	390	320	130	550	560	110
Gd	-	-	-	-	-	-	-
Yb	-	-	-	-	-	-	-
Lu	380	0	0	0	0	680	0
Th	-	-	-	-	-	-	-
U	-	-	-	-	-	-	-

(1) Element abundance in weight percent oxide.
(2) Total iron expressed as FeO.
(3) Trace element abundance in ppm.

APPENDIX II: TITANITE

Chemical compositions of Type B titanite crystals from the Type III pegmatites.

Location	27A-T3-4	27A-T3-5	27A-T3-6	27A-T5-2	27A-T5-3	27A-T1-5	27A-T1-6
PIXE	Apr10_95.066						
Zoning	Dark Sector Zone	Dark Sector Zone	Dark Sector Zone	Dark Sector Zone	Dark Sector Zone	Medium Sector Zone	Medium Sector Zone
SiO2 (1)	30.244	30.524	30.275	30.504	30.367	29.954	30.002
TiO2	32.357	32.025	32.273	32.622	32.33	31.977	32.102
CaO	28.028	28.04	27.974	28.473	28.227	28.308	28.244
FeO T (2)	2.476	4.113	3.904	3.938	3.923	4.459	4.141
Al2O3	2.008	1.933	2.099	1.987	1.963	2.106	2.214
Na2O	0	0	0.015	0.006	0.029	0	0
F	1.697	1.91	1.657	1.404	1.346	1.645	1.557
TOTAL	96.81	98.545	98.197	98.934	98.185	98.449	98.26
Mn (3)	240			527	147	511	256
Sr	74	0	540	0	0	0	0
Co	0	-	-	-	-	-	-
Cu	10	-	-	-	-	-	-
Zn	17	-	-	-	-	-	-
Zr	257	-	-	-	-	-	-
Nb	1710	-	-	-	-	-	-
Ta	160	-	-	-	-	-	-
Pb	59	-	-	-	-	-	-
Sn	110	-	-	-	-	-	-
Mo	33	-	-	-	-	-	-
Y	505	460	500	270	520	660	700
La	2790	0	0	0	0	0	0
Ce	1985	0	0	0	0	0	0
Nd	634	1510	1770	1270	1510	1930	2070
Sm	297	280	180	0	0	520	180
Gd	50	-	-	-	-	-	-
Yb	52	-	-	-	-	-	-
Lu	0	0	0	0	500	30	390
Th	40	-	-	-	-	-	-
U	68	-	-	-	-	-	-

(1) Element abundance in weight percent oxide.
(2) Total iron expressed as FeO.
(3) Trace element abundance in ppm.

APPENDIX II: TITANITE

Chemical compositions of Type B titanite crystals from the Type III pegmatites.

Location	27A-T2-5	27A-T2-6	27A-T3-3	27A-T4-2	27A-T4-3	27A-T4-5	27A-T5-4
PIXE Zoning	Medium Sector Zone	Medium Sector Zone	Medium Sector Zone	Medium Sector Zone	Medium Sector Zone	Medium Sector Zone	Medium Sector Zone
SiO2 (1)	30.126	30.273	30.355	30.288	30.455	30.218	30.498
TiO2	32.277	32.085	32.3	32.087	32.108	32.869	31.998
CaO	28.264	28.195	27.879	28.252	28.283	28.356	28.196
FeO T (2)	4.216	4.104	3.745	4.203	4.039	3.939	4.178
Al2O3	2.282	2.195	2.11	2.178	2.158	1.88	2.131
Na2O	0.031	0	0.002	0.002	0.008	0	0.012
F	1.163	1.266	1.666	1.974	1.579	1.668	1.426
TOTAL	98.359	98.118	98.057	98.984	98.63	98.93	98.439
Mn (3)	759	519	379	689	186	511	372
Sr	0	0	0	0	0	100	0
Co	-	-	-	-	-	-	-
Cu	-	-	-	-	-	-	-
Zn	-	-	-	-	-	-	-
Zr	-	-	-	-	-	-	-
Nb	-	-	-	-	-	-	-
Ta	-	-	-	-	-	-	-
Pb	-	-	-	-	-	-	-
Sn	-	-	-	-	-	-	-
Mo	-	-	-	-	-	-	-
Y	870	750	680	680	790	540	840
La	0	0	0	0	0	0	0
Ce	0	0	0	0	0	0	0
Nd	1840	2270	2310	2030	2030	2020	2160
Sm	260	870	420	0	430	620	570
Gd	-	-	-	-	-	-	-
Yb	-	-	-	-	-	-	-
Lu	0	0	580	170	0	140	510
Th	-	-	-	-	-	-	-
U	-	-	-	-	-	-	-

(1) Element abundance in weight percent oxide.
(2) Total iron expressed as FeO.
(3) Trace element abundance in ppm.

APPENDIX II: TITANITE

Chemical compositions of Type B titanite crystals from the Type III pegmatites.

Location	27ATI-1-2	27ATI-1-4	27ATI-2-2	27ATI-3-2	27A-T1-3	27A-T1-4	27A-T4-1
PIXE Zoning	Bright Sector Zone	Bright Sector Zone	Bright Sector Zone	Bright Sector Zone	Bright Sector Zone	Bright Sector Zone	Bright Sector Zone
SiO2 (1)	30.255	30.094	29.993	30.129	30.423	30.143	30.292
TiO2	32.862	32.215	32.983	32.884	32.911	32.714	32.075
CaO	27.989	27.189	27.822	28.04	28.245	28.072	27.974
FeO T (2)	4.382	4.583	4.129	3.718	3.4	3.647	3.736
Al2O3	1.327	1.276	1.331	1.739	2.04	2.016	2.205
Na2O	0.048	0.081	0.049	0.037	0.023	0.019	0.036
F	1.664	1.437	1.417	1.512	1.367	1.236	1.834
TOTAL	98.527	96.875	97.724	98.059	98.409	97.847	98.152
Mn (3)	658	1479	1224	953	217	240	271
Sr	0	0	330	0	0	0	0
Co	-	-	-	-	-	-	-
Cu	-	-	-	-	-	-	-
Zn	-	-	-	-	-	-	-
Zr	-	-	-	-	-	-	-
Nb	-	-	-	-	-	-	-
Ta	-	-	-	-	-	-	-
Pb	-	-	-	-	-	-	-
Sn	-	-	-	-	-	-	-
Mo	-	-	-	-	-	-	-
Y	1170	3740	1120	960	840	880	1050
La	0	490	0	0	0	0	0
Ce	0	540	0	0	0	0	0
Nd	2300	3170	1940	1960	2760	2040	2710
Sm	160	510	440	170	700	180	390
Gd	-	-	-	-	-	-	-
Yb	-	-	-	-	-	-	-
Lu	0	0	350	0	390	70	0
Th	-	-	-	-	-	-	-
U	-	-	-	-	-	-	-

(1) Element abundance in weight percent oxide.
(2) Total iron expressed as FeO.
(3) Trace element abundance in ppm.

APPENDIX II: TITANITE

Chemical compositions of Type B titanite crystals from the Type III pegmatites.

Location	27A-T4-4	27A-T2-1	27A-T2-2	27A-T3-1	27A-T3-2	27A-T5-1
PIXE				Apr10_95.065		
Zoning	Bright Sector Zone	Overgrowth	Overgrowth	Overgrowth	Overgrowth	Overgrowth
SiO2 (1)	29.954	30.006	29.749	30.081	30.162	30.352
TiO2	32.627	32.877	32.403	32.5	33.171	33.438
CaO	27.709	27.547	27.947	27.837	27.522	28.359
FeO T (2)	4.399	4.291	3.696	1.36	4.143	3.476
Al2O3	1.366	1.375	1.995	1.422	1.319	1.836
Na2O	0.046	0.054	0.035	0.028	0.047	0.027
F	1.297	1.084	1.185	1.805	1.548	1.184
TOTAL	97.398	97.234	97.01	95.033	97.912	98.672
Mn (3)	395	589	635	488	682	542
Sr	0	100	0	154	580	500
Co	-	-	-	58	-	-
Cu	-	-	-	54	-	-
Zn	-	-	-	42	-	-
Zr	-	-	-	150	-	-
Nb	-	-	-	1313	-	-
Ta	-	-	-	122	-	-
Pb	-	-	-	171	-	-
Sn	-	-	-	358	-	-
Mo	-	-	-	0	-	-
Y	1370	650	1270	5172	850	600
La	150	0	0	3338	0	0
Ce	0	0	0	0	0	0
Nd	2380	2410	2900	682	2260	2150
Sm	240	830	80	1003	1120	260
Gd	-	-	-	687	-	-
Yb	-	-	-	821	-	-
Lu	180	0	0	0	0	0
Th	-	-	-	17	-	-
U	-	-	-	47	-	-

(1) Element abundance in weight percent oxide.
(2) Total iron expressed as FeO.
(3) Trace element abundance in ppm.

APPENDIX II: TITANITE

Chemical compositions of titanite crystals from the Type IV pegmatites.

Location	6A4-TI1-2	6A4-TI1-5	6A4-TI1-6	6A4-TI2-1	6A4-TI2-2	6A4-TI3-1
Zoning	Dark Oscillatory Zone	Dark Oscillatory Zone	Dark Oscillatory Zone	Dark Oscillatory Zone	Dark Oscillatory Zone	Dark Oscillatory Zone
SiO2 (1)	29.802	29.907	29.917	30.151	29.696	29.769
TiO2	34.488	33.238	34.475	34.454	34.05	34.594
CaO	27.535	27.315	27.56	27.521	26.993	27.761
FeO T (2)	3.258	3.553	3.29	2.891	3.337	3.248
Al2O3	0.953	1.37	0.944	1.408	0.977	0.977
Na2O	0	0.043	0.031	0.024	0.038	0
F	0.992	1.157	1.312	0.933	0.867	0.925
TOTAL	97.028	96.583	97.529	97.382	95.958	97.274
Mn (3)	101	0	0	232	256	15
Sr	190	100	0	20	20	1080
Y	790	860	730	510	930	590
La	600	100	620	490	2940	500
Ce	2210	1760	2960	870	6160	1920
Nd	5210	5540	5130	4190	7500	4470
Sm	1480	1390	1090	840	1110	820
Lu	0	0	220	0	0	0

Location	6A4-TI3-2	6A4-TI4-1	6A4-TI4-4	6A6B-T1-2	6A6B-T2-1	6A6B-T2-2
Zoning	Dark Oscillatory Zone	Dark Oscillatory Zone	Dark Oscillatory Zone	Dark Oscillatory Zone	Dark Oscillatory Zone	Dark Oscillatory Zone
SiO2 (1)	29.845	29.594	30.217	29.321	29.069	29.311
TiO2	34.522	34.095	34.982	34.147	33.815	33.22301
CaO	27.433	27.498	27.829	27.357	26.897	27.072
FeO T (2)	3.415	3.4	2.79	3.216	3.347	3.466
Al2O3	1.029	1.032	1.015	1.077	0.842	1.253
Na2O	0.042	0.029	0.047	0.016	0.017	0.047
F	0.826	1.201	1.15	0.778	0.693	1.075
TOTAL	97.112	96.849	98.03	95.912	94.68	95.447
Mn (3)	0	170	0	418	217	511
Sr	990	0	0	470	810	60
Y	720	800	610	570	710	1060
La	700	770	640	710	610	470
Ce	2340	2550	1270	1070	1810	670
Nd	5080	5130	4190	4960	5010	5230
Sm	860	840	840	710	1470	780
Lu	0	1020	340	0	360	0

(1) Element abundance in weight percent oxide.

(2) Total iron expressed as FeO.

(3) Trace element abundance in ppm.

APPENDIX II: TITANITE

Chemical compositions of titanite crystals from the Type IV pegmatites.

Location	6A6B-T2-5	6A6B-T2-6	6A8A-T1-1	6A8A-T2-1	6A8A-T2-3	6A8A-T3-1
Zoning	Dark Oscillatory Zone	Dark Oscillatory Zone	Dark Oscillatory Zone	Dark Oscillatory Zone	Dark Oscillatory Zone	Dark Oscillatory Zone
SiO2 (1)	29.805	29.636	29.756	29.835	29.484	28.84
TiO2	32.819	31.269	33.883	33.086	33.394	32.872
CaO	26.967	26.768	26.936	27.202	27.356	27.312
FeO T (2)	3.503	3.834	3.293	3.529	3.102	3.3
Al2O3	1.385	1.825	0.926	1.275	1.455	1.139
Na2O	0.034	0.013	0.024	0.015	0.007	0.039
F	1.113	1.11	1.217	1.068	1.221	2.28
TOTAL	95.626	94.455	96.035	96.01	96.019	95.782
Mn (3)	472	0	31	0	279	85
Sr	0	490	0	310	20	0
Y	1200	1450	870	530	650	940
La	350	290	840	400	530	710
Ce	1050	1720	1900	1270	330	1260
Nd	6270	6890	4960	5280	4550	5540
Sm	1760	1280	1080	1230	1210	1360
Lu	0	510	0	0	80	0

Location	6A8A-T3-3	6A8A-T4-1	6A8A-T4-3	6A8A-T4-4	6A8A-T5-1	6A2-3-1
Zoning	Dark Oscillatory Zone	Dark Oscillatory Zone	Dark Oscillatory Zone	Dark Oscillatory Zone	Dark Oscillatory Zone	Dark Oscillatory Zone
SiO2 (1)	29.217	28.861	29.095	29.681	29.54	29.995
TiO2	32.966	34.063	33.461	34.115	33.945	32.788
CaO	27.01	27.329	27.232	26.996	27.185	26.33
FeO T (2)	3.319	2.988	3.337	3.031	3.409	3.494
Al2O3	1.19	0.916	1.022	0.863	0.886	0.969
Na2O	0.027	0	0.02	0.029	0.04	0.054
F	1.344	1.317	0.967	1.044	0.949	0.797
TOTAL	95.073	95.474	95.134	95.759	95.954	94.427
Mn (3)	85	225	379	651	108	1015
Sr	0	0	0	700	500	330
Y	940	640	800	580	770	990
La	570	560	680	690	750	1320
Ce	1700	1690	1360	2120	1860	4780
Nd	5820	5140	5970	5130	5140	6680
Sm	860	930	1150	420	650	1700
Lu	0	420	0	50	60	410

(1) Element abundance in weight percent oxide.

(2) Total iron expressed as FeO.

(3) Trace element abundance in ppm.

APPENDIX II: TITANITE

Chemical compositions of titanite crystals from the Type IV pegmatites.

Location	6A2-3-2	6A4-1-1	6A4-1-2	6A4-1-3	6A4-1-4	6A4-2-1
Zoning	Dark Oscillatory Zone	Dark Oscillatory Zone	Dark Oscillatory Zone	Dark Oscillatory Zone	Dark Oscillatory Zone	Dark Oscillatory Zone
SiO2 (1)	29.824	30.114	30.651	29.961	30.35	29.894
TiO2	33.773	33.811	33.626	33.543	32.786	33.983
CaO	26.966	27.032	27.046	27.245	27.05	27.341
FeO T (2)	3.366	3.265	3.133	3.336	3.403	3.357
Al2O3	0.968	1.054	1.083	1.284	1.292	0.968
Na2O	0.038	0.019	0.036	0.089	0.054	0.012
F	0.779	0.959	0.815	0.842	0.958	0.962
TOTAL	95.714	96.254	96.39	96.3	95.893	96.517
Mn (3)	232	70	341	201	0	39
Sr	0	0	0	0	510	10
Y	1020	900	1750	760	1900	990
La	790	840	12870	610	5090	490
Ce	2490	2830	33880	2150	42910	2050
Nd	5400	5700	19160	5280	15660	5630
Sm	1370	1060	2840	1050	2150	830
Lu	400	810	740	0	0	320

Location	6A4-2-2	6A4-3-1	6A4-3-2	6A4-3-3	6A4-3-4	6A2-1-7
Zoning	Dark Oscillatory Zone	Dark Oscillatory Zone	Dark Oscillatory Zone	Dark Oscillatory Zone	Dark Oscillatory Zone	Dark Oscillatory Zone
SiO2 (1)	30.146	29.894	30.168	29.877	30.046	30.127
TiO2	33.835	33.706	33.85	34.226	34.076	33.909
CaO	27.338	26.882	27.079	27.113	26.931	27.213
FeO T (2)	2.962	3.179	3.428	3.347	3.204	3.421
Al2O3	1.424	0.943	1.011	0.961	0.869	1.054
Na2O	0.038	0.019	0.04	0.022	0.006	0.023
F	1.063	0.921	0.996	0.96	0.947	0.961
TOTAL	96.806	95.544	96.572	96.506	96.079	96.708
Mn (3)	310	465	279	46	0	372
Sr	0	670	790	530	150	420
Y	550	910	910	880	650	730
La	500	690	840	550	1090	50
Ce	1640	3530	2660	2080	3310	2130
Nd	4500	6140	5850	5270	6140	5530
Sm	980	1360	1280	970	1300	1870
Lu	10	0	960	20	0	0

(1) Element abundance in weight percent oxide.

(2) Total iron expressed as FeO.

(3) Trace element abundance in ppm.

APPENDIX II: TITANITE

Chemical compositions of titanite crystals from the Type IV pegmatites.

Location	6A2-1-8	6A2-2-3	6A2-2-4	6A4-TI1-3	6A4-TI1-4	6A4-TI3-3
Zoning	Dark Oscillatory Zone	Dark Oscillatory Zone	Dark Oscillatory Zone	Bright Oscillatory Zone	Bright Oscillatory Zone	Bright Oscillatory Zone
SiO2 (1)	30.017	29.744	29.927	29.373	29.98	28.842
TiO2	33.956	33.5	33.383	33.614	33.992	31.899
CaO	26.804	27.307	27.271	27.353	27.506	25.22
FeO T (2)	3.454	3.789	3.274	3.481	3.629	3.819
Al2O3	0.982	1.046	1.616	0.835	0.784	1.744
Na2O	0.011	0.022	0.017	0.046	0.077	0.08
F	1.156	1.48	1.005	1.479	1.072	1.249
TOTAL	96.38	96.888	96.493	96.181	97.04	92.853
Mn (3)	256	0	194	364	101	248
Sr	0	1080	0	0	0	70
Y	970	130	820	680	740	1080
La	680	1780	50	490	250	5850
Ce	2430	3240	150	1150	1500	16690
Nd	4690	6520	5660	4120	4580	11410
Sm	3100	670	500	710	1080	1680
Lu	0	2330	1080	280	170	0

Location	6A4-TI3-4	6A4-TI3-5	6A4-TI3-6	6A4-TI4-2	6A4-TI4-3	6A6B-T1-1
Zoning	Bright Oscillatory Zone	Bright Oscillatory Zone	Bright Oscillatory Zone	Bright Oscillatory Zone	Bright Oscillatory Zone	Bright Oscillatory Zone
SiO2 (1)	29.713	29.724	29.535	29.539	29.373	29.428
TiO2	33.954	34.596	33.77	34.231	33.758	33.816
CaO	26.841	27.394	26.581	26.949	26.791	26.613
FeO T (2)	3.246	3.104	3.191	2.951	3.433	3.23
Al2O3	0.903	0.93	0.952	0.927	0.951	0.854
Na2O	0.034	0.018	0.039	0.091	0.053	0.043
F	0.842	0.924	1.023	1.09	1.088	0.427
TOTAL	95.533	96.69	95.091	95.778	95.447	94.411
Mn (3)	0	0	132	116	0	333
Sr	720	630	410	270	0	330
Y	930	810	940	1010	1120	860
La	1510	1810	1630	1420	1900	1230
Ce	5230	4650	6470	5100	6680	4930
Nd	6930	6120	7450	6980	8580	6360
Sm	1480	990	1600	1370	1330	1820
Lu	1260	0	530	0	0	0

(1) Element abundance in weight percent oxide.

(2) Total iron expressed as FeO.

(3) Trace element abundance in ppm.

APPENDIX II: TITANITE

Chemical compositions of titanite crystals from the Type IV pegmatites.

Location	6A6B-T2-3	6A6B-T2-4	6A8A-T1-2	6A8A-T2-2	6A8A-T3-2	6A8A-T4-2
Zoning	Bright Oscillatory Zone	Bright Oscillatory Zone	Bright Oscillatory Zone	Bright Oscillatory Zone	Bright Oscillatory Zone	Bright Oscillatory Zone
SiO2 (1)	29.272	29.264	29.441	29.262	28.511	29.221
TiO2	33.618	33.746	33.975	33.271	33.338	33.743
CaO	26.489	26.727	26.634	26.358	26.526	26.596
FeO T (2)	3.41	3.291	3.038	3.256	3.253	3.189
Al2O3	0.858	0.922	0.808	1.02	0.861	0.852
Na2O	0.007	0.019	0.043	0.017	0.011	0.05
F	0.859	0.902	1.02	1.137	1.19	0.858
TOTAL	94.513	94.871	94.959	94.321	93.69	94.509
Mn (3)	0	186	0	217	0	0
Sr	60	0	360	540	330	0
Y	1350	1010	640	1110	800	910
La	1370	1450	1100	4820	3070	1540
Ce	4370	4920	3580	9400	8540	6720
Nd	6820	7450	5850	10850	8580	7410
Sm	1270	1610	1420	1590	1040	1130
Lu	0	0	420	0	260	470

Location	6A8A-T4-5	6A2-3-3	6A2-3-4	6A4-1-5	6A4-1-6	6A4-1-7
Zoning	Bright Oscillatory Zone	Bright Oscillatory Zone	Bright Oscillatory Zone	Bright Oscillatory Zone	Bright Oscillatory Zone	Bright Oscillatory Zone
SiO2 (1)	29.448	29.846	29.542	29.903	29.892	29.796
TiO2	34.162	33.551	33.765	33.508	33.871	33.65
CaO	26.926	26.833	26.689	26.762	27.089	26.765
FeO T (2)	2.988	3.281	3.083	3.177	3.181	3.419
Al2O3	0.82	0.897	0.83	0.91	0.855	0.957
Na2O	0.033	0.026	0.024	0.036	0.03	0.04
F	0.783	0.894	0.505	0.666	0.723	8230
TOTAL	95.16	95.328	94.438	94.962	95.641	8324.627
Mn (3)	356	279	15	395	0	15
Sr	0	10	530	0	0	490
Y	630	990	1150	1370	890	940
La	1280	1500	1380	2730	1230	1360
Ce	3700	5610	5220	12650	4160	5330
Nd	5830	6850	7210	9370	6600	7100
Sm	870	1350	1480	2270	1430	1510
Lu	220	340	0	40	0	250

(1) Element abundance in weight percent oxide.

(2) Total iron expressed as FeO.

(3) Trace element abundance in ppm.

APPENDIX II: TITANITE

Chemical compositions of titanite crystals from the Type IV pegmatites.

Location	6A4-2-3	6A4-2-4	6A4-3-5	6A4-3-6	6A4-3-7	6A4-3-8
Zoning	Bright Oscillatory Zone	Bright Oscillatory Zone	Bright Oscillatory Zone	Bright Oscillatory Zone	Bright Oscillatory Zone	Bright Oscillatory Zone
SiO2 (1)	29.829	30.039	29.771	29.704	29.74	30.014
TiO2	33.921	33.68	33.553	33.49	34.037	34.373
CaO	26.93	26.544	26.593	26.323	26.674	26.87
FeO T (2)	3.414	3.274	3.231	3.392	3.312	2.98
Al2O3	1.029	0.932	0.862	0.959	0.923	0.922
Na2O	0.035	0.078	0.043	0.042	0.031	0.057
F	1.516	0.812	0.666	0.793	0.98	0.744
TOTAL	96.674	95.359	94.719	94.703	95.697	95.96
Mn (3)	333	263	23	0	0	279
Sr	0	0	550	890	0	90
Y	910	770	830	1170	1000	720
La	1600	2350	1180	1750	1200	900
Ce	4850	6160	4280	7120	4890	3520
Nd	7460	7610	7100	8880	7480	5560
Sm	1230	1340	950	2110	1590	1420
Lu	0	320	0	0	0	50

Location	6A2-1-4	6A2-1-5	6A2-1-6	6A2-2-1	6A2-2-2
Zoning	Bright Oscillatory Zone	Bright Oscillatory Zone	Bright Oscillatory Zone	Bright Oscillatory Zone	Bright Oscillatory Zone
SiO2 (1)	29.828	29.717	29.929	29.907	30.025
TiO2	33.421	33.933	34.408	32.471	32.661
CaO	26.534	26.154	26.896	26.999	26.877
FeO T (2)	3.343	3.128	3.18	3.63	3.671
Al2O3	0.899	0.901	0.913	1.425	1.216
Na2O	0.01	0.016	0.028	0.029	0.033
F	0.643	0.803	0.78	1.165	0.892
TOTAL	94.678	94.652	96.134	95.626	95.375
Mn (3)	573	651	0	271	410
Sr	0	260	580	290	0
Y	1620	670	730	430	1290
La	990	1470	0	880	440
Ce	4230	4320	2880	0	4840
Nd	8350	5970	4430	3550	6300
Sm	710	320	2350	2300	660
Lu	240	1140	210	0	2960

(1) Element abundance in weight percent oxide.

(2) Total iron expressed as FeO.

(3) Trace element abundance in ppm.

APPENDIX II: TITANITE

Trace element composition of a titanite crystal in the Type IV pegmatites.

Location	6A7
PIXE	Apr10_95.064
FeO T (1,2)	3.32
REE2O3 (3)	5.496
Mn (4)	2345
Sr	2463
Co	171
Cu	25
Zn	38
Zr	2028
Nb	1485
Ta	70
Pb	1173
Sn	62
Mo	0
Y	2045
La	12275
Ce	18014
Nd	10996
Sm	2363
Gd	998
Yb	139
Th	56
U	935

(1) Element abundance in weight precent oxide.
(2) Total iron expressed as FeO.
(3) REE2O3 is sum of REE abundances.
(4) Trace element abundance in ppm.

APPENDIX III: ZIRCON

Chemical compositions of zircon crystals from the Type III pegmatites.

Location PIXE Zoning	ZIR1-13 Apr10_95.032 Centre	ZIR1-14 Centre	10C-Z2-5 Dark Oscillatory Zone	10C-Z3-1 Dark Oscillatory Zone	10C-Z3-2 Apr10_95.041 Dark Oscillatory Zone	ZIR2-7 Dark Oscillatory Zone
ZrO2 (1)	50.897	57.162	62.901	51.574	56.281	60.531
SiO2	28.951	29.493	30.088	27.972	27.573	30.28
CaO	1.545	1.129	1.513	3.975	2.735	1.988
FeO T (2)	2.226	1.303	0.822	0.196	1.21	1.03
HfO2	0.256	0.361	0.209	0.191	1.002	0.28
Al2O3	0.501	0.209	0.21	0.757	0.315	0.409
MgO	0	0	0	0	0.014	0
Na2O	0	0	0	0	0	0
TiO2	0	0.012	0.002	0.024	0.022	0
P2O5	0	0	0	0	0	0
UO2	1.838	1.326	0.643	1.634	1.354	1.128
REE2O3 (3)	2.838	2.532	0.317	0.462	1.004	0.671
TOTAL	89.051	93.527	96.705	86.784	91.51	96.316
Cr (4)	41	-	-	-	0	-
Mn	1314	-	-	-	1902	-
Co	578	-	-	-	613	-
Ni	94	-	-	-	79	-
Cu	73	-	-	-	109	-
Zn	59	-	-	-	49	-
Br	67	-	-	-	51	-
Sr	5286	-	-	-	1023	-
Mo	0	-	-	-	2679	-
Ba	1133	-	-	-	93	-
Y	3926	2360	1410	2230	3100	3330
La	3583	3330	0	0	607	40
Ce	8393	12250	260	440	2660	360
Nd	0	2000	100	310	613	240
Sm	0	0	400	0	0	40
Gd	406	-	-	-	156	-
Dy	0	-	-	-	0	-
Er	766	-	-	-	589	-
Yb	1281	710	430	730	624	1150
Lu	5768	820	0	70	0	330
Tl	118	-	-	-	116	-
Pb	471	-	-	-	852	-
Th	1230	21460	250	680	1071	60

(1) Element abundance in weight percent oxide.

(2) Total iron expressed as FeO.

(3) REE2O3 is sum of REE abundances.

(4) Trace element abundance in ppm.

APPENDIX III: ZIRCON

Chemical compositions of zircon crystals from the Type III pegmatites.

Location PIXE Zoning	ZIR3-3 Apr10_95.021 Dark Oscillatory Zone	ZIR3-4 Apr10_p5.020 Dark Oscillatory Zone	10C-Z2-7 Medium Oscillatory Zone	10C-Z2-8 Medium Oscillatory Zone	10C-Z2-9 Medium Oscillatory Zone	5A2-Z1-3 Medium Oscillatory Zone
ZrO2	62.796	63.13	59.738	56.67	57.832	63.893
SiO2 (1)	30.02	30.059	29.987	29.812	30.201	30.402
CaO	0.822	0.749	2.04	2.363	2.321	0.936
FeO T (2)	0.232	0.226	0.309	0.128	0.463	0.258
HfO2	0.202	0.195	0.224	0.173	0.164	0.132
Al2O3	0.042	0.062	0.531	0.522	0.604	0.119
MgO	0	0	0	0	0.016	0
Na2O	0.593	0.457	0	0	0	0
TiO2	0	0	0.002	0.013	0.035	0
P2O5	0.012	0.013	0	0	0	0
UO2	1.04	7.212	1.804	3.189	2.251	0.851
REE2O3 (3)	1.442	1.515	1.063	1.521	1.975	0.538
TOTAL	97.201	103.616	95.698	94.391	95.862	97.129
Cr (4)	0	19	-	-	-	-
Mn	865	1026	-	-	-	-
Co	602	461	-	-	-	-
Ni	44	34	-	-	-	-
Cu	70	56	-	-	-	-
Zn	86	58	-	-	-	-
Br	13	46	-	-	-	-
Sr	273	415	-	-	-	-
Mo	1956	1189	-	-	-	-
Ba	187	187	-	-	-	-
Y	2954	8302	5530	7980	11530	2990
La	0	0	0	0	0	0
Ce	93	439	820	950	950	200
Nd	16	98	650	470	510	500
Sm	59	106	0	420	0	140
Gd	179	279	-	-	-	-
Dy	242	554	-	-	-	-
Er	370	885	-	-	-	-
Yb	1055	1656	1180	1840	2600	530
Lu	7359	0	480	730	390	0
Tl	56	317	-	-	-	-
Pb	2412	14615	-	-	-	-
Th	1007	4408	1640	3880	1950	1120

(1) Element abundance in weight percent oxide.

(2) Total iron expressed as FeO.

(3) REE2O3 is sum of REE abundances.

(4) Trace element abundance in ppm.

APPENDIX III: ZIRCON

Chemical compositions of zircon crystals from the Type III pegmatites.

Location	5A2-Z1-4	5A2-Z1-5	10C-Z2-3	10C-Z2-4	10C-Z1-6	10C-Z1-8
PIXE Zoning	Medium Oscillatory Zone	Medium Oscillatory Zone	Medium Oscillatory Zone	Medium Oscillatory Zone	Medium Oscillatory Zone	Medium Oscillatory Zone
ZrO2	66.253	63.837	63.929	62.681	64.418	61.595
SiO2 (1)	31.093	30.362	30.772	30.756	30.504	30.079
CaO	0.162	0.774	0.862	1.091	0.961	1.343
FeO T (2)	0.422	0.105	0.496	0.176	0.099	0.146
HfO2	0.175	0.141	0.228	0.228	0.213	0.182
Al2O3	0.112	0.025	0.14	0.21	0.077	0.115
MgO	0	0	0	0	0	0
Na2O	0	0	0	0	0	0
TiO2	0.01	0	0	0.038	0.017	0.013
P2O5	0.013	0	0	0	0	0.001
UO2	0.429	0.672	0.572	0.597	1.2	1.208
REE2O3 (3)	0.084	0.454	0.321	0.168	0.783	0.404
TOTAL	98.753	96.37	97.321	95.945	98.272	95.086
Cr (4)	-	-	-	-	-	-
Mn	-	-	-	-	-	-
Co	-	-	-	-	-	-
Ni	-	-	-	-	-	-
Cu	-	-	-	-	-	-
Zn	-	-	-	-	-	-
Br	-	-	-	-	-	-
Sr	-	-	-	-	-	-
Mo	-	-	-	-	-	-
Ba	-	-	-	-	-	-
Y	210	2400	510	910	3080	1380
La	0	0	0	0	0	0
Ce	60	140	390	0	180	70
Nd	210	260	150	0	70	0
Sm	0	0	0	0	250	170
Gd	-	-	-	-	-	-
Dy	-	-	-	-	-	-
Er	-	-	-	-	-	-
Yb	230	620	970	330	1680	1350
Lu	0	280	730	130	1250	410
Tl	-	-	-	-	-	-
Pb	-	-	-	-	-	-
Th	170	810	40	360	0	620

(1) Element abundance in weight percent oxide.

(2) Total iron expressed as FeO.

(3) REE2O3 is sum of REE abundances.

(4) Trace element abundance in ppm.

APPENDIX III: ZIRCON

Chemical compositions of zircon crystals from the Type III pegmatites.

Location PIXE Zoning	10C-Z1-9 Medium Oscillatory Zone	5A2-Z1-8 Medium Oscillatory Zone	5A2-Z1-11 Medium Oscillatory Zone	ZIR2-1 Apr10_95.026 Medium Oscillatory Zone	ZIR2-2 Medium Oscillatory Zone	ZIR2-3 Medium Oscillatory Zone
ZrO2	56.222	69.226	68.246	56.947	56.216	56.759
SiO2 (1)	30.393	32.342	31.898	29.73	29.91	30.33
CaO	2.518	0	0	2.216	2.154	2.215
FeO T (2)	0.077	0.478	0	0.657	1.041	0.814
HfO2	0.179	0.173	0.178	0.165	0.159	0.177
Al2O3	0.49	0	0.014	0.427	0.479	0.56
MgO	0.037	0	0	0.017	0	0
Na2O	0	0	0	0	0	0
TiO2	0	0	0	0.005	0.008	0.029
P2O5	0	0.025	0	0	0	0
UO2	3.257	0.057	0.115	2.895	2.732	2.568
REE2O3 (3)	0.924	0.117	0.015	2.145	0.971	0.886
TOTAL	94.097	102.418	100.466	95.204	93.67	94.339
Cr (4)	-	-	-	23	-	-
Mn	-	-	-	1679	-	-
Co	-	-	-	642	-	-
Ni	-	-	-	52	-	-
Cu	-	-	-	81	-	-
Zn	-	-	-	116	-	-
Br	-	-	-	42	-	-
Sr	-	-	-	657	-	-
Mo	-	-	-	1827	-	-
Ba	-	-	-	0	-	-
Y	4880	0	0	6661	4860	4640
La	160	0	0	0	90	0
Ce	720	180	0	921	890	620
Nd	40	270	0	244	180	60
Sm	0	0	0	84	40	0
Gd	-	-	-	326	-	-
Dy	-	-	-	513	-	-
Er	-	-	-	777	-	-
Yb	1290	380	130	1325	1490	1290
Lu	440	190	0	7180	380	620
Tl	-	-	-	79	-	-
Pb	-	-	-	5045	-	-
Th	2620	210	110	4654	5080	4540

(1) Element abundance in weight percent oxide.

(2) Total iron expressed as FeO.

(3) REE2O3 is sum of REE abundances.

(4) Trace element abundance in ppm.

APPENDIX III: ZIRCON

Chemical compositions of zircon crystals from the Type III pegmatites.

Location	ZIR2-4	ZIR3-5	10C-Z2-1	10C-Z2-2	5A2-Z1-2	ZIR1-3
PIXE Zoning	Medium Oscillatory Zone	Light Oscillatory Zone	Light Oscillatory Zone	Light Oscillatory Zone	Light Oscillatory Zone	Light Oscillatory Zone
ZrO2	61.152	45.286	57.713	56.	68.103	56.226
SiO2 (1)	31.021	25.606	29.146	28.939	32.119	28.311
CaO	1.688	2.359	2.307	1.942	0.008	0.942
FeO T (2)	0.787	0.724	0.315	0.299	0.321	0.064
HfO2	0.201	0.124	0.19	0.227	0.177	0.168
Al2O3	0.432	0.062	0.527	0.339	0.012	0.227
MgO	0	0	0.014	0.002	0	0
Na2O	0	0	0	0	0	0
TiO2	0	0.046	0.022	0.021	0.02	0.036
P2O5	0	0	0	0	0.059	0.073
UO2	1.126	21.825	2.201	1.931	0.031	0.769
REE2O3 (3)	0.8	2.997	0.896	1.029	0.095	0.627
TOTAL	97.207	99.029	93.33	90.729	100.945	87.443
Cr (4)	-	-	-	-	-	-
Mn	-	-	-	-	-	-
Co	-	-	-	-	-	-
Ni	-	-	-	-	-	-
Cu	-	-	-	-	-	-
Zn	-	-	-	-	-	-
Br	-	-	-	-	-	-
Sr	-	-	-	-	-	-
Mo	-	-	-	-	-	-
Ba	-	-	-	-	-	-
Y	3910	16210	4150	6000	0	750
La	0	80	160	0	0	810
Ce	460	900	500	750	40	2940
Nd	0	180	630	170	190	60
Sm	40	360	340	390	0	0
Gd	-	-	-	-	-	-
Dy	-	-	-	-	-	-
Er	-	-	-	-	-	-
Yb	1250	5090	1190	1000	0	740
Lu	900	1590	380	0	600	10
Tl	-	-	-	-	-	-
Pb	-	-	-	-	-	-
Th	450	28960	1690	10	0	570

(1) Element abundance in weight percent oxide.

(2) Total iron expressed as FeO.

(3) REE2O3 is sum of REE abundances.

(4) Trace element abundance in ppm.

APPENDIX III: ZIRCON

Chemical compositions of zircon crystals from the Type III pegmatites.

Location	ZIR1-4	ZIR2-5 Apr10_95.028	ZIR2-9	ZIR2-10	ZIR3-1	ZIR3-2
PIXE Zoning	Light Oscillatory Zone	Light Oscillatory Zone	Light Oscillatory Zone	Light Oscillatory Zone	Light Oscillatory Zone	Light Oscillatory Zone
ZrO2	59.504	58.009	65.957	66.355	59.554	56.536
SiO2 (1)	28.305	30.528	31.403	31.874	29.905	29.611
CaO	2.725	1.871	0.243	0.046	1.832	1.818
FeO T (2)	3.853	0.541	0.764	0.163	0.353	0.522
HfO2	0.188	0.166	0.319	0.319	0.171	0.18
Al2O3	0.14	0.526	0.024	0	0.199	0.328
MgO	0	0	0	0	0	0
Na2O	0	0	0	0	0	0.576
TiO2	0.005	0.018	0.004	0.004	0.011	0.036
P2O5	0.034	0	0.077	0.02	0	0
UO2	1.088	1.682	0.194	0.444	1.361	2.61
REE2O3 (3)	1.557	1.038	0.14	0.135	0.673	1.22
TOTAL	97.399	94.38	99.125	99.36	94.059	93.438
Cr (4)	-	21	-	-	-	-
Mn	-	1237	-	-	-	-
Co	-	719	-	-	-	-
Ni	-	57	-	-	-	-
Cu	-	87	-	-	-	-
Zn	-	102	-	-	-	-
Br	-	22	-	-	-	-
Sr	-	444	-	-	-	-
Mo	-	2045	-	-	-	-
Ba	-	146	-	-	-	-
Y	1860	5198	0	0	2970	6070
La	2960	0	0	0	0	0
Ce	7120	215	50	100	310	1070
Nd	0	109	510	150	90	410
Sm	0	155	0	220	250	430
Gd	-	303	-	-	-	-
Dy	-	438	-	-	-	-
Er	-	699	-	-	-	-
Yb	1230	1382	230	170	1440	1110
Lu	0	0	430	540	490	880
Tl	-	93	-	-	-	-
Pb	-	3171	-	-	-	-
Th	60	1392	0	0	1600	2670

(1) Element abundance in weight percent oxide.
(2) Total iron expressed as FeO.
(3) REE2O3 is sum of REE abundances.
(4) Trace element abundance in ppm.

APPENDIX III: ZIRCON

Chemical compositions of zircon crystals from the Type III pegmatites.

Location PIXE Zoning	ZIR3-9 Apr10_95.023 Light Oscillatory Zone	ZIR3-10 Light Oscillatory Zone	ZIR3-11 Light Oscillatory Zone	ZIR3-12 Apr10_95.025 Light Oscillatory Zone	ZIR3-13 Apr10_95.024 Light Oscillatory Zone
ZrO2	66.077	66.251	67.029	59.884	60.574
SiO2 (1)	31.035	32.194	32.137	30.598	30.313
CaO	0.239	0.008	0	1.674	1.573
FeO T (2)	0.021	0.022	0.068	0.895	0.877
HfO2	0.207	0.342	0.288	0.219	0.248
Al2O3	0.026	0	0	0.343	0.315
MgO	0	0	0	0.01	0
Na2O	0	0	0	0	0
TiO2	0	0.016	0	0.034	0.027
P2O5	0.017	0.033	0	0	0
UO2	0.158	0.13	0.014	1.39	1.457
REE2O3 (3)	1.67	0.011	0.041	1.069	0.896
TOTAL	99.451	99.009	99.577	96.116	96.28
Cr (4)	0	-	-	0	0
Mn	7	-	-	1408	1628
Co	514	-	-	600	522
Ni	46	-	-	55	69
Cu	76	-	-	107	91
Zn	7	-	-	86	110
Br	7	-	-	23	20
Sr	22	-	-	498	450
Mo	0	-	-	1432	1863
Ba	134	-	-	17	27
Y	635	0	0	4856	4110
La	0	10	0	0	0
Ce	0	0	0	366	331
Nd	21	0	0	61	101
Sm	16	0	0	59	41
Gd	17	-	-	220	272
Dy	7	-	-	470	526
Er	3	-	-	712	627
Yb	0	90	0	1073	843
Lu	13911	0	360	990	520
Tl	43	-	-	89	69
Pb	449	-	-	2926	3252
Th	0	0	0	674	598

(1) Element abundance in weight percent oxide.

(2) Total iron expressed as FeO.

(3) REE2O3 is sum of REE abundances.

(4) Trace element abundance in ppm.

APPENDIX III: ZIRCON

Chemical compositions of zircon crystals from the Type III pegmatites.

Location PIXE Zoning	ZIR3-14 Light Oscillatory Zone	5A2-Z1-1 Light Oscillatory Zone	10C-Z1-1 Dark Rim	10C-Z1-2 Dark Rim	10C-Z1-11 Dark Rim	10C-Z3-3 Apr10_95.042 Dark Rim
ZrO2	60.128	68.233	55.699	60.698	50.51	55.637
SiO2 (1)	30.171	31.806	29.567	30.292	27.637	27.519
CaO	1.26	0.028	2.638	1.776	3.901	3.229
FeO T (2)	0.912	0.676	0.036	0.421	0.175	0.503
HfO2	0.269	0.163	0.184	0.245	0.194	2.063
Al2O3	0.221	0.02	0.563	0.248	0.312	0.534
MgO	0.058	0	0	0.002	0	0.001
Na2O	0.194	0	0	0	0	0
TiO2	0.037	0	0.007	0.048	0	0
P2O5	0	0.017	0	0	0	0
UO2	1.232	0.12	3.235	1.908	2.492	0.259
REE2O3 (3)	0.66	0.166	1.122	0.562	0.322	0.881
TOTAL	95.141	101.229	93.051	96.201	85.544	90.625
Cr (4)	-	-	-	-	-	0
Mn	-	-	-	-	-	228
Co	-	-	-	-	-	104
Ni	-	-	-	-	-	77
Cu	-	-	-	-	-	249
Zn	-	-	-	-	-	45
Br	-	-	-	-	-	0
Sr	-	-	-	-	-	168
Mo	-	-	-	-	-	2300
Ba	-	-	-	-	-	0
Y	2960	0	6690	2810	1590	2899
La	0	30	0	0	40	0
Ce	270	60	730	400	610	1230
Nd	180	0	60	290	180	1459
Sm	510	700	0	250	0	375
Gd	-	-	-	-	-	498
Dy	-	-	-	-	-	446
Er	-	-	-	-	-	80
Yb	850	0	1580	840	190	207
Lu	660	650	0	0	10	120
Tl	-	-	-	-	-	76
Pb	-	-	-	-	-	543
Th	690	0	2480	20	0	0

(1) Element abundance in weight percent oxide.

(2) Total iron expressed as FeO.

(3) REE2O3 is sum of REE abundances.

(4) Trace element abundance in ppm.

APPENDIX III: ZIRCON

Chemical compositions of zircon crystals from the Type III pegmatites.

Location	ZIR1-5	ZIR1-6	ZIR1-7	ZIR1-8	ZIR1-12	ZIR2-6
PIXE	Apr10_95.034		Apr10_95.037			
Zoning	Dark Rim	Dark Rim	Dark Rim	Dark Rim	Dark Rim	Dark Rim
ZrO2	46.007	50.112	49.214	48.359	43.839	60.7
SiO2 (1)	28.236	28.241	27.999	28.324	27.359	30.37
CaO	4.364	4.71	4.519	4.482	4.397	1.66
FeO T (2)	1.324	3.174	4.611	0.903	2.052	4.081
HfO2	0.84	0.16	0.668	0.152	0.136	0.238
Al2O3	0.677	0.617	0.671	0.788	0.834	0.301
MgO	0.019	0	0	0.012	0.006	0
Na2O	0	0	0	0	0	0
TiO2	0.013	0.033	0.023	0.01	0.018	0.018
P2O5	0	0.007	0.015	0.054	0	0
UO2	1.848	1.261	1.688	1.459	1.829	0.905
REE2O3 (3)	3.186	1.763	1.892	3.576	3.703	0.435
TOTAL	86.515	90.078	91.301	88.118	84.173	98.708
Cr (4)	86	-	67	-	-	-
Mn	844	-	963	-	-	-
Co	335	-	545	-	-	-
Ni	53	-	158	-	-	-
Cu	97	-	111	-	-	-
Zn	25	-	105	-	-	-
Br	59	-	170	-	-	-
Sr	3276	-	5997	-	-	-
Mo	1472	-	3137	-	-	-
Ba	325	-	2032	-	-	-
Y	2955	2390	2420	3150	5480	2580
La	6315	4190	2275	6270	8210	0
Ce	14593	7100	8165	19200	16120	150
Nd	2042	220	335	870	530	0
Sm	0	0	0	0	0	0
Gd	0	-	1079	-	-	-
Dy	0	-	0	-	-	-
Er	579	-	785	-	-	-
Yb	496	550	837	790	640	790
Lu	0	420	120	0	190	0
Tl	86	-	469	-	-	-
Pb	604	-	298	-	-	-
Th	736	30	5825	740	910	0

(1) Element abundance in weight percent oxide.

(2) Total iron expressed as FeO.

(3) REE2O3 is sum of REE abundances.

(4) Trace element abundance in ppm.

APPENDIX III: ZIRCON

Chemical compositions of zircon crystals from the Type III pegmatites.

Location PIXE Zoning	ZIR2-8 Apr10_95.027 Dark Rim	ZIR3-6 Dark Rim	ZIR3-7 Dark Rim	ZIR3-8 Apr10_95.022 Dark Rim	10C-Z2-12 Medium Rim	10C-Z2-13 Medium Rim
ZrO2	59.13	58.906	60.288	56.532	59.788	64.1
SiO2 (1)	30.003	27.593	28.894	29.444	28.161	30.423
CaO	1.871	2.066	1.387	2.662	1.12	1.211
FeO T (2)	0.509	1.086	0.437	0.531	0.698	0.158
HfO2	0.272	0.169	0.178	0.159	0.272	0.245
Al2O3	0.347	0.121	0.145	0.34	0.157	0.169
MgO	0	0	0	0.003	0	0
Na2O	0	0	0.264	0.558	0	0
TiO2	0.052	0.043	0	0.026	0.028	0.02
P2O5	0	0.02	0.003	0	0.012	0.002
UO2	1.315	1.351	1.005	1.789	0.685	1.375
REE2O3 (3)	0.614	0.248	0.25	1.527	0.245	0.383
TOTAL	94.113	91.602	92.851	93.571	91.167	98.086
Cr (4)	8	-	-	0	-	-
Mn	1004	-	-	3483	-	-
Co	507	-	-	492	-	-
Ni	46	-	-	27	-	-
Cu	88	-	-	62	-	-
Zn	77	-	-	56	-	-
Br	45	-	-	53	-	-
Sr	337	-	-	891	-	-
Mo	1927	-	-	2157	-	-
Ba	59	-	-	65	-	-
Y	3137	900	1130	3589	1050	2070
La	0	0	0	0	0	0
Ce	176	30	60	261	310	410
Nd	58	0	60	126	0	310
Sm	47	0	120	184	210	0
Gd	172	-	-	284	-	-
Dy	257	-	-	368	-	-
Er	466	-	-	430	-	-
Yb	705	720	690	1000	450	320
Lu	0	420	0	6739	0	0
Tl	69	-	-	83	-	-
Pb	2516	-	-	1853	-	-
Th	594	720	0	1788	0	130

(1) Element abundance in weight percent oxide.

(2) Total iron expressed as FeO.

(3) REE2O3 is sum of REE abundances.

(4) Trace element abundance in ppm.

APPENDIX III: ZIRCON

Chemical compositions of zircon crystals from the Type III pegmatites.

Location	10C-Z3-6	10C-Z1-3	10C-Z1-4	10C-Z2-14	10C-Z2-15	10C-Z3-4	10C-Z3-5
PIXE Zoning	Medium Rim	Light Rim	Light Rim	Light Rim	Light Rim	Light Rim	Light Rim
ZrO2	58.078	59.193	62.411	59.238	64.84	51.425	59.855
SiO2 (1)	29.704	29.535	30.318	27.568	30.884	23.335	29.648
CaO	1.199	2.842	1.385	0.604	0.478	0.627	0.129
FeO T (2)	0.189	1.015	0.136	0.173	1.515	0.223	1.102
HfO2	0.24	0.249	0.269	0.289	0.358	0.246	0.325
Al2O3	0.38	0.268	0.228	1.936	0.166	8.197	1.826
MgO	0.003	0.011	0	0	0	0.064	0
Na2O	0	0	0	0	0	0	0
TiO2	0	0.035	0.031	0.031	0.032	0.048	0.014
P2O5	0.006	0	0	0.375	0.017	1.149	0.294
UO2	0.836	2.682	1.171	0.466	0.236	1.524	0.28
REE2O3 (3)	1.378	0.38	0.498	1.341	0.065	2.475	1.255
TOTAL	92.012	96.21	96.447	92.022	98.59	89.312	94.729
Cr (4)	-	-	-	-	-	-	-
Mn	-	-	-	-	-	-	-
Co	-	-	-	-	-	-	-
Ni	-	-	-	-	-	-	-
Cu	-	-	-	-	-	-	-
Zn	-	-	-	-	-	-	-
Br	-	-	-	-	-	-	-
Sr	-	-	-	-	-	-	-
Mo	-	-	-	-	-	-	-
Ba	-	-	-	-	-	-	-
Y	1250	1840	2390	3010	0	10180	5390
La	600	0	0	700	10	0	0
Ce	5120	0	160	3820	230	3310	1630
Nd	3940	0	60	2710	0	4140	1790
Sm	330	390	490	320	0	1370	780
Gd	-	-	-	-	-	-	-
Dy	-	-	-	-	-	-	-
Er	-	-	-	-	-	-	-
Yb	450	890	980	180	0	1150	710
Lu	0	0	0	490	320	190	0
Tl	-	-	-	-	-	-	-
Pb	-	-	-	-	-	-	-
Th	500	1310	180	0	0	3110	490

(1) Element abundance in weight percent oxide.

(2) Total iron expressed as FeO.

(3) REE2O3 is sum of REE abundances.

(4) Trace element abundance in ppm.

APPENDIX III: ZIRCON

Chemical compositions of zircon crystals from the Type III pegmatites.

Location	5A2-Z1-6	5A2-Z1-7	5A2-Z1-9	5A2-Z1-10	ZIR1-9 Apr10_95.033	ZIR1-10	ZIR1-11 Apr10_95.035
PIXE Zoning	Light Rim	Light Rim	Light Rim	Light Rim	Light Rim	Light Rim	Light Rim
ZrO2	68.607	67.879	68.302	67.917	62.3	61.456	48.291
SiO2 (1)	31.64	32.283	31.892	31.882	28.9	28.426	28.359
CaO	0.057	0	0.005	0.007	1.577	2.263	4.701
FeO T (2)	0.551	0.087	0.219	0.077	1.472	0.656	2.684
HfO2	0.16	0.246	0.239	0.225	0.357	0.33	1.828
Al2O3	0.022	0.003	0.014	0	0.088	0.144	0.804
MgO	0	0.005	0.007	0.013	0	0	0
Na2O	0	0	0	0	0	0	0
TiO2	0	0.044	0.011	0	0	0.012	0.002
P2O5	0.048	0	0.024	0.03	0.021	0.004	0
UO2	0.051	0.121	0.049	0.053	0.715	0.632	0.695
REE2O3 (3)	0.148	0.079	0.075	0.008	2.273	1.332	3.478
TOTAL	101.284	100.748	100.837	100.213	97.702	95.254	90.841
Cr (4)	-	-	-	-	0	-	0
Mn	-	-	-	-	1748	-	960
Co	-	-	-	-	396	-	826
Ni	-	-	-	-	52	-	96
Cu	-	-	-	-	98	-	183
Zn	-	-	-	-	23	-	78
Br	-	-	-	-	25	-	31
Sr	-	-	-	-	1141	-	3044
Mo	-	-	-	-	0	-	0
Ba	-	-	-	-	142	-	727
Y	0	0	0	0	2529	1220	12627
La	40	0	0	0	704	790	313
Ce	100	110	20	0	3057	4420	3886
Nd	210	310	0	70	1728	4160	4673
Sm	440	260	0	0	184	690	1298
Gd	-	-	-	-	163	-	1455
Dy	-	-	-	-	0	-	1579
Er	-	-	-	-	531	-	1362
Yb	330	0	150	0	372	0	1302
Lu	160	0	490	0	10255	10	300
Tl	-	-	-	-	0	-	181
Pb	-	-	-	-	440	-	173
Th	0	0	0	150	295	160	872

(1) Element abundance in weight percent oxide.

(2) Total iron expressed as FeO.

(3) REE2O3 is sum of REE abundances.

(4) Trace element abundance in ppm.

APPENDIX III: ZIRCON

Chemical compositions of zircon crystals from the Type III pegmatites.

Location PIXE Zoning	ZIR2-14 Light Rim	10C-Z1-7 Dark part of Mottled Area	10C-Z1-13 Dark part of Mottled Area	ZIR2-11 Apr10_95.029 Dark part of Mottled Area	ZIR2-12 Dark part of Mottled Area	ZIR2-13 Dark part of Mottled Area
ZrO2	64.74	62.291	57.667	60.117	51.999	49.233
SiO2 (1)	30.777	29.744	28.292	28.659	26.622	26.251
CaO	0.271	1.089	2.368	1.263	4.891	0
FeO T (2)	2.15	0.165	0.188	1.414	0.427	1.047
HfO2	0.372	0.177	0.209	0.178	0.134	0.154
Al2O3	0.056	0.136	0.19	0.058	0.446	0.477
MgO	0	0.008	0	0	0.021	0.008
Na2O	0	0.496	0	0	0	4.775
TiO2	0	0.019	0.025	0	0.03	0.019
P2O5	0	0	0	0	0	0
UO2	0.419	1.588	3.349	1.578	2.05	2.447
REE2O3 (3)	0.108	0.647	0.978	1.893	0.997	0.935
TOTAL	98.892	96.36	93.266	95.161	87.616	85.345
Cr (4)	-	-	-	70	-	-
Mn	-	-	-	1557	-	-
Co	-	-	-	945	-	-
Ni	-	-	-	0	-	-
Cu	-	-	-	0	-	-
Zn	-	-	-	82	-	-
Br	-	-	-	33	-	-
Sr	-	-	-	1538	-	-
Mo	-	-	-	0	-	-
Ba	-	-	-	379	-	-
Y	470	2390	5030	5358	5050	5360
La	0	0	20	0	0	0
Ce	0	210	560	213	1080	740
Nd	140	250	280	236	0	140
Sm	0	0	0	323	0	0
Gd	-	-	-	457	-	-
Dy	-	-	-	0	-	-
Er	-	-	-	1049	-	-
Yb	280	1360	1660	1352	1300	1330
Lu	0	1190	440	6998	710	0
Tl	-	-	-	37	-	-
Pb	-	-	-	2168	-	-
Th	0	1000	360	2140	1900	490

(1) Element abundance in weight percent oxide.

(2) Total iron expressed as FeO.

(3) REE2O3 is sum of REE abundances.

(4) Trace element abundance in ppm.

APPENDIX III: ZIRCON

Chemical compositions of zircon crystals from the Type III pegmatites.

Location PIXE Zoning	10C-Z1-5 Light part of Mottled Area	10C-Z1-10 Light part of Mottled Area	10C-Z2-10 Light part of Mottled Area	10C-Z2-11 Light part of Mottled Area	ZIR1-1 Apr10_95.030 Light part of Mottled Area	ZIR1-2 Apr10_95.031 Light part of Mottled Area
ZrO2	63.003	54.471	62.708	66.13	54.289	56.386
SiO2 (1)	30.443	25.523	30.154	30.554	28.291	29.915
CaO	1.212	1.175	1.355	0.615	3.959	2.349
FeO T (2)	1.012	0.23	0.104	0.204	3.712	2.719
HfO2	0.194	0.182	0.189	0.205	0.167	0.787
Al2O3	0.198	0.163	0.203	0.044	0.535	0.288
MgO	0.017	0.006	0.004	0	0	0
Na2O	0	0	0	0	0	0
TiO2	0.047	0.021	0.061	0.018	0	0.026
P2O5	0	0	0	0.017	0	0.012
UO2	0.71	1.153	1.504	0.652	1.495	1.802
REE2O3 (3)	0.413	0.423	0.608	0.295	2.284	3.056
TOTAL	97.249	83.346	96.89	98.734	94.731	97.34
Cr (4)	-	-	-	-	0	57
Mn	-	-	-	-	1626	1141
Co	-	-	-	-	655	558
Ni	-	-	-	-	129	108
Cu	-	-	-	-	119	120
Zn	-	-	-	-	70	49
Br	-	-	-	-	86	76
Sr	-	-	-	-	5798	2328
Mo	-	-	-	-	1606	1524
Ba	-	-	-	-	666	387
Y	1220	2190	2840	980	2650	4462
La	0	0	0	0	3227	7573
Ce	110	0	410	100	4975	10644
Nd	350	0	360	500	0	205
Sm	0	110	0	0	0	0
Gd	-	-	-	-	830	556
Dy	-	-	-	-	0	0
Er	-	-	-	-	785	861
Yb	880	930	1380	880	1005	962
Lu	920	230	0	0	6040	520
Tl	-	-	-	-	0	90
Pb	-	-	-	-	287	304
Th	80	1270	1120	290	4908	2031

(1) Element abundance in weight percent oxide.

(2) Total iron expressed as FeO.

(3) REE2O3 is sum of REE abundances.

(4) Trace element abundance in ppm.

APPENDIX III: ZIRCON

Chemical compositions of zircon crystals from the Type IV pegmatites.

Location	**6A7-Z1-3**	**6A6A-Z1-1**	**6A6A-Z1-2**	**6A7-Z1-4**	**6A7-Z1-5**	**6A7-Z1-6**	**6A7-Z2-5**
PIXE Zoning	**Centre**	**Centre**	**Centre**	**Unzoned**	**Unzoned**	**Unzoned**	**Unzoned**
ZrO2 (1)	67.44	68.132	67.268	64.389	64.135	66.137	66.944
SiO2	32.035	32.11	32.18	31.334	30.445	31.343	31.704
CaO	0.038	0.022	0.077	0.208	0.558	0.145	0.243
FeO T (2)	0	0	0	0.126	0.081	0.104	0
HfO2	0.154	0.172	0.189	0.223	0.19	0.188	0.205
Al2O3	0.012	0.01	0.015	0.104	0	0.011	0.025
MgO	0	0	0.008	0	0	0	0
TiO2	0	0.064	0	0	0.019	0.007	0.012
P2O5	0.031	0.038	0.047	0.077	0	0.006	0.163
UO2	0.059	0.083	0.117	0.074	0.107	0.034	0.088
REE2O3 (3)	0.127	0.191	0.433	0.982	1.067	0.612	2.498
TOTAL	99.896	100.822	100.334	97.517	96.601	98.587	101.882
V (4)	-	-	-	-	-	-	-
Cr	-	-	-	-	-	-	-
Mn	-	-	-	-	-	-	-
Co	-	-	-	-	-	-	-
Ni	-	-	-	-	-	-	-
Cu	-	-	-	-	-	-	-
Zn	-	-	-	-	-	-	-
Br	-	-	-	-	-	-	-
Sr	-	-	-	-	-	-	-
Mo	-	-	-	-	-	-	-
Ba	-	-	-	-	-	-	-
Ta	-	-	-	-	-	-	-
Y	0	650	780	70	5490	1780	1060
La	0	0	150	1290	0	170	2890
Ce	190	120	1610	4350	1080	1870	9400
Nd	150	340	960	2040	570	970	7190
Sm	0	80	0	350	0	0	730
Gd	-	-	-	-	-	-	-
Dy	-	-	-	-	-	-	-
Er	-	-	-	-	-	-	-
Yb	0	0	140	300	940	300	0
Lu	770	400	0	0	610	0	0
Pb	-	-	-	-	-	-	-
Bi	-	-	-	-	-	-	-
Th	0	0	0	0	0	0	80

(1) Element abundances in weight percent oxide.

(2) Total iron expressed as FeO.

(3) REE2O3 is sum of REE abundances.

(4) Trace element abundance in ppm.

APPENDIX III: ZIRCON

Chemical compositions of zircon crystals from the Type IV pegmatites.

Location	6A7-Z2-6	6A7-Z2-7	6A7-Z2-8	6A7-Z1-1	6A7-Z1-2	6A7-Z2-3
PIXE				Apr10_95.044		
Zoning	Unzoned	Unzoned	Unzoned	Overgrowth	Overgrowth	Overgrowth
ZrO2	68.313	68.531	68.554	68.567	66.515	66.442
SiO2 (1)	31.664	31.788	31.974	31.895	31.778	31.547
CaO	0.026	0.005	0.002	0.044	0.126	0.091
FeO(2)	0	0.006	0.053	0.018	0.136	0
HfO2	0.241	0.212	0.269	0.208	0.312	0.226
Al2O3	0	0	0.013	0	0.019	0
MgO	0.017	0	0	0.001	0.024	0.007
TiO2	0.031	0.016	0	0	0.028	0.033
P2O5	0.073	0	0	0.046	0.018	0
UO2	0.041	0.01	0.044	1.141	0.123	0.085
REE2O3 (3)	0.249	0.096	0.149	2.527	1.049	0.985
TOTAL	100.654	100.664	101.059	104.447	100.127	99.416
V (4)	-	-	-	85	-	-
Cr	-	-	-	231	-	-
Mn	-	-	-	0	-	-
Co	-	-	-	1319	-	-
Ni	-	-	-	89	-	-
Cu	-	-	-	102	-	-
Zn	-	-	-	0	-	-
Br	-	-	-	21	-	-
Sr	-	-	-	2841	-	-
Mo	-	-	-	0	-	-
Ba	-	-	-	0	-	-
Ta	-	-	-	473	-	-
Y	0	0	0	13707	0	60
La	0	0	0	73	1840	510
Ce	1050	420	450	480	4290	5320
Nd	410	300	630	2174	1890	2150
Sm	370	0	200	1173	0	350
Gd	-	-	-	966	-	-
Dy	-	-	-	656	-	-
Er	-	-	-	368	-	-
Yb	310	100	0	369	0	20
Lu	0	0	0	540	970	10
Pb	-	-	-	3475	-	-
Bi	-	-	-	383	-	-
Th	450	0	0	7935	0	0

(1) Element abundances in weight percent oxide.

(2) Total iron expressed as FeO.

(3) REE2O3 is sum of REE abundances.

(4) Trace element abundance in ppm.

APPENDIX III: ZIRCON

Chemical compositions of zircon crystals from the Type IV pegmatites.

Location	6A7-Z2-4	6A6A-Z1-3	6A6A-Z1-4	6A7-Z2-1	6A7-Z2-2	6A6A-Z1-6
PIXE Zoning	Overgrowth	Overgrowth	Overgrowth	Mottled Area	Mottled Area	Mottled Area
ZrO2	67.151	67.749	68.633	61.588	60.866	65.812
SiO2 (1)	31.384	32.312	32.433	29.245	28.399	31.224
CaO	0.054	0.158	0.2	1.415	2.452	0.265
FeO (2)	0.092	0.046	0	0.141	0.035	0.031
HfO2	0.272	0.176	0.171	0.174	0.167	0.201
Al2O3	0.004	0.052	0	0.001	0.03	0.01
MgO	0	0	0	0.027	0	0
TiO2	0	0.031	0.02	0	0	0.019
P2O5	0.007	0.054	0.035	0.028	0	0.054
UO2	0.228	0.166	0.174	0.431	0.439	0.126
REE2O3 (3)	0.341	1.908	3.069	0.538	0.388	1.215
TOTAL	99.534	102.652	104.735	93.589	92.776	98.957
V (4)	-	-	-	-	-	-
Cr	-	-	-	-	-	-
Mn	-	-	-	-	-	-
Co	-	-	-	-	-	-
Ni	-	-	-	-	-	-
Cu	-	-	-	-	-	-
Zn	-	-	-	-	-	-
Br	-	-	-	-	-	-
Sr	-	-	-	-	-	-
Mo	-	-	-	-	-	-
Ba	-	-	-	-	-	-
Ta	-	-	-	-	-	-
Y	350	780	960	1830	1820	520
La	200	3920	6030	0	0	1600
Ce	740	10010	9050	910	640	5610
Nd	330	720	8370	400	440	2430
Sm	120	670	540	320	0	180
Gd	-	-	-	-	-	-
Dy	-	-	-	-	-	-
Er	-	-	-	-	-	-
Yb	370	130	160	750	270	0
Lu	810	0	1080	260	0	0
Pb	-	-	-	-	-	-
Bi	-	-	-	-	-	-
Th	0	0	0	60	0	0

(1) Element abundances in weight percent oxide.

(2) Total iron expressed as FeO.

(3) REE2O3 is sum of REE abundances.

(4) Trace element abundance in ppm.

APPENDIX III: ZIRCON

Chemical compositions of zircon crystals from the Type IV pegmatites.

Location	**6A6A-Z1-5**
PIXE	
Zoning	**Mottled**
	Area
ZrO2	66.043
SiO2 (1)	31.365
CaO	0.451
FeO (2)	0.019
HfO2	0.196
Al2O3	0.022
MgO	0
TiO2	0
P2O5	0.026
UO2	0.205
REE2O3 (3)	0.673
TOTAL	99.001
V (4)	-
Cr	-
Mn	-
Co	-
Ni	-
Cu	-
Zn	-
Br	-
Sr	-
Mo	-
Ba	-
Ta	-
Y	1090
La	350
Ce	2220
Nd	1230
Sm	60
Gd	-
Dy	-
Er	-
Yb	430
Lu	300
Pb	-
Bi	-
Th	40

(1) Element abundances in weight percent oxide.
(2) Total iron expressed as FeO.
(3) REE2O3 is sum of REE abundances.
(4) Trace element abundance in ppm.

APPENDIX III: ZIRCON

XRD data for a zircon crystal from the Type III pegmatites.

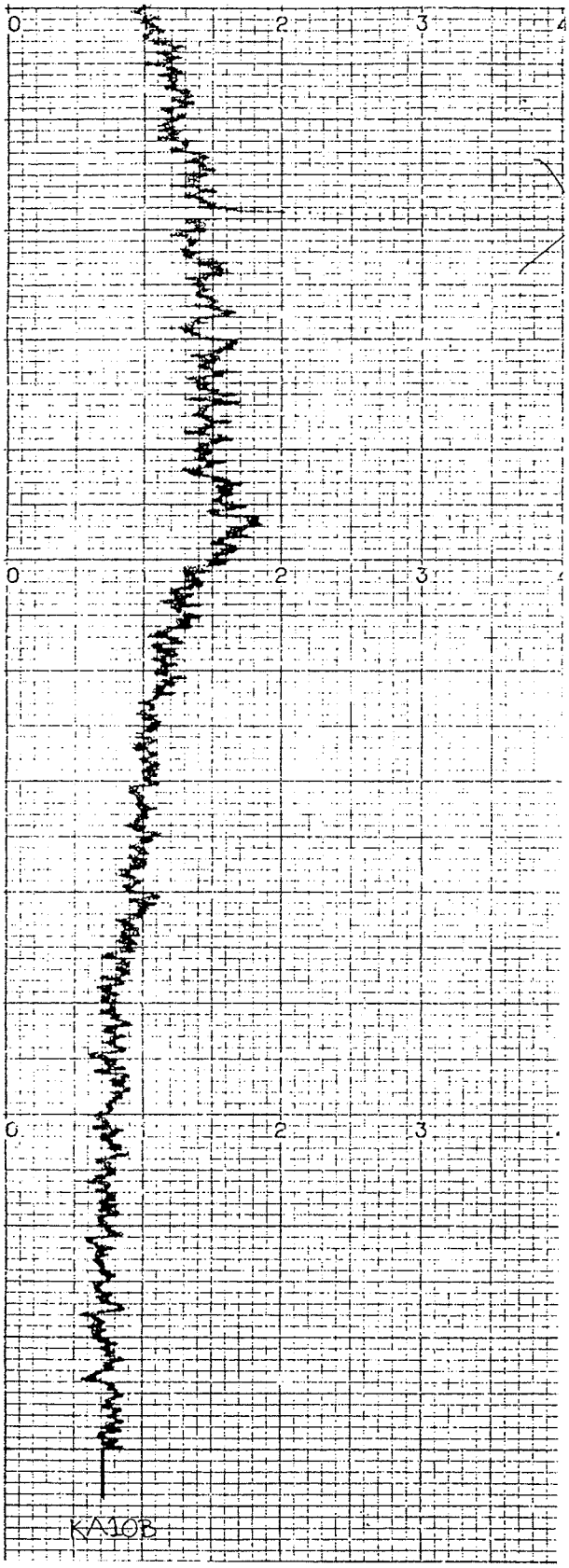

APPENDIX IV: BRITHOLITE

Chemical compositions of unaltered and altered britholite grains from the Type IV pegmatites.

Location	6A2-B1-1	6A2-B1-2	6A2-B1-4	6A2-B1-5	6A2-B2-1	6A2-B2-2
	Unaltered	Unaltered	Unaltered	Unaltered	Unaltered	Unaltered
SiO2 (1)	18.705	19.289	19.021	19.039	18.874	19.076
FeO T (2)	0	0	0	0	0	0
CaO	16.816	15.478	15.9	15.463	16.267	16.001
Al2O3	0	0	0	0	0	0
TiO2	0.002	0	0	0	0	0.026
UO2	0.743	0.744	0.841	0.8	0.794	0.802
ThO2	1.123	0.91	1.029	1.046	0.978	1.139
Y2O3	1.896	1.96	1.854	1.901	1.904	1.87
La2O3	8.859	8.894	8.683	8.893	8.538	8.544
Ce2O3	24.757	24.902	24.806	24.884	24.657	24.62
Nd2O3	12.774	12.91	12.656	12.859	12.699	12.862
Sm2O3	1.738	1.921	1.934	1.814	1.788	1.77
Gd2O3	1.357	1.064	0.992	1.18	1.057	1.152
Dy2O3	0.52	0.567	0.469	0.485	0.526	0.516
Eu2O3	0.293	0.275	0.365	0.344	0.245	0.361
P2O5	4.669	3.479	3.987	3.398	4.435	3.817
F	3.254	2.866	3.445	3.835	3.229	3.237
Cl	0.018	0.062	0.004	0.021	0.015	0.031
TOTAL	97.524	95.321	95.986	95.962	96.006	95.824

Location	6A2-B2-3	6A2-B2-4	6A2-B2-5	6A2-B2-6	6A2-B2-7	6A4-B1-4
	Unaltered	Unaltered	Unaltered	Unaltered	Unaltered	Unaltered
SiO2 (1)	19.566	19.233	19.138	19.216	19.156	20.398
FeO T (2)	0	0	0	0	0	0
CaO	15.27	15.91	16.214	15.779	16.051	13.057
Al2O3	0	0	0	0	0	0
TiO2	0	0	0	0	0	0
UO2	0.817	0.752	0.814	0.867	0.812	0.837
ThO2	0.913	0.909	0.936	1.002	0.914	1.194
Y2O3	1.923	1.915	1.83	1.917	1.941	2.12
La2O3	9.023	8.852	8.742	8.564	8.754	8.699
Ce2O3	25.151	25.185	24.523	24.853	24.681	26.351
Nd2O3	12.817	13.095	12.819	13.122	12.859	14.396
Sm2O3	1.929	1.892	1.852	1.7	1.839	2.145
Gd2O3	1.196	1.14	1.143	1.06	1.199	1.421
Dy2O3	0.558	0.477	0.405	0.622	0.581	0.57
Eu2O3	0.293	0.386	0.339	0.305	0.379	0.429
P2O5	3.383	3.873	3.911	3.814	3.769	1.723
F	3.022	3.146	3.567	3.145	3.248	2.776
Cl	0.037	0.024	0.027	0.029	0.038	0.031
TOTAL	95.898	96.789	96.26	95.995	96.221	96.147

(1) Element abundance in weight percent oxide.

(2) Total iron expressed as FeO.

APPENDIX IV: BRITHOLITE

Chemical compositions of unaltered and altered britholite grains from the Type IV pegmatites.

Location	6A4-B1-5	6A4-B1-10	6A4-B2-1	6A4-B2-5	6A4-B2-6	6A8A-B1-1
	Unaltered	Unaltered	Unaltered	Unaltered	Unaltered	Unaltered
SiO2 (1)	20.046	19.319	20.205	20.002	20.223	19.276
FeO T (2)	0	0	0	0	0	0
CaO	13.572	13.577	13.379	12.897	13.012	15.912
Al2O3	0	0	0	0	0	0.127
TiO2	0	0	0	0	0	0
UO2	0.918	0.763	1.004	0.854	0.701	0.962
ThO2	1.248	1.229	1.216	1.167	1.186	1.11
Y2O3	2.18	2.112	2.21	2.231	2.265	1.838
La2O3	8.703	8.559	8.314	8.354	8.22	8.363
Ce2O3	26.064	25.839	25.648	25.943	26.197	24.616
Nd2O3	13.981	14.324	14.345	14.404	14.632	13.139
Sm2O3	2.094	1.978	2.092	2.189	2.341	1.906
Gd2O3	1.338	1.188	1.367	1.357	1.327	1.222
Dy2O3	0.486	0.588	0.533	0.596	0.59	0.515
Eu2O3	0.32	0.358	0.43	0.337	0.37	0.342
P2O5	1.928	2.55	1.808	1.769	1.674	3.817
F	2.818	2.825	2.617	2.474	3.016	3.27
Cl	0.039	0.094	0.038	0.097	0.045	0.035
TOTAL	95.735	95.303	95.206	94.671	95.799	96.45

Location	6A8A-B1-2	6A8A-B2-1	6A8A-B2-2	6A8A-B2-3	6A8A-B2-4	6A8A-B2-5
	Unaltered	Unaltered	Unaltered	Unaltered	Unaltered	Unaltered
SiO2 (1)	19.129	19.178	19.097	19.098	19.021	19.06
FeO T (2)	0	0	0	0	0	0
CaO	15.983	16.099	16.095	16.268	16.286	16.279
Al2O3	0.109	0.034	0.037	0.05	0.024	0.072
TiO2	0	0	0	0.064	0	0
UO2	0.768	0.764	0.805	0.86	0.705	0.839
ThO2	0.873	0.972	0.993	0.92	0.879	0.7
Y2O3	1.834	1.832	1.852	1.868	1.782	1.864
La2O3	8.668	8.764	8.781	8.449	8.612	8.653
Ce2O3	24.683	24.971	24.581	24.59	24.47	24.425
Nd2O3	12.993	12.796	13.165	13.01	12.975	12.8
Sm2O3	1.909	1.943	2.002	1.75	1.708	1.824
Gd2O3	1.141	1.128	1.27	1.171	1.193	1.255
Dy2O3	0.538	0.565	0.589	0.52	0.466	0.376
Eu2O3	0.233	0.364	0.287	0.311	0.306	0.242
P2O5	3.731	4.046	3.977	4.133	4.046	4.191
F	2.761	3.255	3.31	3.311	3.352	3.453
Cl	0.027	0.032	0.019	0.033	0.035	0.026
TOTAL	95.38	96.743	96.86	96.406	95.86	96.059

(1) Element abundance in weight percent oxide.

(2) Total iron expressed as FeO.

APPENDIX IV: BRITHOLITE

Chemical compositions of unaltered and altered britholite grains from the Type IV pegmatites.

Location	6A8A-B3-1	6A8A-B3-3	6A8A-B3-6	6A8A-B3-7	6A8A-B3-10	6A6B-B1-1
	Unaltered	Unaltered	Unaltered	Unaltered	Unaltered	Unaltered
SiO2 (1)	19.307	18.941	19.385	19.265	19.044	19.091
FeO T (2)	0	0	0	0	0	0
CaO	15.4	16.166	15.605	15.779	16.038	15.887
Al2O3	0.011	0.003	0.031	0.045	0.038	0.008
TiO2	0	0	0	0	0	0
UO2	0.886	0.758	0.848	0.766	0.847	0.831
ThO2	0.787	0.864	0.943	0.877	0.917	0.873
Y2O3	1.817	1.819	1.923	1.837	1.809	1.897
La2O3	8.788	8.721	8.665	8.842	8.897	8.499
Ce2O3	24.713	24.639	25.042	24.946	24.775	24.795
Nd2O3	13.172	12.77	13.115	13.029	12.664	13.296
Sm2O3	1.922	1.843	2.003	1.896	2.033	1.841
Gd2O3	1.443	1.112	1.217	1.228	1.174	1.279
Dy2O3	0.377	0.492	0.528	0.425	0.506	0.578
Eu2O3	0.322	0.269	0.324	0.283	0.283	0.294
P2O5	3.252	3.962	3.73	3.625	3.776	3.82
F	3.698	2.746	2.76	3.42	2.946	2.887
Cl	0.044	0.029	0.028	0.035	0.021	0.063
TOTAL	95.939	95.134	96.147	96.298	95.768	95.939

Location	6A6B-B1-3	6A6B-B2-1	6A6B-B2-2	6A6B-B2-3	6A6B-B3-1	6A6B-B3-4
	Unaltered	Unaltered	Unaltered	Unaltered	Unaltered	Unaltered
SiO2 (1)	19.305	19.231	19.182	19.204	19.158	19.4
FeO T (2)	0	0	0	0	0	0
CaO	15.779	15.891	15.743	15.913	16.015	16.014
Al2O3	0	0.098	0.038	0.059	0.04	0
TiO2	0	0	0	0	0	0
UO2	0.727	0.739	0.676	0.735	0.781	0.701
ThO2	0.844	0.713	0.793	0.941	0.825	0.717
Y2O3	1.864	1.94	1.928	1.909	1.864	1.869
La2O3	8.624	8.774	8.635	8.648	8.776	8.634
Ce2O3	24.7	24.964	24.722	24.67	24.753	24.589
Nd2O3	13.146	12.913	12.898	13.093	13.067	12.867
Sm2O3	1.93	1.782	1.811	1.939	1.855	1.974
Gd2O3	1.129	1.263	1.157	1.198	1.174	1.108
Dy2O3	0.5	0.498	0.432	0.499	0.466	0.64
Eu2O3	0.335	0.286	0.237	0.432	0.321	0.29
P2O5	3.823	3.939	3.788	3.871	3.881	3.84
F	2.98	3.246	3.343	3.294	2.78	3.169
Cl	0.043	0.038	0.029	0.039	0.043	0.051
TOTAL	95.729	96.315	95.412	96.444	95.799	95.863

(1) Element abundance in weight percent oxide.

(2) Total iron expressed as FeO.

APPENDIX IV: BRITHOLITE

Chemical compositions of unaltered and altered britholite grains from the Type IV pegmatites.

Location	6A6B-B3-5	6A6B-B3-6	6A6B-B3-10	6A2-B-1	6A2-B-2	6A4-B-1
	Unaltered	Unaltered	Unaltered	Unaltered	Unaltered	Unaltered
SiO2 (1)	19.211	19.13	19.245	19.458	19.134	20.023
FeO T (2)	0	0	0	0	0	0
CaO	15.922	16.37	15.678	15.245	15.705	12.983
Al2O3	0.025	0.069	0.014	0.021	0	0.009
TiO2	0.035	0	0	0	0	0
UO2	0.793	0.827	0.79	0.861	0.887	0.942
ThO2	0.951	0.877	0.704	0.943	0.987	1.141
Y2O3	1.904	1.888	1.908	1.976	1.942	2.255
La2O3	8.453	8.37	8.632	8.992	9.13	8.502
Ce2O3	24.594	24.392	24.948	25.458	25.562	25.688
Nd2O3	13.174	13.185	13.101	13.156	13.195	14.272
Sm2O3	1.981	1.999	2.096	1.909	1.864	2.176
Gd2O3	1.045	1.19	1.177	1.093	1.042	1.283
Dy2O3	0.627	0.531	0.594	0.497	0.455	0.566
Eu2O3	0.338	0.322	0.339	0.331	0.375	0.393
P2O5	3.67	4.077	3.529	3.266	3.724	1.699
F	3.254	3.229	3.533	3.07	3.585	2.392
Cl	0.032	0.021	0.027	0.026	0.022	0.097
TOTAL	96.009	96.477	96.315	96.302	97.609	94.421

Location	6A4-B-2	6A4-B-3	6A6A-B1-1	6A6A-B1-3	6A6A-B1-4	6A6A-B1-9
	Unaltered	Unaltered	Unaltered	Unaltered	Unaltered	Unaltered
SiO2 (1)	19.866	19.54	18.887	19.119	18.286	19.143
FeO T (2)	0	0	0	0	0	0
CaO	12.739	13.722	16.636	16.107	17.048	16.298
Al2O3	0	0	0.057	0.017	0.087	0.016
TiO2	0.126	0	0.015	0	0	0
UO2	0.762	0.976	0.892	0.848	0.72	0.805
ThO2	1.198	1.255	0.735	1.105	0.803	0.722
Y2O3	2.301	2.263	1.913	1.822	1.806	1.811
La2O3	8.205	8.341	8.397	8.502	8.172	8.573
Ce2O3	25.548	25.516	24.396	24.286	23.67	24.549
Nd2O3	14.545	14.28	12.677	13.009	12.62	12.929
Sm2O3	2.312	2.314	1.843	1.767	1.931	1.949
Gd2O3	1.477	1.382	1.023	1.11	1.16	1.148
Dy2O3	0.58	0.546	0.417	0.437	0.516	0.424
Eu2O3	0.362	0.339	0.251	0.275	0.262	0.262
P2O5	1.617	2.513	4.699	4.168	4.876	4.279
F	2.26	2.399	3.689	3.004	3.527	3.344
Cl	0.085	0.068	0.09	0.072	0.032	0.033
TOTAL	93.983	95.454	96.617	95.648	95.516	96.285

(1) Element abundance in weight percent oxide.

(2) Total iron expressed as FeO.

APPENDIX IV: BRITHOLITE

Chemical compositions of unaltered and altered britholite grains from the Type IV pegmatites.

Location	6A6A-B1-10	6A6A-B2-4	6A6A-B2-5	6A6A-B2-6	6A6A-B3-1	6A6A-B3-4
	Unaltered	Unaltered	Unaltered	Unaltered	Unaltered	Unaltered
SiO2 (1)	18.966	19.053	19.425	19.137	19.418	19.234
FeO T (2)	0	0	0	0	0	0
CaO	16.582	16.183	15.278	16.143	15.553	16.212
Al2O3	0.049	0.053	0.013	0.034	0.016	0.095
TiO2	0	0.009	0	0	0.001	0
UO2	0.766	0.808	0.869	0.735	0.72	0.777
ThO2	1.055	0.873	0.974	0.83	0.826	0.892
Y2O3	1.857	1.872	1.95	1.869	1.929	1.897
La2O3	8.518	8.76	8.715	8.656	8.507	8.515
Ce2O3	24.56	24.788	25.117	24.64	24.817	24.166
Nd2O3	12.889	12.932	13.267	12.964	13.269	12.865
Sm2O3	2.124	1.927	1.93	1.897	2.006	1.708
Gd2O3	1.052	1.164	1.153	1.156	1.314	1.123
Dy2O3	0.452	0.367	0.474	0.503	0.465	0.574
Eu2O3	0.324	0.299	0.223	0.251	0.334	0.314
P2O5	4.602	4.012	3.516	4.28	3.79	4.077
F	3.112	3.469	3.215	3.374	3.071	3.029
Cl	0.036	0.051	0.032	0.036	0.034	0.045
TOTAL	96.944	96.62	96.151	96.505	96.07	95.523

Location	6A6A-B3-6	6A6A-B3-7	6A6A-B3-9	6A6A-B4-1	6A6A-B4-3	6A6A-B4-5
	Unaltered	Unaltered	Unaltered	Unaltered	Unaltered	Unaltered
SiO2 (1)	19.054	19.052	19.57	19.36	19.465	19.529
FeO T (2)	0	0	0	0	0	0
CaO	16.27	16.255	15.567	15.822	15.793	15.54
Al2O3	0.064	0.07	0.082	0.093	0.133	0.12
TiO2	0	0	0	0	0	0
UO2	0.758	0.898	0.849	0.777	0.762	0.775
ThO2	0.814	0.921	0.894	0.79	0.802	0.742
Y2O3	1.849	1.893	1.938	1.938	1.966	1.925
La2O3	8.619	8.751	8.663	8.616	8.674	8.756
Ce2O3	24.474	24.735	25.055	24.812	24.823	25.269
Nd2O3	12.878	12.992	13.522	13.006	13.089	13.243
Sm2O3	1.809	1.859	1.871	1.982	1.996	1.934
Gd2O3	1.115	1.095	1.258	1.184	1.091	1.062
Dy2O3	0.481	0.514	0.53	0.444	0.428	0.51
Eu2O3	0.329	0.306	0.339	0.282	0.333	0.311
P2O5	4.135	4.223	3.391	3.886	3.706	3.668
F	3.067	3.26	3.515	3.187	3.243	2.635
Cl	0.031	0.028	0.033	0.032	0.033	0.04
TOTAL	95.747	96.852	97.077	96.211	96.337	96.059

(1) Element abundance in weight percent oxide.

(2) Total iron expressed as FeO.

APPENDIX IV: BRITHOLITE

Chemical compositions of unaltered and altered britholite grains from the Type IV pegmatites.

Location	6A6A-B5-1	6A6A-B5-2	6A6A-B5-5	6A2-B1-7	6A2-B1-8	6A2-B1-9
	Unaltered	Unaltered	Unaltered	Altered	Altered	Altered
SiO2 (1)	19.563	19.491	19.286	18.686	18.381	19.555
FeO T (2)	0	0	0	0	0	0
CaO	15.488	15.684	16.389	15.871	16.101	11.649
Al2O3	0.183	0.139	0.134	0	0.09	0.037
TiO2	0.048	0	0	0	0	0
UO2	0.722	0.912	0.821	0.745	0.829	0.714
ThO2	0.981	0.96	0.78	1.001	0.965	1.081
Y2O3	1.975	1.855	1.869	1.885	0.189	1.886
La2O3	8.576	9.043	8.608	8.554	8.444	8.366
Ce2O3	24.992	25.208	24.455	24.301	23.964	23.839
Nd2O3	13.172	13.027	13.05	12.655	12.536	12.555
Sm2O3	1.934	1.826	1.864	1.83	1.891	1.895
Gd2O3	1.131	1.169	1.066	1.113	1.088	1.102
Dy2O3	0.53	0.632	0.581	0.403	0.28	0.458
Eu2O3	0.431	0.228	0.231	0.335	0.331	0.311
P2O5	3.491	3.49	4.138	4.074	4.283	2.201
F	3.252	3.335	3.119	2.42	1.987	3.571
Cl	0.046	0.032	0.027	0.11	0.217	0.141
TOTAL	96.515	97.031	96.418	93.983	91.576	89.361

Location	6A2-B1-10	6A2-B1-11	6A2-B1-12	6A2-B2-8	6A2-B2-9	6A2-B2-10
	Altered	Altered	Altered	Altered	Altered	Altered
SiO2 (1)	18.615	20.037	19.02	19.106	19.169	18.305
FeO T (2)	0	0.016	0	0	0	0
CaO	16.212	16.185	15.083	15.245	15.426	16.723
Al2O3	0	0.158	0	0	0	0
TiO2	0	0.008	0	0	0	0
UO2	0.844	0.561	0.867	0.791	0.74	0.77
ThO2	1.115	0.94	0.942	0.988	0.756	0.949
Y2O3	1.865	1.78	1.972	1.874	1.904	1.835
La2O3	8.47	8.251	8.503	8.593	8.504	8.326
Ce2O3	21.819	23.137	24.246	24.501	24.241	23.792
Nd2O3	12.517	12.203	12.99	12.774	12.645	12.115
Sm2O3	1.778	1.834	1.849	1.805	1.759	1.73
Gd2O3	1.166	1.144	1.253	1.147	1.087	1.157
Dy2O3	0.45	0.445	0.393	0.527	0.487	0.481
Eu2O3	0.288	0.228	0.335	0.384	0.263	0.294
P2O5	4.42	3.441	3.932	3.443	3.666	5.074
F	2.569	2.556	2.565	2.513	2.129	2.424
Cl	0.045	0.119	0.021	0.026	0.123	0.096
TOTAL	92.173	93.043	93.971	93.717	92.899	94.071

(1) Element abundance in weight percent oxide.

(2) Total iron expressed as FeO.

APPENDIX IV: BRITHOLITE

Chemical compositions of unaltered and altered britholite grains from the Type IV pegmatites.

Location	6A2-B2-11	6A2-B2-12	6A4-B1-1	6A4-B1-2	6A4-B1-3	6A4-B1-6
	Altered	Altered	Altered	Altered	Altered	Altered
SiO2 (1)	18.5	19.268	19.911	20.177	20.18	19.742
FeO T (2)	0	0	0	0	0	0
CaO	15.471	16.413	12.859	12.502	12.711	13.858
Al2O3	0	0.095	0	0	0	0
TiO2	0.001	0	0.059	0	0	0
UO2	0.695	0.683	0.967	0.626	0.968	0.92
ThO2	0.931	0.882	1.067	1.106	1.215	1.019
Y2O3	1.866	1.872	2.15	2.18	2.146	2.178
La2O3	8.407	8.178	8.319	8.401	8.366	8.319
Ce2O3	23.939	23.36	25.373	25.561	25.56	24.911
Nd2O3	12.26	12.341	13.714	14.613	14.279	13.595
Sm2O3	1.184	1.883	1.978	2.063	2.064	1.863
Gd2O3	1.062	1.212	1.318	1.257	1.398	1.344
Dy2O3	0.525	0.274	0.632	0.584	0.62	0.614
Eu2O3	0.288	0.334	0.305	0.295	0.316	0.341
P2O5	4.063	4.023	1.537	1.355	1.452	2.391
F	2.183	2.309	2.151	2.025	2.327	2.444
Cl	0.175	0.108	0.204	0.085	0.04	0.019
TOTAL	91.55	93.235	92.544	92.83	93.642	93.558

Location	6A4-B1-7	6A4-B1-8	6A4-B1-9	6A4-B2-2	6A4-B2-3	6A4-B2-4
	Altered	Altered	Altered	Altered	Altered	Altered
SiO2 (1)	19.829	20.45	19.857	20.16	20.073	19.491
FeO T (2)	0	0	0	0	0	0
CaO	13.255	12.683	14.239	12.68	12.745	13.726
Al2O3	0	0	0.011	0	0	0
TiO2	0	0	0.066	0.028	0	0.025
UO2	0.925	0.606	0.899	1.048	1.091	0.995
ThO2	1.17	1.039	1.511	1.38	1.275	1.17
Y2O3	2.187	2.297	2.286	2.282	2.333	2.294
La2O3	8.173	7.898	7.557	7.864	8.016	7.684
Ce2O3	25.09	25.164	23.085	25.288	24.976	24.488
Nd2O3	13.931	14.561	12.939	14.513	14.43	13.952
Sm2O3	2.085	2.201	2.016	2.151	2.002	2.181
Gd2O3	1.245	1.36	1.45	1.355	1.396	1.293
Dy2O3	0.546	0.583	0.613	0.613	0.592	0.448
Eu2O3	0.392	0.311	0.406	0.372	0.405	0.358
P2O5	2.298	1.479	2.329	1.545	1.584	2.504
F	2.658	2.362	2.125	2.469	2.302	2.282
Cl	0.114	0.134	0.151	0.078	0.027	0.086
TOTAL	93.898	93.128	91.54	93.826	93.247	92.977

(1) Element abundance in weight percent oxide.

(2) Total iron expressed as FeO.

APPENDIX IV: BRITHOLITE

Chemical compositions of unaltered and altered britholite grains from the Type IV pegmatites.

Location	6A8A-B1-3	6A8A-B1-4	6A8A-B2-6	6A8A-B2-7	6A8A-B2-8	6A8A-B2-9
	Altered	Altered	Altered	Altered	Altered	Altered
SiO2 (1)	18.667	18.608	18.428	18.736	18.99	19.036
FeO T (2)	0	0	0	0	0	0
CaO	15.587	15.228	15.859	15.82	14.699	16.004
Al2O3	0.047	0.015	0.03	0.046	0.05	0.051
TiO2	0	0	0	0	0	0.028
UO2	0.805	0.74	0.823	0.904	0.942	0.813
ThO2	0.878	0.916	0.899	0.873	1.004	0.921
Y2O3	1.804	1.825	1.838	1.802	1.896	1.852
La2O3	8.458	8.308	8.266	8.208	8.488	8.187
Ce2O3	24.021	24.215	23.625	23.519	24.339	23.544
Nd2O3	12.773	12.858	12.83	12.797	13.031	12.618
Sm2O3	1.958	1.99	1.817	1.968	1.899	1.817
Gd2O3	1.168	1.179	1.141	1.199	1.156	1.304
Dy2O3	0.488	0.475	0.518	0.573	0.441	0.353
Eu2O3	0.36	0.284	0.292	0.333	0.247	0.283
P2O5	4.145	4.208	4.211	3.98	3.307	4.159
F	2.133	2.183	2.735	2.616	2.926	2.427
Cl	0.211	0.149	0.144	0.116	0.192	0.074
TOTAL	93.503	93.181	93.456	93.49	93.607	93.471

Location	6A8A-B2-10	6A8A-B3-2	6A8A-B3-4	6A8A-B3-5	6A8A-B3-8	6A8A-B3-9
	Altered	Altered	Altered	Altered	Altered	Altered
SiO2 (1)	18.418	18.68	18.495	18.522	18.559	18.971
FeO T (2)	0	0	0	0	0	0
CaO	15.437	15.705	15.62	16.275	15.921	15.468
Al2O3	0.008	0.047	0.027	0.054	0	0.058
TiO2	0.108	0.001	0	0	0	0.003
UO2	0.814	0.807	0.73	0.697	0.756	0.725
ThO2	0.934	0.982	0.78	0.902	0.822	0.786
Y2O3	1.777	1.815	1.815	1.805	1.746	1.852
La2O3	8.434	8.453	8.325	8.261	8.196	7.958
Ce2O3	23.881	23.848	24.005	23.694	23.794	23.51
Nd2O3	12.61	12.877	12.482	12.561	12.789	12.698
Sm2O3	1.819	1.805	1.73	1.766	1.792	1.938
Gd2O3	1.277	1.157	1.223	1.176	1.202	1.273
Dy2O3	0.437	0.399	0.506	0.37	0.511	0.494
Eu2O3	0.258	0.238	0.309	0.399	0.322	0.394
P2O5	3.762	4.197	4.084	4.621	4.265	3.792
F	2.294	2.841	2.415	2.79	2.603	2.528
Cl	0.188	0.053	0.124	0.04	0.154	0.144
TOTAL	92.456	93.905	92.67	93.933	93.432	92.592

(1) Element abundance in weight percent oxide.

(2) Total iron expressed as FeO.

APPENDIX IV: BRITHOLITE

Chemical compositions of unaltered and altered britholite grains from the Type IV pegmatites.

Location	6A6B-B1-2	6A6B-B1-4	6A6B-B2-4	6A6B-B2-5	6A6B-B2-6	6A6B-B3-2
	Altered	Altered	Altered	Altered	Altered	Altered
SiO2 (1)	19.181	18.865	19.1	18.498	18.466	18.838
FeO T (2)	0	0.001	0	0	0	0
CaO	14.838	15.75	15.158	15.527	16.239	15.499
Al2O3	0.017	0.041	0.015	0.056	0.104	0.013
TiO2	0.012	0	0.063	0.033	0.004	0
UO2	0.874	0.739	0.788	0.801	0.772	0.797
ThO2	0.856	0.905	0.891	0.764	0.792	0.883
Y2O3	2.007	1.915	1.912	1.848	1.79	1.894
La2O3	8.27	8.106	8.432	8.409	8.333	8.316
Ce2O3	24.509	23.403	24.355	24.136	23.836	23.953
Nd2O3	13.683	12.611	13.267	12.934	12.864	12.767
Sm2O3	1.979	1.826	1.932	1.878	1.825	1.985
Gd2O3	1.296	1.312	1.286	1.326	1.131	1.241
Dy2O3	0.613	0.569	0.521	0.324	0.487	0.417
Eu2O3	0.355	0.328	0.285	0.409	0.213	0.34
P2O5	3.182	3.865	3.566	4.297	4.424	3.838
F	2.385	2.445	2.394	2.646	3.165	2.373
Cl	0.116	0.144	0.035	0.025	0.078	0.138
TOTAL	94.173	92.825	94	93.911	94.523	93.292

Location	6A6B-B3-3	6A6B-B3-7	6A6B-B3-8	6A6B-B3-9	6A2-B-3	6A2-B-4
	Altered	Altered	Altered	Altered	Altered	Altered
SiO2 (1)	19.164	18.349	18.944	18.569	18.532	18.512
FeO T (2)	0.038	0	0	0	0	0
CaO	15.607	15.71	15.9	15.831	15.451	15.924
Al2O3	0.009	0.056	0.017	0.24	0.005	0
TiO2	0	0.042	0.017	0	0	0.053
UO2	0.804	0.881	0.802	0.81	0.782	0.764
ThO2	0.764	0.827	0.804	0.791	0.891	0.85
Y2O3	1.951	1.824	1.833	1.864	1.909	1.871
La2O3	8.134	8.314	8.401	8.183	8.572	8.404
Ce2O3	23.435	23.696	24.077	23.548	24.311	23.91
Nd2O3	12.818	12.767	12.883	12.755	12.478	12.424
Sm2O3	1.919	1.874	1.919	1.85	1.804	1.771
Gd2O3	1.27	1.219	1.154	1.277	0.986	1.094
Dy2O3	0.523	0.427	0.528	0.562	0.422	0.538
Eu2O3	0.279	0.324	0.335	0.354	0.348	0.321
P2O5	3.918	4.352	3.889	4.161	3.896	4.112
F	2.742	2.592	3.023	2.94	2.72	2.731
Cl	0.082	0.174	0.038	0.13	0.16	0.122
TOTAL	93.457	93.428	94.564	93.865	93.267	93.401

(1) Element abundance in weight percent oxide.

(2) Total iron expressed as FeO.

APPENDIX IV: BRITHOLITE

Chemical compositions of unaltered and altered britholite grains from the Type IV pegmatites.

Location	6A4-B-4	6A4-B-5	6A4-B-6	6A6A-B1-2	6A6A-B1-5	6A6A-B1-6
	Altered	Altered	Altered	Altered	Altered	Altered
SiO2 (1)	20.446	19.757	19.882	18.605	19.031	18.611
FeO T (2)	0.134	0	0	0	0	0
CaO	13.805	15.913	13.354	15.745	14.936	15.718
Al2O3	0.023	0.057	0	0.026	0.041	0
TiO2	0	0	0	0	0	0
UO2	0.874	0.889	0.655	0.845	0.806	0.782
ThO2	1.209	1.238	1.292	0.872	1.005	0.857
Y2O3	2.463	2.309	2.239	1.862	1.777	1.869
La2O3	6.822	7.35	8.22	8.121	8.087	8.17
Ce2O3	23.241	22.887	25.415	23.414	23.465	23.677
Nd2O3	14.143	13.608	13.922	12.582	12.698	12.444
Sm2O3	2.296	2.237	2.283	1.845	1.81	1.908
Gd2O3	1.494	1.431	1.398	0.996	1.139	1.172
Dy2O3	0.629	0.625	0.54	0.48	0.413	0.463
Eu2O3	0.346	0.455	0.326	0.283	0.267	0.241
P2O5	2.368	2.697	2.199	4.366	3.337	4.509
F	2.293	1.999	2.41	2.72	2.665	2.534
Cl	0.12	0.363	0.148	0.142	0.156	0.2
TOTAL	92.706	93.815	94.283	92.904	91.633	93.155

Location	6A6A-B1-7	6A6A-B1-8	6A6A-B2-1	6A6A-B2-2	6A6A-B2-3	6A6A-B3-2
	Altered	Altered	Altered	Altered	Altered	Altered
SiO2 (1)	18.26	18.371	18.546	18.465	19.151	18.649
FeO T (2)	0	0	0	0	0	0
CaO	16.446	16.531	16.465	16.377	15.032	16.006
Al2O3	0	0.01	0.041	0.027	0.004	0.039
TiO2	0	0	0.012	0	0.035	0
UO2	0.651	0.795	0.818	0.699	0.774	0.933
ThO2	0.717	0.841	0.836	0.834	0.86	0.969
Y2O3	1.742	1.774	1.848	1.76	1.85	1.828
La2O3	8.128	8.3	8.215	8.349	8.567	8.26
Ce2O3	23.05	23.628	23.433	23.844	24.335	23.559
Nd2O3	12.149	12.376	12.366	12.607	12.981	12.693
Sm2O3	1.668	1.964	1.729	1.961	1.854	1.63
Gd2O3	1.154	1.188	1.009	1.153	1.106	1.104
Dy2O3	0.505	0.389	0.454	0.569	0.363	0.507
Eu2O3	0.25	0.363	0.336	0.339	0.216	0.323
P2O5	4.455	4.61	4.476	4.385	3.521	4.618
F	2.876	2.868	2.689	2.911	2.788	2.714
Cl	0.208	0.107	0.078	0.069	0.037	0.147
TOTAL	92.259	94.115	93.351	94.349	93.474	93.979

(1) Element abundance in weight percent oxide.

(2) Total iron expressed as FeO.

APPENDIX IV: BRITHOLITE

Chemical compositions of unaltered and altered britholite grains from the Type IV pegmatites.

Location	6A6A-B3-5	6A6A-B3-8	6A6A-B3-10	6A6A-B4-2	6A6A-B4-4	6A6A-B4-6
	Altered	Altered	Altered	Altered	Altered	Altered
SiO2 (1)	18.961	18.985	18.582	20.502	18.931	18.927
FeO T (2)	0	0	0	0.156	0	0
CaO	16.037	15.745	16.001	16.472	15.292	15.373
Al2O3	0.034	0.027	0.007	0.257	0.031	0.052
TiO2	0	0	0	0	0	0
UO2	0.816	0.797	0.809	0.746	0.765	0.799
ThO2	0.952	0.814	0.803	0.837	0.667	0.888
Y2O3	1.878	1.935	1.83	1.847	1.938	1.901
La2O3	8.278	8.816	8.503	7.74	8.232	8.298
Ce2O3	23.574	23.654	23.807	22.752	23.913	23.887
Nd2O3	12.634	12.85	12.714	12.101	12.817	12.907
Sm2O3	1.892	2.151	1.84	1.957	1.913	1.917
Gd2O3	1.1	1.191	1.258	1.188	1.307	1.288
Dy2O3	0.464	0.489	0.518	0.504	0.492	0.347
Eu2O3	0.266	0.193	0.334	0.287	0.183	0.29
P2O5	4.329	3.969	4.092	3.493	3.848	3.744
F	2.503	3.093	2.649	2.471	2.541	2.683
Cl	0.104	0.108	0.08	0.098	0.121	0.088
TOTAL	93.822	94.817	93.827	93.408	92.991	93.389

Location	6A6A-B3-3	6A6A-B5-3	6A6A-B5-4	6A6A-B5-6
	Altered	Altered	Altered	Altered
SiO2 (1)	19.938	18.642	18.788	19.312
FeO T (2)	0	0	0	0
CaO	15.325	15.721	16.046	15.452
Al2O3	0.043	0.076	0.053	0.112
TiO2	0.033	0.04	0	0
UO2	0.912	0.766	0.808	0.877
ThO2	0.954	0.718	0.786	0.794
Y2O3	1.953	1.804	1.876	1.942
La2O3	8.336	8.093	8.251	8.033
Ce2O3	24.064	23.194	23.879	23.561
Nd2O3	13.262	12.295	12.627	12.886
Sm2O3	1.841	1.956	1.876	1.92
Gd2O3	1.165	1.174	1.27	1.422
Dy2O3	0.405	0.411	0.478	0.55
Eu2O3	0.356	0.337	0.384	0.338
P2O5	3.811	4.203	4.228	3.987
F	2.806	2.761	2.603	2.778
Cl	0.114	0.083	0.099	0.061
TOTAL	95.318	92.274	94.052	94.025

(1) Element abundance in weight percent oxide.

(2) Total iron expressed as FeO.

APPENDIX IV: BRITHOLITE

Water contents of britholite determined on a Mitsubishi Moisture Meter. Samples contain both unaltered and altered britholite and are identified by thin section number.

Sample	Water content (weight percent)
6A6	1.6787
6A2	1.5382
6A3	1.5318
6A1	1.1736
8-4D	1.4205
Average	1.46856

APPENDIX IV: BRITHOLITE

Interfacial angles measurements from triple junctions of britholite polygonal boundaries.

Sample	Interfacial Angles
6A1C-AP1-A	126-119-115
6A1C-AP1-B	122-118-120
6A1C-AP1-C	115-112-132
6A1C-AP1-D	101-157-102
6A1C-AP1-E	104-137-119
6A1C-AP1-F	169-56-135
6A1C-AP1-G	180-90-90
6A1C-AP1-H	101-86-173
6A1C-AP1-I	62-134-164
6A1C-AP1-J	92-133-135
6A1C-AP1-K	158-91-111
6A1C-AP1-L	169-52-139
6A1C-AP1-M	180-90-90
6A1C-AP1-N	90-83-187
6A1C-AP1-O	100-142-118
6A1C-AP1-P	145-102-113
6A5-AP2-A	136-127-97
6A5-AP2-B	90-135-135
6A5-AP2-C	135-119-106
6A5-AP2-D	150-110-100
6A5-AP2-E	129-109-122
6A5-AP2-F	55-141-164
6A5-AP2-G	147-71-142
6A5-AP2-H	113-108-139
6A5-AP2-I	155-61-144
6A5-AP2-J	100-138-122
6A5-AP2-K	90-126-144
6A5-AP2-L	135-107-118
6A5-AP2-M	119-137-104
6A5-AP2-N	150-120-90
6A5-AP2-O	131-73-156
6A4-BP1-A	135-108-117
6A4-BP1-B	135-90-135
6A4-BP1-C	90-170-100

Sample	Interfacial Angles
6A4-BP1-D	135-104-121
6A4-BP1-E	98-136-126
6A4-BP1-F	130-140-90
6A4-BP1-G	105-120-135
6A4-BP1-H	180-45-135
6A4-BP1-I	45-159-156
6A4-BP1-J	180-34-146
6A4-BP1-K	180-51-129
6A4-BP1-L	111-114-135
6A4-BP1-M	135-121-104
6A4-BP1-N	135-95-130
6A4-BP1-O	135-45-180
6A4-BP1-P	103-135-122
6A4-AP1-A	125-117-118
6A4-AP1-B	90-127-143
6A4-AP1-C	114-128-118
6A4-AP1-D	90-135-135
6A4-AP1-E	145-95-120
6A4-AP1-F	143-80-135
6A4-AP1-G	145-114-101
6A4-AP1-H	65-128-167
6A4-AP1-I	108-101-151
6A4-AP1-J	151-134-75
6A4-AP1-K	115-95-150
6A4-AP1-L	135-90-135
6A4-AP1-M	135-135-90
6A4-AP1-N	130-121-109
6A4-AP1-O	97-138-135
6A4-AP1-P	135-90-135
6A4-AP1-Q	126-112-122
6A4-AP1-R	77-148-135
6A4-AP1-S	128-102-130
6A4-AP1-T	135-135-90
6A4-AP1-U	135-111-114

APPENDIX V: ALLANITE

Chemical compositions of allanite grains from the Type IV pegmatites.

Location	6A7-AL3-4	6A2-AL2-2	6A2-AL5-2	6A2-AL5-4	6A2-AL6-2	6A2-AL6-9
Zoning	Dark	Dark	Dark	Dark	Dark	Dark
SiO2 (1)	29.912	29.981	27.969	28.227	28.273	28.169
FeO T (2)	16.581	15.447	19.01	20.721	17.076	20.235
Al2O3	8.452	8.171	9.554	8.356	6.368	8.386
CaO	11.356	11.433	10.628	10.075	10.687	9.921
MnO	0.435	0.827	0.552	0.667	0.719	0.487
MgO	0.385	0.529	0.548	0.605	0.456	0.68
TiO2	0.808	0.983	0.657	0.859	1.334	1.019
Y2O3	0	0	0.098	0.039	0.023	0
La2O3	4.845	6.013	7.326	8.101	6.674	7.917
Ce2O3	12.438	12.325	12.496	14.209	12.158	13.406
Nd2O3	4.867	3.453	3.412	2.773	3.385	2.811
Sm2O3	0.365	0.141	0.317	0.08	0.217	0.181
Gd2O3	0.025	0.089	0.092	0.049	0.054	0.007
Yb2O3	0.006	0.06	0.041	0	0	0
ThO2	0.341	0.13	0.025	0.005	0.212	0.112
P2O5	0.018	0.029	0.04	0	0.013	0.034
F	0.383	0.279	0.211	0.218	0.498	0.255
Cl	0.078	1.09	0.006	0.014	0.037	0.009
TOTAL	91.296	90.98	92.982	94.998	88.184	93.629

Location	6A4-AL1-5	6A4-AL1-6	6A4-AL1-8	6A4-AL2-3	6A4-AL2-4	6A4-AL2-7
Zoning	Dark	Dark	Dark	Dark	Dark	Dark
SiO2 (1)	28.99	28.536	33.058	28.511	28.62	28.975
FeO T (2)	18.339	18.35	9.35	19.584	19.403	17.647
Al2O3	9.977	9.938	7.069	8.815	8.525	8.896
CaO	10.331	10.24	5.397	10.11	9.61	9.338
MnO	0.609	0.61	0.82	0.684	0.718	0.633
MgO	0.735	0.735	0.34	0.71	0.747	0.671
TiO2	0.857	0.851	0.832	0.894	0.869	0.945
Y2O3	0	0.001	0.759	0	0	0.019
La2O3	7.363	7.493	5.676	7.515	7.903	7.818
Ce2O3	13.116	13.205	12.848	13.388	13.739	13.33
Nd2O3	3.034	2.939	5.648	2.958	2.837	2.978
Sm2O3	0.079	0.114	0.807	0.203	0.244	0.063
Gd2O3	0	0	0.351	0	0	0.121
Yb2O3	0	0	0.068	0	0.049	0
ThO2	0.089	0	0.228	0.077	0.063	0.063
P2O5	0.029	0.044	0.063	0	0.018	0
F	0.249	0.217	0.938	0.287	0.12	0.23
Cl	0.011	0.017	0.034	0.042	0.013	0.011
TOTAL	93.81	93.29	84.29	93.78	93.48	91.74

(1) Element abundances in weight percent oxide.

(2) Total iron expressed as FeO.

APPENDIX V: ALLANITE

Chemical compositions of allanite grains from the Type IV pegmatites.

Location	6A4-AL3-1	6A4-AL3-2	6A4-AL4-2	6A4-AL4-3	6A2-AL4-2	6A2-AL5-1
Zoning	Dark	Dark	Dark	Dark	Light	Light
SiO2 (1)	29.16	28.524	28.587	28.415	27.941	28.486
FeO T (2)	18.97	19.806	20.069	19.523	19.267	20.146
Al2O3	9.275	8.807	8.236	7.977	8.477	9.136
CaO	10.049	10.21	9.586	9.613	9.997	10.429
MnO	0.577	0.617	0.564	0.539	0.66	0.595
MgO	0.74	0.568	0.671	0.593	0.558	0.497
TiO2	0.97	0.866	0.832	0.802	0.617	0.694
Y2O3	0.019	0	0	0.032	0	0.009
La2O3	8.052	7.788	8.044	7.94	7.716	7.414
Ce2O3	13.565	13.187	13.805	13.771	13.305	12.696
Nd2O3	2.76	2.686	3.063	3.29	3.161	3.031
Sm2O3	0.194	0.003	0.165	0.199	0.176	0.107
Gd2O3	0.141	0	0.018	0.02	0	0.002
Yb2O3	0	0	0.066	0	0.015	0.011
ThO2	0	0	0.016	0.01	0	0.131
P2O5	0.022	0	0.025	0.004	0	0
F	0.54	0.309	0.196	0.34	0.385	0.205
Cl	0.016	0	0.011	0.01	0.026	0.02
TOTAL	95.05	93.372	93.954	93.078	92.3	93.609

Location	6A2-AL5-3	6A2-AL6-1	6A2-AL6-3	6A2-AL6-8	6A4-AL1-7	6A4-AL2-1
Zoning	Light	Light	Light	Light	Light	Light
SiO2 (1)	28.301	28.679	28.421	27.121	28.125	28.226
FeO T (2)	20.79	20.007	20.938	21.368	18.924	21.025
Al2O3	8.122	8.039	8.096	7.564	8.588	7.923
CaO	9.88	9.677	9.961	9.535	9.598	9.735
MnO	0.596	0.542	0.56	0.553	0.74	0.547
MgO	0.771	0.664	0.612	0.53	0.75	0.468
TiO2	0.771	1.152	1.026	0.67	0.634	0.863
Y2O3	0.013	0	0.009	0	0	0.103
La2O3	8.124	8.225	8.138	7.614	7.203	6.611
Ce2O3	13.351	13.532	13.216	13.862	13.527	13.355
Nd2O3	2.833	2.988	2.769	3.401	3.654	4.115
Sm2O3	0.104	0.126	0.126	0.09	0.1	0.325
Gd2O3	0.003	0.045	0.04	0	0	0.09
Yb2O3	0.046	0	0	0	0.046	0
ThO2	0.014	0.034	0	0.031	0.107	0.019
P2O5	0.002	0.005	0	0	0.034	0
F	0.487	0.243	0.223	0.357	0.328	0.32
Cl	0.021	0.03	0.01	0.02	0.031	0.006
TOTAL	94.23	93.99	94.14	92.72	92.39	93.73

(1) Element abundances in weight percent oxide.

(2) Total iron expressed as FeO.

APPENDIX V: ALLANITE

Chemical compositions of allanite grains from the Type IV pegmatites.

Location	6A4-AL2-6	6A4-AL3-3	6A4-AL3-4	6A4-AL4-1	6A4-AL4-4	6A7-AL1-1
Zoning	Light	Light	Light	Light	Light	Unzoned
SiO2 (1)	28.47	28.519	28.232	28.853	28.579	29.879
FeO T (2)	20.416	20.521	20.756	20.249	19.887	18.885
Al2O3	7.931	8.424	7.775	7.787	6.611	9.91
CaO	9.574	10.033	9.65	9.373	8.689	10.854
MnO	0.586	0.676	0.547	0.715	0.68	0.369
MgO	0.628	0.559	0.62	0.79	0.656	0.551
TiO2	0.867	0.877	0.874	1.055	0.71	0.964
Y2O3	0	0	0	0.004	0.057	0.02
La2O3	7.643	8.167	8.131	8.004	8.284	7.235
Ce2O3	13.734	13.668	13.732	13.802	14.222	12.618
Nd2O3	3.495	2.754	2.81	2.978	3.094	2.808
Sm2O3	0.173	0.128	0.111	0.131	0.055	0.111
Gd2O3	0	0.021	0.005	0.117	0.083	0
Yb2O3	0	0.017	0.031	0.023	0	0
ThO2	0.003	0.091	0.086	0	0	0.166
P2O5	0.022	0	0	0	0.016	0.004
F	0.119	0.209	0.195	0.254	0.461	0.272
Cl	0.04	0	0.001	0.003	0	0.009
TOTAL	93.701	94.663	93.556	94.138	92.084	94.655

Location	6A7-AL1-2	6A7-AL2-1	6A7-AL2-2	6A7-AL2-3	6A7-AL2-4	6A7-AL2-5
Zoning	Unzoned	Unzoned	Unzoned	Unzoned	Unzoned	Unzoned
SiO2 (1)	29.958	29.66	29.619	29.437	29.673	29.67
FeO T (2)	17.399	18.316	18.422	19.197	18.768	18.894
Al2O3	10.524	9.393	9.244	8.875	9.162	8.973
CaO	10.917	10.24	10.157	10.093	10.092	10.282
MnO	0.441	0.496	0.612	0.607	0.575	0.591
MgO	0.62	0.665	0.66	0.706	0.709	0.663
TiO2	0.981	0.947	0.931	0.959	0.94	1.055
Y2O3	0	0	0	0	0	0.006
La2O3	6.867	6.883	6.979	7.086	7.057	7.22
Ce2O3	12.7	13.522	13.553	13.745	13.785	13.399
Nd2O3	2.838	2.904	3.385	3.181	3.279	3.013
Sm2O3	0.158	0.235	0.137	0.07	0.169	0.112
Gd2O3	0	0	0	0	0	0
Yb2O3	0.041	0	0.008	0	0	0.027
ThO2	0.085	0.126	0.146	0.113	0.069	0.118
P2O5	0.007	0.022	0	0.029	0.009	0.027
F	0.345	0.369	0.301	0.221	0.31	0.286
Cl	0.02	0.017	0.021	0.014	0.036	0.031
TOTAL	93.9	93.8	94.17	94.33	94.63	94.37

(1) Element abundances in weight percent oxide.

(2) Total iron expressed as FeO.

APPENDIX V: ALLANITE

Chemical compositions of allanite grains from the Type IV pegmatites.

Location	6A7-AL2-6	6A7-AL2-7	6A7-AL2-8	6A7-AL2-9	6A7-AL2-10	6A7-AL3-1
Zoning	Unzoned	Unzoned	Unzoned	Unzoned	Unzoned	Unzoned
SiO2 (1)	29.827	29.52	29.693	29.513	29.713	29.501
FeO T (2)	19.165	18.531	18.679	18.219	19.01	18.605
Al2O3	9.123	9.296	9.211	9.157	9.153	9.316
CaO	10.189	9.974	10.119	9.752	10.143	10.21
MnO	0.542	0.548	0.512	0.633	0.583	0.651
MgO	0.745	0.696	0.696	0.727	0.738	0.711
TiO2	1.139	1.01	1.051	0.879	1.063	0.94
Y2O3	0	0.025	0.009	0	0	0
La2O3	7.05	7.34	6.843	6.234	7.243	6.755
Ce2O3	13.696	13.726	13.566	13.958	13.641	13.669
Nd2O3	3.209	3.248	3.357	3.84	3.118	3.328
Sm2O3	0.148	0.07	0.17	0.169	0.109	0.18
Gd2O3	0	0	0	0	0	0
Yb2O3	0.03	0	0.015	0.024	0	0
ThO2	0.157	0.189	0.124	0.303	0.11	0.172
P2O5	0.025	0.007	0	0	0	0
F	0.269	0.221	0.322	0.435	0.269	0.233
Cl	0.023	0.028	0	0.043	0.023	0.026
TOTAL	95.336	94.429	94.367	93.886	94.916	94.296

Location	6A7-AL3-2	6A7-AL3-3	6A7-AL3-5	6A7-AL4-1	6A7-AL4-2	6A7-AL4-3
Zoning	Unzoned	Unzoned	Unzoned	Unzoned	Unzoned	Unzoned
SiO2 (1)	29.712	29.625	29.608	29.593	29.744	29.484
FeO T (2)	19.478	18.319	18.348	18.403	18.737	18.384
Al2O3	9.011	9.546	9.408	9.493	9.341	9.369
CaO	10.301	10.276	10.255	10.347	10.263	10.205
MnO	0.577	0.462	0.432	0.53	0.574	0.52
MgO	0.611	0.683	0.673	0.659	0.687	0.645
TiO2	1.103	0.925	1.077	1.006	0.933	1.059
Y2O3	0	0	0.009	0	0	0.005
La2O3	7.524	7.34	7.471	7.148	6.913	6.776
Ce2O3	13.525	13.382	13.458	13.592	13.785	13.49
Nd2O3	2.802	2.944	2.981	3.205	3.426	3.397
Sm2O3	0.094	0.015	0.104	0.071	0.159	0.284
Gd2O3	0	0.02	0	0	0	0
Yb2O3	0	0	0	0.026	0.01	0
ThO2	0.109	0.155	0.053	0.061	0	0.159
P2O5	0	0	0	0.013	0.029	0
F	0.201	0.313	0.159	0.233	0.264	0.393
Cl	0	0.022	0.008	0.007	0	0.025
TOTAL	95.05	94.03	94.04	94.39	94.87	94.19

(1) Element abundances in weight percent oxide.

(2) Total iron expressed as FeO.

APPENDIX V: ALLANITE

Chemical compositions of allanite grains from the Type IV pegmatites.

Location	6A7-AL4-4	6A7-AL4-5	6A7-AL5-1	6A7-AL5-2	6A7-AL5-3	6A7-AL5-4
Zoning	Unzoned	Unzoned	Unzoned	Unzoned	Unzoned	Unzoned
SiO2 (1)	29.466	29.864	29.712	29.384	29.579	29.558
FeO T (2)	18.445	18.931	18.457	19.015	18.139	18.816
Al2O3	9.398	9.259	9.387	9.038	10.425	9.187
CaO	10.182	10.252	10.23	9.963	10.735	10.306
MnO	0.511	0.518	0.579	0.517	0.58	0.562
MgO	0.663	0.687	0.666	0.693	0.577	0.645
TiO2	0.984	0.891	0.944	1.057	0.667	1.082
Y2O3	0.011	0.023	0	0.009	0	0.002
La2O3	7.169	6.792	6.811	7.486	6.033	7.302
Ce2O3	13.779	13.682	13.432	13.809	12.966	13.494
Nd2O3	3.206	3.344	3.43	3.18	3.541	3.089
Sm2O3	0.112	0.133	0.068	0.14	0.21	0.135
Gd2O3	0	0	0	0	0.055	0
Yb2O3	0	0	0	0.047	0	0.014
ThO2	0.082	0.084	0.072	0.228	0.102	0.034
P2O5	0.042	0.004	0.015	0.02	0.002	0.042
F	0.269	0.327	0.313	0.288	0.375	0.223
Cl	0.014	0	0.039	0.025	0.011	0.029
TOTAL	94.334	94.791	94.156	94.898	93.997	94.519

Location	6A7-AL5-5	6A7-AL6-1	6A7-AL6-2	6A7-AL6-3	6A6A-AL1-1	6A6A-AL1-2
Zoning	Unzoned	Unzoned	Unzoned	Unzoned	Unzoned	Unzoned
SiO2 (1)	29.547	29.829	29.541	29.793	29.204	29.677
FeO T (2)	18.49	19.243	18.566	19.286	18.763	19.235
Al2O3	9.713	9.531	9.419	9.314	9.11	9.126
CaO	10.192	10.464	9.982	10.346	9.983	10.309
MnO	0.425	0.432	0.453	0.514	0.595	0.62
MgO	0.68	0.644	0.683	0.619	0.723	0.663
TiO2	1.028	0.843	0.948	0.893	0.999	0.877
Y2O3	0.013	0	0.004	0.015	0	0.009
La2O3	7.361	6.414	6.719	6.803	8.684	8.447
Ce2O3	13.255	13.463	13.732	13.423	13.503	13.178
Nd2O3	3.15	3.454	3.482	3.475	2.623	2.532
Sm2O3	0.048	0.194	0.124	0.143	0	0.208
Gd2O3	0	0	0	0	0	0
Yb2O3	0.049	0.001	0.006	0	0.023	0.02
ThO2	0.066	0.163	0.13	0.155	0.079	0
P2O5	0.038	0.02	0	0.042	0.029	0.06
F	0.17	0.344	0.179	0.219	0.263	0.28
Cl	0.015	0.006	0.033	0.038	0.006	0.012
TOTAL	94.24	95.04	94.	95.08	94.59	95.25

(1) Element abundances in weight percent oxide.

(2) Total iron expressed as FeO.

APPENDIX V: ALLANITE

Chemical compositions of allanite grains from the Type IV pegmatites.

Location	6A6A-AL1-3	6A6A-AL1-4	6A6A-AL1-5	6A6A-AL2-1	6A6A-AL2-2	6A6A-AL2-3
Zoning	Unzoned	Unzoned	Unzoned	Unzoned	Unzoned	Unzoned
SiO2 (1)	29.467	29.215	29.438	29.674	29.893	29.636
FeO T (2)	18.881	18.517	18.756	18.364	18.199	18.203
Al2O3	9.554	9.653	9.526	10.148	9.137	9.941
CaO	10.244	10.352	10.278	10.357	9.701	10.362
MnO	0.58	0.569	0.488	0.449	0.608	0.442
MgO	0.691	0.715	0.755	0.735	0.768	0.789
TiO2	0.824	0.794	1.023	0.645	0.765	0.856
Y2O3	0	0	0	0	0	0
La2O3	8.118	7.912	8.375	7.937	8.494	8.37
Ce2O3	13.247	13.156	13.317	13.129	13.657	12.994
Nd2O3	2.738	2.77	2.615	2.845	3.062	2.663
Sm2O3	0.245	0.072	0	0.146	0.068	0.066
Gd2O3	0	0	0	0	0	0
Yb2O3	0.023	0.027	0	0	0	0.025
ThO2	0.028	0.046	0.023	0.033	0.047	0.051
P2O5	0.02	0.013	0	0.085	0.029	0.118
F	0.406	0.254	0.28	0.387	0.307	0.249
Cl	0.022	0.02	0.022	0.01	0.033	0
TOTAL	95.088	94.084	94.896	94.944	94.768	94.765

Location	6A6A-AL2-4	6A6A-AL2-5	6A6A-AL2-6	6A6A-AL2-7	6A6A-AL3-1	6A6A-AL3-2
Zoning	Unzoned	Unzoned	Unzoned	Unzoned	Unzoned	Unzoned
SiO2 (1)	29.616	29.33	29.696	29.795	29.021	29.375
FeO T (2)	17.507	17.971	18.843	18.03	17.583	18.11
Al2O3	10.16	9.188	9.297	10.2	9.494	9.267
CaO	10.262	10.022	10.08	10.49	9.713	9.691
MnO	0.609	0.569	0.607	0.568	0.711	0.537
MgO	0.79	0.688	0.738	0.72	1.04	0.807
TiO2	0.741	0.838	0.901	0.76	0.872	0.935
Y2O3	0	0.005	0.013	0.025	0.057	0.011
La2O3	8.107	8.444	8.518	7.879	8.614	8.891
Ce2O3	13.173	13.26	13.488	13.073	12.694	13.49
Nd2O3	2.763	2.662	2.613	2.774	3.048	2.666
Sm2O3	0.073	0.1	0.058	0.129	0	0.094
Gd2O3	0	0	0	0	0	0
Yb2O3	0	0	0	0	0	0.039
ThO2	0	0	0	0.025	0.056	0.01
P2O5	0.055	0.053	0.052	0.045	0.38	0.04
F	0.277	0.243	0.347	0.346	0.385	0.246
Cl	0.017	0	0	0.014	0.03	0.006
TOTAL	94.15	93.37	95.25	94.87	93.7	94.22

(1) Element abundances in weight percent oxide.

(2) Total iron expressed as FeO

APPENDIX V: ALLANITE

Chemical compositions of allanite grains from the Type IV pegmatites.

Location	6A6A-AL3-3	6A2-AL1-1	6A2-AL1-2	6A2-AL2-3	6A2-AL2-4	6A2-AL3-1
Zoning	Unzoned	Unzoned	Unzoned	Unzoned	Unzoned	Unzoned
SiO2 (1)	29.525	28.426	28.287	28.729	28.62	29.333
FeO T (2)	18.647	18.682	18.801	19.089	18.382	17.777
Al2O3	9.564	9.769	9.103	9.337	9.568	10.636
CaO	10.239	10.215	9.818	10.035	9.975	10.542
MnO	0.588	0.56	0.52	0.582	0.469	0.55
MgO	0.81	0.75	0.85	0.744	0.765	0.663
TiO2	0.962	0.863	0.917	0.882	0.809	0.665
Y2O3	0.011	0	0.004	0	0.004	0.019
La2O3	8.417	7.965	8.541	8.274	8.105	7.203
Ce2O3	13.348	13.062	13.467	13.177	13.342	13.007
Nd2O3	2.663	2.903	2.925	2.698	2.759	3.352
Sm2O3	0.153	0.059	0.082	0.166	0.097	0.139
Gd2O3	0	0.024	0.024	0.097	0.021	0.037
Yb2O3	0	0	0.006	0.005	0	0.016
ThO2	0.002	0.014	0.058	0.019	0.09	0.038
P2O5	0.045	0.016	0.004	0.005	0.024	0.02
F	0.217	0.259	0.302	0.278	0.283	0.319
Cl	0.031	0.018	0.01	0.007	0.028	0.012
TOTAL	95.222	93.586	93.72	94.123	93.341	94.328

Location	6A2-AL3-2	6A2-AL3-3	6A2-AL3-4	6A2-AL4-1	6A2-AL4-3	6A2-AL6-4
Zoning	Unzoned	Unzoned	Unzoned	Unzoned	Unzoned	Unzoned
SiO2 (1)	28.946	29.042	28.183	28.349	28.372	28.16
FeO T (2)	18.278	18.379	18.629	19.229	20.091	21.3
Al2O3	9.969	10.267	10.041	9.407	8.899	7.549
CaO	10.14	10.352	10.148	10.373	10.264	9.729
MnO	0.586	0.552	0.601	0.483	0.57	0.531
MgO	0.774	0.74	0.667	0.647	0.584	0.589
TiO2	0.798	0.702	0.537	0.671	0.703	0.931
Y2O3	0.013	0.018	0	0	0	0.02
La2O3	7.75	7.913	7.686	7.521	7.971	7.832
Ce2O3	12.883	13.095	13.077	12.944	12.746	13.536
Nd2O3	3.027	2.9	2.768	3.027	2.736	3.059
Sm2O3	0.107	0.043	0.064	0.104	0.078	0.008
Gd2O3	0.007	0.014	0.009	0.016	0.037	0.021
Yb2O3	0	0	0	0	0.044	0.054
ThO2	0	0.08	0.048	0.02	0.053	0
P2O5	0.053	0.025	0.009	0	0.013	0.016
F	0.302	0.16	0.358	0.289	0.252	0.33
Cl	0.036	0.009	0	0	0	0
TOTAL	93.67	94.29	92.83	93.08	93.41	93.67

(1) Element abundances in weight percent oxide.

(2) Total iron expressed as FeO.

APPENDIX V: ALLANITE

Chemical compositions of allanite grains from the Type IV pegmatites.

Location	6A2-AL6-5	6A2-AL6-6	6A2-AL6-7	6A4-AL1-1	6A4-AL1-2	6A4-AL1-3
Zoning	Unzoned	Unzoned	Unzoned	Unzoned	Unzoned	Unzoned
SiO2 (1)	27.68	27.337	28.244	28.429	28.76	28.368
FeO T (2)	22.312	22.48	20.52	18.639	17.898	18.601
Al2O3	6.659	6.356	8.131	9.635	10.583	9.479
CaO	9.419	9.564	9.854	10.219	10.409	10.128
MnO	0.494	0.535	0.498	0.574	0.57	0.622
MgO	0.587	0.604	0.662	0.759	0.746	0.693
TiO2	0.877	1.132	1.014	0.909	0.646	0.872
Y2O3	0.014	0.032	0	0.021	0.012	0
La2O3	7.915	8.209	8.021	7.768	7.843	7.885
Ce2O3	13.756	13.76	13.457	13.196	13.074	12.916
Nd2O3	3.131	2.901	2.96	2.804	2.918	2.661
Sm2O3	0.111	0.096	0.028	0.144	0.016	0.036
Gd2O3	0.045	0	0.053	0.022	0	0.007
Yb2O3	0.025	0	0.024	0.019	0.034	0
ThO2	0.047	0.042	0.036	0.055	0.118	0
P2O5	0.031	0	0.018	0	0.029	0
F	0.199	0.25	0.332	0.296	0.335	0.227
Cl	0.009	0.001	0	0	0.005	0
TOTAL	93.31	93.3	93.852	93.489	93.997	92.494

Location	6A4-AL1-4	6A4-AL2-5	6A4-AL4-5	6A4-AL4-6	6A8A-AL1-1	6A8A-AL1-2
Zoning	Unzoned	Unzoned	Unzoned	Unzoned	Unzoned	Unzoned
SiO2 (1)	28.024	28.564	28.597	28.771	30.7	28.685
FeO T (2)	17.668	19.785	20.867	20.563	16.178	18.005
Al2O3	9.229	8.591	7.746	8.01	12.007	8.743
CaO	9.803	10.01	9.932	9.948	11.666	9.712
MnO	0.61	0.612	0.592	0.57	0.558	0.711
MgO	0.683	0.734	0.631	0.59	0.66	0.713
TiO2	0.67	0.901	0.803	0.859	0.65	0.728
Y2O3	0.006	0.001	0.014	0	0.015	0.066
La2O3	7.391	7.738	7.697	7.658	6.336	8.432
Ce2O3	13.301	13.396	13.713	13.6	11.912	12.98
Nd2O3	2.978	2.875	3.299	3.265	3.323	2.971
Sm2O3	0.147	0.167	0.093	0.279	0.096	0.22
Gd2O3	0	0.006	0.012	0.017	0	0.066
Yb2O3	0	0	0.03	0	0.017	0.02
ThO2	0.048	0	0.035	0.143	0.126	0.08
P2O5	0.045	0.024	0	0.027	0.035	0.293
F	0.42	0.205	0.222	0.269	0.229	0.37
Cl	0	0.004	0.007	0.006	0.007	0.035
TOTAL	91.02	93.61	94.29	94.58	94.52	92.83

(1) Element abundances in weight percent oxide.

(2) Total iron expressed as FeO.

APPENDIX V: ALLANITE

Chemical compositions of allanite grains from the Type IV pegmatites.

Location	6A8A-AL1-3	6A8A-AL1-4	6A8A-AL2-1	6A8A-AL2-2	6A8A-AL2-3	6A8A-AL2-4
Zoning	Unzoned	Unzoned	Unzoned	Unzoned	Unzoned	Unzoned
SiO2 (1)	29.44	28.838	29.048	29.341	29.238	29.732
FeO T (2)	18.7	20.633	20.074	18.148	17.588	17.76
Al2O3	9.745	7.925	8.514	10.139	9.95	10.492
CaO	10.243	9.757	10.098	10.139	10.426	10.554
MnO	0.625	0.492	0.526	0.518	0.532	0.43
MgO	0.701	0.63	0.575	0.803	0.767	0.697
TiO2	0.459	0.491	0.775	0.884	0.858	0.69
Y2O3	0	0.01	0.01	0	0	0
La2O3	7.987	7.906	7.779	8.236	8.182	6.664
Ce2O3	13.579	13.532	13.056	13.314	13.396	13.123
Nd2O3	3.033	3.262	3.154	2.805	2.808	3.476
Sm2O3	0.177	0.137	0.109	0.175	0.104	0.161
Gd2O3	0.091	0.095	0	0.005	0	0
Yb2O3	0	0	0.048	0.01	0.034	0
ThO2	0	0.069	0	0.014	0.011	0.036
P2O5	0.039	0.015	0.09	0.017	0.057	0.024
F	0.346	0.24	0.323	0.352	0.45	0.243
Cl	0.016	0.009	0	0.006	0.025	0.033
TOTAL	95.18	94.042	94.179	94.906	94.427	94.115

Location	6A8A-AL2-5	6A8A-AL2-6	6A8A-AL2-7	6A8A-AL3-1	6A8A-AL3-2	6A8A-AL4-1
Zoning	Unzoned	Unzoned	Unzoned	Unzoned	Unzoned	Unzoned
SiO2 (1)	29.593	29.387	29.64	29.199	29.19	29.58
FeO T (2)	17.242	18.024	17.743	16.585	17.454	16.507
Al2O3	10.681	9.662	10.449	8.762	9.61	11.285
CaO	10.444	9.894	10.612	9.39	10.117	10.525
MnO	0.702	0.579	0.56	0.754	0.65	0.55
MgO	0.742	0.781	0.742	0.961	0.86	0.863
TiO2	0.697	0.875	0.646	0.831	0.88	0.56
Y2O3	0	0	0	0.074	0.025	0
La2O3	7.387	8.174	7.033	8.576	8.424	8.189
Ce2O3	12.986	13.111	13.053	13.28	13.268	13.156
Nd2O3	3.013	2.874	3.437	2.972	2.661	2.628
Sm2O3	0.224	0.104	0.121	0.271	0.1	1.113
Gd2O3	0.051	0.055	0.023	0.054	0.012	0
Yb2O3	0.022	0.015	0	0	0	0
ThO2	0.074	0	0.148	0.03	0	0.041
P2O5	0.046	0.138	0	0.152	0.084	0.004
F	0.287	0.401	0.372	0.425	0.375	0.195
Cl	0	0.004	0	0.009	0.011	0.001
TOTAL	94.19	94.08	94.58	92.33	93.72	95.2

(1) Element abundances in weight percent oxide.

(2) Total iron expressed as FeO.

APPENDIX V: ALLANITE

Chemical compositions of allanite grains from the Type IV pegmatites.

Location	6A8A-AL4-2	6A8A-AL4-3	6A6B-AL1-1	6A6B-AL1-2	6A6B-AL1-3
Zoning	Unzoned	Unzoned	Unzoned	Unzoned	Unzoned
SiO2 (1)	29.373	30.03	29.362	29.143	29.756
FeO T (2)	17.514	16.72	19.184	18.056	18.31
Al2O3	9.929	11.152	8.979	10.405	9.375
CaO	10.363	10.505	9.981	10.192	10.02
MnO	0.763	0.556	0.61	0.523	0.749
MgO	0.904	0.897	0.65	0.614	0.627
TiO2	1.022	0.63	0.85	0.377	0.737
Y2O3	0.02	0.006	0	0	0.014
La2O3	8.538	7.605	8.402	8.184	8.363
Ce2O3	13.321	13.142	13.33	13.358	13.139
Nd2O3	2.831	3.009	2.747	2.879	2.642
Sm2O3	0.075	0.138	0.109	0.031	0.172
Gd2O3	0.008	0	0	0.001	0.069
Yb2O3	0.044	0	0	0.069	0.01
ThO2	0	0.041	0.024	0.102	0
P2O5	0.039	0	0	0	0.092
F	0.291	0.201	0.297	0.362	0.327
Cl	0.019	0.019	0.027	0.007	0
TOTAL	95.054	94.651	94.552	94.304	94.402

Location	6A6B-AL1-4	6A6B-AL1-5	6A6B-AL1-6	6A6B-AL1-7	6A6B-AL2-1
Zoning	Unzoned	Unzoned	Unzoned	Unzoned	Unzoned
SiO2 (1)	29.697	29.683	28.7	29.208	28.852
FeO T (2)	18.03	17.787	20.728	19.827	17.755
Al2O3	10.829	10.734	7.452	8.307	8.85
CaO	10.679	10.721	9.6	10.068	9.78
MnO	0.55	0.55	0.699	0.56	0.528
MgO	0.656	0.638	0.628	0.651	0.686
TiO2	0.621	0.62	0.898	0.875	0.93
Y2O3	0	0	0.094	0	0.055
La2O3	7.771	7.676	8.89	8.459	8.367
Ce2O3	13.026	12.995	14.058	13.185	13.221
Nd2O3	2.974	2.907	3.208	2.638	2.794
Sm2O3	0.155	0.233	0.16	0.196	0.109
Gd2O3	0.075	0.078	0.143	0.024	0.055
Yb2O3	0	0	0	0.002	0.016
ThO2	0.051	0	0.034	0.003	0.003
P2O5	0.02	0	0.031	0.007	0.213
F	0.248	0.379	0.296	0.165	0.467
Cl	0.001	0.01	0.017	0.007	0.016
TOTAL	95.38	95.01	95.63	94.18	92.7

(1) Element abundances in weight percent oxide.

(2) Total iron expressed as FeO.

APPENDIX V: ALLANITE

Chemical compositions of allanite grains from the Type IV pegmatites.

Location	6A6B-AL2-2	6A6B-AL2-3	6A6B-AL2-4	6A6B-AL2-5	6A6B-AL3-1	6A6B-AL3-2
Zoning	Unzoned	Unzoned	Unzoned	Unzoned	Unzoned	Unzoned
SiO2 (1)	28.972	28.564	29.043	28.852	29.161	29.1
FeO T (2)	18.433	19.452	18.486	19.478	17.972	17.857
Al2O3	9.136	8.802	9.276	8.96	10.253	9.796
CaO	10.15	10.22	10.344	10.336	10.362	10.137
MnO	0.604	0.643	0.576	0.682	0.556	0.49
MgO	0.731	0.686	0.69	0.635	0.769	0.936
TiO2	1.077	0.91	0.822	0.81	0.584	0.78
Y2O3	0	0.005	0.015	0	0	0.015
La2O3	8.171	8.293	8.242	8.235	8.065	7.778
Ce2O3	13.205	13.179	13.136	13.087	13.313	12.506
Nd2O3	2.788	2.649	2.841	2.648	2.754	2.745
Sm2O3	0.108	0.154	0.057	0.006	0.095	0.117
Gd2O3	0	0.018	0.006	0.094	0.037	0.117
Yb2O3	0.034	0	0.01	0.014	0	0.098
ThO2	0	0.088	0	0	0.106	0.101
P2O5	0.017	0.038	0.017	0	0.007	0
F	0.262	0.436	0.273	0.171	0.262	0.339
Cl	0	0.02	0	0.002	0	0.021
TOTAL	93.687	94.157	93.834	94.009	94.295	92.933

Location	6A6B-AL3-3	6A6B-AL3-4	6A6B-AL4-1	6A6B-AL4-2	6A6B-AL4-3	6A6B-AL4-4
Zoning	Unzoned	Unzoned	Unzoned	Unzoned	Unzoned	Unzoned
SiO2 (1)	28.71	29.07	28.989	29.335	29.221	28.985
FeO T (2)	19.284	19.198	18.97	18.335	18.901	18.707
Al2O3	9.07	9.13	9.574	10.11	9.273	0.9535
CaO	10.254	10.247	10.323	10.644	10.62	10.468
MnO	0.586	0.597	0.549	0.577	0.456	0.585
MgO	0.654	0.71	0.57	0.641	0.662	0.692
TiO2	0.897	0.933	0.795	0.633	0.962	0.888
Y2O3	0	0.037	0	0	0	0
La2O3	8.28	8.299	8.08	7.994	7.861	8.301
Ce2O3	13.214	13.	13.084	12.946	13.054	13.183
Nd2O3	2.748	2.812	2.796	2.721	2.931	2.676
Sm2O3	0.066	0.132	0.086	0.096	0.052	0.154
Gd2O3	0.021	0.141	0.055	0.102	0.012	0.002
Yb2O3	0	0.022	0	0.002	0.023	0.025
ThO2	0.042	0	0	0.075	0.044	0
P2O5	0.027	0.007	0.04	0.015	0	0.028
F	0.356	0.294	0.182	0.291	0.274	0.241
Cl	0.004	0	0	0.028	0.001	0
TOTAL	94.21	94.63	94.09	94.55	94.35	85.89

(1) Element abundances in weight percent oxide.

(2) Total iron expressed as FeO.

APPENDIX V: ALLANITE

Chemical compositions of allanite grains from the Type IV pegmatites.

Location	**6A6B-AL4-5**
Zoning	**Unzoned**
SiO2 (1)	28.824
FeO T (2)	19.119
Al2O3	8.979
CaO	10.21
MnO	0.516
MgO	0.668
TiO2	0.981
Y2O3	0
La2O3	8.32
Ce2O3	13.127
Nd2O3	2.706
Sm2O3	0.104
Gd2O3	0.062
Yb2O3	0.016
ThO2	0.067
P2O5	0.009
F	0.155
Cl	0.001
TOTAL	93.864

(1) Element abundances in weight percent oxide.
(2) Total iron expressed as FeO.

APPENDIX V: ALLANITE

Trace element compositions of allanite grains from the Type IV pegmatites.

Location	6A7-B	6A7-B	6A5-A	6A5-A	6A5-A
PIXE	Apr10_95.062	Apr10_95.061	Apr10_95.060	Apr10_95.059	Apr10_95.058
FeO T (1,2)	13.896	17.189	16.003	16.796	10.199
MnO	0.459	0.409	0.49	0.522	0.366
Y2O3	0.185	0.037	0.043	0.019	0.039
La2O3	4.826	5.805	6.571	7.126	4.283
Ce2O3	8.994	9.592	9.66	10.369	6.514
Nd2O3	2.908	2.129	1.915	1.952	1.433
ThO2	0.233	0.169	0.103	0.09	0.064
UO2	0.231	0.011	0.018	0.007	0.017
Co (3)	0	0	0	1430	0
Ni	32	46	26	29	16
Cu	23	23	0	0	27
Zn	537	676	789	769	534
Ga	29	35	34	30	23
Sr	3886	1414	4558	1454	1057
Mo	0	11	13	0	0
Pb	749	108	118	46	101

Location	6A7-A
PIXE	Apr10_95.043
FeO T (1,2)	5.247
MnO	0.159
Y2O3	0.033
La2O3	2.02
Ce2O3	3.414
Nd2O3	0.8
ThO2	0.035
UO2	0.034
Co (3)	464
Ni	12
Cu	12
Zn	228
Ga	10
Sr	1132
Mo	0
Pb	73

(1) Element abundances in weight percent oxide.
(2) Total iron expressed as FeO.
(3) Trace element abundance in ppm.

APPENDIX VI: ANDRADITE

Chemical compositions of unaltered and altered andradite crystals from the Type III pegmatites.

Location	27A-GT1-2	27A-GT2-3	27A-GT2-4	27A-GT3-1	27A-GT4-2	27A-GT5-1
Zoning	**Centre**	**Centre**	**Centre**	**Centre**	**Centre**	**Centre**
SiO2 (1)	35.212	35.379	35.109	35.39	34.965	34.895
CaO	31.816	31.669	31.444	31.489	31.591	31.336
Fe2O3 T (2)	27.806	28.136	28.986	28.53	28.273	28.093
Al2O3	2.104	2.032	1.906	1.97	1.968	1.961
TiO2	1.103	0.974	0.808	0.885	1.007	0.937
MnO	0.855	0.952	1.014	1.106	1.015	1.035
MgO	0	0	0	0	0	0
TOTAL	98.896	99.142	99.267	99.37	98.819	98.257
V (3)	1270	1490	1060	850	850	800
Zr	0	780	0	0	0	590
Y	2230	2280	2630	2620	2360	2530
La	70	0	0	0	0	110
Ce	90	0	50	330	260	0
Nd	250	140	400	250	600	70
Yb	30	540	390	340	570	530
Lu	0	680	0	350	0	0
U	30	0	0	0	490	100

Location	27A-GT6-3	27A-GT6-6	27A-GT1-1	27A-GT2-1	27A-GT3-2	27A-GT5-2
Zoning	**Centre**	**Centre**	**Edge**	**Edge**	**Edge**	**Edge**
SiO2 (1)	34.874	34.754	34.987	35.382	35.08	35.388
CaO	31.613	31.345	31.341	31.687	30.493	31.683
Fe2O3 T (2)	27.786	28.761	29.235	28.968	30.917	28.133
Al2O3	1.903	1.809	1.455	1.362	1.178	1.949
TiO2	1.011	0.827	0.626	0.677	0.469	1
MnO	1.005	1.033	1.168	1.014	1.346	0.887
MgO	0	0	0	0	0	0
TOTAL	98.192	98.529	98.812	99.09	99.483	99.04
V (3)	1400	1220	40	1130	1370	550
Zr	0	400	240	0	50	740
Y	2220	2260	1650	2630	2450	2080
La	0	10	0	0	0	0
Ce	0	0	0	120	0	420
Nd	290	500	0	200	370	170
Yb	430	250	710	710	260	560
Lu	0	0	0	0	220	350
U	0	0	0	0	20	110

(1) Element abundance in weight percent oxide.

(2) Total iron expressed as Fe2O3.

(3) Element abundance in ppm.

APPENDIX VI: ANDRADITE

Chemical compositions of unaltered and altered andradite crystals from the Type III pegmatites.

Location	27A-GT6-2	27A-GT1-3	27A-GT2-2	27A-GT2-5	27A-GT4-1	27A-GT6-1
Zoning	**Edge**	**Altered**	**Altered**	**Altered**	**Altered**	**Altered**
SiO2 (1)	34.755	34.619	35.045	35.115	35.014	34.283
CaO	31.528	30.479	30.72	30.206	30.574	29.945
Fe2O3 T (2)	28.008	30.273	30.294	31.128	30.645	30.041
Al2O3	1.829	1.082	1.072	1.011	0.945	0.967
TiO2	0.894	0.606	0.646	0.582	0.627	0.642
MnO	1.033	1.543	1.314	1.331	1.188	1.501
MgO	0	0	0	0	0.006	0
TOTAL	98.047	98.602	99.091	99.373	98.999	97.379
V (3)	1110	1280	920	1190	990	1530
Zr	0	690	0	0	0	270
Y	2020	2530	2350	2400	2870	2630
La	60	0	0	0	0	0
Ce	30	0	530	210	580	0
Nd	250	370	310	450	410	330
Yb	620	380	290	50	340	430
Lu	0	0	1090	390	0	460
U	260	0	180	360	0	50

Location	27A-GT6-4	27A-GT6-5
Zoning	**Altered**	**Altered**
SiO2 (1)	34.735	34.643
CaO	30.205	30.848
Fe2O3 T (2)	30.17	29.035
Al2O3	0.961	1.129
TiO2	0.656	0.6
MnO	1.282	1.395
MgO	0	0
TOTAL	98.009	97.65
V (3)	1340	660
Zr	0	0
Y	2740	2260
La	60	100
Ce	0	500
Nd	350	140
Yb	260	290
Lu	0	1300
U	100	0

(1) Element abundance in weight percent oxide.

(2) Total iron expressed as Fe2O3.

(3) Element abundance in ppm.

APPENDIX VII: AEGIRINE-AUGITE

Chemical compositions of aegirine-augite crystals from the Type III pegmatites.

Location	5A7-PY1-6	5A7-PY1-7	5A1-PY1-4	5A1-PY1-5	5A1-PY1-7	5A1-PY2-1
Zoning	Dark	Dark	Dark	Dark	Dark	Dark
SiO2 (1)	52.43	52.024	51.693	51.454	51.065	51.818
TiO2	0.045	0	0.034	0.036	0.029	0.011
Al2O3	2.084	0.39	0.545	0.451	0.439	0.481
Fe2O3 (2)	16.884	16.672	16.317	16.725	16.167	15.235
MnO	0.912	0.872	1.044	1.101	1.066	1.168
MgO	13.035	8.027	8.026	8.174	8.089	8.631
CaO	11.456	20.771	19.792	20.219	20.245	19.782
Na2O	1.022	1.63	1.753	1.82	1.85	1.994
V2O5	0.011	0.016	0	0.02	0.03	0.03
La2O3	0.006	0.002	0	0	0	0
Ce2O3	0.008	0	0.014	0.006	0.016	0.056
Yb2O3	0	0.01	0	0.008	0.006	0
Lu2O3	0	0	0	0	0	0
TOTAL	97.893	100.415	99.218	100.013	99.002	99.207

Location	5A1-PY2-4	5A7-PY1-1	5A7-PY1-2	5A7-PY1-3	5A7-PY1-4	5A7-PY1-5
Zoning	Dark	Light	Light	Light	Light	Light
SiO2 (1)	51.926	50.926	52.048	51.44	52.591	51.635
TiO2	0.013	0.044	0.034	0.046	0.02	0.01
Al2O3	0.468	0.773	0.405	0.77	0.401	0.647
Fe2O3 (2)	15.904	21.05	16.659	21.696	16.723	19.56
MnO	1.085	0.704	1.165	0.802	1.051	0.864
MgO	8.157	5.919	8.079	5.655	8.116	6.745
CaO	19.823	19.451	20.427	19.398	20.818	19.852
Na2O	1.857	2.204	1.774	2.234	1.769	2.039
V2O5	0	0.136	0	0.129	0.1	0.012
La2O3	0	0	0	0	0	0
Ce2O3	0.005	0	0	0.019	0	0.043
Yb2O3	0.007	0	0.002	0	0.006	0
Lu2O3	0	0	0	0	0	0
TOTAL	99.245	101.207	100.593	102.188	101.595	101.408

(1) Element abundance in weight percent oxide.

(2) Total iron expressed as Fe2O3.

APPENDIX VII: AEGIRINE-AUGITE

Chemical compositions of aegirine-augite crystals from the Type III pegmatites.

Location	5A7-PY1-8	5A1-PY1-1	5A1-PY1-2	5A1-PY1-3	5A1-PY1-6	5A1-PY1-8
Zoning	Light	Light	Light	Light	Light	Light
SiO2 (1)	51.28	51.774	51.402	50.498	50.886	50.453
TiO2	0.001	0.026	0.016	0.025	0.026	0
Al2O3	0.639	0.466	0.488	0.792	0.772	0.789
Fe2O3 (2)	21.195	17.676	17.195	20.494	20.347	20.201
MnO	0.663	0.974	0.91	0.717	0.689	0.695
MgO	5.844	7.361	7.641	6.034	5.879	6.119
CaO	19.551	20.248	20.069	19.445	19.157	19.24
Na2O	2.204	1.897	1.937	2.206	2.211	2.111
V2O5	0.043	0.054	0	0	0.12	0.055
La2O3	0	0	0	0	0	0.009
Ce2O3	0	0.016	0	0.006	0.013	0
Yb2O3	0.002	0	0	0	0.034	0
Lu2O3	0	0	0	0	0	0
TOTAL	101.422	100.492	99.658	100.217	100.134	99.673

Location	5A1-PY2-2	5A1-PY2-3
Zoning	Light	Light
SiO2 (1)	50.295	50.531
TiO2	0.044	0.061
Al2O3	0.823	0.784
Fe2O3 (2)	20.706	20.455
MnO	0.761	0.652
MgO	5.854	5.74
CaO	18.713	18.832
Na2O	2.347	2.269
V2O5	0.05	0.027
La2O3	0.005	0
Ce2O3	0	0
Yb2O3	0.034	0.03
Lu2O3	0	0
TOTAL	99.632	99.38

(1) Element abundance in weight percent oxide.
(2) Total iron expressed as Fe2O3.

APPENDIX VII: AEGIRINE-AUGITE

Chemical compositions of aegirine-augite crystals from the Type IV pegmatites.

Location	6A6B-PY1-3	6A6B-PY1-4	6A6B-PY2-1	6A1C-PY1-3	6A1C-PY2-1	6A1C-PY3-1
Zoning	Centre	Centre	Centre	Centre	Centre	Centre
SiO2 (1)	50.841	50.655	50.699	50.852	51.446	51.179
TiO2	0.045	0.022	0.039	0	0.028	0
Al2O3	0.356	0.492	0.839	0.406	0.58	0.406
Fe2O3 (2)	21.551	22.779	22.438	22.739	19.718	21.589
MnO	1.194	1.138	1.164	1.215	1.079	1.17
MgO	5.387	4.846	5.037	4.945	6.265	5.595
CaO	19.029	18.752	18.707	18.584	19.438	19.336
Na2O	2.335	2.473	2.569	2.454	2.197	2.227
V2O5	0.043	0.046	0.009	0.116	0.016	0.016
La2O3	0	0.007	0	0.002	0	0
Ce2O3	0	0.039	0.019	0	0.016	0.014
Yb2O3	0	0	0	0	0	0
Lu2O3	0	0	0	0	0	0
TOTAL	100.781	101.249	101.52	101.313	100.783	101.532

Location	6A6B-PY1-1	6A6B-PY1-2	6A6B-PY2-2	6A1C-PY1-2	6A1C-PY2-2	6A1C-PY3-2
Zoning	Rim	Rim	Rim	Rim	Rim	Rim
SiO2 (1)	49.791	47.744	50.889	50.403	51.395	52.364
TiO2	0.016	0.001	0.073	0	0	0.014
Al2O3	0.711	4.681	0.568	0.285	0.468	0.384
Fe2O3 (2)	22.803	18.436	21.542	20.289	18.965	15.989
MnO	1.097	1.026	1.141	1.197	1.169	1.061
MgO	4.93	6.447	5.383	6.185	6.755	8.713
CaO	19.285	17.263	19.132	20.152	20.338	21.686
Na2O	2.128	1.817	2.383	1.873	1.861	1.253
V2O5	0	0.096	0.016	0.014	0.055	0.002
La2O3	0	0.03	0.005	0.008	0	0
Ce2O3	0.01	0	0.097	0.078	0.051	0.01
Yb2O3	0	0	0	0		0
Lu2O3	0	0	0	0	0	0
TOTAL	99.245	101.207	100.593	102.188	101.595	101.408

(1) Element abundance in weight percent oxide.

(2) Total iron expressed as Fe2O3.

APPENDIX VII: AEGIRINE-AUGITE

Chemical compositions of aegirine-augite crystals from the Type IV pegmatites.

Location	6A1C-PY1-4	6A1C-PY3-3	6A1C-PY3-4
Zoning	Altered	Altered	Altered
SiO2 (1)	52.763	51.547	52.335
TiO2	0.022	0.017	0.018
Al2O3	0.434	0.215	0.243
Fe2O3 (2)	13.851	14.726	13.888
MnO	1.011	1.055	1.048
MgO	10.029	9.034	9.7
CaO	22.13	21.602	21.983
Na2O	1.068	1.148	0.995
V2O5	0	0.059	0
La2O3	0	0	0
Ce2O3	0	0.071	0.056
Yb2O3	0	0.005	0.002
Lu2O3	0	0	1.274
TOTAL	101.308	99.479	101.542

(1) Element abundance in weight percent oxide.

(2) Total iron expressed as Fe2O3.

APPENDIX VIII: FELDSPAR

Chemical compositions of K-feldspar crystals from the Type III pegmatites.

Location	5A7-KF1-1 K-feldspar	5A7-KF1-2 K-feldspar	5A7-KF1-3 K-feldspar	5A7-KF1-4 K-feldspar	10C-KF1-1 K-feldspar	10C-KF1-2 K-feldspar
SiO2 (1)	63.647	63.58	64.158	63.944	64.442	64.711
Al2O3	18.806	18.909	18.733	18.53	18.421	18.469
Fe2O3	0.183	0.109	0.136	0.141	0.213	0.26
CaO	0	0	0	0	0	0
Na2O	0.644	0.762	0.696	0.336	0.213	0.35
K2O	15.624	15.556	15.693	16.632	16.909	16.641
BaO	0.406	0.655	0.654	0.63	0.066	0.025
SrO	0.311	0.164	0.121	0.108	0	0
TOTAL	99.621	99.736	100.191	100.32	100.264	100.456
La (2)	0	0	0	0	0	120
Ce	1950	2260	1840	1440	230	250
Nd	0	110	80	0	0	120
Sm	200	0	0	40	0	50
Eu	0	70	80	0	0	130
Yb	0	0	300	130	10	120
Hf	810	660	410	870	730	770

Location	10C-KF1-4 K-feldspar	10C-KF1-5 K-feldspar
SiO2 (1)	64.04	63.976
Al2O3	18.462	18.644
Fe2O3	0.06	0.097
CaO	0	0
Na2O	0.15	0.345
K2O	16.831	16.427
BaO	0.499	0.259
SrO	0	0.07
TOTAL	100.042	99.818
La (2)	0	0
Ce	1120	1700
Nd	350	0
Sm	260	0
Eu	0	80
Yb	0	60
Hf	800	780

(1) Element abundance in weight percent oxide.

(2) Trace element abundance in ppm.

APPENDIX VIII: FELDSPAR

Chemical compositions of plagioclase grains from the Type III pegmatites.

Location	5A7-NP1-1 Plagioclase	5A7-NP1-2 Plagioclase	5A7-NP1-3 Plagioclase	5A7-NP1-4 Plagioclase	10C-NP1-1 Plagioclase
SiO2 (1)	68.164	69.257	67.812	65.933	68.377
Al2O3	20.114	20.194	20.033	21.919	19.747
Fe2O3	0.054	0.032	0.13	0.053	0.363
CaO	0.264	0.059	0.181	0.255	0.066
Na2O	11.448	10.507	11.599	11.128	11.429
K2O	0.07	0.091	0.084	0.14	0.16
BaO	0.067	0	0	0.049	0.025
SrO	0.436	0.121	0.148	0.053	0.066
TOTAL	100.617	100.261	99.987	99.53	100.233
La (2)	0	0	0	0	0
Ce	30	110	0	90	40
Nd	170	0	0	0	160
Sm	70	0	0	0	270
Eu	0	120	0	0	300
Yb	30	0	0	0	40
Hf	0	0	0	0	0

Location	10C-NP1-2 Plagioclase	10C-NP1-3 Plagioclase	10C-NP1-4 Plagioclase
SiO2 (1)	68.256	67.991	68.269
Al2O3	19.471	19.623	19.662
Fe2O3	0.337	0.273	0.269
CaO	0.065	0.095	0.069
Na2O	11.588	11.471	11.662
K2O	0.158	0.134	0.072
BaO	0	0	0
SrO	0.066	0	0.092
TOTAL	99.941	99.587	100.095
La (2)	0	0	0
Ce	0	0	0
Nd	0	0	0
Sm	0	80	30
Eu	190	30	0
Yb	190	0	120
Hf	0	0	0

(1) Element abundance in weight percent oxide.

(2) Trace element abundance in ppm.

APPENDIX VIII: FELDSPAR

Chemical compositions of K-feldspar crystals from the Type IV pegmatites.

Location	6A1C-KF1-1	6A1C-KF1-2	6A1C-KF2-1	6A1C-KF2-2	6A1C-KF2-3	6A1C-KF2-4
	K-feldspar	K-feldspar	K-feldspar	K-feldspar	K-feldspar	K-feldspar
SiO2 (1)	63.116	63.171	63.958	63.584	63.738	64.474
Al2O3	18.802	19.014	18.78	18.465	18.839	18.727
Fe2O3	0.044	0.08	0.167	0.414	0.062	0.159
CaO	0	0	0	0	0	0
Na2O	0.363	0.614	0.605	0.685	0.504	0.624
K2O	16.133	15.816	16.097	15.453	16.124	16.112
BaO	0.477	0.574	0.3494645	0.408	0.435	0.316
SrO	0.119	0.272	0.21523502	0.194	0.123	0.186
TOTAL	99.054	99.541	100.172	99.202	99.825	100.598
La (2)	0	0	30	0	0	0
Ce	2060	2050	1420	1320	1200	1020
Nd	0	170	0	190	0	30
Sm	30	0	290	140	0	0
Eu	0	180	160	0	0	0
Yb	0	0	290	0	0	200
Hf	980	900	590	550	650	900

Location	6A1C-KF2-5
	K-feldspar
SiO2 (1)	63.709
Al2O3	18.893
Fe2O3	0.095
CaO	0
Na2O	0.582
K2O	15.811
BaO	0.452
SrO	0.189
TOTAL	99.731
La (2)	0
Ce	1760
Nd	170
Sm	0
Eu	0
Yb	0
Hf	590

(1) Element abundance in weight percent oxide.
(2) Trace element abundance in ppm.

APPENDIX VIII: FELDSPAR

Chemical compositions of plagioclase grains from the Type IV pegmatites.

Location	6A1C-NP1-3 Plagioclase	6A1C-NP3-1 Plagioclase	8-4C-PG1 Plagioclase	8-4C-PG2 Plagioclase	8-4C-PG3 Plagioclase
SiO2 (1)	67.624	67.774	69.7	68.691	68.847
Al2O3	20.368	20.384	20.031	20.634	20.478
Fe2O3	0.861	0.107	0.119	0.11	0.056
CaO	0.464	0.634	0.107	0.62	0.451
Na2O	11.363	11.094	11.509	11.089	11.195
K2O	0.129	0.224	0.21	0.164	0.081
BaO	0	0	0.132	0	0.025
SrO	0.183	0.272	0	0.33	0.303
TOTAL	100.992	100.489	101.808	101.638	101.435
La (2)	0	0	0	0	0
Ce	50	90	120	170	60
Nd	20	190	70	60	0
Sm	270	0	0	180	220
Eu	40	130	0	60	0
Yb	0	0	0	80	0
Hf	0	0	0	0	0

(1) Element abundance in weight percent oxide.

(2) Trace element abundance in ppm.